

# Hakone XVII



August 21st – 25th, 2022 Rolduc Abbey, Kerkrade, The Netherlands.

# **Contents**

1	Introduction	2
	1.1 Scope & Format	. 2
	1.2 Venue	. 2
	1.3 Conference Topics	. 3
	1.4 Information for Presenters	. 3
2	Committees	4
	2.1 Local Organizing Committee	. 4
	2.2 International Scientific Committee	. 4
3	Sponsors	5
4	Program	6
	4.1 Program table	. 6
	4.2 Detailed program including social program	
5	Venue maps	17
6	Abstracts	19

#### 1 Introduction

HAKONE XVII will be held in the south of the Netherlands in the former Abbey Rolduc, August 21st – 25th, 2022. The biennial HAKONE symposium series started in Hakone (Japan) in 1987 and is devoted to the fundamentals and applications of non-thermal plasmas and their chemistry at elevated pressures.

#### 1.1 Scope & Format

HAKONE brings together scientists and engineers from academia and industry working on high pressure and low temperature plasma chemistry. The symposium aims to connect more traditional subjects such as ozone synthesis, basic oxidants generation, water treatment and environmental protection to the emerging and innovative fields of biomedical applications, micro-plasmas and alternative materials.

#### 1.2 Venue



HAKONE XVII will be held at the Rolduc abbey in Kerkrade, which is one of the most important religious monuments in the Netherlands. The abbey's rich history dates back more than 900 years. Rolduc is the largest abbey complex in the Benelux and one of the Dutch UNESCO Top 100 monuments. Rolduc abbey can be reached by public transport from Amsterdam Schiphol airport ( $\approx$ 3:30 hrs), Düsseldorf airport ( $\approx$ 2:00 hrs) and Maastricht airport ( $\approx$ 1:30 hrs).

We will provide a shuttle bus between Herzogenrath railway station (Germany) and the conference venue, and possibly between Kerkrade railway station and the venue as well. We will likely start with this around 13:00 on Sunday. If you would like to use this then please let us know when and where you expect to arrive.

#### WIFI

WIFI is available on an open network without requiring a password.

#### 1.3 Conference Topics

- T01 Fundamental problems of high pressure discharges
- T02 Modelling and diagnostics
- T03 Molecular synthesis and decomposition
- T04 Ozone generation and applications
- T05 Generation of radiation in high-pressure discharges
- T06 Depollution and environmental applications
- T07 Surface processing and technology (cleaning, coating, etching and modification, equipment)
- **T08** Biological applications
- T09 Miscellaneous

#### 1.4 Information for Presenters

Orals are 20 minutes (16 min + 4 min questions), while invited presentation and the Ulrich Kogelschatz Lecture Award are 50 minutes (45 min + 5 min questions). Please upload your presentation to the central laptop well in advance of your scheduled presentation block.

Posterboards will be 1.25 meter high and 1.00 meter wide. Posters can be mounted on the poster boards inside the lecture hall for the entire symposium. Furthermore, all poster presenters are requested to submit a one-page slide latest on Sunday, Aug. 21st for the one-minute poster presentation introduction. Please submit a PDF, preferably in 16:9 aspect ratio.

#### 2 Committees

#### 2.1 Local Organizing Committee

- · Sander Nijdam (chair), Eindhoven University of Technology
- · Behnaz Bagheri, Eindhoven University of Technology
- Ute Ebert, Centre for Mathematics and Computer Science (CWI) Amsterdam
- · Tom Huiskamp, Eindhoven University of Technology
- · Gerrit Kroesen, Eindhoven University of Technology
- · Gerard van Rooij, Maastricht University
- · Ana Sobota, Eindhoven University of Technology

#### 2.2 International Scientific Committee

- · Mirko Černák (chair), Czech Republic
- · Ronny Brandenburg, Germany
- · Nicolas Naude, France
- · Tony Herbert, Ireland
- · Tomáš Hoder, Czech Republic
- · Indrek Jõgi, Estonia
- · Kirill V. Kozlov, Russia
- · Štefan Matejčík, Slovakia
- · Jerzy Mizeraczyk, Poland
- · Naoki Osawa, Japan
- · Cristina Paradisi, Italy
- · Yi-Kang Pu, China
- · Henryka D. Stryczewska, Poland
- · Fumiyoshi Tochikubo, Japan

# 3 Sponsors

Hakone XVII is sponsored by the Dutch Research Council (NWO) and Plasma Matters B.V.





# 4 Program

### 4.1 Program table

	Sun, Aug 21		Mon, Aug 22		Tue, Aug 23		Wed, Aug 24	Thu, Aug 25
		08:00	Breakfast	08:00	Breakfast	08:00	Breakfast	Breakfast
		09:00	Opening	09:00	102 - Koichi Sasaki	09:00	104 - Deborah O'Connel	105 - Xin Pei Lu
		09:10	Françoise Massines	09:50	C09 - Vlasta Štěpánová	09:50	C17 - Alex Destrieux	C29 - Yury Gorbanev
		10:00	C01 - Elizabeth Mercer	10:10	C10 - Julia Mrotzek	10:10	C18 - Anne Limburg	C30 - Ursel Fantz
		10:20	Coffee break	10:30	Coffee break	10:30	Coffee break	Coffee break
		10:50	C02 - Roman Přibyl	11:00	C11 - Kristian Wende	11:00	C19 - David Prokop	C31 - Mostafa Hassan
		11:10	C03 - Antoine Belinger	11:20	C12 - Mark Kushner	11:20	C20 - Siebe Dijcks	C32 - David Sawtell
		11:30	C04 - Fumiyoshi Tochiku	11:40	C13 - Jan Cech	11:40	Organ concert	C33 - Chiel Ton
		11:50	C05 - Corentin Bajon	12:00	C14 - Ravi Patel	12:00	Organ concert	Closing ceremony
		12:30	Lunch	12:30	Lunch	12:30	Lunch	Lunch
		14:00	Poster 1-slide presenta	14:00	C15 - Perla Trad	14:00	103 - Luc Stafford	Bus to Eindhoven
		14:40 P	Poster session	14:20	C16 - Jeroen van Oorsch	14:50	C21 - Markus Becker	(optional)
				-		15:10	C22 - Mohammad Hasar	(optional)
						15:30	Coffee break	Labtour Eindhoven (optional)
						16:00	C23 - Hans Höft	
						16:20	C24 - Hani Francisco	
		16:40	I01 - Judith Golda			16:40	C25 - Thijs van der Gaag	
		17:00	C06 - Naoki Osawa	15:00	Excursion + banquet	17:00	C26 - Davide Del Cont-B	
	<b>—</b>	17:20	C07 - Thomas Orrière			17:20	C27 - Francisco Pontiga	
		17:40	C08 - Kazuki Watanabe			17:40	C28 - Lucia Kuthanová	
18:00	Formal registration	18:00	Free time			18:00	Free time	
		18:30	Dinner			18:30	Dinner	
19:00	Welcome reception					19:30	ISC-meeting	

**Ulrich Kogelschatz Award Lecture** 

Invited lecture

Contributed lecture

### 4.2 Detailed program including social program

#### Sun, Aug 21

#### **18:00 - 20:00** Formal registration

Chance to register for the conference. Hotel rooms will be available starting from 15:00. Conference registration is in Aula Minor (E on the map), while hotel registration is at the reception (R).

#### **19:00 - 22:00** Welcome reception

A welcome reception is organized in the hotel bar ('De Verloren Zoon', 'The Lost Son') located in the cellar.

#### Mon, Aug 22

#### 08:00 - 09:00 Breakfast

In the large dining room ('Grote Eetzaal')

#### 09:00 - 09:10 Opening

In the Aula Minor (building opposite to the reception).

#### Session chair: Mirko Černák

#### 09:10 - 10:00 Ulrich Kogelschatz Lecture Award UKL: Françoise Massines T01

CNRS, France.

Physics of diffuse DBDs and on line thin film treatment: History, recent developments and new challenges

#### 10:00 - 10:20 Contributed CO1: Elizabeth Mercer TO1

University of Antwerp, Belgium.

Effects of Post-Plasma Mixing in a CO<sub>2</sub> Microwave Plasma on Conversion and Energy Efficiency

#### 10:20 - 10:50 Coffee break

Fover + terrace

#### Session chair: Ronny Brandenburg

#### 10:50 - 11:10 Contributed CO2: Roman Přibyl TO1

Masaryk University, Czech Republic.

Alumina ceramic tapes doped by various dopants and their effect on properties of coplanar dielectric barrier discharge

#### 11:10 - 11:30 Contributed CO3: Antoine Belinger TO1

LAPLACE, Université de Toulouse, France.

Influence of the dielectric on a Diffuse Dielectric Barrier Discharge in air at atmospheric pressure

#### 11:30 - 11:50 Contributed CO4: Fumiyoshi Tochikubo TO1

Tokyo Metropolitan University, Japan.

Characteristics of Trichel Pulse Discharge from Taylor Cone with AC Superimposed DC Voltage

#### 11:50 - 12:10 Contributed C05: Corentin Bajon T01

Laboratoire Plasmas et conversion d'énergie, France.

Dielectric Barrier Discharge in  ${\it CO}_2$ : electrical and optical characterization

#### 12:30 - 14:00 Lunch

Foyer + terrace

#### **14:00 - 14:40** Poster 1-slide presentations

A quick introduction to all posters. All poster presenters are requested to submit a one-page slide latest on Sunday, Aug. 21st.

#### 14:40 - 16:40 Poster session

Including some refreshments.

P01: Indrek Jõgi T08

University of Tartu, Estonia.

Virus and aerosol removal by electrostatic precipitator

#### P02: Kubra Ulucan-Altuntas T06

University of Padua, Italy.

Degradation of Perfluorooctanoic Acid (PFOA) in Water by Non-Thermal Plasma Enhanced by Boron-Doped Reduced Graphene Oxide

P03: Sean Kelly T06

University of Antwerp, Belgium.

Microwave plasma-based conversion of methane and carbon dioxide

P04: Francisco Pontiga T06

Universidad de Sevilla, Spain.

Carbon dioxide conversion using ac and pulsed dielectric barrier discharge

P05: **Tian Tian** T06

GREMI, UMR7344, CNRS/Université d'Orléans, France.

Removal of amoxicillin and sulfamethoxazole in water using non-thermal plasma

P07: Rezvan Hosseini Rad T06

Leibniz Institute for Plasma Science and Technology (INP), Germany.

Electrical Characterization of a Coaxial Dielectric Barrier Discharges for  $CO_2$  splitting at Elevated Pressure

P08: **Shahriar Mirpour** T01

Eindhoven university of technology, Netherlands.

Investigating CO<sub>2</sub> streamer inception in repetitive pulsed discharges

P09: Lucia Švandová T01

Masaryk University, Czech Republic.

Properties of Cr-doped  $Al_2O_3$  as a dielectric barrier layer

P10: Mária Cíbiková T01

University of Comenius, Faculty of Mathematics, Physics and Informatics, Bratislava, Slovakia, Slovakia.

Characterization of emission current generated by pulse electric field in microdischarge electrode system

#### P11: Lucia Kuthanová T01

Masaryk University, Czech Republic.

Spatiotemporal memory effects in barrier discharge at water interface

P12: Simon Dap T01

LAPLACE - Toulouse University, France.

Pre-ionization in atmospheric pressure townsend discharges (APTD): surface vs volume mechanisms

P13: Hiroshi Arai T01

Chiba Institute of Technology, Japan.

Linearized Penning effect in gas mixture with small amount of  $H_2O$  content in He

P14: Haruo Itoh T01

Chiba Institute of Technology, Japan.

Increase of Penning ionization coefficient proportional to small amount of water vapor admixed with helium

P15: Shuai Zhao T09

Eindhoven University of Technology, Netherlands.

Microelectrode-assisted atmospheric pressure air discharge and its extended applications

P16: Nicolas Naudé T09

Université de Toulouse, France.

Dielectic barrier discharges: from spatially resolved electrical measurements to a reconfigurable electrode

#### P17: Zdenek Navratil T02

Masaryk University, Czech Republic.

2D-resolved electric field measurement in helium coplanar DBD using multi-wavelength single photon counting

#### P18: Emanuel Mat'aš T02

Faculty of Mathematics, Physics and Informatics, Comenius University, Slovakia.

Ion Mobility Spectrometry diagnostics of NOx generated in kHz driven DBD plasma jet in Argon

#### P19: Sara Ceulemans T02

University of Antwerp, Belgium.

Effect of quenching on the afterglow temperature to improve  ${\rm CO_2}$  conversion in a rotating gliding arc plasma reactor

#### P20: **Dennis Bouwman** T02

Centrum Wiskunde & Informatica (CWI), Netherlands.

Theoretical approximations for macroscopic parameters of positive streamer discharges

#### P21: Tomas Hoder T02

Masaryk University, Czech Republic.

Kinetics of the  $N_2(A^3\Sigma_u^+, v)$  state in atmospheric pressure townsend discharge in  $N_2$ 

#### P22: Tomas Hoder T02

Masaryk University, Czech Republic.

Development of a method for determination of the electric field in transient argon discharges

### P23: Omar Biondo T02

University of Antwerp, Belgium.

Gas heating dynamics in a CO<sub>2</sub> pulsed glow discharge resolved by kinetic modeling

#### P24: Yihao Guo T02

Eindhoven University of Technology, Netherlands.

3D reconstruction and analysis of branching streamer discharges in air

#### P25: **David Rauner** T02

Leibniz Institute for Plasma Science and Technology (INP), Germany.

Spectroscopic determination of rotational and vibrational temperatures in molecular MW plasmas for gas conversion

#### P26: Julia Mrotzek T02

HAWK, Germany.

Characterization of the plasma torch of an APPJ for thin film deposition

#### P27: Gerard van Rooij T03

Maastricht University, Netherlands.

Unravelling Transport in CO<sub>2</sub> Microwave Plasma by Comparing Flow Geometries

#### P28: **Hemaditya Malla** T04

Centrum Wiskunde & Informatica, Netherlands.

Identifying the Major Reactive Oxygen-Nitrogen Species in a Pulsed Streamer Discharge

#### P29: Dušan Kováčik T07

Masaryk University, Czech Republic.

Air plasma treatment for improving the safety properties of laminated glasses containing ionoplast interlayer used in civil engineering

#### P30: Katerina Polaskova T07

Brno University of Technology, Czech Republic.

Effect of Plasma and Light Irradiation on Morphology of Deposited  $TiO_2$  Nanoparticles

#### P31: Richard Krumpolec T07

Masaryk University, Czech Republic.

Ultra-fast low temperature atmospheric plasma triggered reduction-exfoliation of highly porous aerogel-like graphene oxide

#### P32: Maria Luíza de Azevedo T07

Maastricht University, Netherlands.

Fast pyrolysis in methane plasma

P33: Wouter Graef T02

Plasma Matters, Netherlands.

Status report on the LXCat project

P34: Daan Boer T02

Eindhoven University of Technology, Netherlands.

A Novel Data Platform for Low-Temperature Plasma Physics

P35: Jakub Kelar T07

Masaryk University, Czech Republic.

High quality UV digital printing on various materials with plasma enhanced surface

P36: **Tao Zhu** T07

Leibniz Institute for Plasma Science and Technology, Germany.

Tracing model of in-flight particles during a plasma spray process

#### Session chair: Nicolas Naudé

#### 16:40 - 17:00 Invited IO1: Judith Golda T06

Ruhr-University Bochum, Germany.

Cold Atmospheric Pressure Plasmas for Plasma Catalytic Applications: Characteristics, Constraints and Challenges

#### 17:00 - 17:20 Contributed C06: Naoki Osawa T01

Kanazawa Institute of Technology, Japan.

Comparison of surface charge density distribution generated by diffuse and filamentary barrier discharges in atmospheric pressure air

#### 17:20 - 17:40 Contributed CO7: Thomas Orrière TO1

Université de Poitiers, France.

3D Topography of a liquid surface interacting with an Argon plasma jet

#### 17:40 - 18:00 Contributed C08: Kazuki Watanabe T01

Kanazawa Institute of Technology, Japan.

Effect of surface resistivity on surface charge density and diffuse dielectric barrier discharge in atmospheric pressure air

**18:00 - 18:30** Free time

#### 18:30 - 20:00 Dinner

Zaal 2, afterwards, the hotel bar (De Verloren Zoon in the cellar) is open.

#### Tue, Aug 23

#### 08:00 - 09:00 Breakfast

In the large dining room ('Grote Eetzaal')

#### Session chair: Indrek Jõgi

#### 09:00 - 09:50 Invited I02: Koichi Sasaki T02

Hokkaido University, Japan.

Detection of negative ions in dc glow and streamer discharges produced in ambient air

#### 09:50 - 10:10 Contributed CO9: Vlasta Štěpánová TO7

Masaryk University, Czech Republic.

Adhesion improvement of LLDPE/PA tubular foil used as sausage casing after a very short atmospheric-pressure roll-to-roll plasma treatment

#### 10:10 - 10:30 Contributed C10: Julia Mrotzek T07

HAWK, Germany.

OES as tool for characterization of an APPI for thin film deposition

#### 10:30 - 11:00 Coffee break

Foyer + terrace

#### Session chair: Naoki Osawa

#### 11:00 - 11:20 Contributed C11: Kristian Wende T08

Leibniz Institute for Plasma Science and Technology, Germany.

Biomolecule oxidation by gas phase species – the role of the gas-liquid interphase

#### 11:20 - 11:40 Contributed C12: Mark Kushner T08

University of Michigan, United States of America.

Atmospheric pressure plasma treatment of organics in liquid: extending reaction mechanisms into solution

#### 11:40 - 12:00 Contributed C13: Jan Cech T06

Masaryk University, Faculty of Science, Czech Republic.

CaviPlasma – The new tool for energy-efficient large-scale treatment of liquids

#### 12:00 - 12:20 Contributed C14: Ravi Patel T06

Eindhoven University of Technology, Netherlands.

Filamentary DBD plasma for ignition stabilized combustion

#### 12:30 - 14:00 Lunch

Foyer + terrace

#### Session chair: Behnaz Bagheri

#### 14:00 - 14:20 Contributed C15: Perla Trad T06

Laboratoire de Physique des Gaz et des Plasmas, France.

Influence of the applied HV-pulse rise time on the removal efficiency of n-hexane in a DBD

#### 14:20 - 14:40 Contributed C16: Jeroen van Oorschot T06

Eindhoven University of Technology, Netherlands.

Real-Time In-Situ Characterization of Plasma Activated Water

#### **14:40 - 21:40** Excursion + banquet

The excursion will be to the Zonneberg caves near Maastricht, followed by a boat-tour with dinner on the Maas (Meuse) river. The caves have a temperature of about 11 degrees all year round. Keep this in mind with regard to your clothes and put on sturdy shoes! The caves are basically accessible to everyone. However, the walk from the meeting point to the entrance is a difficult climb.

#### Wed, Aug 24

#### 08:00 - 09:00 Breakfast

In the large dining room ('Grote Eetzaal')

#### Session chair: Fumiyoshi Tochikubo

#### 09:00 - 09:50 Invited I04: Deborah O'Connell T01

Dublin City University, Ireland.

Controlling vibrational kinetics through energy input into repetitively pulsed atmospheric pressure nitrogen discharges

#### 09:50 - 10:10 Contributed C17: Alex Destrieux T02

Laval University, Canada.

Toward a better understanding of the electrical properties in a dielectric barrier discharge during long-time operation

#### 10:10 - 10:30 Contributed C18: Anne Limburg T02

Eindhoven University of Technology, Netherlands.

Influence of probing laser beam and electric field properties in E-FISH measurements

#### 10:30 - 11:00 Coffee break

Foyer + terrace

#### Session chair: Ute Ebert

#### 11:00 - 11:20 Contributed C19: David Prokop T02

Masaryk University, Czech Republic.

Spatiotemporal spectroscopic characterization of nanosecond pulsed volume barrier discharge in argon

#### 11:20 - 11:40 Contributed C20: Siebe Dijcks T02

Eindhoven University of Technology, Netherlands.

Corona Imaging

#### 11:40 - 12:20 Organ concert

An organ concert by the TU/e organist, Jan Verschuren in the Rolduc Abbey Church (Abdijkerk).

#### 12:30 - 14:00 Lunch

Foyer + terrace

#### Session chair: Tom Huiskamp

#### 14:00 - 14:50 Invited I03: Luc Stafford T07

Université de Montreal, Canada.

Advanced surface engineering of cellulose nanomaterials using dielectric barrier discharges at atmospheric pressure

#### 14:50 - 15:10 Contributed C21: Markus Becker T02

Leibniz Institute for Plasma Science and Technology (INP), Germany.

Combining modelling and experiment for advanced plasma diagnostics

#### 15:10 - 15:30 Contributed C22: Mohammad Hasani T02

Eindhoven University of Technology, Netherlands.

Charge detection of plasma exposed surfaces using quantum dots photoluminescence

#### 15:30 - 16:00 Coffee break

Foyer + terrace

#### Session chair: Gerrit Kroesen

#### 16:00 - 16:20 Contributed C23: Hans Höft T02

INP Greifswald, Germany.

Impact of dielectric-covered electrode proximity on streamer propagation in pulsed-driven dielectric barrier discharges

#### **16:20 - 16:40** Contributed C24: **Hani Francisco** T02

Centrum Wiskunde & Informatica, Netherlands.

The propagation and chemistry of positive streamers in lightning and sprite discharges at different air densities

#### 16:40 - 17:00 Contributed C25: Thijs van der Gaag T02

Tokyo Institute of Technology, Japan.

EEDF measurement of cold atmospheric-pressure plasma by OES

#### 17:00 - 17:20 Contributed C26: Davide Del Cont-Bernard T02

Maastricht University, Netherlands.

Development of the EFISH technique for electric field measurements in nanosecond repetitively pulsed discharges

#### 17:20 - 17:40 Contributed C27: Francisco Pontiga T02

Universidad de Sevilla, Spain.

Distribution of neutral species in a corona discharge: effect of the electrohydrodynamic gas motion

#### 17:40 - 18:00 Contributed C28: Lucia Kuthanová T09

Masaryk University, Czech Republic.

Liquid displacement by atmospheric pressure plasma in microgap

**18:00 - 18:30** Free time

#### 18:30 - 20:00 Dinner

Zaal 2, afterwards, the hotel bar (De Verloren Zoon in the cellar) is open.

19:30 - 22:00 ISC-meeting

#### Thu, Aug 25

#### 08:00 - 09:00 Breakfast

In the large dining room ('Grote Eetzaal')

#### Session chair: TBD

#### 09:00 - 09:50 Invited I05: Xin Pei Lu T01

HuaZhong University of Science and Technology, China.

Atmospheric Pressure Plasma

#### 09:50 - 10:10 Contributed C29: Yury Gorbanev T03

University of Antwerp, Belgium.

Pulsed plasma jet for nitrogen fixation: Fundamentals and prospective technologies

#### 10:10 - 10:30 Contributed C30: Ursel Fantz T03

Max-Planck-Institut fuer Plasmaphysik, Germany.

Enhancement of  $CO_2$  conversion at atmospheric pressure by influencing the gas quenching in the effluent of a microwave plasma torch

#### 10:30 - 11:00 Coffee break

Foyer + terrace

#### Session chair: Tomáš Hoder

#### 11:00 - 11:20 Contributed C31: Mostafa Hassan T03

Faculty of Mathematics, Physics and Informatics, Comenius University, Slovakia. The role of gas-water interface size on solvation of gaseous species to water

### 11:20 - 11:40 Contributed C32: David Sawtell T03

Manchester Metropolitan University, United Kingdom.

Insights into nitrogen fixation using microfluidic plasma devices

#### 11:40 - 12:00 Contributed C33: Chiel Ton T04

Eindhoven University of Technology, Netherlands.

Transient plasma for air purification using 400 kV pulses

#### **12:00 - 12:20** Closing ceremony

#### 12:30 - 14:00 Lunch

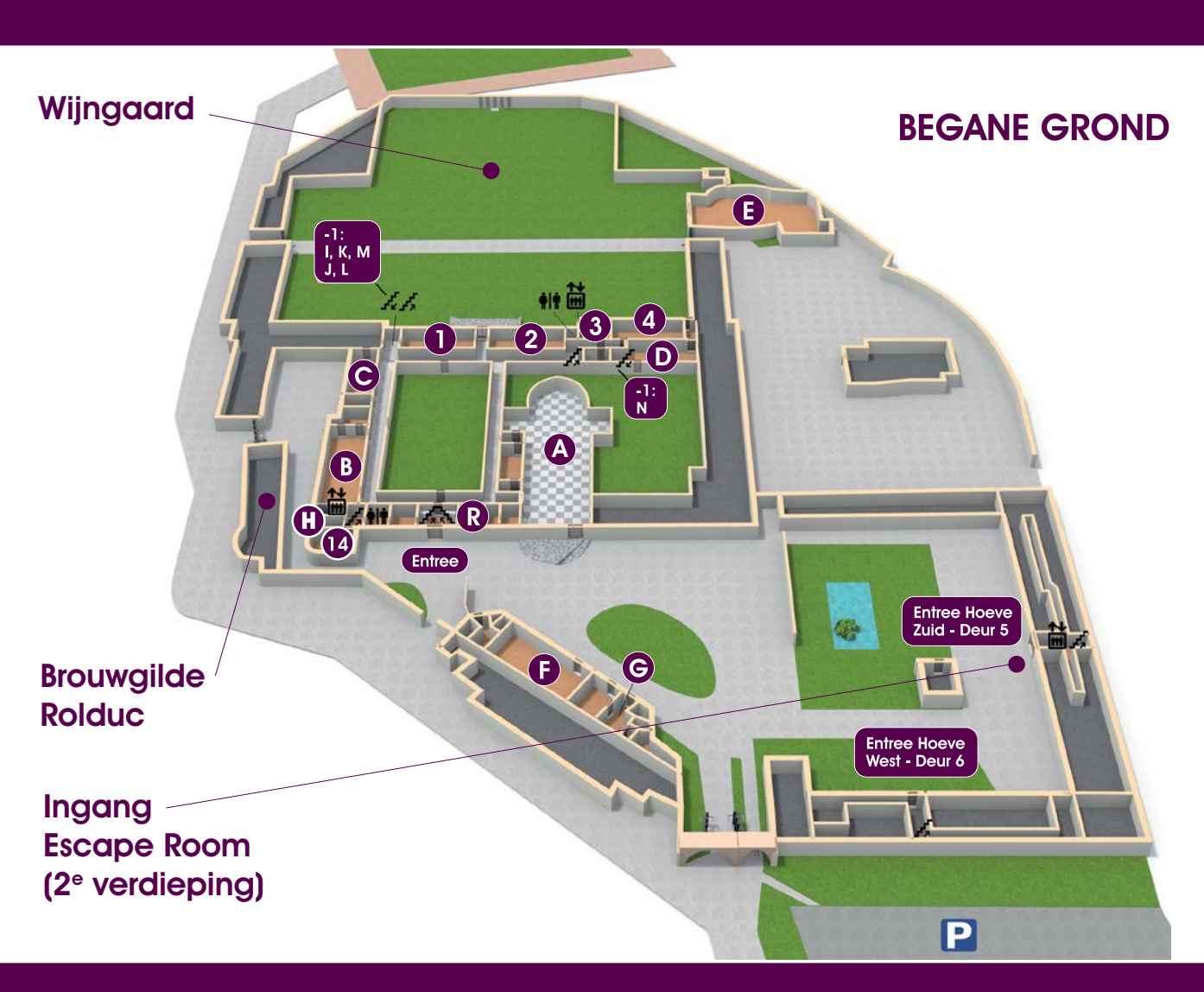
Foyer + terrace

#### **14:00 - 15:30** Bus to Eindhoven (optional)

If you would like to join the lab tour and have not registered yet, then please do this as soon as possible.

#### 15:30 - 17:30 Labtour Eindhoven (optional)





## **BEGANE GROND**

- A Abdijkerk
- **B** Grote Eetzaal
- C Brasserie De Kanunnik
- D Foyer
- E Aula Major (buiten)
- Aula Minor (buiten)
- G Fietsenstalling (buiten)
- H Bagageruimte
- Receptie R

### **BEGANE GROND**

- Zaal 1
- 2 Zaal 2
- Zaal 3
- Zaal 4
- 14 Zaal 14

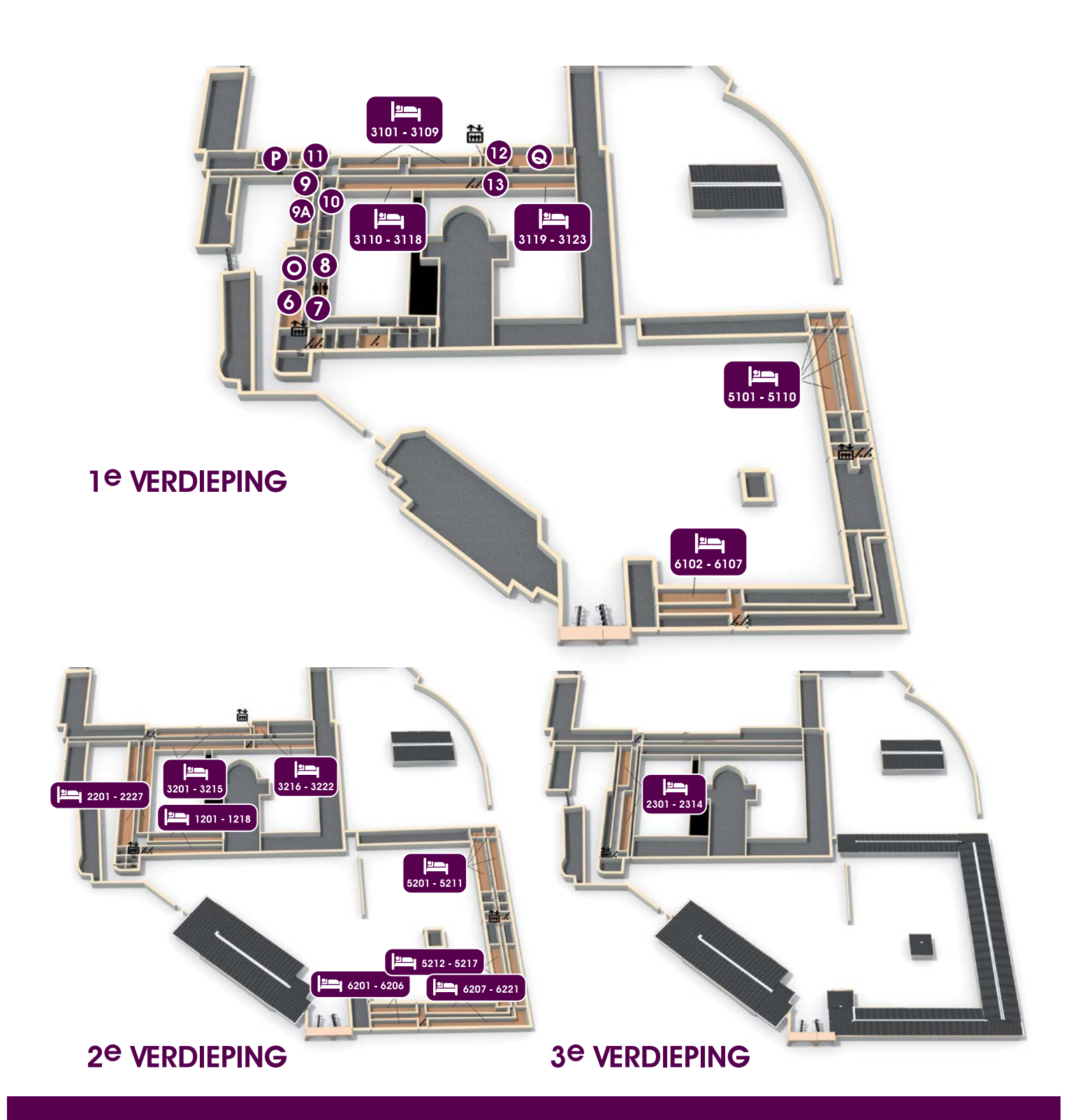
## KELDER (-1)

- De Verloren Zoon
- Zwaantie
- Rookruimte
- Kana 1
- M Kana 2
- Boerenkelder

www.rolduc.com **f** 







# 1e VERDIEPING

0 Kleine EetzaalP Bisschopszaal

**Q** Rococo-bibliotheek

# 1e VERDIEPING

6 Zaal 6

7 Zaal 7

8 Zaal 8

9 Zaal 9

9A Zaal 9A

10 Zaal 10

11 Zaal 11<sup>8</sup>

12 Zaal 12

13 Zaal 13

# المال

### 1<sup>e</sup> VERDIEPING

3101 - 3123 (hoofdgebouw)

5101 - 5110 (Hoeve)

6102 - 6107 (Hoeve)

#### 2<sup>e</sup> VERDIEPING

1201 - 1218 (hoofdgebouw)

2201 - 2227 (hoofdgebouw)

3201 - 3222 (hoofdgebouw)

5201 - 5217 (Hoeve)

6201 - 6221 (Hoeve)

### 3<sup>e</sup> VERDIEPING

2301 - 2314 (hoofdgebouw)



Lift



#### 6 Abstracts

#### Ulrich Kogelschatz Lecture - Françoise Massines

Fundamental problems of high pressure discharges

# PHYSICS OF DIFFUSE DBDs AND ON LINE THIN FILM TREATMENT: HISTORY, RECENT DEVELOPMENTS AND NEW CHALLENGES

Françoise Massines <sup>1</sup>CNRS PROMES, Rambla de la Thermodynamique, 66100 Perpignan, France

E-mail: françoise.massines@promes.cnrs.fr

The use of dielectric barrier discharges, DBDs, for roll to roll surface treatment is an old story still relevant. It started with corona treatment more than 50 years ago, continues with thin film coatings of higher and higher quality and now nanocomposite thin films having well controlled multifunctional properties. Such evolution is related to new discharge modes, new discharge physics and new ways of thinking thin film processing to take advantages of the different DBDs. The aim of this talk is to illustrate the very large possibilities offered by sinusoidal voltages applied to parallel electrodes to answer surface treatment challenges... or how to have fun with plasma physics while seeking solutions to new applications.

The discharges involved in corona treatment formed a linear plasma, produced in a millimetric gap between a linear high-voltage electrode of rather small radius and a counter electrode which is usually a cylinder or a plate. The smaller is the radius of the electrode, the lower is the breakdown voltage of the corona discharge. However, to increase the throughput of the process, the voltage is increased to such a point that the discharge is no more a corona discharge as streamers connect the two electrodes. The transition to arc is avoided thanks to a solid dielectric in the discharge current path which automatically decreases the gas voltage just after the gas breakdown. Thus the discharge is a DBD<sup>1,2</sup>. In such reactors, the substrate width determines the electrodes length; meters are fully possible. Substrate displacement allows treating kilometer square of substrates like polymer films, fabrics, metal sheets, glass plates... In the industrial system, the discharge is a filamentary DBD. Until the end of the 90s, the application was only surface activation. Then, DBDs free of microdischarges were pointed out by S. Okazaki<sup>3</sup>. These discharges appeared relevant to atmospheric pressure plasma enhanced thin film deposition (AP-PECVD). Such DBDs are obtained in well-defined conditions allowing a pre-ionization of the gas and a rather low increase or level of the ionization.<sup>4</sup> Different DBDs are considered for AP-PECVD: APGD (atmospheric pressure glow discharge)<sup>5</sup>, APTD (atmospheric pressure Townsend discharges) first achieved in nitrogen by Massines team<sup>6</sup>, Glow like DBDs achieved by Van de Sanden team<sup>7</sup>, RF-DBD (radio frequency)<sup>8</sup>...

All of them are able to produce dense, well controlled, thin films. However, a key point for AP-PECVD development is the growth rate of the thin film. The growth rate is limited by the power of the discharge and the quantity of precursors which can be injected in the gas without streamer formation. As a DBD is a pulsed discharge the main idea to increase the power is to decrease the time off between two discharges. The other advantage of this approach is to increase the memory effect from one discharge to the following one and thus decrease the influence of the chemical composition of the gas on the quenching of energetic species during time off. This approach motivated the development of current power supply for Townsend DBD in nitrogen or air and Naudé *et al.* <sup>9</sup> reach the power of 100 W/cm<sup>2</sup>. For glow DBD the solution to increase the power and the stability of the discharge is to increase the sinusoidal voltage frequency. A first optimum was found around 200 kHz which is still in the range where ions mobility is high

enough to allow secondary emission of electrons. Around this frequency, Van de Sanden et al. <sup>10</sup> get a high-power glow-like DBD free of microdischarge. For higher frequencies, the ions trapping in the gas bulk transform the glow DBD in a Townsend-like DBD <sup>11</sup>. Since 1 MHz the ohmic or alpha RF mode can be observed <sup>11</sup>. It is characterized by a drastic decrease in the gas breakdown voltage, an increase of the power and the occurrence of a continuum emission. As it will be shown, the physics of these different DBDs free of microdischarge are fully different. This is illustrated by the values of the maximum electron density ranging from 10<sup>8</sup> to 10<sup>12</sup> cm<sup>-3</sup> for a maximum metastable density from 10<sup>13</sup> to 10<sup>9</sup> cm<sup>-3</sup>.

Well-controlled multifunctional coating is now the challenge of AP-PECVD. These thin films are composed of nanoparticles (NPs) of a material included in a matrix of another material. They combine the properties of the two materials, like TiO<sub>2</sub> NPs for antiUV in a SiO<sub>2</sub> barrier layer <sup>12</sup>. They can also produce a hierarchical multiscale surface texture <sup>13</sup> that is super -hydrophobic or –hydrophilic. They can be synthesized on very different substrates including foam <sup>13</sup> or wood <sup>12</sup>. Such materials are obtained by mixing gas, liquid and solid precursors able to form particles in the gas phase <sup>14</sup> or from an aerosol of a stable dispersion of NPs in a thin film precursor12,<sup>13,15</sup>. Whatever the precursor the plasma should be adapted to control the gas or liquid polymerization and the NPs transport to the surface. From there came the idea of coupling different plasma frequencies during the same process. This coupling can be done at different time scales of the process: ns (time scale of the discharge development), µs (time scale of the ions transport), ms (time scale of NPs transport and chemistry in the gas and at the surface), tens of ms (time scale of the gas residence time in the plasma), seconds or minutes (time scale of thin film growth).

The idea of coupling different frequencies leads to dual frequency discharges which generate new DBDs modes. Such dual frequency DBD are easy to set up as each electrode of a DBD can be powered by a different voltage. When the frequency of the two voltages are close to each other, the power and the stability of the discharge are increased <sup>16</sup>. When the frequencies of the two voltages are very different, like low frequencies (LF) (1 to 200 kHz) applied on a  $\alpha$ -RF discharge, the behavior largely depends on the low frequency voltage amplitude <sup>17</sup>. For low values, the discharge tends to extinguish because of the decrease of the ion density in the gas bulk. For higher values of the low frequency amplitude, the secondary electrons generate a  $\gamma$ -RF mode when the two voltages have the same polarity and an amplitude large enough. Thus, during one LF cycle, the discharge alternates from  $\alpha$  to  $\gamma$  modes depending on the LF amplitude <sup>17</sup>. In Ar, the contribution of photoionization is also enhanced by the excimer formation. The  $\gamma$  mode increases the ion bombardment of the cathode and thus densifies the thin film <sup>16</sup>.

Work is still in progress...

```
<sup>1</sup> U. Kogelschatz, Plas. Chem. & Plas. Proc. 2003, 23 (1) 1
<sup>2</sup> R. Brandenburg, Plasma Sources Sc.&Tech. 2017, 26 (5) 053001
 Kanazawa et al., J. Phys. D - Ap. Phys. 1988, 21 (5) 838
<sup>4</sup> F. Massines et al., Plasma Proc. & Polym. 2012, 9 (11-12) 1041
<sup>5</sup> T. Yokoyama et al., J. Phys. D - Ap. Phys. 1990, 23 (3) 374
<sup>6</sup> N. Gherardi et al., J. of Phys. D - Ap. Phys. 2000, 33 (19) 104
 S. Starostine et al., Plasma Proc. & Polym. 2007, 4 (440)
<sup>8</sup> R. Bazinette et al., Plasma Proc. & Polym, 2016, 13 (10) 1015
<sup>9</sup> X. Bonin Eur. Phys. J. Appl. Phys. 2013 (64) 10901
<sup>10</sup> S. Starostine et al., Plasma Sources Sc.&Tech. 2009, 18 (4)
<sup>11</sup> R. Bazinette et al., Plasma Sources Sc. & Tech. 2014, 23 035008 / J. S. Boisvert et al., J. of Phys. D - Ap. Phys. 2016, 49 (32)
<sup>12</sup> J. Profili et al., J. Appl. Phys. 2016, 120 (5) / J. Profili et al., Surf.&Coat. Tech. 2017, 309 (729)
<sup>13</sup> F. Fanelli et al., Langmuir 2014, 30 (3) 857 / F. Fanelli et al., Plasma Proc. & Polym. 2016, 13 (4) 470
<sup>14</sup> E. Nadal et al., Nanotechnology, 2021, 32 (17)
<sup>15</sup> P. Brunet et al., Langmuir 2018, 34, (5) 1865
<sup>16</sup> R. Bazinette et al., Plasma Sources Sc. & Tech. 2020, 29 (9)
<sup>17</sup> R. Magnan et al., Plasma Sources Sc. & Tech. 2020, 29 (3) / R. Magnan et al., Plasma Sources Sc. & Tech. 2021, 30 (1)
```

#### Invited IO1 - Judith Golda

Depollution and environmental applications

# COLD ATMOSPHERIC PRESSURE PLASMAS FOR PLASMA CATALYTIC APPLICATIONS: CHARACTERISTICS, CONSTRAINTS AND CHALLENGES

Judith Golda<sup>1</sup>, David Steuer<sup>1</sup>, Steffen Schüttler<sup>1</sup>, Sascha Chur<sup>1</sup>, Emanuel Jeß<sup>1</sup>, Henrik van Impel<sup>1</sup>, Robin Labenski<sup>1</sup>, Volker Schulz-von der Gathen<sup>2</sup>, Marc Böke<sup>2</sup>

<sup>1</sup>Plasma Interface Physics, Ruhr-University Bochum, Germany

<sup>2</sup>Experimental Physics II, Ruhr-University Bochum, Germany

E-mail: judith.golda@rub.de

Atmospheric pressure plasmas provide the platform for a multitude of applications ranging from plasma chemistry, surface modification, thin films, and plasma medicine to plasma catalysis. At the heart of these applications is the distinct non-equilibrium character of atmospheric pressure plasmas and their interaction with surfaces. For example, heat-sensitive materials, such as biological tissue in plasma medicine, require a low gas temperature whereas the electron temperature and density have to be high in order to efficiently generate relevant reactive species interacting with the treated substrate. The complexity of this interaction makes the understanding rather challenging and requires dedicated experimental setups, diagnostics, and simulations.

In this talk, we will introduce three different examples of atmospheric pressure plasmas used for catalytic applications. We will show Conversion of volatile organic compounds (VOCs) in a surface dielectric barrier discharge, chemical and structural changes of surfaces for electrolysis using laser and plasma modification as well as hydrogen peroxide production for biocatalysis using a plasma jet in contact with liquids. We will show measurements of electrical power, absolute species densities, and conversion efficiencies and highlight current constraints and challenges.

This research is funded within CRC 1316 in projects A6, B2, and B11.

#### Invited IO2 - Koichi Sasaki

Modelling and diagnostics

# DETECTION OF NEGATIVE IONS IN DC GLOW AND STREAMER DISCHARGES PRODUCED IN AMBIENT AIR

#### Koichi Sasaki

Division of Applied Quantum Science and Engineering, Hokkaido University, Kita-13, Nishi-8, Kita-ku, Sapporo 060-8628, Japan

E-mail: sasaki@qe.eng.hokudai.ac.jp

It is quite sure that atmospheric-pressure plasmas produced in ambient air contain significant amounts of negative ions. This is because oxygen and water vapor are typical electronegative gases. In contrast to the importance, experimental investigations of negative ions in atmospheric-pressure plasmas are seriously insufficient to date except some works employing mass spectrometry. A problem of mass spectrometry is the difficulty in sampling negative ions from active plasma zone. In this talk, we will report two diagnostic works which are based on laser photdetachment.

The first work was carried out using a dc glow discharge [1]. A miniature helium flow was applied from a nozzle electrode toward a planar electrode in ambient air. The planar electrode was replaced with the surface of NaCl solution in some experiments. By connecting a dc power supply between the two electrodes, we obtained a glow discharge along the helium flow. A pulsed laser beam, which was yielded from tunable lasers (a dye laser and an optical parametric oscillator), was injected into the discharge from the radial direction. As a result, we observed the pulsed increase in the discharge current at the timing of the pulsed laser injection. It was confirmed that the amplitude of the pulsed increase in the discharge current was proportional to the amount of electrons produced from negative ions by photodetachment. We scanned the laser wavelength around the threshold photon energy for photodetachment to identify the major negative ion species. According to the experimental results, the dominant negative ion was O in the active glow discharge, and the fractional abundance of O<sub>2</sub> is lower than that of O in the fractional abundance of H was negligible. OH was another major negative ion when the NaCl solution worked as the cathode of the dc discharge.

The second experiment was carried out using a streamer discharge in air. The streamer discharge was produced by applying a pulsed voltage of 15 kV between needle and planar electrodes. The duration of the high voltage was approximately 40 ns. The distance between the electrodes was 7.5 mm. We measured the temporal variation of the negative ion density by cavity ringdown absorption spectroscopy (CRDS). The discharge was placed inside of an optical cavity which was composed of two concave mirrors with high reflectivities. A pulsed laser beam at a wavelength of 777 nm was injected into the cavity, and we recorded the temporal variation of the intensity of the laser pulse transmitted through the cavity. The laser beam at 777 nm can work for photodetachment of O-, O2-, and H-. Since a photon is lost by a photodetachment reaction, we can deduce the negative ion density from the weak optical absorption detected by CRDS. The negative ion density was lower than the detection limit until

 $0.6~\mu s$  after the initiation of the discharge. The negative ion density began the increase at  $0.6~\mu s$ , and it arrived at the peak at  $2~\mu s$  after the initiation of the discharge. The maximum negative ion density was approximately  $2x10^{13}~cm^{-3}$ . After the peak, we observed the decrease in the negative ion density until 8-9  $\mu s$ . The decrease was slower than the rate that is expected by mutual neutralization between positive and negative ions. We observed the second maximum of the negative ion density at 9-12  $\mu s$ . This is an unexpected result, and we do not have reasonable explanation for the physics of the second maximum.

[1] K. Sasaki, R. Hosoda and N. Shirai, Plasma Sources Sci. Technol. 29, 085012 (2020).

#### Invited I03 - Luc Stafford

Surface processing and technology (cleaning, coating, etching and modification, equipment)

# Advanced surface engineering of cellulose nanomaterials using dielectric barrier discharges at atmospheric pressure

#### Luc Stafford

<sup>1</sup>Chaire de recherche du Canada en physique des plasmas hautement réactifs (PPHARE), Département de physique, Université de Montréal, Montréal, Québec, Canada

E-mail: luc.stafford@umontreal.ca

Wood components have been used as a building material for centuries. In light of the growing concern over the environmental impact of human industrial activity, woody biomass has taken on a new importance worldwide. The main advantages of this widely distributed and renewable resource lie in its versatility, strength-to-weight characteristics, ease of processing, aesthetics, and its sustainability as a green-material. Its bio-polymeric structure, however, renders it susceptible to degradation due to moisture, water, microorganisms, insects, fire, and ultraviolet radiation. Over the last decade, we have shown that dielectric barrier discharges at atmospheric pressure operated in either glow or Townsend homogeneous mode represent a very promising approach for tailoring the surface properties of wood-based materials for both improvement of existing protection systems [1,2] or as standalone treatment for the growth of (multi)functional coatings [3–5]. Such treatments bourght additional plasma processing features, including self-organized light emission patterns along the anisotropic materials [6] and modification of discharge regimes and plasma fundamental properties due to substrate outgassing [7].

More recently, inspired by the development of advanced methods for deconstructing the delignified wood tracheids (fibres) into micro and nano fibres on an industrial scale, we have explored the plasma-assisted functionalization of highly porous microfibrillated cellulose (MFC) films and foams using plane-to-plane dielectric barrier discharges (DBDs) operated in presence of organosilicon precursors. In the case of films, plasma-deposited coating followed the roughness of the porous cellulosic substrate. While spatially homogeneous coatings were obtained on silicon substrates, significant variations of the coatings' thickness, organicity, and water contact angle were observed along the gas flow lines. In addition, significant in-depth penetration of plasma-generated species was observed [8,9], a feature that was linked to the porosity level of the woody biomass films.

In the case of MFC foams taking up the entirety of the gas gap of the DBD cell, discharge ignition and propagation mostly occurs through the foam from one electrode to the other (volume discharge). In addition, over the range of experimental conditions investigated, filamentary discharges were generated, and burn-like damage was produced. This resulted in highly inhomogeneous organosilicon deposits having both hydrophilic and hydrophobic domains. MFC foams taking up only a portion of the gas gap volume generated a homogeneous discharge and induced cellulose defibrillation. They generated effective hydrophobic surfaces on both the top and bottom of the foams. Oleophilicity measurements were also carried out, which support the possibility of an effective separation of oily wastewater using a green and renewable material [10,11].

In this presentation, the scientific and technological accomplishments associated with advanced surface engineering of cellulose nanomaterials in plane-to-plane dielectric barrier discharges are reviewed. Novel applications of such atmospheric pressure plasma processes toward more sustainable aqueous Li-ion batteries are also discussed.

- [1] Prégent J, Vandsburger L, Blanchard V, Blanchet P, Riedl B, Sarkissian A and Stafford L 2015 Determination of active species in the modification of hardwood samples in the flowing afterglow of N2 dielectric barrier discharges open to ambient air *Cellulose* 22 811–27
- [2] Prégent J, Vandsburger L, Blanchard V, Blanchet P, Riedl B, Sarkissian A and Stafford L 2015 Modification of hardwood samples in the flowing afterglow of N2–O2 dielectric barrier discharges open to ambient air *Cellulose* 22 3397–408
- [3] Levasseur O, Stafford L, Gherardi N, Naudé N, Blanchard V, Blanchet P, Riedl B and Sarkissian A 2012 Deposition of Hydrophobic Functional Groups on Wood Surfaces Using Atmospheric-Pressure Dielectric Barrier Discharge in Helium-Hexamethyldisiloxane Gas Mixtures *Plasma Process. Polym.* **9** 1168–75
- [4] Levasseur O, Vlad M, Profili J, Gherardi N, Sarkissian A and Stafford L 2017 Deposition of fluorocarbon groups on wood surfaces using the jet of an atmospheric-pressure dielectric barrier discharge *Wood Sci. Technol.* **51** 1339–52
- [5] Profili J, Levasseur O, Koronai A, Stafford L and Gherardi N 2017 Deposition of nanocomposite coatings on wood using cold discharges at atmospheric pressure *Surf. Coatings Technol.* **309** 729–37
- [6] Levasseur O, Profili J, Gangwar R K, Naudé N, Clergereaux R, Gherardi N and Stafford L 2014 Experimental and modelling study of organization phenomena in dielectric barrier discharges with structurally inhomogeneous wood substrates *Plasma Sources Sci. Technol.* **23** 054006
- [7] Levasseur O, Kumar Gangwar R, Profili J, Naudé N, Gherardi N and Stafford L 2017 Influence of substrate outgassing on the plasma properties during wood treatment in He dielectric barrier discharges at atmospheric pressure *Plasma Process. Polym.* **14** 1600172
- [8] Babaei S, Profili J, Asadollahi S, Sarkassian A, Dorris A, Beck S and Stafford L 2020 Analysis of transport phenomena during plasma deposition of hydrophobic coatings on porous cellulosic substrates in plane-to-plane dielectric barrier discharges at atmospheric pressure *Plasma Process. Polym.* 17 2000091
- [9] Profili J, Asadollahi S, Vinchon P, Dorris A, Beck S, Sarkassian A and Stafford L 2020 Recent progress on organosilicon coatings deposited on bleached unrefined Kraft paper by non-thermal plasma process at atmospheric pressure *Prog. Org. Coatings* 147 105865
- [10] Meunier L-F, Profili J, Babaei S, Asadollahi S, Sarkissian A, Dorris A, Beck S, Naudé N and Stafford L 2021 Characterization of non-thermal dielectric barrier discharges at atmospheric pressure in presence of microfibrillated cellulosic foams *Plasma Sources Sci. Technol.* 30 095019
- [11] Meunier L, Profili J, Babaei S, Asadollahi S, Sarkissian A, Dorris A, Beck S, Naudé N and Stafford L 2021 Modification of microfibrillated cellulosic foams in a dielectric barrier discharge at atmospheric pressure *Plasma Process. Polym.* **18** 2000158

#### Invited I04 - Deborah O'Connell

Fundamental problems of high pressure discharges

# Controlling vibrational kinetics through energy input into repetitively pulsed atmospheric pressure nitrogen discharges.

Helen L. Davies<sup>1</sup>, Andrew R. Gibson<sup>2</sup>, Marjan van der Woude<sup>3</sup>, Vasco Guerra<sup>4</sup>, Timo Gans<sup>5</sup>, <u>Deborah</u> O'Connell<sup>5</sup>

<sup>1</sup>York Plasma Institute, Department of Physics, University of York, UK
<sup>2</sup>Institute of Electrical Engineering and Plasma Technology, Ruhr-University Bochum,
Germany

<sup>3</sup>York Biomedical Research Institute and Hull York Medical School, University of York, Heslington, YO10 5DD

<sup>4</sup>Instituto de Plasmas e Fusão Nuclear, Instituto Superior Técnico, Universidade de Lisboa, Portugal

<sup>5</sup>School of Physical Sciences & National Centre for Plasma Science and Technology, Dublin City University, Ireland

Nitrogen-based, atmospheric pressure plasma sources are of importance for many applications. Particularly, repetitively pulsed sources are of interest and understanding the chemical kinetics that control the production of reactive species is vital. The practical importance of being able to control the population of high level vibrationally excited nitrogen species is seen when considering the large amounts of energy they can carry. Nitrogen can exist in many electronically and vibrationally excited states. In nitrogen, the electron impact cross sections for the excitation of vibrational states from the ground state are large. This means that low lying vibrationally excited states are significantly populated by electron-impact excitation, and their production is a major energy loss mechanism for electrons. On top of this, due to the strong nitrogen bond and associated high dissociation energy of the nitrogen molecule, vibrationally excited states of nitrogen can carry significant energies. Vibrationally excited nitrogen molecules can actively participate in the plasma chemistry by influencing molecular metastable densities that lie at similar energy levels.

Here, using a 0-dimensional global plasma chemistry model, the kinetics of vibrationally excited nitrogen species are investigated. Simulations predict that the kinetics of vibrationally excited states undergo a switch in behaviour as the energy input to the discharge is varied, either by altering the peak pulse power or the pulse repetition frequency. Above a certain energy input threshold, it appears that the control of the vibrationally excited state concentrations and vibrational distribution function (VDF) shape is controlled by vibration-vibration (V-V) and vibration-translation (V-T) energy transfer processes. Prior to the threshold being reached, the VDF remains underpopulated and the concentrations of vibrationally excited states are controlled by electron-impact processes. It is also shown, through pathways analysis, that energy in vibrationally excited species can be transferred to electronically excited states, which then results in an increased rate of Penning ionisation and an increased average electron density. Overall, this study investigates the potential for delineating the processes by which electronically and vibrationally excited species are produced, thus highlighting potential routes by which plasma chemistry could be tailored. This could have significant implications for the design of LTPs for various applications in the fields of technological, agricultural and biomedical plasmas.

#### Invited I05 - XinPei Lu

Fundamental problems of high pressure discharges

#### **Atmospheric Pressure Plasma**

#### XinPei Lu

School of Electrical and Electronic Engineering, Huazhong University of Science and Technology, Wuhan, HuBei, 430074, P. R. China

E-mail: luxinpei@hotmail.com

In this talk, firstly, several plasma sources developed in our group will be presented, including a nobble gas plasma jet for root canal treatment and four air plasma jet devices [1, 2]. Secondly, several interesting physics phenomena of plasma jets are introduced, such as the repeatability of the plasma bullet, the plasma interruption behavior, the plasma transfer dielectric phenomenon, and the appearance of multiple plasma bullet per voltage pulse [2-4]. Thirdly, the state-of-the-art on the measurement of VUV emission of atmospheric pressure air plasma is discussed and our results by using differential pumping system as EUV window are presented [5]. Finally, several different configurations of nonequal gap distance DBD are described [6, 7].

- 1) Z. Li, J. Liu, X. Lu, A large atmospheric pressure nonequilibrium open space air plasma based on a rotating electrode, *Plasma Sources Sci. Technol.* 29, 045015 (2020)
- 2) X. Lu\*, G. Naidis, M. Laroussi, K. Ostrikov, Guided ionization waves: Theory and experiments. *Physics Reports*, 540,123-166 (2014)
- 3) X. Lu\*, and Kostya (Ken) Ostrikov, Guided ionization waves: The physics of repeatability, *Appl. Phys, Rev*, 5, 031102 (2018)
- 4) J. Liu, L. Nie, Y. Xian, X. Lu\*, The twisted behavior of a rotating electrode atmospheric-pressure argon plasma jet, *J. Phys. D: Appl. Phys.* 54, 185201 (2021)
- 5) F Liu, L Nie, X Lu, J Stephens and K Ostrikov, Atmospheric plasma VUV photon emission, *Plasma Sources Sci. Technol.* 29, 065001(2020)
- 6) Z. Li, S. Jin, Y. Xian, L. Nie, D. Liu, X. Lu\*, A non-equal gap distance dielectric barrier discharge: between a wedge-shaped and a plane-shaped electrode, *Plasma Sources Sci. Technol.* 30, 065026 (2021)
- 7) S. Jin, Z. Li, Y. Xian, L. Nie, X. Lu\*, A non-equal gap distance dielectric barrier discharge: Between cone-shape and cylinder-shape electrodes, *High Voltage*, 1-9 (2021)

#### Contributed CO1 - Elizabeth Mercer

Fundamental problems of high pressure discharges

# Effects of Post-Plasma Mixing in a CO<sub>2</sub> Microwave Plasma on Conversion and Energy Efficiency

<u>Elizabeth Mercer</u><sup>1</sup>, Senne Van Alphen<sup>1</sup>, Cas van Deursen<sup>2</sup>, Tim Righart<sup>3</sup>, Waldo Bongers<sup>2</sup>, Annemie Bogaerts<sup>1</sup>, Richard van de Sanden<sup>2</sup>, and Floran Peeters<sup>2</sup>.

<sup>1</sup>University of Antwerp, Universiteitsplein 1, 2610 Antwerpen, Belgium <sup>2</sup>Dutch Institute of Fundamental Energy Research, De Zaale 20, 5612 AJ Eindhoven, Netherlands

<sup>3</sup>Maastricht University, P.O. Box 616, 6200 MD Maastricht, Netherlands

E-mail: elizabeth.mercer@uantwerpen.be

Power-to-X (P2X) pathways seek to decarbonize our electricity by harnessing intermittent sustainable energy sources; developing and employing plasma reactors is one way to achieve a P2X route. Plasmolysis is a central research topic that will aid in realizing the closure of the human-induced carbon cycle. Presented is an investigation of the effects of implementing postplasma mixing in a vortex stabilized 2.45 GHz microwave plasma reactor for CO<sub>2</sub> dissociation. The study focuses on induced mixing with a converging-diverging nozzle (CDN), where the results showed promising advances in energy efficiency and conversion, exhibiting improved performance for high flow rates near-atmospheric pressure with the introduction of a CDN.

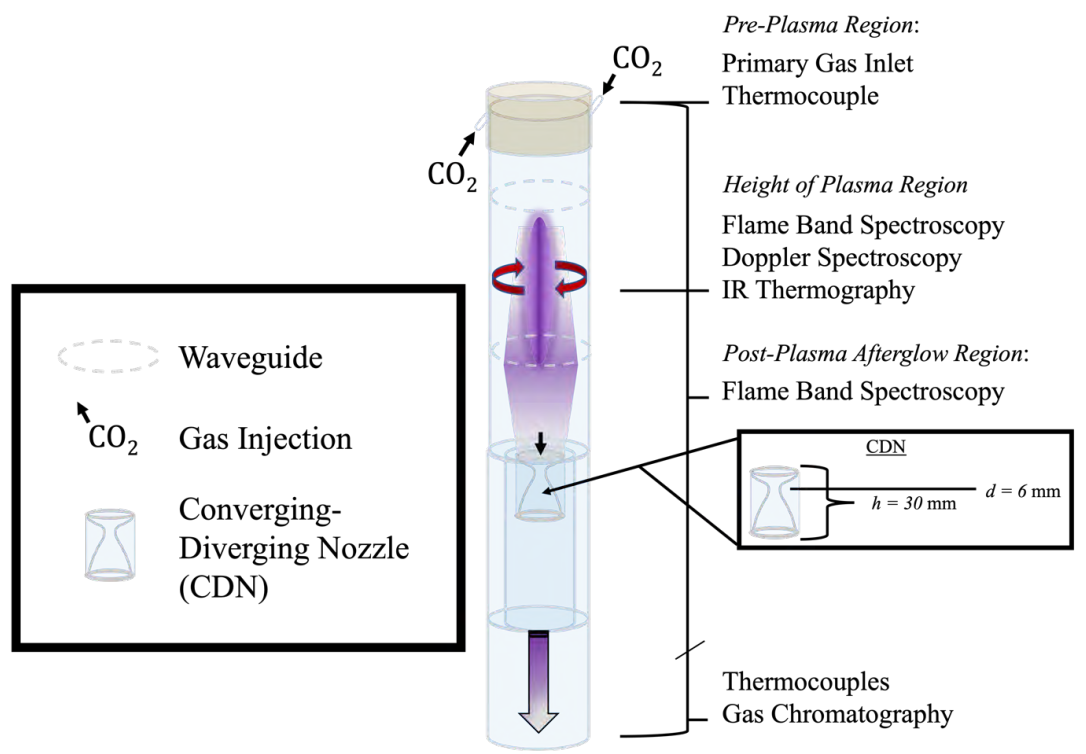


**Fig. 1**: Overview of experimental setup with list of diagnostic techniques used in this work. A diagram of the CDN is also shown to highlight the shape and dimension.

As shown in **Fig. 1**, several diagnostic techniques, including Doppler Broadening<sup>1</sup> and Flame Band Spectroscopy<sup>2</sup> were used to investigate the temperature profiles both within the plasma

region and in the post-plasma region, which allowed for a deeper investigation into how the changes in flow can affect the energy efficiency of conversion. Infrared Thermography was also employed to measure heat lost through the wall at the height of the plasma.

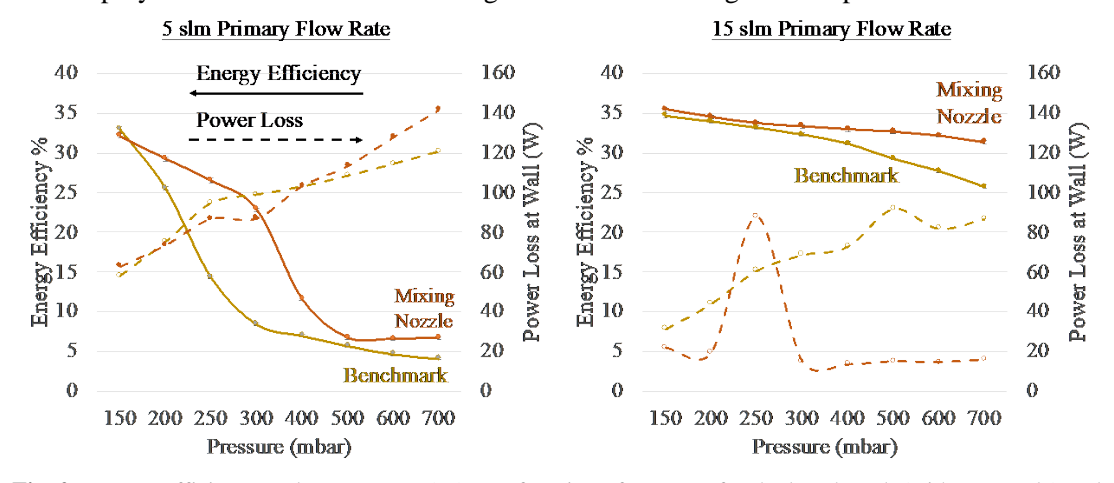


**Fig. 2**: Energy Efficiency and Power Loss (W) as a function of pressure for the benchmark (without nozzle) and with nozzle (CDN), where an increase in the energy efficiency is observed after introducing the CDN.

In **Fig. 2**, it is shown that the overall energy efficiency at higher flow rates and pressure with the CDN increased by 22% compared to benchmark conditions. Furthermore, higher flow rates without the nozzle showed a larger decay in the radially averaged temperature and a more considerable loss of heat to the environment within the plasma region compared to conditions with the CDN. The radial temperature and heat lost to the environment showed a significant effect on conversion.

A fully-coupled 3D COMSOL Multiphysics model was employed to further investigate the flow changes within the reactor upon introduction of the CDN. The model showed good agreement with the conversion and radial temperature profiles reported in the experimental results. The radial and axial temperature distribution within the reactor was related to conversion using the fully coupled model, outlining conditions for which performance can be optimized.

It was found that the increase in conversion relates to additional species transport from the area of conversion at higher flow rates. The CDN accelerates induced mixing, with the flow geometry preferentially circulating the input gas within the reactor, leading to a well-mixed flow regardless of where the flow originates. The results indicate that the addition of a CDN can be an effective method for achieving higher conversion and energy efficiency, if it is placed relative to the flow velocity as it relates to the flow rate and pressure of a given condition in order to maximize performance.

<sup>1.</sup> T. W. H. Righart, "Gas Temperatures and Residence Times in a Vortex Stabilized CO2 Microwave Plasma,"

<sup>2.</sup> G. J. C. Raposo *et al.*, "Flame Bands: CO + O chemiluminescence as a measure of gas temperature," *J. Phys. D. Appl. Phys.*, 2021.

#### Contributed CO2 - Roman Přibyl

Fundamental problems of high pressure discharges

## Alumina ceramic tapes doped by various dopants and their effect on properties of coplanar dielectric barrier discharge

Roman Přibyl<sup>1</sup>, Michal Pazderka<sup>1,2</sup>, Jakub Kelar<sup>1</sup>, Lucia Švandová<sup>1</sup>, Přemysl Šťastný<sup>3</sup>, Zlata Kelar Tučeková<sup>1</sup>, Martin Trunec<sup>3</sup>, Mirko Černák<sup>1</sup>

<sup>1</sup>Faculty of Science, Department of Physical Electronics, R&D Center for Plasma and Nanotechnology Surface Modifications, CEPLANT, Kotlářská 267/2, 611 37 Brno, Czech Republic

<sup>2</sup>Department of Theoretical Physics and Astrophysics, Faculty of Science, Masaryk University, Kotlářská 2, 611 37 Brno, Czech Republic <sup>3</sup>CEITEC BUT, Brno University of Technology, Purkyňova 123, 612 00 Brno, Czech Republic

E-mail: roman.pribyl@mail.muni.cz

This presentation is concluding current results of long-term research in development of new specialized ceramic substrates for Dielectric Barrier Discharges (DBDs), in our case coplanar DBDs.

We have developed unique method for capturing ignition and quenching voltage [1]. This device is using simple RC high-pass filter, which simply suppress high-voltage signal with frequencies around tens of kHz, whereas low-voltage signal with high-frequency is nearly unaffected. That means that this simple RC high-pass filter can be used for capturing ignition/quenching voltage, thanks to occurrence of high-frequency voltage drops during plasma ignition/quenching (voltage drops are caused due to non-zero impedance of high voltage source).

Effectivity of this approach was studied on commonly used ceramic tapes used in industry for Diffuse Coplanar Dielectric Barrier Discharge (DCSBD) [2]. After evaluation of data reproducibility on these types of ceramic tapes, new ceramic tapes with potentially better chemical and physical properties were made [3].

The innovational ceramics tapes were made by tape-casting method incorporating different dopants into aluminum oxide ( $Al_2O_3$ ) matrix. In our results, the most advantageous and interesting dopants were magnesium alumina oxide ( $MgAl_2O_4$ ) and chromium oxide ( $Cr_2O_3$ ). Examples of used ceramic tapes are shown in Figure 1.



Fig. 1: Photography of used ceramic tapes. From left: ELCERAM ceramic tape, 5 vol. % Cr<sub>2</sub>O<sub>3</sub> in alumina, 50 vol. % MgAl<sub>2</sub>O<sub>4</sub> in alumina.

Complex study of new ceramic tapes was also made by several other methods like AFM, SEM (EDX), XRD, XPS, permittivity measurement, noncontact electrostatic voltmeter, etc. The most usable and interesting results from these measurements are that doping by 1 vol. % Cr<sub>2</sub>O<sub>3</sub> into Al<sub>2</sub>O<sub>3</sub> matrix, which can decrease ignition voltage about 10 % for 0.3 mm gap between electrodes and about 3 % 1.0 mm gap between electrodes. Despite the fact that MgAl<sub>2</sub>O<sub>4</sub> doped ceramic tapes reported nearly similar or higher ignition voltage than commonly used alumina oxide, other interesting phenomena were observed.

One of the most interesting result/phenomena on these types of ceramic tapes is that on 20 vol. % MgAl<sub>2</sub>O<sub>4</sub> doped into Al<sub>2</sub>O<sub>3</sub>, the unpredictable type of discharge was observed. This type of discharge could be explained by sharp change in permittivity and loss-tangent, whereas due to the immiscibility of MgAl<sub>2</sub>O<sub>4</sub> into Al<sub>2</sub>O<sub>3</sub> the sharp changes in surface roughness could also led to such type of discharge. This type of discharge is shown in Figure 2 e) and f).

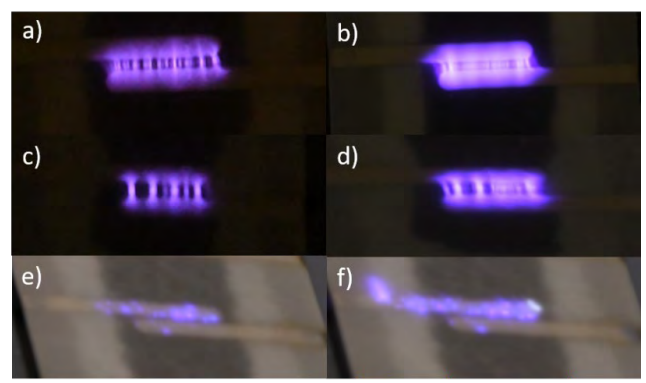


Fig. 2: Photographs of plasma discharges on different materials. a) pure alumina (f/9, ISO-12800, exp. time 1/60 s), b) pure alumina prolonged exposure time (f/9, ISO-400, exp. time 1 s), c) 10 vol. % of MgAl<sub>2</sub>O<sub>4</sub> (f/9, ISO-12800, exp. time 1/60 s), d) 10 vol. % of MgAl<sub>2</sub>O<sub>4</sub> prolonged exposure time (f/9, ISO-400, exp. time 1 s), e) 20 vol. % of MgAl<sub>2</sub>O<sub>4</sub> (f/9, ISO-100, exp. time 10 s), f) 20 vol. % of MgAl<sub>2</sub>O<sub>4</sub> with higher voltage power input (f/9, ISO-100, exp. time 10 s) [3]

#### Acknowledgment

This research was supported by project LM2018097 funded by the Ministry of Education, Youth and Sports of the Czech Republic

#### References

- [1] PAZDERKA, Michal, Roman PŘIBYL, Miroslav ZEMANEK, Jakub KELAR, Tomáš PLŠEK, Zlata KELAR TUČEKOVÁ a Mirko CERNAK. Robust current peak detection method for dielectric barrier discharges. Journal of Physics D: Applied Physics [online]. ISSN 0022-3727. doi:10.1088/1361-6463/abc916
- [2] ZEMANEK, M, R PRIBYL, J KELAR, M PAZDERKA, P STASTNY, J KUDELCIK, M TRUNEC a M CERNAK. Electrical properties of alumina-based ceramic barrier layers for dielectric barrier discharge. Plasma Sources Science and Technology [online]. 2019, 28(7). ISSN 1361-6595. doi:10.1088/1361-6595/ab28fa
- [3] PRIBYL, R, P STASTNY, M PAZDERKA, J KELAR, Z KELAR TUCEKOVA, M ZEMANEK, M TRUNEC a M CERNAK. Properties of MgAl2O4 doped alumina barrier layers for dielectric barrier discharge. Journal of Physics D: Applied Physics [online]. 2020, 53(50). ISSN 0022-3727. doi:10.1088/1361-6463/abb0ba

#### Contributed CO3 - Antoine Belinger

Fundamental problems of high pressure discharges

# Influence of the dielectric on a Diffuse Dielectric Barrier Discharge in air at atmospheric pressure

Antoine BELINGER<sup>1</sup>, Simon DAP<sup>1</sup>, Erwan SAMMIER<sup>1</sup>, Nicolas NAUDE<sup>1</sup>

<sup>1</sup> LAPLACE, Université de Toulouse, CNRS, INPT, UPS, Toulouse, 31062, France

e-mail: belinger@laplace.univ-tlse.fr

The Dielectric Barrier Discharge is an easy and robust way to obtain a cold plasma at atmospheric pressure. The discharges produced by this device are generally constituted by many microdischarges or filaments independent from each other. They have a short lifetime (1-10 ns) and are randomly distributed throughout the discharge volume. The energy is then not uniformly and optimally transferred to the discharge. This property is a significant obstacle to the use of DBD in some applications, such as plasma coating or surface treatment. Hopefully, it is possible to obtain a diffuse discharge, although it is an outstanding event only observable under restricted conditions. As a rule of thumb, diffuse discharge is always the result of a memory effect related to the previous discharges that creates seed electrons before the ignition of the discharge. Diffuse discharge can be divided into two kinds of discharges: the atmospheric pressure glow discharge (APGD) and the atmospheric pressure Townsend discharge (APTD). The APGD is obtained in noble gases with a penning mixture, while APTD was first obtained in Nitrogen.

The origin of the discharge homogeneity of the APGD and the APTD in Nitrogen is now well known and related to a memory effect in the bulk caused by long lifetime metastable [1]. For the APTD in Nitrogen, we recently pointed out the role of the  $N_2(A)$  and associative ionization reaction [2]. In air, the lifetime of this  $N_2(A)$  metastable is very low due to the strong quenching by the oxidizing species. It is why it was considered for a long time that it is impossible to obtain a diffuse discharge in air. However, in 2011 Osawa et al. presented a homogeneous discharge in air at low frequency (below 1 kHz) [3]. We observed such discharge at a higher frequency as presented in Fig 1. Its electrical characteristics are presented Fig 1. a, whereas short ICCD images taken perpendicular to the gas flow direction (position 1) are presented **Fig** 1.b. The two first images (noted + and -) are taken respectively on the positive and negative polarities with an exposure time equal to the half period. The discharge is diffuse, covering the whole electrode. The bright region is always located on the anode side, and no filament is observed. The images numbered from 1 to 6 are taken with a shorter exposure time (250 ns) to show the discharge development for each polarity. These six images are samples from a record of 2000 images. Then, it is possible to quantify the light emitted by the discharge during the whole period. When the discharge turn-on the light increases slowly with the current, moreover no light is present between the two discharges. The luminous intensity follows the evolution of the discharge current (I<sub>d</sub>). The current shows clearly one large peak for each half period and no series of many narrow peaks distinctive to the filamentary discharge. On each half-cycle, from ignition to extinction the light is always located close to the anode, and the gas voltage of the discharge is almost constant during the discharge. In summary, we can say that: the

homogeneous discharge obtained in air is a Townsend discharge like the APTD obtained in Nitrogen.

This observation is remarkable, but the origin of this regime is not yet understood. It is not likely due to a memory effect in the gas bulk but probably to a production of seed electrons on the surface of the dielectrics. To go in this direction, we focus this work on obtaining such discharge in air and the key role of the dielectric properties on the discharge. Then, the role of the dielectric material on the discharge homogeneity will be pointed out.

To go further, we can note that the production of seed electrons is *sine qua non* but not the only requirement to obtain a diffuse discharge. It is also important to prevent the transition from electron avalanches to streamer, which can be done by limiting the discharge current. It is possible to do it by changing the capacitance of the dielectrics covering the electrodes. The influence of the dielectric capacitance on the discharge behavior is studied by varying the dielectric thickness.

Finally, the effect of the intrinsic properties of the dielectric on the power transferred to the discharge will be discussed. We will explain how to obtain a diffuse discharge in air at a frequency up to 5 kHz.

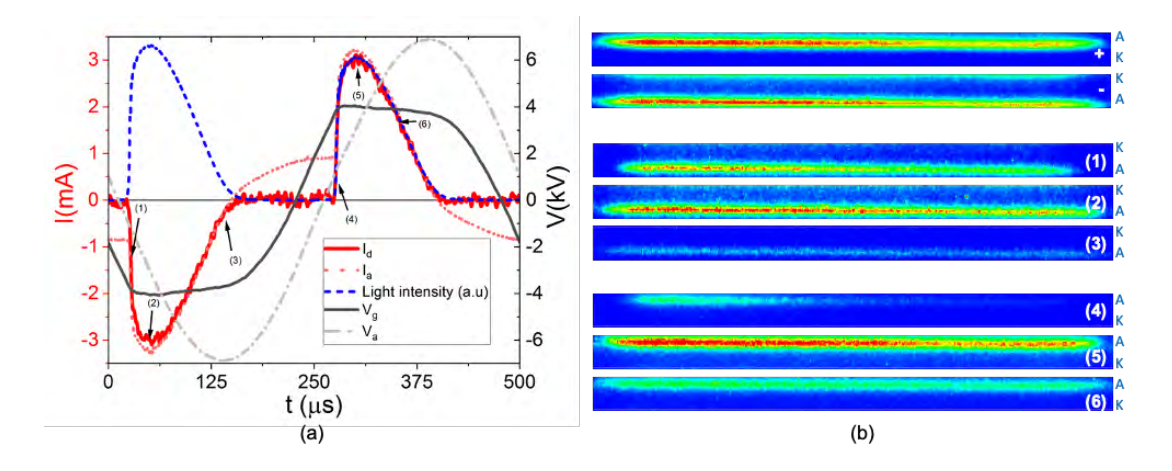


Fig 1. Homogeneous discharge in air at f=2kHz and  $V_{pp}$  =13.8 kV.  $I_a$  and  $I_d$  are the current applied to the DBD and the discharge current.  $V_g$  and  $V_a$  are the gas voltage and the applied voltage.

#### References

- [1] Massines F. et al. Eur. Phys. J. Appl. Phys. (2009) 47, 22805 (10pp).
- [2] Tyl C. et al. J. Phys. D: Appl. Phys (2018), **51** 354001 (10pp).
- [3] Osawa N. et al. IEEE Trans. Plasma. Sci. (2011), 40, pp 2-8

#### Contributed CO4 - Fumiyoshi Tochikubo

Fundamental problems of high pressure discharges

# CHARACTERISTICS OF TRICHEL PULSE DISCHARGE FROM TAYLOR CONE WITH AC SUPERIMPOSED DC VOLTAGE

Fumiyoshi Tochikubo<sup>1</sup>, Most Tauhida Tabassum<sup>1</sup>, Yusuke Nakagawa<sup>1</sup> *Tokyo Metropolitan University, 1-1, Minami-Osawa, Hachioji, Tokyo 192-0397, Japan* 

E-mail: tochi@tmu.ac.jp

When a DC high voltage is applied to a liquid in a capillary, the liquid surface forms a conical shape named Taylor cone. Then, the electrically charged fine droplets are emitted from the cone tip when the electrostatic repulsion by the surface-induced charge exceeds the surface tension of the liquid, which is called electrospray. Further, when the electric field at the cone tip reaches the corona onset electric field, corona discharge occurs. The generation of corona discharge is generally avoided in electrospray. However, the combination of electrospray and discharge plasma has been studied recently in the application of plasma-liquid interaction such as plasma medicine [1]. Therefore, the understanding of interaction between electrospray and corona discharge is important. Sugimoto *et al* reported that the discharge pulses from the water cone with negative DC high voltage are likely Trichel pulses [2]. We showed that the peculiar Trichel pulse-like discharge current is caused by the dynamic change of the electric field at the cone tip due to the vibration of Taylor cone [3]. In terms of dynamic changes in the electric field at the Taylor cone tip, the corona discharge and droplet emission can be controlled by controlling the applied voltage waveform. In this report, we show the characteristics of Trichel pulse discharge from Taylor cone with AC superimposed DC voltage.

The experimental setup is shown in Fig. 1. A grounded stainless-steel nozzle electrode with inner and outer diameters of 0.5 and 0.8 mm, respectively, are placed 10 mm below the plate electrode with a diameter of 40 mm. As liquid, either 1 wt% sodium dodecyl sulfate (SDS) solution or ethylene glycol (EG) was supplied to the nozzle through a U-shaped tube. A DC or AC superimposed DC high voltage is applied to the plate electrode through a current-limiting resistor of 141 k $\Omega$ . The high voltage source consisted of an AC/DC amplifier and a signal generator. The applied voltage and discharge current were monitored on an oscilloscope. The behavior of the Taylor cone and the droplets emitted from the cone tip was observed using a high-speed camera with a magnifying lens. The transport of the droplets was visualized by Mie scattering of laser light by the droplets.

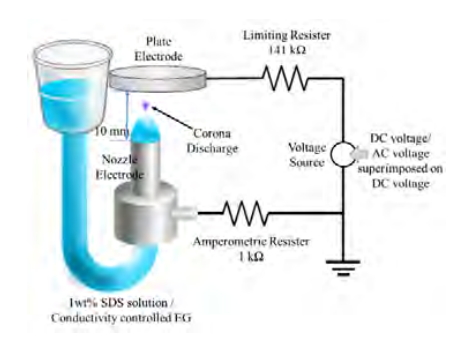
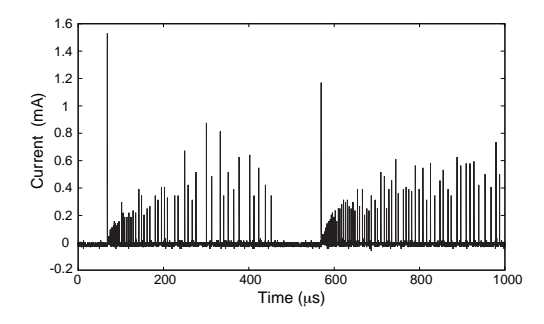


Fig. 1: Schematic of the experimental system.

Typical Trichel pulse-like current waveform with EG and DC applied voltage is shown in Fig. 2. There are multiple current pulse trains, where the first pulse in each train has the maximum peak, the second pulse has almost the minimum peak, and the subsequent pulses have gradually increasing peaks and intervals. From the observation of cone tip shape using a high-speed camera, we found that the cone tip is vibrating vertically in synchronization with the appearance of pulse trains. The first current pulse appears when the cone tip position is highest, and its curvature radius is smallest. Droplets were emitted from the cone tip coincident with the first pulse. The interval between the pulse train is affected by the liquid viscosity and the applied voltage (electric field). Since EG has large viscosity compared with SDS, the interval between the pulse train was long, approximately 500 µs in the present case.

We applied AC superimposed DC voltage to change the external electric field for controllable cone tip movements and discharges. Fig. 3 shows the cone tip displacement and current waveform with applying AC superimposed DC voltage using EG. The voltage for DC and AC (peak-to-peak) were 5.8 kV and 1.0 kV, respectively, and the AC frequency was 8 kHz. The current pulses were in the form of a Trichel pulse-like pulse train similar to the case of DC applied voltage. The pulse train appears in synchronization with the AC period (125 µs), which is shorter than the pulse train interval in Fig. 2. This means that the external AC field controls the cone tip movement and also the droplet emission. One-dimensional simulation of negative corona discharge was performed with applied voltage of AC superimposed DC voltage assuming the cone tip vibration. The calculated results agree qualitatively with the experimental observation.



**Fig. 2**: Typical Trichel pulse-like current waveform with EG (1.07 mS/cm) and DC voltage of 7 kV.

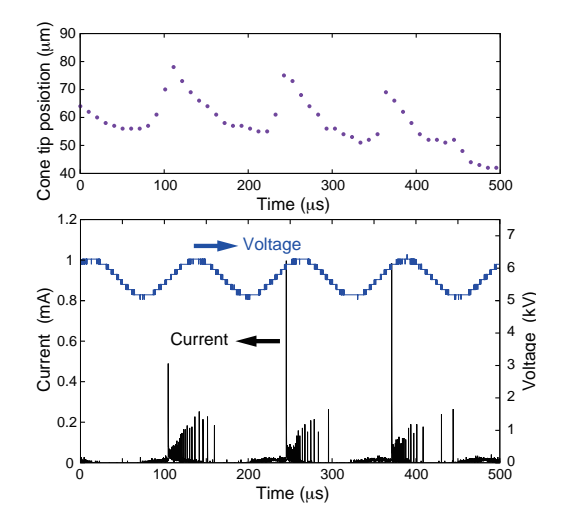


Fig. 3: Temporal profile of Taylor cone tip position with the current waveform for EG (V=5.8~kV~DC and 1.0~kVpp~AC with 8~kHz).

#### References

- [1] Z. Machala, B. Tarabová, D. Sersenová, M. Janda, K. Hensel, J. Phys. D 52, 034002 (2019)
- [2] T. Sugimoto, K. Asano, Y. Higashiyama, J. Electrost. 53, 25-38, 2001.
- [3] Y. Nakagawa, K. Nagao, F. Tochikubo, J. Phys. D 54, 305201 (2021).

# Contributed CO5 - Corentin Bajon

Fundamental problems of high pressure discharges

# Dielectric Barrier Discharge in CO<sub>2</sub>: electrical and optical characterization

C.Bajon<sup>1</sup>, S.Dap<sup>1</sup>, A.Belinger<sup>1</sup>, O.Guaitella<sup>2</sup>, T.Hoder<sup>3</sup>, N.Naudé<sup>1</sup>

<sup>1</sup>LAPLACE, Université de Toulouse, CNRS, INPT, UPS, Toulouse, France

<sup>2</sup> Laboratoire de Physique des Plasmas, Ecole Polytechnique, Route de Saclay, F-91128,

Palaiseau Cedex, France

<sup>3</sup>Department of Physical Electronics, Faculty of Science, Masaryk University, Kotlářská 2,

61137 Brno, Czech Republic

E-mail: cbajon@laplace.univ-tlse.fr

In the past ten years, studies on CO<sub>2</sub> have known a growing interest [1] [2]. Among them, CO<sub>2</sub> recycling [3], design of spacecraft shields for atmosphere re-entry, or oxygen production [4] [5] in the frame of the future Mars missions are of major concern. Non-equilibrium plasmas are an excellent way to induce chemistry in gases. At atmospheric pressure, dielectric barrier discharges (DBD) are widely used to generate cold plasmas, avoiding the transition to the arc regime. Usually, at this pressure, DBDs are filamentary and homogeneous DBD are only reported for few gas compositions such as Nitrogen or noble gases (Ar, He, Ne) with a Penning admixture. In this work, we will present the very first results obtained in a homogeneous dielectric barrier discharge at atmospheric pressure in pure CO<sub>2</sub>.

In such conditions, the discharge works in the well-known Townsend regime. The measured current (Fig.1) presents a large peak during one half-period as typically reported in the literature for Atmospheric Pressure Townsend Discharge (APTD). This operating regime is confirmed by optical measurements (Fig. 2), showing that the maximum light is located on the anode side, which is a characteristic of an APTD.

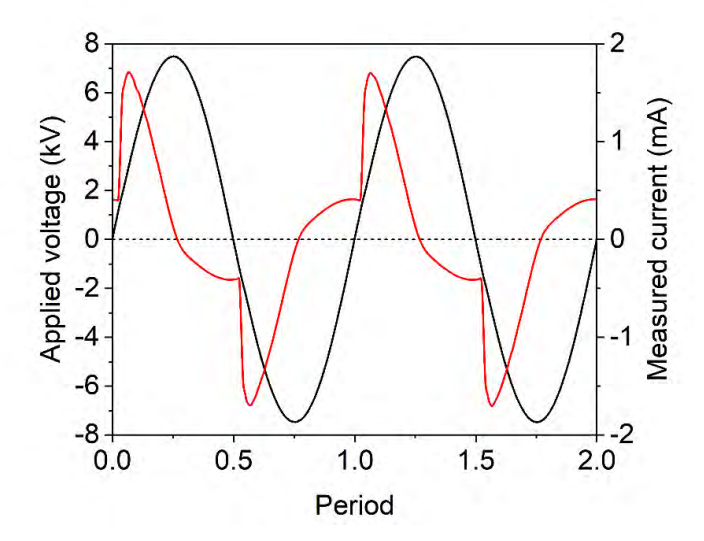
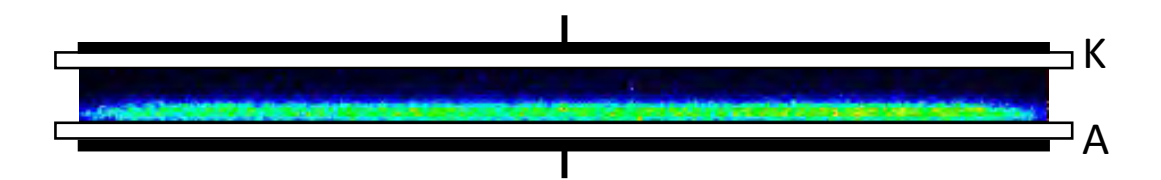


Fig. 1: Voltage and current measured in pure CO<sub>2</sub> DBD at atmospheric pressure.



**Fig. 2**: ICCD image of light emission during one half-period of the applied voltage in pure CO<sub>2</sub> (aperture time=1/4 period).

This work will present the first experimental characterization of the homogeneous discharge in CO<sub>2</sub> using electrical measurements, imaging and optical emission spectroscopy. On the basis of these results, the possible mechanisms involved in this discharge regime will be discussed.

#### References

- [1] A. Fridman, Plasma chemistry, Cambridge: Cambridge University Press, 2008.
- [2] L. D. Pietanza, O. Guaitella, V. Aquilanti, I. Armenise, A. Bogaerts, M. Capitelli, G. Colonna, V. Guerra, R. Engeln, E. Kustova, A. Lombardi, F. Palazzetti et T. Silva, Advances in non-equilibrium CO2 plasma kinetics: a theoretical and experimental review, Eur. Phys. J. D, 2021.
- [3] G. Centi et S. Perathoner, «Opportunities and prospects in the chemical recycling of carbon dioxide to fuels,» *Catalysis today 148*, pp. 191-205, 2009.
- [4] V. Guerra, T. Silva, P. Ogloblina, M. Grofulovic, L. Terraz, M. L. da Silva, C. D. Pintassilgo, L. L. Alves et O. Guaitella, «The case for in situ resource utilisation for oxygen production on Mars by non-equilibrium plasmas,» *Plasma Sources Sci. Technol. 26*, 2017.
- [5] D. Premathilake, R. A. Outlaw, R. A. Quinlan et C. E. Byvik, «Oxygen generation by carbon dioxide glow discharge and separation by permeation trhough ultarthin silver membranes,» *Earth an Space Science 6*, pp. 557-564, 2018.

#### Contributed C06 - Naoki Osawa

Fundamental problems of high pressure discharges

# COMPARISON OF SURFACE CHARGE DENSITY DISTRIBUTION GENERATED BY DIFFUSE AND FILAMENTARY BARRIER DISCHARGES IN ATMOSPHERIC PRESSURE AIR

Naoki Osawa, Kazuki Watanabe, Yoshio Yoshioka Kanazawa Institute of Technology, 7-1 Ohgigaoka, Nonoichi Ishikawa 921-8501, Japan

E-mail: n.osawa@neptune.kanazawa-it.ac.jp

#### 1. INTRODUCTION

Dielectric Barrier Discharges (DBDs) are promising technology for material processing, biomedical applications and so on. So far, we succeeded in generating diffuse DBD in atmospheric pressure dry air,  $N_2$  (purity: 99.95%) and  $O_2$  (purity: 99.5%) at low frequency [1]. There is a report that in  $N_2$  discharge, secondary electrons emitted by collision of metastable states  $N_2(A^3\Sigma_u^+)$  to the dielectric surface become seed electrons, and it is an important mechanism for the stable generation of diffuse DBD. If a small amount of  $O_2$  is mixed in  $N_2$ , metastable states  $N_2(A^3\Sigma_u^+)$  is quenched by the molecular oxygen, and the diffuse DBD changes to filamentary DBD [2]. Since our diffuse DBD is generated in the dry air and  $O_2$ , we believe that another mechanism to generate seed electrons from the barrier surface exists. Recently, we developed the DBD device which consists of a hemisphere rod electrode and alumina coated plane electrode and the surface potential scanning device which consists of a non-contacting electrostatic voltmeter and an electrical actuator. In this work, we compared surface charge density distribution on barrier before and after diffuse DBD with filamentary DBD.

#### 2. EXPERIUMENTAL SET UP

Fig. 1 shows an experimental setup. The hemisphere rod electrode type DBD device and surface potential scanning system were placed in a transparent box in order to observe discharge occurrence and control humidity. The relative humidity was set to 25%. Gas pressure in the box was 0.1 MPa. The radius of the hemisphere rod electrode tip and the gap length were 5 mm and 3 mm, respectively. Alumina (Material code: A473 and A440, Kyocera) was used as barrier material. A sinusoidal voltage of 12 kVp and 50 Hz was applied to the hemisphere rod electrode by a high-speed high-voltage power amplifier (model 20/20C-HS, Trek) and function generator (AFG-3022C, Tektronix). The applied voltage was interrupted at various voltage phase in order to analyze the surface charge density distribution before and after DBDs. The distribution was measured by the non-contacting electrostatic voltmeter (model 341HV, Trek).

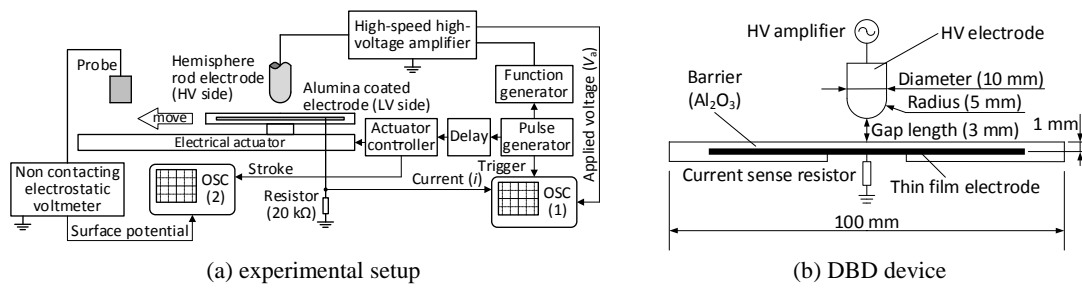
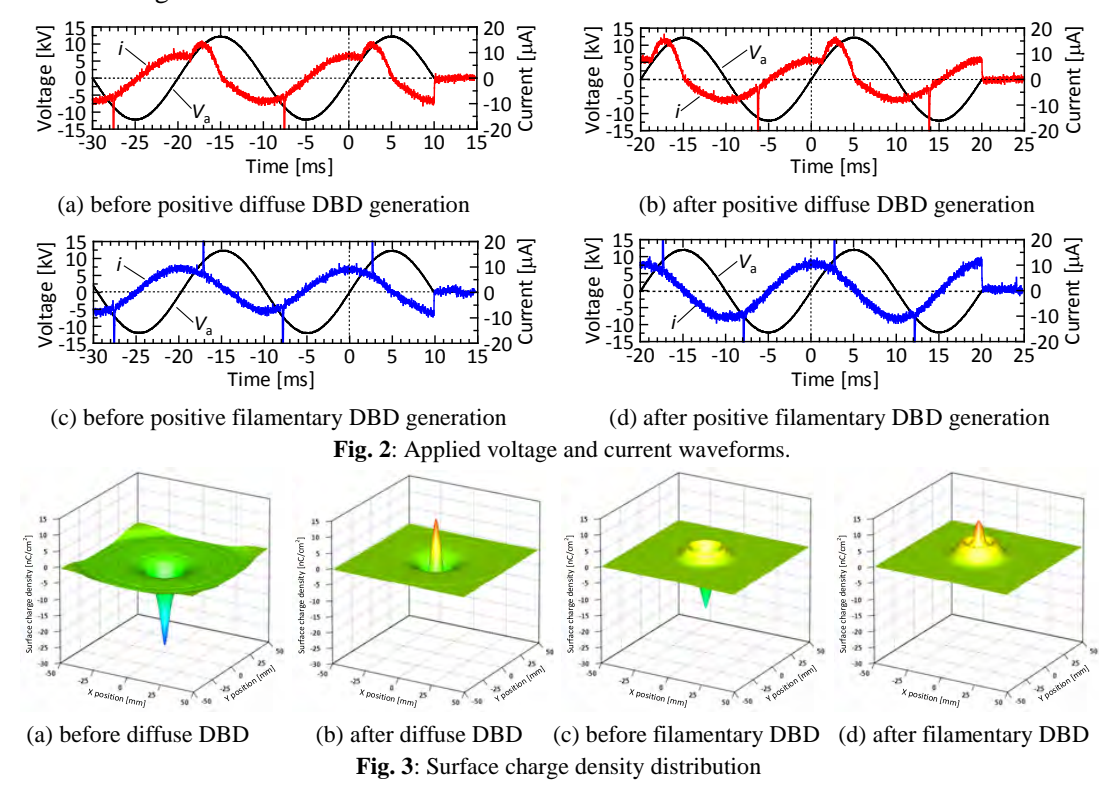


Fig. 1: Experimental setup.

#### 3. RESULTS

Fig. 2(a) – (d) show waveforms of the applied voltage and the current. Here, t = 0 ms is the instant of 35 cycles after the application of sinusoidal voltage. Fig. 2(a) and 2(b) show the waveform of the discharge when A473 alumina barrier was used. It is recognized that positive APTD generated at -18.5 ms and 1.5 ms. On the other hand, when A440 alumina barrier was used, positive filamentary DBDs were generated at -17.4 ms and 2.7 ms. We interrupted the applied voltage at 10 ms in the case of Fig. 2(a) and Fig. 2(c), and at 20 ms in the case of Fig. 2(b) and Fig. 2(d), respectively, and measured the surface potential distributions after discharge. These four cases make clear the difference of surface charge density distribution between A473 and A440 alumina barrier. Fig. 3(a) – (d) show surface charge density distribution before and after diffuse DBD and filamentary DBD. It is interesting to see the difference of surface charge profile of two materials. Namely, from figures 3(a) and 3(c), the maximum negative surface charge density before diffuse DBD and filamentary DBD appeared at the center of the barrier. The density by generating diffuse DBD was higher than that of generating filamentary DBD. This means that the amount of seed electrons from the barrier surface by an A473 alumina barrier is larger than that of an A440 alumina barrier.



This work was supported by JSPS KAKENHI (JP19K04360). We would like to thank Kyocera Corporation for providing the alumina coated electrode.

#### REFFERENCES

- [1] N. Osawa, Y. Yoshioka, IEEE Trans. Plasma Sci., Vol.40, No.1, pp.2-8, 2012.
- [2] K. V. Kozlov, R. Brandenburg, H.-E. Wagner, A. M. Morozov, P. Michel, J. Phys. D: Appl. Phys. 38, pp.528-529, 2005.

#### Contributed CO7 - Thomas Orrière

Fundamental problems of high pressure discharges

# 3D Topography of a liquid surface interacting with an Argon plasma jet

<u>Thomas Orrière</u>, Joao Vitor Olivira, Guillaume Gomit Institut PPRIME - UPR 3346 CNRS - Université de Poitiers - ISAE/ENSMA Futuroscope Chasseneuil Cedex, France

E-mail: thomas.orriere@univ-poitiers.fr

The aim of this work is to develop a diagnostic to measure the three-dimensional topography of a liquid surface exposed by a DC argon plasma jet in air at atmospheric pressure. Plasmas interacting with liquids are a promising solution in many research fields such as nanoparticles synthesis, pollutant removal, chemical synthesis or biomedical applications. Considerable efforts has been made to understand the the plasma-liquid chemistry. However, less work has been done in the electro-hydrodynamic phenomena occurring at the interface.

The shape of the liquid is an important aspect to consider both from an application point of view or for fundamental studies because high species density gradients can be measured at the liquid interface. Furthermore, it affects key plasma parameters such as the electric field and the transfer efficiency between the plasma and the liquid depends on the exchange area between the two phases. Usually, the dimple forming at the plasma-liquid interface is measured by using shadowgraphy or imaging. However, when the dimple is too small, the resolution of these diagnostics is to low to measure the topology. The free-surface synthetic Schlieren (FS-SS) should be a useful tool to reach greater sensitivities and the three-dimensional shape of the interface can be measured. However, the diagnostic has never been used to study plasma-liquid interactions.

We studied an argon microplasma jet interacting with deionized water with the experimental setup shown on figure 1a. The plasma is generated by applying a DC voltage via a 250 k $\Omega$  ballast resistor to a capillary tube with a 1.65 mm external diameter and a 180 um internal diameter. The liquid is grounded with a Pt Wire. The gap distance was set to 1 mm and measured afterward. The light source was a high-power led luminous CBT-120 and the camera was THORLABS DCC1645C. The method FS-SS work by watching a pattern across the gas-liquid surface. The pattern remains unchanged while the surface is flat. However, when the shape of the surface is modified, the pattern is distorted. The distortion can be quantified by using a displacement algorithm (the same as particle imaging velocimetry or PIV). Then the liquid-air surface topography can be calculated by using an integration method. In this study, we used PIVlab to calculate the displacement field and the integration algorithm *Intgrad2*, both available on Matlab. The surface roughness of the jet is a good pattern usable for the measurement as shown on figure 1b. However, a larger pattern has been mounted on the jet. Two lenses (f = 10 cm and f = 20 cm) were used to focus on the nozzle of the jet with a magnification of 2.

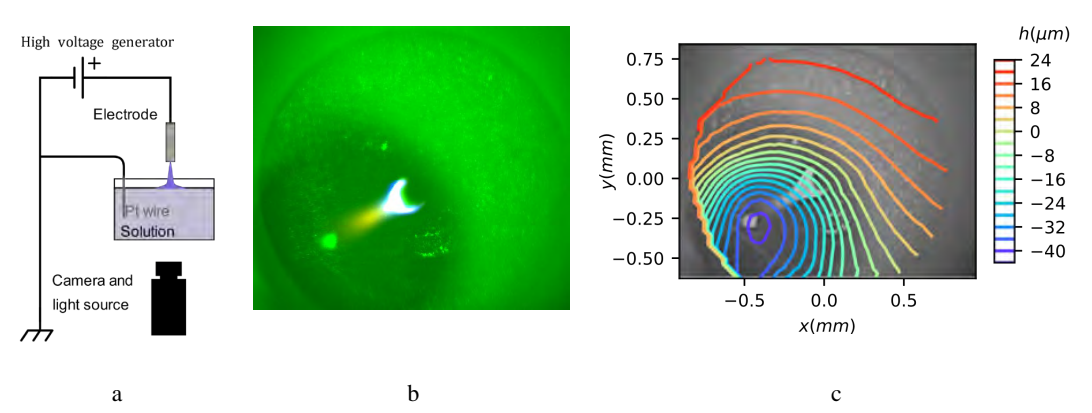


**Fig. 1a**: Experimental setup of the plasma liquid system studied by FS-SS; **Fig. 1b**: an image of the plasma jet taken with the experimental setup of figure (1a), the pattern is the roughness of the electrode and the voltage was negative; **Fig. 1c**: calculated liquid surface topology with the image of figure 2.

To test the method, the results obtained with the FS-SS are compared with side view shadowgraphy images and shows a good agreement without plasma. The range of argon flow rates were 0 to 25 SCCM. In our conditions, the dimple depth was 60 µm with the highest flow rate. The shadowgraphy cannot be used when a plasma is generated because of its low sensitivity and the 3D structure of the dimple.

An example of image is presented on figure 1b when the plasma is ignited with a DC current of 4.5 mA, a negative voltage applied to the tube and a 25 SCCM argon flow rate. The discharged is generated between the jet nozzle and the liquid. The contact of the discharge with the liquid is not centered with the nozzle. By comparing it with a image taken without plasma and without argon flow, the liquid surface topography has been calculated and is shown on figure 1c. Figure 1c shows the contour map of the height of the liquid superimposed with figure 1b in black and white and shows that the dimple follows the discharge.

When increasing the current from 1.5 mA to 4.5 mA, the dimple is deeper and when increasing the argon flow rate from 5 SCCM to 25 SCCM, the dimple shift and depth are greater. The results shows that the plasma restructure the flow thanks to an electro-hydrodynamic phenomenon. The limits of the method will also be discussed and the conditions when it is not usable will be presented.

#### Contributed C08 - Kazuki Watanabe

Fundamental problems of high pressure discharges

# EFFECT OF SURFACE RESISTIVITY ON SURFACE CHARGE DENSITY AND DIFFUSE DIELECTRIC BARRIER DISCHARGE IN ATMOSPHERIC PRESSURE AIR

<u>Kazuki Watanabe</u>, Naoki Osawa Kanazawa Institute of Technology, 7-1 Ohgigaoka, Nonoichi Ishikawa 921-8501, Japan

E-mail: c7200032@st.kanazawa-it.ac.jp

Dielectric Barrier Discharges (DBDs) are composed of many streamer discharges. We succeeded in generating an Atmospheric Pressure Townsend Discharge (APTD) in air by using a specific alumina barrier [1]. So far, we developed the method for changing surface resistivity of barrier material by using water vapor and clarified that the APTD does not generate when the surface resistivity of barrier material is low in spite of using the same barrier material [2]. We considered that the amount of negative charge accumulated on the barrier is influenced by the surface resistivity of barrier material. In this work, we investigated the effect of surface resistivity on the surface charge density distribution before APTD inception by the noncontacting electrostatic voltmeter.

A DBD system consists of a hemispherical rod electrode and an alumina coated plane electrode (thickness: 1 mm, material code: A473, Kyocera). The radius of the hemisphere rod electrode tip and the gap length were 5 mm and 3 mm, respectively. A sinusoidal voltage of 12 kVp and 50 Hz was applied to the hemispherical rod electrode. The surface charge density distribution on the barrier was measured by the non-contacting electrostatic voltmeter. The surface resistivity of the barrier was changed from over  $9.99 \times 10^{15} \Omega/\text{sq}$  to  $5.70 \times 10^{11} \Omega/\text{sq}$  by exposing purified water mist.

Fig. 1 shows applied voltage and current waveforms. In the case of  $\rho_s > 9.99 \times 10^{15}~\Omega/\text{sq}$ , APTD was generated at 3.0 ms. On the other hand, when  $\rho_s = 5.70 \times 10^{11}~\Omega/\text{sq}$ , filamentary DBD occurred at 3.0 ms. Fig. 2 shows surface charge density distribution just before APTD generation (obtained at 0 ms). We confirmed that the surface charge density at the center of the barrier by  $\rho_s > 9.99 \times 10^{15}~\Omega/\text{sq}$  was higher than that of by  $\rho_s = 5.70 \times 10^{11}~\Omega/\text{sq}$ . From these results, we confirmed that since the amount of accumulated negative charge is low, APTD did not generate by using specific alumina barrier.

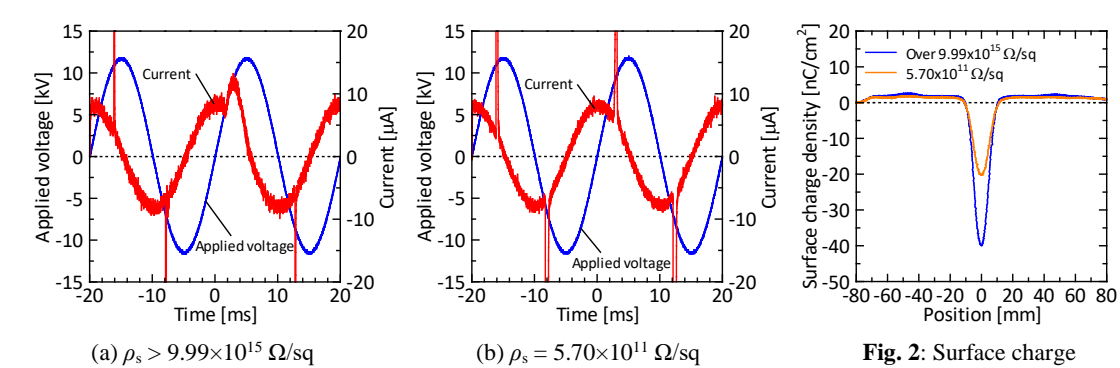


Fig. 1: Applied voltage and current waveforms.

density distribution (t = 0ms).

This work was supported by JSPS KAKENHI (JP19K04360). We would like to thank Kyocera Corporation for providing the alumina coated electrode.

# REFFERENCES

- [1] N. Osawa, Y. Yoshioka: IEEE Trans. Plasma Sci., Vol.40, No.1, pp.2-8, 2012.
- [2] K. Watanabe, K. Yamada, N. Osawa: Inst. Electrostat. Jpn. Spring meeting, pp.13-14, 2022.

# Contributed CO9 - Vlasta Štěpánová

Surface processing and technology (cleaning, coating, etching and modification, equipment)

# Adhesion improvement of LLDPE/PA tubular foil used as sausage casing after a very short atmospheric-pressure roll-to-roll plasma treatment

<u>Vlasta Štěpánová</u>, Petra Šrámková, Slavomír Sihelník, Jana Jurmanová, Monika Stupavská,
Dušan Kováčik

Department of Physical Electronics, CEPLANT, Faculty of Science, Masaryk University,
Kotlářská 2, 611 37 Brno, Czech Republic

E-mail: <u>vstepanova@mail.muni.cz</u>

This research aimed to optimize the diffuse coplanar surface barrier discharge (DCSBD) rollto-roll (R2R) treatment of multi-layer tubular foil as a very efficient plasma technology using several types of rollers differing in material resistance. Multi-layer tubular foils are commonly utilized in the meat processing industry as sausage or ham casings. The effect of ambient air plasma generated by coplanar and volume dielectric barrier discharge, so-called "industrial corona", on the surface characteristics of tubular foil formed from the outside by polyamide and from the inner side by linear low-density polyethylene (LLDPE) was studied. During the roll-to-roll treatment, the plasma acts from outside of the LLDPE/PA tubular foil, whereas the inside LLDPE surface is affected by plasma as well in dependence on the material of the roller used in combination with the DCSBD plasma unit. Various rollers differing in their electrical properties (conductivity, resistance) were utilized for experiments and compared. Based on these findings, the utility model "Device for plasma treatment of tubular foils" focused on DCSBD plasma in the roll-to-roll arrangement was registered [1]. It has been experimentally verified that a non-conductive roller constructed from plastic does not allow the surface discharge to be superimposed by microfilaments generated perpendicular to the film surface. This finding clarified the different effects of plasma treatment achieved using plastic and metalrubber roller on the surface properties of LLDPE foil. Applied exposure times of DCSBD treatment were in the range of 0.5-2 seconds. Evident wettability improvement of LLDPE foil surface after the plasma treatment was observed with the naked eye, while the pristine LLDPE foil surface repelled water solution of methylene blue used to visualize the plasma effect. The desired increase in peel resistance in the case of 0.5 s exposure time when comparing plastic and metal-rubber roller was three times higher for the second one. Peel resistance of untreated LLDPE foil was so low that it was unmeasurable. Best results were obtained for 2 s plasma exposure, where the peel resistance achieved using the metal-rubber roller was 31 % higher than for the plastic roller. The industrial corona treatment of the LLDPE/PA tubular foil was less effective compared to the DCSBD treatment under the same working conditions (exposure time, square power density of plasma). DCSBD plasma treatment in the roll-to-roll arrangement can improve the adhesion properties of the outer (better printability, dyeability) and the inner surface (enhanced adhesion of the meat mixture) of LLDPE/PA tubular foil simultaneously in combination with the appropriate roller.

#### Reference

[1] D. Kováčik, V. Štěpánová, M. Zemánek, S. Sihelník, P. Šrámková. Utility model PUV2019-36369 "Device for plasma treatment of tubular foils", 2019.

# Acknowledgement

This research has been supported by the project TG02010067 funded by the Technology Agency of the Czech Republic, and by the project LM2018097 funded by the Ministry of Education, Youth and Sports of the Czech Republic.

#### Contributed C10 - Julia Mrotzek

Surface processing and technology (cleaning, coating, etching and modification, equipment)

# Characterization of the plasma torch of an APPJ for thin film deposition

Julia Mrotzek<sup>1,2</sup>, Wolfgang Viöl<sup>1,2</sup>

<sup>1</sup>Laboratory of Laser and Plasma Technologies, University of Applied Sciences and Arts, Von-Ossietzky-Str. 99, 37085 Göttingen, Germany

E-mail: julia.mrotzek@hawk.de

Plasma powder deposition by means of an Atmospheric Pressure Plasma Jet (APPJ) allows the deposition of thin films of metal, metal oxide or polymers also on temperature sensitive surfaces such as paper or wood. In the process, particles are melted in the plasma and applied to the surface. For broad application, understanding of the underlying mechanisms and influence of relevant parameters is necessary, while process stability must be guaranteed.

In this study, the afterglow plasma of a pulsed DC arc jet (2 kW input power, 50 kHz repetition frequency, pulse period 5–10  $\mu$ s) was studied using optical emission spectroscopy (Figure 1). The development of reactive species along the gas flow direction was investigated for different process gases (N<sub>2</sub>, air) and gas flow rates. Spectra are dominated by N<sub>2</sub><sup>+</sup> (B-X), N<sub>2</sub> (C-B) and NI. With increasing distance to the nozzle, the intensity of species (OH, NO) originating from the surrounding atmosphere is increasing due to the turbulent flow. Determination of plasma temperatures proofed, that the jet is far from LTE conditions with rotational temperatures at the nozzle exit around 4500 K and excitation temperatures around 6000 K.

In a next step, investigations will be carried out during injection of metallic powders.

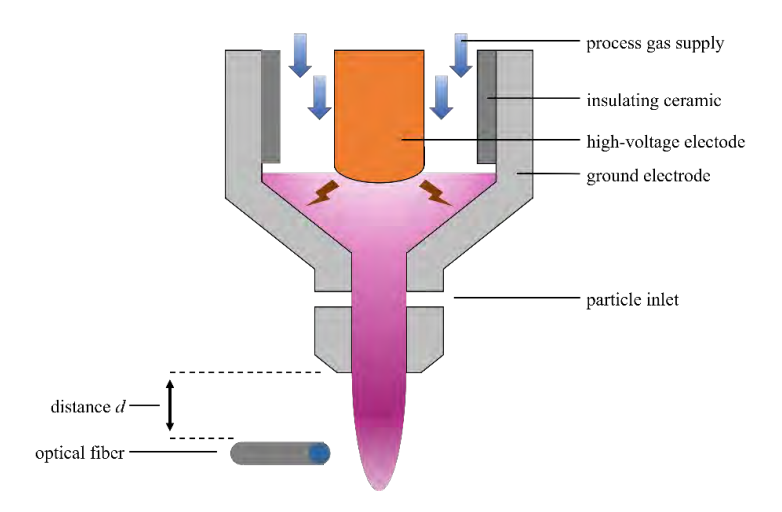


Fig. 1: Schematic Setup of the Atmospheric Pressure Plasma Jet (APPJ).

<sup>&</sup>lt;sup>2</sup>Application Center for Plasma and Photonics, Fraunhofer Institute for Surface Engineering and Thin Films, Ossietzky-Str. 100, 37085 Göttingen, Germany

#### Contributed C11 - Kristian Wende

Biological applications

# Biomolecule oxidation by gas phase species – the role of the gas-liquid interphase

Wende, Kristian<sup>1</sup>, Nasri, Zara<sup>1</sup>, Striesow, Johanna<sup>1</sup>, Ahmadi, Mohsen<sup>1</sup>, Minkus, Lara<sup>1</sup>, Weltmann, Klaus-Dieter<sup>1</sup>, Bekeschus, Sander<sup>1</sup>, von Woedtke, Thomas<sup>1,2</sup>,

<sup>1</sup>Leibniz Institute for Plasma Science and Technology, Felix-Hausdorff-Str. 2, Greifswald, Germany <sup>2</sup>Institute for Hygiene and Environmental Medicine, University Medicine Greifswald, Greifswald, Germany E-mail: kristian.wende@inp-greifswald.de

Biomolecules such as amino acids, lipids, proteins, and carbohydrates are relevant targets for reactive species due to the presence of sensitive chemical structures, such as electron-rich heteroatoms, (conjugated) double bonds, or aromatic rings. In plasma medicine, the successful application of plasmas for curative or preventive measures has been established. Besides electrical fields, predominantly reactive oxygen and nitrogen species were attributed to be most relevant for the observed effects. While it is accepted that long-lived species such as hydrogen peroxide can penetrate into (model) tissues, the fate of atomic and singlet oxygen or peroxynitrite remains to be clarified. Starting from amino acids (tyrosine, cysteine) and phospholipids (POPC), we found distinctive oxidation products and could show the incorporation of gas-and liquid phase derived atoms indicative for gas-liquid interphase reactions. Via model lipids and peptides, isolated proteins and carbohydrates, and complex protein samples a site and sub-structure specificity of plasma-derived reactive species could be shown (1-3). In catalase, phospholipase, or filamentary proteins, the newly introduced chemical modifications modulated protein activity and recognition and subsequently changed cell physiology. Accordingly, it can be stated that the oxidative modification of biomolecules is a regular event in plasma medicine that modulates or even controls downstream physiologic processes.



Fig. 1. Inflammation related enzyme Phospholipase A2: the oxidation of the Tryptophan 128 by singlet oxygen leads to structural changes inhibiting lipid membrane approach and ultimately enzymatic activity

#### Acknowledgement

This work was supported by the German Ministry of Research and Education (BMBF), grants no. 03Z22DN12 (to K. W.), 03Z22DN11 (To S.B.), and 03Z22Di1 (to K.-D. W.).

#### References

- [1] Wenske S, Lackmann JW, Busch L, Bekeschus S, von Woedtke T, Wende K, Journal of Applied Physics 129 (2021).
- [2] Nasri Z, Memari S, Wenske S, Clemen R, Martens U, Delcea M, Bekeschus S, Weltmann KD, von Woedtke T, Wende K, Chemistry - A European Journal 27 (59), 14702-14710
- [3] Wenske S, Lackmann JW, Bekeschus S, Weltmann KD, von Woedtke T, Wende K, Biointerphases 15, 061008 (2020).

#### Contributed C12 - Mark Kushner

Biological applications

# ATMOSPHERIC PRESSURE PLASMA TREATMENT OF ORGANICS IN LIQUID: EXTENDING REACTION MECHANISMS INTO SOLUTION

Jordyn Polito<sup>1</sup>, Sanjana Kerketta<sup>1</sup>, Katharina Stapelmann<sup>2</sup> and Mark J. Kushner<sup>1</sup> University of Michigan, Ann Arbor, Michigan 48109-2122 USA <sup>2</sup>North Carolina State University, Raleigh, North Carolina 27607 USA

E-mail: mjkush@umich.edu

One of the motivating applications for investigation of atmospheric pressure plasma interactions with liquids is the treatment of organic materials – the field of plasma biology. Fundamental investigations to date have focused on the production of reactive oxygen and nitrogen species (RONS) in water. More applied investigations have addressed the outcome of these RONS on, for example, deactivating bacteria and viruses. The fundamental reaction mechanisms of those RONS interacting with organic material (proteins to cell membranes) in the activated solution are less clear. Investigations have shown that reactions of RONS with organic molecules in solution (e.g., simple amino acids such as cysteine) significantly deplete the RONS while producing oxidation products that are not unlike the reaction of similar organic molecules with gas phase plasmas [1]. Extending these results to cell membranes would be the next step. While mechanisms are available for reactions of gas phase plasmas with organic molecules and polymers, such mechanisms are generally not available for analogous processes in solution.

In this paper, we report on a computational investigation of atmospheric pressure plasma jet treatment of water and saline solutions having simple proteins and amino acids. The goal of this work is to provide insights as to whether gas phase reaction mechanisms of RONS with organic molecules can be extended to solution. These investigations were performed with a 2-dimensional plasma hydrodynamics model [2] and a global plasma chemistry model adapted for plasma-liquid interactions [3]. The scaling of plasma activation of water and saline solutions by plasma jets sustained in He/O<sub>2</sub> and Ar/O<sub>2</sub> flowing into air will be briefly discussed with a focus on the generation of oxidizing (e.g., OH, H<sub>2</sub>O<sub>2</sub>) and biocidal (e.g., OCl<sup>-</sup>) species in solution. Using analogous reactions as for gas phase processes, the interaction of these RONS with simple amino acids and proteins in solution will discussed. Comparisons will be made to available experimental data.

- [1] K. Stapelmann et al., J. Phys. D Appl. Phys. **54**, 434003 (2021).
- [2] G. Parsey et al., J. Phys. D: Appl. Phys. **54**, 045206 (2021).
- [3] S. Mohades, et al., J. Phys. D: Appl. Phys. **53**, 435206 (2020).

### Contributed C13 - Jan Cech

Depollution and environmental applications

# CAVIPLASMA – THE NEW TOOL FOR ENERGY-EFFICIENT LARGE-SCALE TREATMENT OF LIQUIDS

Jan Čech¹, Pavel St'ahel¹, Lubomír Prokeš¹, Jozef Ráhel²l, Pavel Rudolf², Eliška Maršálková³,
Blahoslav Maršálek³, Petr Lukeš⁴, Aleksandra Lavrikova⁵, Zdenko Machala⁵

<sup>1</sup>Masaryk University, Faculty of Science, Dept. of Physical Electronics, Kotlarska 2, CZ-611

37 Brno, Czechia

<sup>2</sup>Brno University of Technology, Faculty of Mechanical Engineering, V. Kaplan Dept. of Fluid Engineering, Technicka 2896/2, CZ-616 69 Brno, Czechia

<sup>3</sup>Institute of Botany, Czech Academy of Sciences, Lidicka 25/27, CZ-602 00 Brno, Czechia <sup>4</sup>Institute of Plasma Physics of the Czech Academy of Sciences, U Slovanky 2525/1a, 182 00 Prague 8, Czechia

<sup>5</sup>Division of Environmental Physics, Faculty of Mathematics, Physics and Informatics, Comenius University, Mlynská Dolina, 842 48 Bratislava, Slovakia

E-mail: cech@physics.muni.cz

Generation of reactive oxidizing species in liquids (esp. water) became a highly developed field of plasma physics [1]. Various liquid discharge technologies found their application primarily in cross-discipline environmental, or bio-medical plasma research [2,3]. However, the main obstacle remains in place even after two decades of focused research effort – the effective method for large-volume liquid treatment. In our contribution, we introduce a novel approach to overcome this technological barrier named CaviPlasma (Fig. 1). It employs a synergistic combination of hydrodynamic cavitation phenomenon with the plasma generation in the cavitation vapor cloud – see more details in patent [4], or [5].

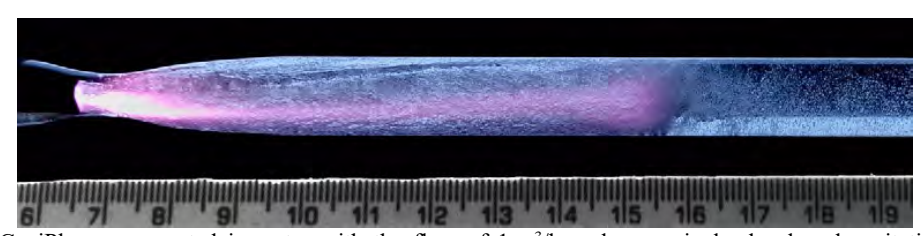


**Fig. 1**: CaviPlasma generated in water with the flow of 1 m³/h under massively developed cavitation cloud conditions. Plasma channel was generated using a high-frequency sine-wave generator (3 kV @ 64 kHz), with the total input power of 400 W. Bare electrode is immersed in Venturi nozzle. Exposure time 1/20 s, rear-curtain flash backfill to freeze the cavitation cloud state (scale bar in cm/unit).

The generation of electrical discharges in liquids can be divided into two distinct categories. The first category features extremely high-pressure discharges generated in a genuinely liquid environment. The second category makes use of discharge generation in a subsidiary gas-phase environment with subsequent mixing of plasma produced species into the liquid. The typical representatives of the latter approach are plasma jets immersed in liquid volume, discharges generated above the liquid level or in liquid aerosol, or discharges incited inside the gas microbubbles introduced or formed inside the liquid volume. The technique of CaviPlasma is a representative of such an approach.

The CaviPlasma uses an energy-efficient generation of developed hydrodynamic cavitation cloud (HCC) which proves to be a highly suitable gas-phase environment to (i) sustain electrical discharge between the pair of properly positioned electrodes, and (ii) efficiently mix and dissolve plasma generated radicals into the liquid. The HCC comprises an ample number of tiny voids (cavities) with the internal pressure of liquid vapors of a few kPa only. In this way, an advantageous low-pressure environment is formed inside the flowing liquid, where even a moderate high-voltage field can sustain a considerable volume of discharge plasma.

The CaviPlasma generated in our lab-scale unit and operated at  $Q=1~\mathrm{m}^3/\mathrm{h}$  was subject to diagnostics. Typical voltage and current waveforms are shown in Fig. 2a. The current is dominantly formed by its resistive component. No clear or distinctive discharge current peaks were found. The optical emission spectroscopy (Fig. 2b) confirmed the decomposition of water vapors in cavities into the OH radicals, accompanied by H and O atoms. The state-by-state fitting of OH emission [6] revealed high non-equilibrium of OH rotational state population. The water analysis revealed high production rate of  $H_2O_2$  of  $G(H_2O_2)=6~\mathrm{g/kWh}$  (incl. pumps). The presence of OH radicals was confirmed using terephthalic acid fluorescence measurement. The strong oxidizing effects was confirmed using phenol degradation resulting in  $G(\mathrm{phenol})=2.5~\mathrm{g/kWh}$  ( $P_{\mathrm{discharge}}=0.5~\mathrm{kW}$ ). Exceptionally high efficacy of CaviPlasma can be demonstrated also on single-pass cyanobacteria (Microcystis~aeruginosa) treatment [5], where combined action of HCC and discharge led to a removal with no increase in microcystin concentration in the treated water. In actual numbers, 6 l of water ( $5\times10^5~\mathrm{cells/ml}$ ) was disinfected in  $<15~\mathrm{sec}$ .

Acknowledgement: This research has been supported by the Czech Science Foundation under the project No. GA22-11456S and also by the projects of Technological Agency of Czech Republic under the project No. SS01020006 and Slovak Research and Development Agency APVV-17-0382. This work results within the collaboration of the COST Action CA19110.

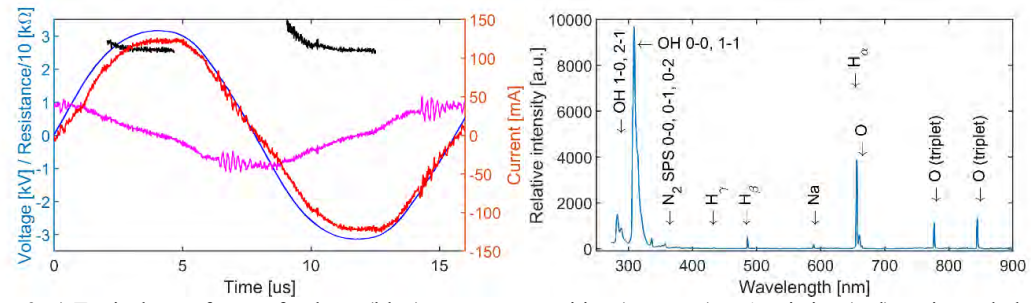


**Fig. 2**: a) Typical waveforms of voltage (blue), current: capacitive (magenta) and resistive (red); estimated plasma environment resistance (black); b) Typical optical emission spectrum consisting of OH, H and O emission.

#### Reference:

- [1] Bruggeman, P J et al., Plasma Sources Sci. Technol. 2016, 25, 053002.
- [2] Brandenburg, R et al., Plasma Process Polym. 2019, 16, e1700238.
- [3] Kaushik, N K et al., Biological Chemistry 2018, 400 (1), 39-62.
- [4] CZ Patent No. 308 532 (Industrial Property Office, Czech Republic)
- [5] Maršálek, B et al., Water 2020, 12, 8.
- [6] massiveOES: https://bitbucket.org/OES\_muni/massiveoes/src/master/

#### Contributed C14 - Ravi Patel

Depollution and environmental applications

# Filamentary DBD plasma for ignition stabilized combustion

Ravi Patel<sup>1,2</sup>, Nico dam<sup>2</sup>, Sander Nijdam<sup>3</sup>

<sup>1</sup>Department of Applied Physics, Eindhoven University of Technology, the Netherlands

<sup>2</sup>Department of Mechanical Engineering, Eindhoven University of Technology, the

Netherlands

E-mail: r.b.patel@tue.nl

More than 80 % of the world's energy is produced by fossil fuel combustion. Besides the energy sector, the transportation sector is also dominated by combustion in the form of internal combustion (IC) engines for automobile vehicles or as turbojets for aviation applications. A major downside of over reliance on combustion is global warming. So, there is an urgent need to minimize emissions of combustion exhaust products like CO<sub>2</sub>, NO<sub>x</sub>, and soot. One of the possible ways to make combustion cleaner is to operate in lean conditions. However, ignition and flame stabilization are difficult in these conditions. In recent years, plasma-assisted combustion (PAC) is investigated to facilitate better ignition and flame stabilization in lean conditions. Especially, nanosecond repetitive pulse driven non-equilibrium plasmas have the potential to support lean combustion by producing atomic radicals (like O, H, etc.) at low temperatures [1, 2].

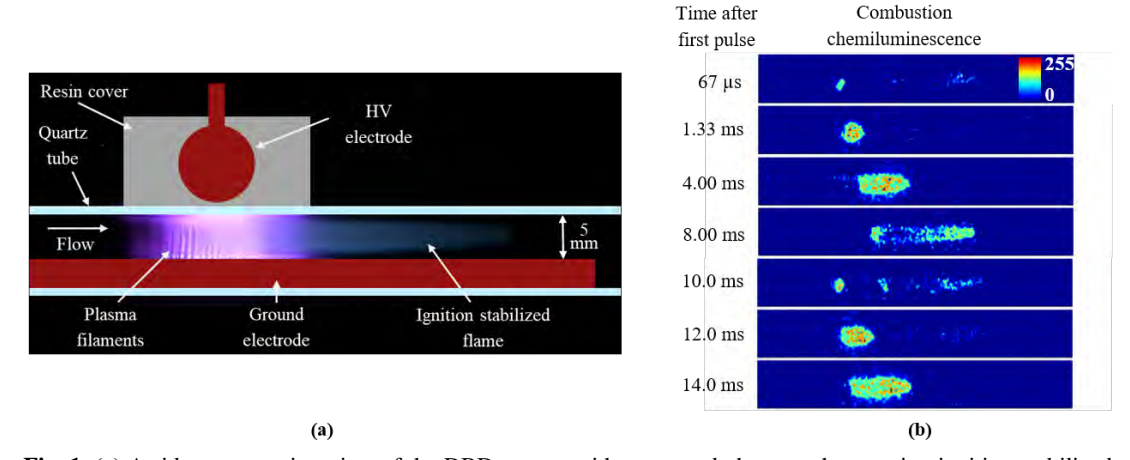


Fig. 1: (a) A side cross section view of the DBD reactor with a cropped photograph capturing ignition-stabilized combustion at  $\phi = 0.7$ , 150 cm/s flow speed, and 2 kHz PRR & (b) a set of high-speed intensified combustion chemiluminescence images at  $\phi = 0.7$  and 100 cm/s flow speed.

In this work, we experimentally investigate a dielectric barrier discharge (DBD) plasma as a repetitive ignition source in methane-air flows near atmospheric pressure conditions. We use a quartz flow reactor incorporated with a DBD configuration as shown in Fig. 1(a). A discharge is produced using 23 kV pulses of 10 ns duration at up to 3 kHz pulse repetition rate (PRR). The figure also includes a digital camera photograph capturing ignition stabilized combustion at 150 cm/s flow speed and an equivalence ratio  $\varphi = 0.7$ . A "stable looking flame" is seen at the downstream of the plasma, that is due to repetitively ignited kernels which are blowing out with the flow. To visualize these dynamics better, a set of high-speed intensified combustion chemiluminescence images is shown in Fig. 1(b). These images capture the repetitive ignition

dynamics at  $\phi = 0.7$  which includes ignition, kernel expansion and splitting, extinction, and reignition.

A systematic parametric study has been performed in a continuous plasma mode to explore plasma and repetitive ignition dynamics, plasma  $NO_x$  production, and plasma energy coupling. This work was continued for a plasma burst mode. The minimum number of pulses required for ignition and the pulse-to-pulse gas temperature have been evaluated. For these analyses, we used passive optical diagnostics like high-speed imaging and optical emission spectroscopy. A summary of all these studies will be presented during the conference.

#### References

- [1] Y. Ju, W. Sun, Progress in Energy and Combustion Science 48 (2015) 21-83.
- [2] A. Starikovskiy, N. Aleksandrov, Progress in Energy and Combustion Science 39 (2013) 61-110.

### Acknowledgement

This work is part of the research programme "Making plasma assisted combustion efficient" with project number 16480, which is partly financed by the Dutch Research Council (NWO).

#### Contributed C15 - Perla Trad

Depollution and environmental applications

# Influence of the applied HV-pulse rise time on the removal efficiency of n-hexane in a DBD

Perla Trad<sup>1,3</sup>, Nicole Blin-Simiand<sup>1</sup>, Michel Fleury<sup>1</sup>, Fabien Gerardin<sup>3</sup>, Michel Heninger<sup>2</sup>,

Pascal Jeanney<sup>1</sup>, Stéphane Pasquiers<sup>1</sup>

<sup>1</sup> Université Paris-Saclay, CNRS, Laboratoire de Physique des Gaz et des Plasmas - Orsay

(France)

<sup>2</sup> Université Paris-Saclay, CNRS, Institut de Chimie Physique - Orsay (France) <sup>3</sup> PROCEP, INRS, Vandœuvre-lès-Nancy (France)

perla.trad@universite-paris-saclay.fr

Non-thermal plasmas are now a recognized efficient method for reducing VOCs in the context of air depollution [1, 2]. However, it suffers a disadvantage in by-product formation at low energy deposition in the electric discharge. As a result, plasmas are often combined with other techniques (mainly catalysts) to overcome this limitation.

The present study is done in a filamentary plasma produced by dielectric barrier discharge (DBD) in synthetic air  $N_2/O_2$  (20%) at room temperature and atmospheric pressure. N-hexane ( $C_6H_{14}$ ) is selected as the model pollutant molecule. It is frequently used as a solvent in various industries for different purposes, such as extracting vegetable oils and formulating multiple products such as paints and printer inks, and is considered an indoor pollutant. We use a DBD with a cylinder-rod geometry connected to a high voltage (HV) pulsed power supply. The reactor is an alumina tube with a thickness of 2.5 mm and an internal diameter of 10 mm. In the tube's central axis is placed a tungsten rod (diameter of 1 mm) connected to the high voltage pulsed power supply, and on its surface is rolled a copper tape that acts as the ground electrode. The discharge volume is 3.89 cm<sup>3</sup>.

This study aims to evaluate and understand the effect of voltage waveform on n-hexane in terms of removal efficiency, given further coupling to a complementary removal process.

Residual n-hexane in the treated gas stream is measured using gas-phase chromatography. Voltage and current waveforms are measured using adapted probes (LeCroy PPE20KV high voltage passive probe, TM Research Products SBNC-5-5) connected to a fast digital LeCroy oscilloscope (Waverunner 204 MXi-A, 2 GHz, 10 GS s<sup>-1</sup>). The influence of various parameters such as applied voltage, HV-pulse repetition frequency, and the voltage waveform's temporal evolution (rise time) is examined in terms of n-hexane removal.

Figure 1 shows the two HV pulses delivered by the power supplies used in this study. The HV-pulse of  $A_1$  is a half-sinusoidal waveform with a rise time of 90 ns, and the pulse of  $A_2$  is a square waveform with a rise time of 50 ns. The  $A_2$  power supply produces a current with a higher amplitude (32 A) than the one produced with  $A_1$  (7 A). The current produced with the  $A_2$  power supply also presents a negative peak at the end of the pulse at 500 ns that isn't observed with the  $A_1$  power supply. The difference in breakdown voltage between the two power supplies explains the higher values of current obtained with  $A_2$ . The breakdown voltage obtained with the  $A_2$  power supply is 17 kV which is much higher compared to the breakdown voltage of  $A_1$ , which is 11.5 kV. This also creates a difference in the energies deposited in the plasma; we have 2.7 mJ with the  $A_1$  power supply and 11 mJ with the  $A_2$  power supply.

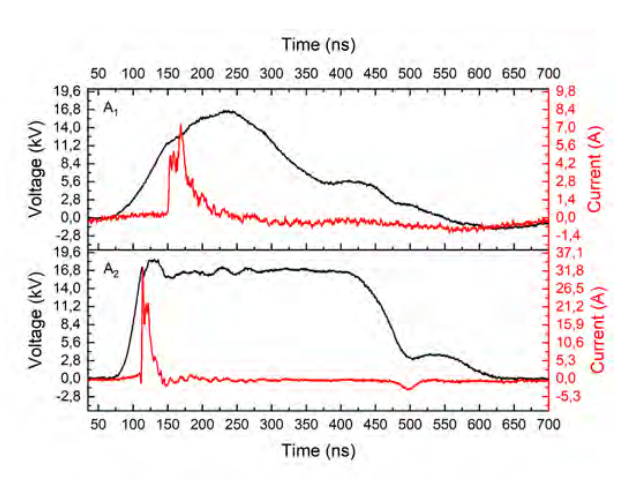


**Fig. 1**: Voltage and current waveforms temporal evolutions at 17.5 kV and 16.5 kV applied voltage, 500 Hz and 500 mL/min with an inlet concentration of 25 ppm of n-hexane for the  $A_1$  and  $A_2$  power supplies, respectively.

Figure 2 shows the evolution of the residual n-hexane measured at the exit of the reactor as a function of the SED (J/L), the specific energy density, defined as the energy deposited in the plasma as per unit of volume of the gas stream.

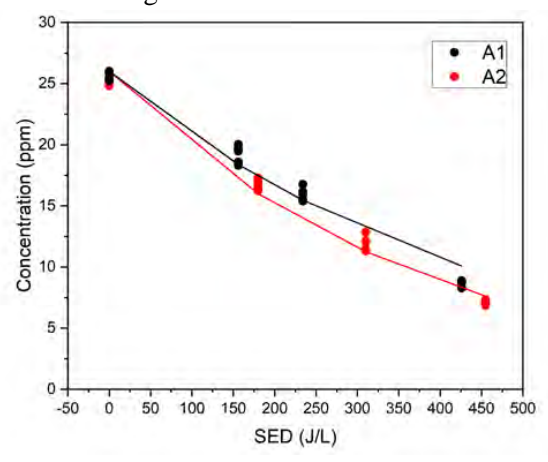


Fig. 2: Residual n-hexane in the treated gas stream with an inlet concentration of 25 ppm as a function of the SED at 500 Hz and 500 mL/min for  $A_1$  (black) and  $A_2$  (red) power supplies.

The results obtained with the A<sub>2</sub> power supply show a slightly better removal efficiency of n-hexane.

The presence of n-hexane in the discharge also increased its stability compared to when the discharge is done in the  $N_2/O_2$  mixture for both power supplies: real-time ozone and energy measurements present significantly less variations when the discharge is operated in the polluted gas stream.

#### References

- [1] A. Vandenbroucke et al., J. Hazard. Mat. 195 (2011) 30-54.
- [2] M. Schiavon et al., Water Air Soil Pollut. 228 (2017) 388 (20pp).

# Contributed C16 - Jeroen van Oorschot

Depollution and environmental applications

#### Real-Time In-Situ Characterization of Plasma Activated Water

J. J. van Oorschot<sup>1</sup>, A.J.M. Pemen<sup>1</sup>, T. Huiskamp<sup>1</sup>

<sup>1</sup> Eindhoven University of Technology, 5612az Eindhoven, The Netherlands

In this contribution we present an in-situ sensor system to monitor the generation of plasma activated water in real time.

Plasma activated water is a promising solution for producing both fertilizer and disinfectant from normal tap water, by generating an atmospheric pressure plasma near the water surface. This plasma generates free oxygen and nitrogen radicals from the ambient air, which dissolve in the water as mainly  $NO_2^-$ ,  $NO_3^-$ ,  $HNO_2$  and  $H_2O_2$ .

At Eindhoven University we develop pulse generators to generate flexible high voltage pulses for plasma generation. These high voltage (10-20kV) pulses can be changed in pulse length, pulse repetition rate, rise-time. Also, bursts of a few pulses can be applied, spaced only nanoseconds apart. By changing the high-voltage waveform, we can tune the plasma and as such the composition of species in the water.

To measure the effect of a certain high voltage pulse waveform on the plasma, we developed a continuous measurement system. This system pumps water from our reactor (a beaker) and through pH, ORP and conductivity sensors. Then the water flows through a UV flow cell, where the UV-absorption of the water is measured, which tells us the concentration of the species of interest. Finally, the water flows back to the reactor.

Both PAW measurements and electrical measurements are read by a computer which shows the measured values and water composition in real time. In the future this allows for a real time feedback system, where the high voltage pulses can be adapted to changing parameters over time.

#### Contributed C17 - Alex Destrieux

Modelling and diagnostics

# Toward a better understanding of the electrical properties in a dielectric barrier discharge during long-time operation

A. Destrieux<sup>1,2</sup>, J. Profili<sup>2</sup>, M. Laurent<sup>3</sup>, G. Laroche<sup>1,2</sup>

<sup>1</sup>Laboratoire d'Ingénierie de Surface, Département de génie des mines, de la métallurgie et des matériaux, Centre de Recherche sur les Matériaux Avancés, Université Laval, Québec, OC, Canada

<sup>2</sup>Centre de recherche du CHU de Québec, Hôpital St-François d'Assise, Québec, QC, Canada

<sup>3</sup>Saint-Gobain North America, Northborough, Massachusetts, USA.

E-mail: alex.destrieux.1@ulaval.ca

Atmospheric pressure dielectric barrier discharges (APDBD) are recently gaining a lot of interest for several applications due to the varieties of non-equilibrium regimes that can be produced. The possibility to operate APDBDs at room temperature make them suitable for surface modification of different thermosensitive materials such as polymers. Compared to low pressure plasmas, where expensive pumping system and closed environment limit the amount of material that can be treated, atmospheric pressure systems enable in-line modifications and are more suitable for industrial applications.

The physical phenomena as well as the chemistry occurring in APDBD are very sensitive to the gas composition, the electrodes' geometry, or the electrical excitation used. As an example, in nitrogen operating plasma, few tenth of ppm of impurities added can lead to a stabilized homogenous regime, while few hundreds of ppm strongly change the regime to a filamentary one<sup>1</sup>. This strongly affects the surface modifications of the plasma-treated materials and highlights the importance to gain more insight, with different diagnostics, in the physical phenomena of the discharge.

One of the diagnostics widely employed for plasma characterization at atmospheric pressure is the electrical measurements. Electrical signals such as the applied voltage, the current or the charge flowing through the discharge enable to retrieve the dissipated power or the capacitances of the system. One of the advantages of these measurements is that can easily be implemented on a production line to follow possible changes during the process, allowing the creation of feedback control loops during the treatments. In this work, the longtime operation of an atmospheric pressure dielectric barrier discharge (APDBD) in nitrogen is investigated by using electrical diagnostics. The experimental setup is shown in Figure 1a.

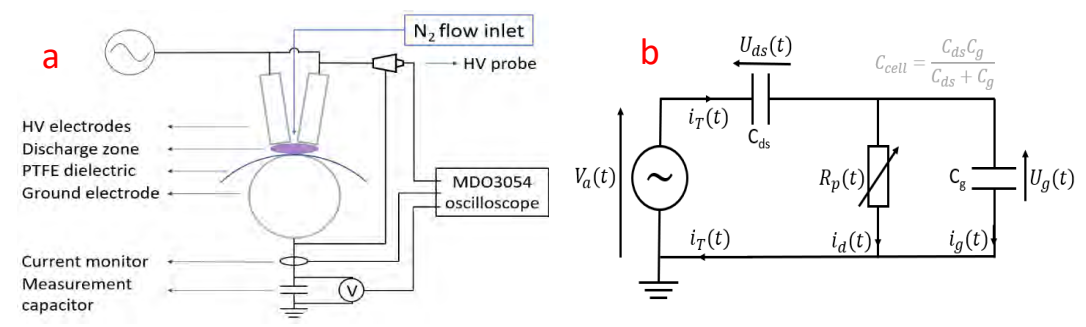


Figure 1 : Schematic of the experimental setup (a) and equivalent circuit of the DBD (b)

The applied voltage, current and charge are acquired in real time during the process. A simple equivalent circuit (Figure 1b) and the Lissajous figures have been used to evaluate the power dissipated, the "effective" gap voltage  $U_g$ , the deposited charge  $Q_0$ , and the capacitances (of the dielectric,  $C_{ds}$ , and of the cell,  $C_{cell}$ ). Modifications of these parameters are followed over one hour of operation. The results highlight no significant change for the dissipated power. However, interesting changes have been observed in the shape of the Lissajous figures, as depicted in Figure 2a. In some conditions, while the discharge operates,  $U_g$  falls over time by 20% and  $Q_0$  is rising by the same percentage. Modification of the slopes of the Lissajous figures have also been observed. While left and right sides slopes do not change over time, they increase with the applied voltage. Hence, the determination of  $C_{ds}$  require particular attention, in agreement with similar observations made by Kriegseis et al<sup>2</sup>.

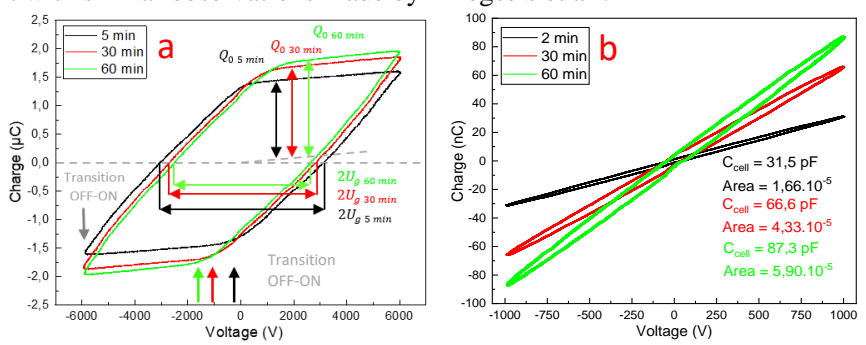


Figure 2: Evolution of the Lissajous figures over time with discharge (a) and without discharge (b)

To investigate modifications of  $C_{cell}$ , measurements without discharge have also been performed over one hour. Examples of the obtained Q-V plots are shown in Figure 2b. Two major observations may be highlighted. First, the area of the figures increases over time. This indicates that the measured electrical "power" in the circuit changes during OFF time from 1.29 mW.cm<sup>-2</sup> to 5.23 mW.cm<sup>-2</sup> (+305%). Second, this increase may be linked with the rise of the cell capacitance, highlighted by the modification of the slope of the Q-V plots. At the beginning,  $C_{cell} = 31.5 \ pF$ , which is close to the calculated theoretical value of  $C_{cell}$  (23.64 pF). After one hour,  $C_{cell}$  reaches 87.3 pF, hence increasing by 177% its initial measured value. Remarkably, the same behavior has been observed for different amplitudes, frequencies, and duty cycles.

All these observations clearly indicate that some physical modifications affect the regime of the discharge in time. Since the applied voltage is the sum of the gap  $(U_g)$  and dielectric voltage  $(U_{ds})$ , the decrease of the effective  $U_g$  (Figure 1a) might be correlated with an increase of  $U_{ds}$ , which directly represents the charge held by the dielectrics. In addition,  $C_{cell}$  is mainly governed by the gas capacitance  $C_g$ , while  $C_{ds}$  has a very small influence on it. To explain the evolution of the  $C_{cell}$  over time, one might make the hypothesis that the capacitance is influenced by its environment, hence the charge accumulation on the dielectrics over time.

In conclusion, long-time operation of an APDBD leads to modifications of the electrical properties of the discharge. Parameters like the capacitances may not be constant over time. Since these parameters are key in the determination of other electrical quantities, their accurate determination is crucial. From an industrial point of view, this means that the surface chemistry of plasma-treated materials is likely to change between the beginning and the end of a procedure that lasts several minutes.

- Tyl, C. et al. Investigation of memory effect in atmospheric pressure dielectric barrier discharge in nitrogen with small oxygen or nitric oxide addition. J. Phys. D. Appl. Phys. 51, 354001 (2018).
- Kriegseis, J. et al. Power consumption, discharge capacitance and light emission as measures for thrust production of dielectric barrier discharge plasma actuators. J. Appl. Phys. 110, 013305 (2011).

# **Contributed C18 - Anne Limburg**

Modelling and diagnostics

# INFLUENCE OF PROBING LASER BEAM AND ELECTRIC FIELD PROPERTIES IN E-FISH MEASUREMENTS

A.A.A. Limburg<sup>1</sup>, R.F.E. Pleijers<sup>1</sup>, Y. Guo<sup>1</sup>, S. Nijdam<sup>1</sup>

Department of Applied Physics, Eindhoven University of Technology, PO box 513, 5600 MB

Eindhoven, The Netherlands

E-mail: a.a.a.limburg@tue.nl

One of the most important parameters of a plasma is its electric field. It defines quantities such as particle transport, gas temperature, electron energy distribution function and creation of energetic particles. Recently, a promising laser-based optical diagnostic technique is introduced for electric field measurements called Electric Field Induced Second-Harmonic generation (E-FISH). In this technique, a pulsed, focused laser beam interacts non-linearly with the ambient electric field in a medium, which results in frequency doubled light. The intensity of these second harmonics (SH) scales quadratically with the electric field. In this way, a polarization resolved electric field distribution can be obtained for (almost) any kind of plasma. Nevertheless, the validity of common assumptions regarding the probing laser beam, most notably the plane-wave approximation (PWA), that are made in previous works by multiple groups, is not yet thoroughly investigated. Preliminary results suggest that neglecting phasematching could lead to a misinterpretation of the results, and thereby inaccurate conclusions. Therefore, the goal of this research is to investigate the validity of these assumptions. This is done based on a fundamental analysis of the physics behind the method. To this end, a numerical and experimental study have been performed on the influence of the properties of the probing laser beam and electric field on the E-FISH signal.

We found that by including phase-matching, not only the magnitude of the electric field, but also its length and distribution start to have a profound effect on the generation of the E-FISH signal. For example, let us consider the influence of the distribution of the electric field. Two different electric field shapes are evaluated, a homogeneous field

$$E_{ext}(z) = \begin{cases} E_0, & \text{for } |z| \le \frac{L}{2} \\ 0, & \text{otherwise,} \end{cases}$$
 (1)

and a semi-homogeneous field

$$E_{ext}(z) = \begin{cases} \frac{1}{2}E_0, & \text{for } -\frac{L}{2} < z \le 0\\ \frac{3}{2}E_0, & \text{for } 0 < z < \frac{L}{2}\\ 0, & \text{otherwise,} \end{cases}$$
 (2)

with  $E_0$  the electric field strength. Both fields have the same length L and integrating the field over its length both results in  $E_0L$ . Only the distribution slightly differs. In Fig. 1a, the evolution of the SH intensity is plotted for two values of the wavevector mismatch  $\Delta k$  and a field length of about two times the coherence length of the laser. A significant difference can be observed in the final SH signal probing the inhomogeneous and homogeneous field for a wavevector mismatch of  $\Delta k = 50$  cm<sup>-1</sup>, which can be explained by a varying absolute phase difference between the induced polarization wave and the SH wave inside the electric field. This results

in a non-linear relation between the magnitude of the electric field at a certain position and the contribution of SH signal to the final intensity at that position. Thus, two fields with the same length and integrated value do not necessarily have to yield the same SH intensity. Moreover, this and other effects related to the properties of the electric field are amplified by focusing the probing beam. This results in the E-FISH signal being unevenly generated along the electric field, which we attribute to the combination of the Gouy phase shift together with the longitudinal intensity profile of the beam. The effect of the Gouy phase shift on the E-FISH signal is most significant for field lengths up to the coherence length. In general, this additional phase shift results in a lower SH intensity for a more focused laser beam, which can be observed in Fig. 1b. Here, the electric field length is equal to the coherence length.

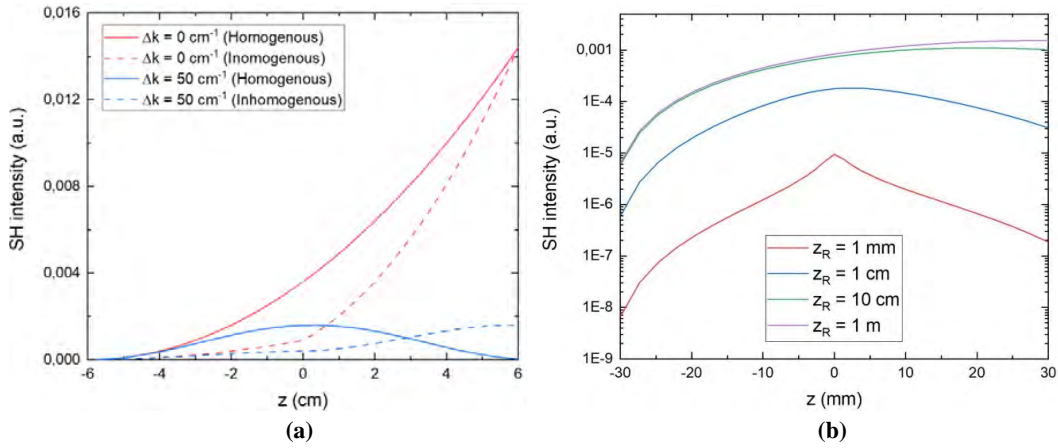


**Fig. 1**: Simulation of the evolution of the SH signal (a) for the PWA inside the electric fields as given in (1) and (2) in and (b) for different Rayleigh lengths  $z_R$  as function of z coordinate within an electric field as given in (1). Since this imposes difficulties for calibration purposes, we conclude that the reduced PWA-based calibration method is not suitable for absolute field measurements. However, the Gaussian beam solution can be a good representation of a focused laser beam used in E-FISH experiments, as is shown in Fig. 2. Parallel plate electrodes are used to generate an electric field.

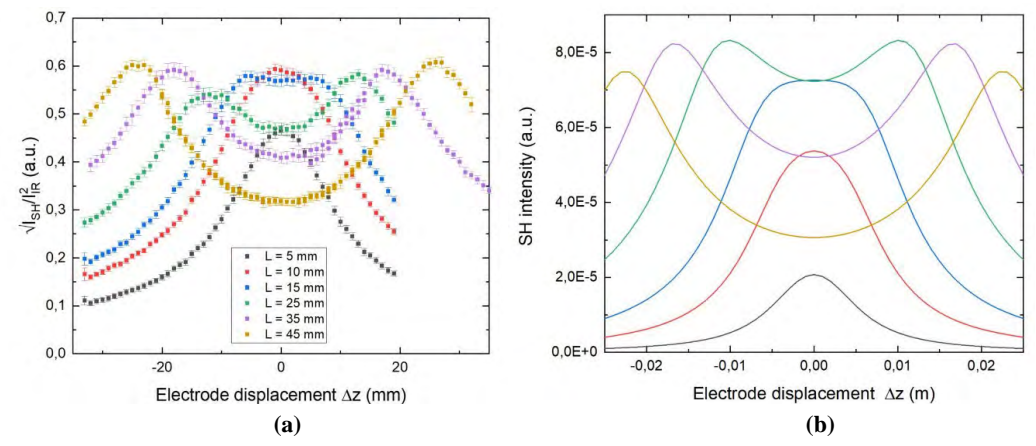


Fig. 2: (a) The measured E-FISH signal and (b) the simulated SH intensity, both as function of the electrode displacement  $\Delta z$  for different electrode widths L. A 200 mm focusing lens and 8 kV high voltage pulses are used. The omission of the influence of the properties of the probing laser beam and the electric field, might have led to incorrect conclusions in previous works. From this research, improvements for future applications of the E-FISH diagnostic can be retrieved.

# Contributed C19 - David Prokop

Modelling and diagnostics

# SPATIOTEMPORAL SPECTROSCOPIC CHARACTERIZATION OF NANOSECOND PULSED VOLUME BARRIER DISCHARGE IN ARGON

<u>David Prokop</u><sup>1</sup>, Lukáš Kusýn<sup>1</sup>, Zdeněk Navrátil<sup>1</sup>, Tomáš Hoder<sup>1</sup>

<sup>1</sup>Department of Physical Electronics, Faculty of Science, Masaryk University, Kotlářská 2, 611 37 Brno, Czech Republic

E-mail: david.prokop@mail.muni.cz

In our work, the main focus was given to the utilization of time-correlated single photon counting (TCSPC) for spatiotemporal spectroscopic characterization of volume barrier discharge in atmospheric pressure argon. Similar investigations were made by Kloc et al. [1] for argon discharge driven by sinusoidal high-voltage waveform. Here, the discharge was produced by applying high-voltage nanosecond pulses to a pair of metallic electrodes, with one electrode covered in aluminum oxide. Using TCSPC measurements we were able to obtain spatiotemporal evolution of different phases of argon discharge, see Fig. 1, namely transition from rapid electron avalanching to streamer to transient glow discharge, which ended with surface discharge upon reaching the lower electrode. From the obtained data we were also able to determine the approximate velocity of a streamer. Motivated by the detailed spectroscopic analysis of the nanosecond pulsed coplanar discharge in argon as done by Simek et al. [2] we increase the temporal resolution of such investigation of selected radiative 2p states (Paschen notation). Using TCSPC with far sub-nanosecond resolution we also measured temporal profiles of line intensities corresponding to these individual states. Furthermore, a detailed electrical characterization was made using an equivalent electrical circuit [3] and the concept of the effective capacity or effective gas gap voltage was analyzed thoroughly.

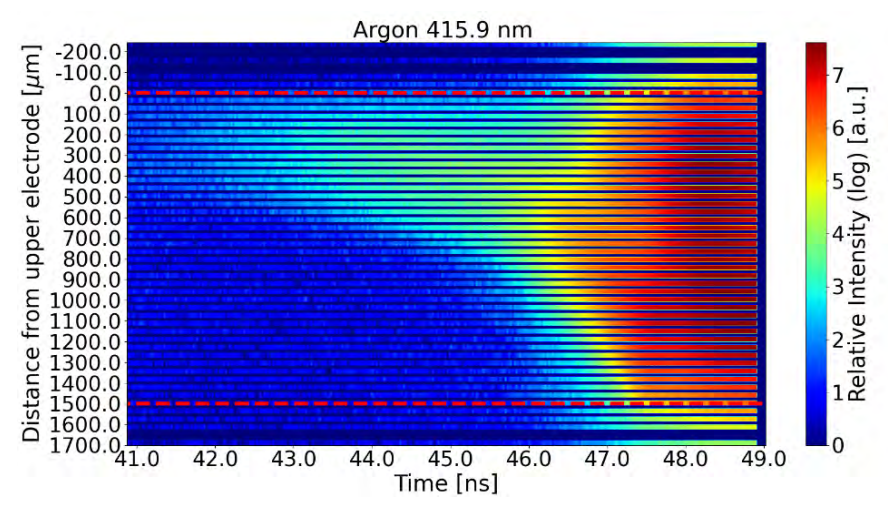


**Fig. 1**: Spatiotemporal TCSPC scan of the 3p<sub>6</sub> radiative state emission focused on the initial phases of the discharge. Red dashed lines highlight the positions of the electrodes.

#### **References:**

- [1] P. Kloc, H-E Wagner, D. Trunec, Z. Navrátil, and G. Fedoseev. "An investigation of dielectric barrier discharge in Ar and Ar/NH3 mixture using cross-correlation spectroscopy." Journal of Physics D 43 (2010): 345205.
- [2] M. Šimek, P.F. Ambrico, T. Hoder, V. Prukner, G. Dilecce, S. De Benedictis and V. Babický. "Nanosecond imaging and emission spectroscopy of argon streamer micro-discharge developing in coplanar surface DBD." Plasma Sources Science and Technology 27 (2018): 055019.
- [3] A. V. Pipa, J. Koskulics, R. Brandenburg and T. Hoder. "The simplest equivalent circuit of a pulsed dielectric barrier discharge and the determination of the gas gap charge transfer." The Review of scientific instruments 83 11 (2012): 115112.

#### **Acknowledgments:**

This work is supported by the Internal Grant Agency of Masaryk University, project no. 1188/202, by Czech Science Foundation project GAČR No. 21-16391S and by project LM2018097 funded by the Ministry of Education, Youth and Sports of the Czech Republic.

# Contributed C20 - Siebe Dijcks

Modelling and diagnostics

# **Corona Imaging**

<u>Siebe Dijcks</u><sup>1</sup>, Lukáš Kusýn<sup>2</sup>, Jesper Janssen<sup>3</sup>, Xiaoran Li<sup>4</sup>, Sander Nijdam<sup>1</sup>

<sup>1</sup>Eindhoven University of Technology, Eindhoven, The Netherlands

<sup>2</sup>Masaryk University, Brno, Czechia

<sup>3</sup>Plasma Matters BV, Eindhoven, The Netherlands

<sup>4</sup>Centrum Wiskunde & Informatica, Amsterdam, The Netherlands

s.j.dijcks@tue.nl

Streamers are a type of discharge which can develop when strong local fields are applied to a gaseous medium. The paths of these growing 'fingers' are paved by a strong space charge layer, locally enhancing the electric field strength and thereby propagating the streamer.

Since streamers are a precursor to short-circuits, they are generally undesirable in high voltage engineering and therefore something to actively avoid. However, their non-equilibrium nature makes them of interest in various gas treatments.

In this research an experiment is developed where streamers can be generated by tunable rectangular voltage pulses (< 50 kV, > 180 ns) applied to opposing disk electrodes inside a discharge vessel (filled with N<sub>2</sub>/Air/CO<sub>2</sub> @ 1-1000 mbar). Active and passive optical diagnostics are applied in tandem with electrical diagnostics to these streamers.

The morphology of the streamer development is studied in detail with stereoscopic and stroboscopic imaging techniques to reconstruct the time resolved in 3D. Regimes of certain voltage, repetition-rate, pressure and gas composition are found where streamers are repetitive and stable. These are compared to 2D streamer models of Afivo from CWI, and show good agreement.

Using the stable repetitive streamers, phase resolved optical emission spectroscopy is performed. From this the emission from the  $N_2[C]$  and  $N_2^+[B]$  species is tracked in space and time, showing the response of the nitrogen containing gas to the strong local electric field of the streamer. Using a Global model in PLASIMO this response is used to model the E/n field of the streamer causing the measured response. This E/n dependency can then be related to the velocity, diameter and potential in the streamer head, giving more tools to morphologically investigate streamer images.

#### Contributed C21 - Markus Becker

Modelling and diagnostics

# COMBINING MODELLING AND EXPERIMENT FOR ADVANCED PLASMA DIAGNOSTICS

Markus M. Becker<sup>1</sup>, Ihda Chaerony Siffa<sup>1</sup>, Torsten Gerling<sup>1</sup>, Hans Höft<sup>1</sup>, Aleksandar P. Jovanović<sup>1</sup>, Lukáš Kusýn<sup>2</sup>, Detlef Loffhagen<sup>1</sup>, Marjan N. Stankov<sup>1</sup>, Tomáš Hoder<sup>2</sup>

<sup>1</sup>Leibniz Institute for Plasma Science and Technology (INP), 17489 Greifswald, DE <sup>2</sup>Department of Physical Electronics, Fac.Sci., Masaryk University, 611 37 Brno, CZ

E-mail: markus.becker@inp-greifswald.de

Plasma modelling has emerged over the last decades as a powerful tool for the fundamental analysis and development of technological applications of non-thermal plasmas. At the same time, measurement methods have also evolved tremendously, offering new opportunities for model validation. This provides the basis for the development of novel diagnostic tools that directly combine measurements and modelling approaches.

The present contribution reports on current activities and recent results of the analysis of transient phenomena in non-thermal atmospheric pressure plasmas, which have been obtained by combining fast current measurements as well as optical diagnostics with different modelling approaches. This includes

- solution of the ion dispersion relation for identification of ion-acoustic waves and ion density determination by means of highly resolved current measurements in a transient spark discharge;
- validation and application of an extended reaction-kinetic argon model for experimental determination of the electric field in a single-filament dielectric barrier discharge (DBD) by spectrally resolved optical measurements of 2p argon levels with sub-ns time resolution;
- fluid-Poisson modelling combined with electrical measurements and iCCD and streakcamera imaging for a detailed understanding of streamer inception, propagation and surface interaction in single-filament DBDs in air-like gas mixtures.

The results show the great potential of close cooperation between experimental laboratories and modelling facilities going far beyond the traditional way of comparing measured data with modelling results. As an example, figure 1 illustrates how current and voltage measurements were combined with modelling results to estimate the pre-ionisation level in pulsed single-filament DBDs for different slopes of the high voltage pulse.

The remaining challenges include systematic verification and validation of the models used as well as reproducibility testing of the measurement results. The establishment of a common database in which measurement and modelling data are seamlessly integrated by means of standardised data formats and metadata can then open up new possibilities for the application of data-driven diagnostic methods.

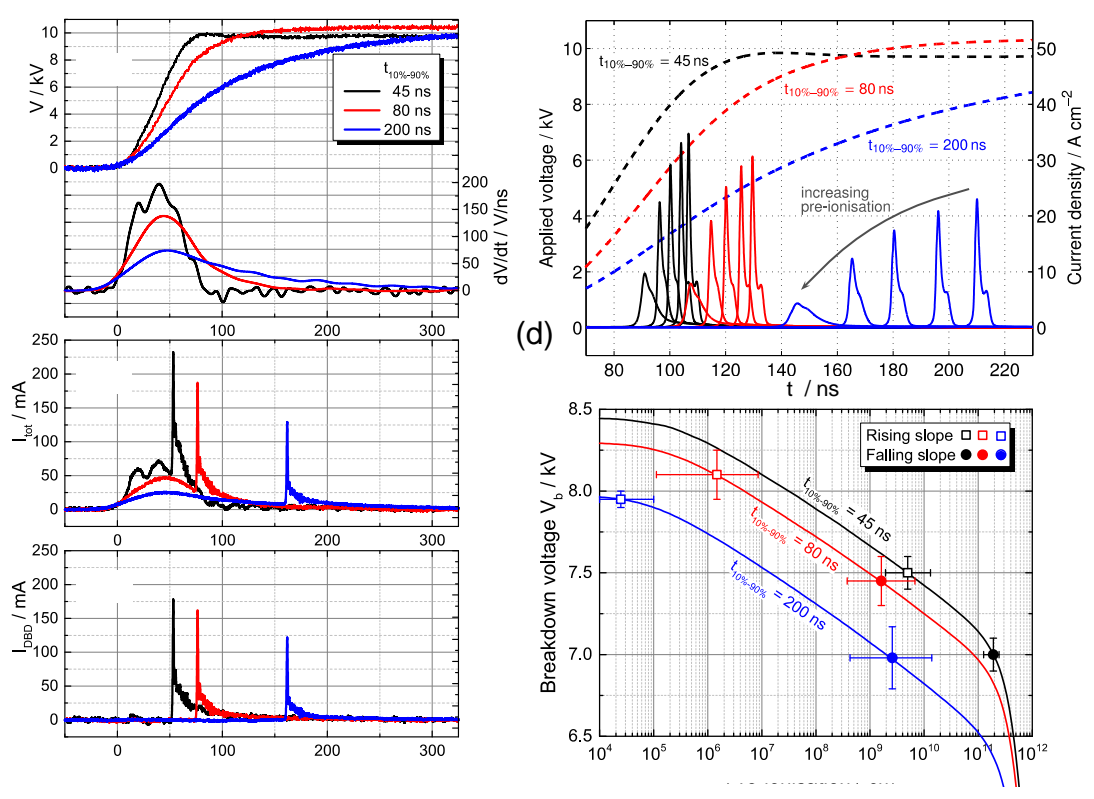


Fig. 1: Analysis of the influence of the slope steepness of the HV pulse on the characteristics of pulsed DBDs in a symmetric single-filament arrangement with 1 mm gas gap and a gas mixture with  $0.1 \text{ vol}\% \text{ O}_2$  in  $N_2$  at atmospheric pressure [1]. The left panel shows measured voltage and current signals for three different voltage slopes, i.e. HV pulse slope and its steepness (a), measured total and discharge current (b,c). The upper right panel (d) represents results of a time-dependent and spatially one-dimensional fluid-Poisson model for different pre-ionisation levels using the measured voltage pulse as input. The lower right panel (e) shows the breakdown voltages predicted by the fluid model in dependence on the pre-ionisation (lines) and measured breakdown voltages (data points). It thus combines measured and calculated data to estimate the pre-ionisation in the DBD arrangement depending on the HV slope.

[1] H. Höft, M. M. Becker, D. Loffhagen and M. Kettlitz, "On the influence of high voltage slope steepness on breakdown and development of pulsed dielectric barrier discharges", *Plasma Sources Sci. Technol.* **25** (2016) 064002.

This work has been partly funded by the German Research Foundation (DFG) – project numbers 368502453, 407462159, 408777255 and 466331904 as well as the Federal Ministry of Education and Research (BMBF) – project number 16QK03A. TH and LK acknowledge the support of the Czech Science Foundation project GAČR No. 21-16391S and project LM2018097 funded by the Ministry of Education, Youth and Sports of the Czech Republic.

#### Contributed C22 - Mohammad Hasani

Modelling and diagnostics

# Charge detection of plasma exposed surfaces using quantum dots photoluminescence

Mohammad Hasani, Guido Klaassen, Zahra Marvi, Job Beckers

Department of Applied Physics, Eindhoven University of Technology, Eindhoven, 5600 MB, The Netherlands

E-mail: m.hasani@tue.nl

Excess charges resting on an electrically floating substrate immersed in a low temperature argon plasma are qualitatively detected by recording time-resolved photoluminescence (PL) spectra of surface deposited quantum dots (QDs). For this purpose, QDs with the size of a few nanometers are excited by a laser and the variations of their PL spectra peak before, during and after plasma exposure are measured. It has been observed that a redshift of the PL peak spectra is generated as a result of local electrical fields induced by electrons residing near the QDs' surfaces, a phenomenon called the Quantum-confined Stark effect (QCSE)<sup>1</sup>. The detected amount of Stark shift – typically 0.04 nm for a collection of QDs on a silicon substrate - is measured using enhanced measurement schemes with better accuracy compared to previous attempts<sup>1</sup>, illustrated in Figure 1 for short plasma exposure of 0.7 s. With these accurate measurements, dependencies between global plasma parameters - such as the gas pressure and the input power - and the amount of Stark shift is pinpointed. Lower amounts of Stark shifts are observed with relatively increasing gas pressures and decreasing input powers. This work demonstrates the possibility of using QDs as in-situ, quantum (nano-)sensors for surface charge.

\_

<sup>&</sup>lt;sup>1</sup> Marvi, Z., Donders, T.J.M., Hasani, M., Klaassen, G. and Beckers, J., 2021. Quantum dot photoluminescence as a versatile probe to visualize the interaction between plasma and nanoparticles on a surface. Applied Physics Letters, 119(25), p.254104.

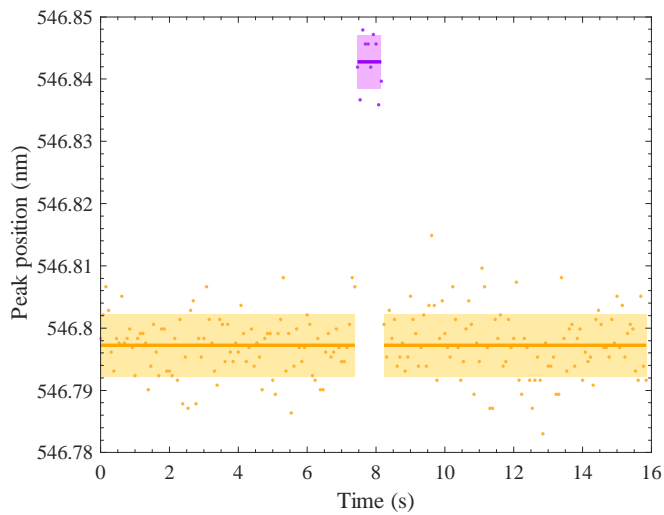


**Fig. 1**: Stark shift measured independently for 0.7 s plasma exposure of an electrically floating surface with QDs deposited on them. For the specific plasma parameters of 40 W (power) and 4 Pa (pressure), the plasma-exposure-caused Stark shift is measured to be 0.046  $\pm 0.001$  nm.

Modelling and diagnostics

# IMPACT OF DIELECTRIC-COVERED ELECTRODE PROXIMITY ON STREAMER PROPAGATION IN PULSED-DRIVEN DIELECTRIC BARRIER DISCHARGES

<u>Hans Höft</u>, Jente R. Wubs, Manfred Kettlitz, Markus M. Becker, Aleksandar P. Jovanović, Klaus-Dieter Weltmann Leibniz Institute for Plasma Science and Technology (INP) Felix-Hausdorff-Straße 2, 17489 Greifswald, Germany

E-mail: hans.hoeft@inp-greifswald.de

Dielectric barrier discharges (DBDs) are a common tool for the generation of non-thermal plasmas at atmospheric pressure [1]. These discharges are filamentary in air-like gas mixtures at atmospheric pressure, i.e. they feature thin constricted channels in the volume. The breakdown mechanism in filamentary DBDs is the so-called cathode-directed streamer, i.e. a fast propagating ionisation front moving from towards the cathode. In most application-relevant cases, the gas gap distances in volume DBDs are in the (sub-)mm range.

For this contribution, the impact of the electrode proximity on the streamer breakdown and development was investigated for pulsed-driven DBDs. They were ignited in a symmetric double-sided, single-filament arrangement [2] using a gas mixture of 0.1 vol% O<sub>2</sub> in N<sub>2</sub> at 0.6 bar and 1.0 bar. Different gas gap distances were selected to change the streamer propagation length in a confined arrangement. This gas gap distance was varied from 0.5 mm to 1.5 mm, while the applied voltage was adapted correspondingly to create comparable breakdown conditions in the gap, i.e. similar values of the reduced electric field strength E/n. Fast electrical measurements provided insight into relevant discharge characteristics such as the transferred charge and consumed energy. The development of the DBDs was recorded by an iCCD and a streak camera system, which enabled sub-ns temporal and  $\mu$ m spatial resolution. In Fig. 1, the side-on recorded 2D emission structure of individual discharge events is shown for the three investigated gas gap distances at 1.0 bar. A constricted discharge channel, which is widened near the anode, and spreading surface discharges on the dielectric are clearly visible.

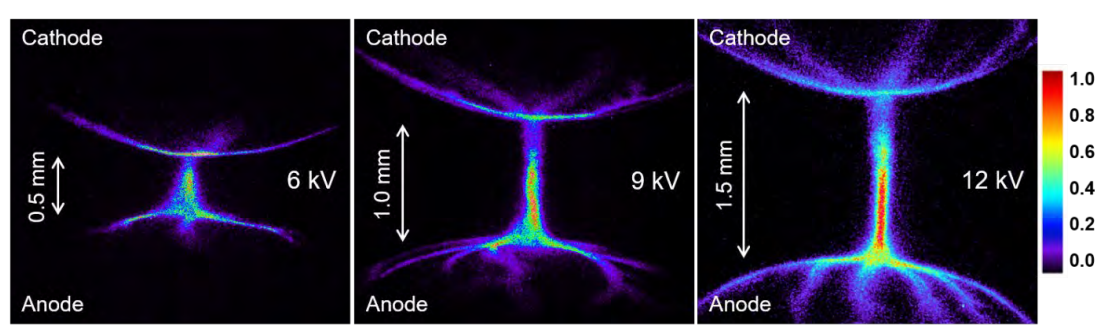


**Fig. 1**: Spectrally-integrated discharge emission structure at rising slopes of the HV pulse for the three investigated gas gap distances at different HV pulse amplitudes recorded by an iCCD camera (gate widths 150 ns). Each image displays a single discharge event at atmospheric pressure.

An analysis of the discharge emission diameter revealed that the widening of the 'footpoint' near the anode (which occurs after the streamer has crossed the gap) depends only on the distance to the anode and not on the gas gap distance.

The streak camera measurements were used to track the propagation of the cathode-directed streamer in the gap. In Fig. 2, the streamer velocities are plotted as a function of the distance to the cathode for all investigated gas gap distances and both used pressures. The results demonstrate that breakdown in a smaller gap is characterised by a slower streamer propagation but a significantly higher acceleration. It can therefore be concluded that the proximity of the cathode has a strong impact on the characteristics of the streamer breakdown. Similar behaviour was found for both pressures. In addition, the maximal streamer velocity, which is reached in front of the cathode, increases with the gap distance.

As an outlook, the streamer propagation phase will be investigated by a time-dependent and spatially 2D fluid-Poisson model using the HV waveforms and the actual single-filament arrangement geometry as input. The plan is to gain more insight into similarities and differences during the propagation phase, focusing on the streamer behaviour as it approaches the dielectric surface when different gas gap distances are used. The upcoming results will be utilised, for example, to examine the streamer acceleration under the influence of the surface in more detail.

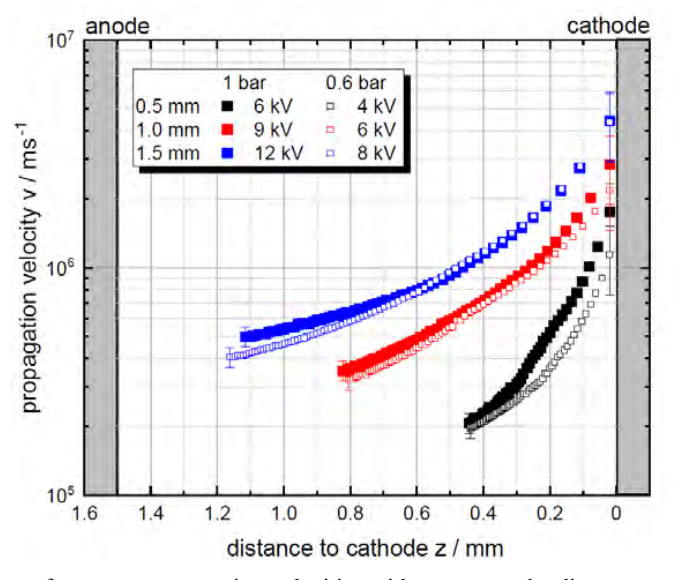


**Fig. 2**: Comparison of streamer propagation velocities with respect to the distance to the cathode, for the three investigated gas gap distances at 1.0 and 0.6 bar.

Additional information can be found in this recently published work [3].

This work was partly funded by the DFG in the framework of the MultiFil project (project number 408777255) and the MAID project (project number 466331904).

- [1] U. Kogelschatz, Plasma Chem. Plasma Process. 23 1-46 (2003)
- [2] M. Kettlitz, H. Höft, T. Hoder, S. Reuter, K.-D. Weltmann, R. Brandenburg, J. Phys. D: Appl. Phys. 45 245201 (2012)
- [3] J. R. Wubs, H. Höft, M. Kettlitz, M. M. Becker, K.-D. Weltmann, *Plasma Sources Sci. Technol.* **31** 035006 (2022)

# Contributed C24 - Hani Francisco

Modelling and diagnostics

# The propagation and chemistry of positive streamers in lightning and sprite discharges at different air densities

Hani Francisco<sup>1,2</sup>, Ute Ebert<sup>1,2</sup>

<sup>1</sup>Multiscale Dynamics, Centrum Wiskunde & Informatica, Amsterdam, The Netherlands <sup>2</sup>Department of Applied Physics, Technische Universiteit Eindhoven, The Netherlands

E-mail: Hani.Francisco@cwi.nl

Streamers are gas discharges that can propagate in an electric field below breakdown because of local field enhancement ahead of its curves space charge layer. They are observed at different altitudes in the atmosphere in the form of sprite discharges and streamer coronas ahead of lightning leaders. These atmospheric phenomena occur at different conditions, but the relation between them can be estimated by similarity laws that describe how the discharges scale with the gas number density.

The idea of streamer scaling follows from the understanding that as long as electrons gain the same kinetic energy between collisions, dynamics governed by electron acceleration and electron-molecule collisions would behave similarly. Townsend scaling describes how to scale the electric field, the time scales, and the length scales to get similar discharge behavior with a different gas number density. For the densities of charged species, there is a scaling law specific for streamers that takes into consideration space charge effects and ionization growth [1].

In [2], photoionization was shown to introduce corrections to the streamer scaling properties at sprite altitudes due to the absence of the quenching of states responsible for photoionizing radiation. We extend this discussion by looking at a greater range of densities and background electric fields and considering other factors that might break the similarity laws at lower densities, such as a different dominating electron attachment reaction. As reported in [3], in gases with low number densities, the electron attachment reaction that dominates in the streamer channel is the two-body attachment reaction to oxygen. The three-body attachment reaction, which dominates in high density gases, is suppressed.

Our investigation is relevant in the study of gas chemistry, as these streamers at different altitudes can have different effects on the chemical composition of the gas they propagate in. Oxidant and NO<sub>x</sub> production of lightning has been reported in [4] and [5] respectively, which reveals how atmospheric electricity plays a role in changing the chemical composition of the atmosphere. We investigate this further by considering greenhouse gases in the atmosphere and analyzing how their concentrations are affected by streamer discharges.

- [1] S. Nijdam, J. Teunissen, U. Ebert Plasma Sources Sci. Technol. 29 (2020) 103001.
- [2] N. Liu, V.P. Pasko J. Geopys. Res. 109 (2004) A04301.
- [3] A. Luque, F.J. Gordillo-Vázquez Nat. Geosci. 5 (2012) 22-25.
- [4] W.H. Brune et al. Science **372** (2021) 711-715.

[5] V. Cooray, M. Rahman, V. Rakov J. Atmos. Sol.-Terr Phys. **71** (2009) 1877-1889.

# Contributed C25 - Thijs van der Gaag

Modelling and diagnostics

# EEDF measurement of cold atmospheric-pressure plasma by OES

Thijs van der Gaag, Hiroshi Akatsuka
Tokyo Institute of Technology, 2-12-1-N1-10, Ookayama, Meguro-ku, Tokyo 152-8550 Japan
E-mail: <a href="mailto:van.t.ab@m.titech.ac.ip">van.t.ab@m.titech.ac.ip</a>

Cold atmospheric-pressure plasma (CAPP) applications have become numerous and diverse. The appeal of these non-thermal plasmas has been noticed by various fields such as medicine, agriculture and other industries. Describing the behavior of these CAPP discharges is a complicated and not fully discovered problem. Multiple molecular species, multiple phases, applications that have to satisfy medical safety regulations make it difficult to accurately predict the plasma state. Through elaborate empirical study, the behavior of CAPP can be mapped. This approach can support the studied application at hand, but the results do not necessarily provide any insight beyond that. In order to increase our understanding of the processes that happen inside a CAPP, fundamental plasma diagnostics study is required<sup>1)</sup>.

CAPP discharges are in thermal non-equilibrium, meaning that the electron temperature can be several 10,000 K while the gas temperature remains around room temperature. Being the highly energetic particles in CAPP, the electrons are mainly responsible for causing the desired effect in a plasma application. This can be direct electron collision with the target or the generation of a certain concentration of a reactive species within the plasma. As such, the state of the electron population is heavily tied to the application characteristics. Usually, an electron-involving reaction requires an electron with a certain threshold electron energy  $E_{th}$  or a higher energy. For calculation of this reaction rate, the electron energy distribution function (EEDF) should be known to statistically determine how many electrons have an energy  $E_{th}$ . Common practice in low-pressure plasma diagnostics is to estimate the usage of electron temperature  $T_e$  and electron number density  $n_e$  as a summary of the electron energy distribution. Then, by assuming a distribution model such as the Maxwell distribution  $\sim \exp\left(-\frac{E}{kT_e}\right)$  or less frequently used Druyvesteyn distribution  $\sim \exp\left(-\frac{E}{kT_e}\right)^2$ , the EEDF can be created from  $T_e$  and  $n_e$ . For low-pressure plasmas, the validity of these distributions has been thoroughly investigated. This is not the case for CAPP due to its shorter history, making the accuracy of

and  $n_e$ . For low-pressure plasmas, the validity of these distributions has been thoroughly investigated. This is not the case for CAPP due to its shorter history, making the accuracy of these EEDF models unknown. Instead, direct measurement of the arbitrary EEDF should be considered. This is not a trivial task for CAPP since conventional EEDF measurement techniques such as probe measurement and Thomson scattering are not available through theoretical or practical difficulties.

In this work, a CAPP electron diagnostics tool will be presented that is capable of determining arbitrary EEDF from optical emission spectroscopy (OES) measurement<sup>2)</sup>. For this, the continuum emission part of the spectrum is used. In the generally weakly ionized CAPP, the continuum spectrum is dominated by electron-neutral bremsstrahlung emission<sup>1)</sup>. The neutral bremsstrahlung emissivity is related to the EEDF through equation (1). Here  $\varepsilon_{ea}(hv)$ , f(E) and R(hv, E) are the electron-neutral bremsstrahlung emissivity, EEDF and kernel function

respectively with variables electron energy E and photon energy  $h\nu$  both with unit electronvolt. For the evaluation of the kernel function is shown in equation (2), only the electron-neutral momentum-transfer cross section  $Q_{ea}^{mom}(E)$  is required, which is readily available in low-temperature plasma database vs.

$$\varepsilon_{ea}(h\nu) = \int_{h\nu}^{\infty} R(h\nu, E) f(E) dE \tag{1}$$

$$R(h\nu, E) = \frac{2\sqrt{2}}{3\pi^2} \cdot \frac{\alpha n_e n_a}{hc^3 m_e^{3/2}} (h\nu)^2 \left( E - \frac{h\nu}{2} \right) \sqrt{E - h\nu} \cdot Q_{ea}^{mom}(E)$$
 (2)

To obtain the EEDF from the continuum spectrum, integral equation (1) has to be inverted. Since only a limited part of the continuum spectrum can be measured, the input data to invert this integral is incomplete. Because of this, a machine learning method has to be used, which can obtain a partial EEDF by reconstructing the continuum spectrum to closely fit the experimental continuum through EEDF simulation. The visible OES spectrum of 800-300 nm corresponds to 1.5-4 eV photon energy, which roughly allows the determination of the EEDF in the 1.5-4 eV electron energy region. The 4-20 eV EEDF section can be determined, but has to be assumed a straight line in a semilogarithmic plot.

Figure 1 shows the resulting partial EEPF (electron energy probability function = EEDF/ $\sqrt{E}$ ). The input for these results is the spectrum shown in figure 2. The best fit obtained by the machine learning method is almost identical to the measured continuum spectrum. The EEPF shown in figure 1 is clearly deviating from a Maxwell EEPF. The dip observed in the EEPF around 2.3 eV is often contributed to vibrational transitions of N2 contamination.

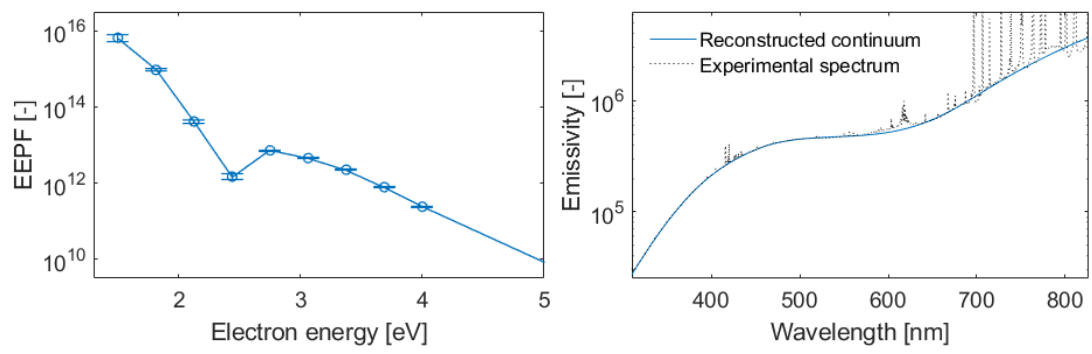


Fig. 1: Arbitrary EEPF reconstructed from an OES Fig. 2: OES measurement of a CAPP argon DBD measurement. Its range is from 1.5-4 eV with a single datapoint at 20 eV.

plasma and the reconstructed continuum spectrum corresponding to the EEPF shown in figure 1.

Determination of arbitrary EEDF in CAPP is difficult with existing diagnostics method. The new method presented here gives the opportunity to obtain a partial EEDF from simple OES measurement in CAPP, making it highly accessible for CAPP application developers.

#### References

- 1) S. Park, W. Choe, S. Y. Moon and S. J. Yoo, Adv. Phys. X 4, 1526114 (2019).
- 2) T. van der Gaag, H. Onishi and H. Akatsuka, Phys. Plasmas 28, 33511 (2021).

#### Contributed C26 - Davide Del Cont-Bernard

Modelling and diagnostics

16<sup>th</sup> High Pressure Low Temperature Plasma Chemistry Symposium

# DEVELOPMENT OF THE EFISH TECHNIQUE FOR ELECTRIC FIELD MEASUREMENTS IN NANOSECOND REPETITIVELY PULSED DISCHARGES

Davide Del Cont-Bernard<sup>1</sup>, Deanna A. Lacoste<sup>1</sup>

<sup>1</sup>King Abdullah University of Science and Technology (KAUST), Clean Combustion Research Center, Thuwal 23955-6900, Saudi Arabia

E-mail: davide.delcontbernard@kaust.edu.sa

The Electric-Field Induced Second-Harmonic generation (EFISH) technique gained considerable popularity in the past five years for electron field measurements [1]. In this work, we apply this diagnostic technique to the study of nanosecond repetitively pulsed (NRP) discharges in a plasma-assisted flame. Indeed, recent works have shown the potential of NRP discharges for combustion-related applications [2], such as enhancing ignition, stabilizing combustion, and promoting deflagration-to-detonation transition, fully justifying fundamental studies to unravel the effects of the plasma on the combustion chemistry. The electric field plays a key role in determining plasma properties, and its characterization is needed for a quantitative description of the plasma. Interestingly, the short time and spatial scales of the phenomenon, the complex dynamics of spatial charges, and the inhomogeneity of the medium posed a combination of novel challenges for an EFISH measurement.

The plasma-assisted burner consists of a wall-stabilized axially symmetric methane-air flame. On the centerline of the burner, two electrodes are used to generate the NRP discharges across the flame. Plasma develops in both the fresh and burned gases (Fig. 1a). A conventional EFISH experimental setup is used. A picosecond Nd:YAG laser generates a beam at 1064 nm that is focused on the region of interest. The second harmonic signal is collected with a photomultiplier. Scanning in both time and space allows us to obtain spatially and time-resolved data.

A fact often overlooked in most previous works on EFISH is that the signal builds up non-linearly along the laser beam [3]. Point measurements are objectively not feasible in conventional EFISH setups. A novel deconvolution-like procedure is proposed to overcome this limitation and obtain calibrated and spatially resolved data. A combined numerical and experimental approach is used in this part.

The proposed deconvolution procedure requires a preliminary characterization of the EFISH generation process using known electric fields. Known electric fields are also used to validate the overall procedure.

A key observation is that higher transverse modes in the laser beam can lead to poor results if the EFISH generation model only accounts for a Gaussian TEM 00 mode.

Considering higher modes in the calculation could lead to better results; however, determining them and accounting for them is challenging.

Despite the mentioned challenges, space and time-resolved measurements of the electric field in the plasma-assisted burner are also presented, showing interesting and reasonable space charge dynamics but lower than expected electric fields (Fig. 1b). Results are discussed in light of the limitations in the EFISH generation process and in the EFISH deconvolution procedure. Based on the results, recommendations for future EFISH measurements are provided. The work on the EFISH methodology has broad validity, and it can be readily exported to potentially improve any (conventional) EFISH measurements.

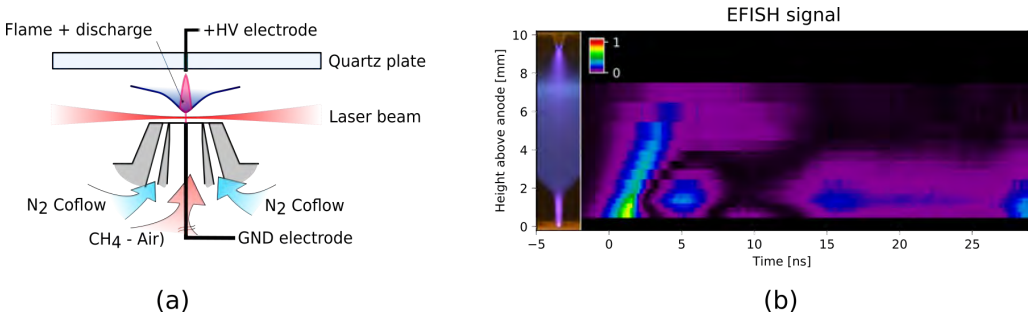


**Fig. 1**: (a) The plasma-assisted burner considered in this study. (b) Sample results of space- and time-resolved EFISH map during a discharge.

- [1] Dogariu, Arthur, et al. "Species-independent femtosecond localized electric field measurement." Physical Review Applied 7.2 (2017): 024024.
- [2] Ju, Yiguang, and Wenting Sun. "Plasma assisted combustion: Dynamics and chemistry." Progress in Energy and Combustion Science 48 (2015): 21-83.
- [3] Chng, Tat Loon, Svetlana M. Starikovskaia, and Marie-Claire Schanne-Klein. "Electric field measurements in plasmas: how focusing strongly distorts the E-FISH signal." Plasma Sources Science and Technology 29.12 (2020): 125002.

#### Contributed C27 - Francisco Pontiga

Modelling and diagnostics

### DISTRIBUTION OF NEUTRAL SPECIES IN A CORONA DISCHARGE: EFFECT OF THE ELECTROHYDRODYNAMIC GAS MOTION

M. R. Bouazza<sup>1</sup>, M. Bouadi<sup>1</sup>, A. Chelih<sup>1</sup>, K. Yanallah<sup>1</sup>, <u>F. Pontiga</u><sup>2</sup>, P. Vázquez<sup>3</sup>

<sup>1</sup>Laboratoire de Génie Electrique et des Plasmas, University of Tiaret, Tiaret, Algeria

<sup>2</sup>Departamento de Física Aplicada II, Universidad de Sevilla, Sevilla, Spain

<sup>3</sup>Departamento de Física Aplicada I, Universidad de Sevilla, Sevilla, Spain

E-mail: pontiga@us.es

In a corona discharge, inelastic collisions of electrons with neutral molecules lead to a rich plasma chemistry that generates positive and negative ions, short-lived radicals, and new neutral molecules. Charged species migrate towards the electrodes under the action of the electric field, exchanging momentum with the neutral molecules through collisions. This exchange of momentum generates an electrohydrodynamic (EHD) force [1], which sets the fluid in motion. The EHD flow thus generated is frequently called electric wind, or ionic wind, and may have a strong influence on the spatial distribution of neutral species and radicals, although it is frequently omitted due to its intrinsic complexity.

This work presents a comparative study of positive and negative corona discharge in air, in which the EHD flow generated by the electrical discharge is considered. The corona discharge is assumed to be generated by a thin wire of radius  $100 \,\mu m$  lodged between two plates. The wire and the plates are parallel to each other, and the distance between the wire and the plates is  $0.5 \, \text{cm}$ . The lower plate acts as the grounding electrode, while the upper plate is a dielectric, and its only purpose is to confine the flow. Air is fed into the corona reactor with inlet air velocity  $2.5 \, \text{cm/s}$  parallel to the plates and perpendicular to the wire. In addition to  $N_2$  and  $O_2$ , the plasma chemical model of the corona discharge includes electrons and 8 neutral species  $(O, N, O_3, NO, NO_2, NO_3, N_2O, N_2O_5)$ , and  $24 \, \text{reactions}$ .

Assuming a fluid modelling and a stationary corona discharge, the equations governing the spatial distribution of species can be written as

$$\nabla \cdot (N_i \mathbf{V} - D_i \nabla N_i) = S_i, \tag{1}$$

where  $N_j$  is the number density of the neutral species j,  $D_j$  its diffusion coefficient, and  $S_j$  its gain/loss rate, and V the gas velocity. Since the EHD flow induced by the corona discharge is turbulent, the gas velocity must be obtained by solving the Reynolds-averaged Navier-Stokes equations,

$$\rho(\mathbf{V}\cdot\nabla)\mathbf{V} = -\nabla P + \lambda\nabla^2\mathbf{V} + \nabla\cdot\mathbf{\tau}_R + \mathbf{F},$$
(2)

$$\nabla \cdot \mathbf{V} = 0. \tag{3}$$

where  $\rho$  is the dynamic viscosity, **V** is the time-averaged gas velocity, *P* is the time-averaged gas pressure,  $\lambda$  is the dynamic viscosity,  $\tau_R$  is the Reynolds stress tensor, and **F** is the EHD force density, which will be approximated by means of an semi-analytical expression derived in previous works [2].

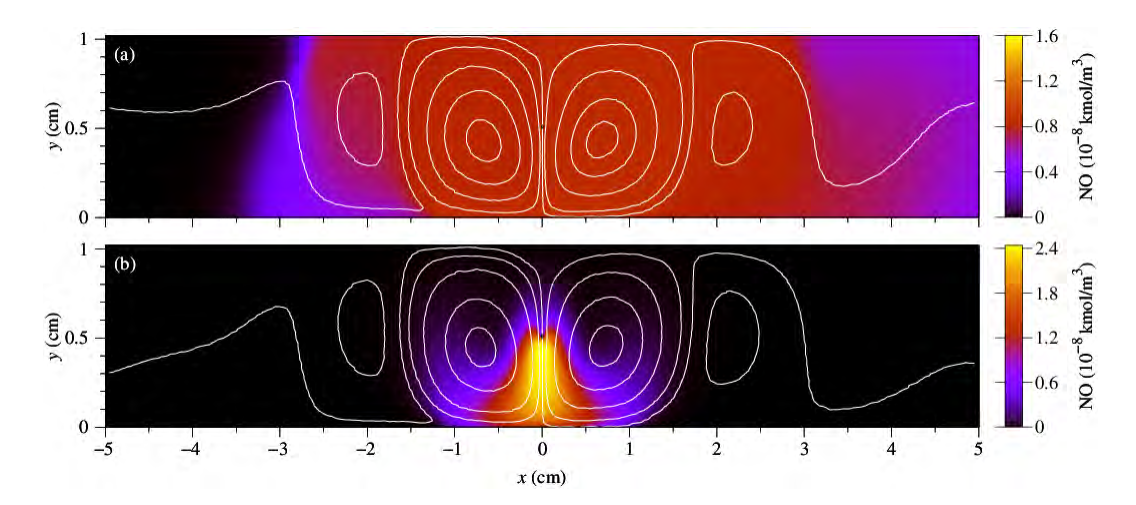


Fig. 1: Streamlines and 2D spatial distribution of nitric oxide inside the reactor in (a) positive corona, and (b) negative corona. The wire is subjected to +9 kV (positive corona) or -9 kV (negative corona).

Figure 1 shows an example of how the polarity of the corona discharge and the EHD motion of the gas can drastically affect the spatial distribution of some species, such as the case of nitric oxide. In the active zone of the corona discharge (i.e., the zone of higher electron density), N and O are generated by electronic dissociation of N2 and O2, and these atomic species constitute the raw material for the formation of nitric oxide  $(N + O_2 \rightarrow NO + O)$  and ozone  $(O + O_2 + M \rightarrow O_3 + M)$ . While in the positive corona the active zone is very close to the wire, in the negative corona it is separated from the wire by several hundred microns and has a greater spatial extension. As a result, the ozone density in the negative corona discharge is several orders of magnitude higher than in the positive corona. Since NO is also destroyed in the active zone by recombining with atomic nitrogen (NO + N  $\rightarrow$  N<sub>2</sub>O), it tends towards an equilibrium concentration of the order of 10<sup>-8</sup> kmol/m<sup>3</sup>. However, as NO leaves the active zone by the effect of the EHD gas motion, its oxidation with ozone (NO + O<sub>3</sub>  $\rightarrow$  NO<sub>2</sub> + O<sub>2</sub>) contributes to its decomposition. In the positive corona, owing to the low concentration of O<sub>3</sub>, the lifetime of NO is relatively long (~ seconds), and the action of the EHD motion contributes to homogenizing its spatial distribution (Fig. 1a). In contrast, in the negative corona, the lifetime of NO is of the order of milliseconds and, thus, this species can only travel a few millimeters before being oxidized by O<sub>3</sub>. Consequently, its spatial distribution is highly localized inside the corona reactor, as shown in Fig. 1b.

#### References

- [1] J. P. Boeuf, L. C. Pitchford, J. Appl. Phys., 97, 103307 (2005).
- [2] M. R. Bouazza, K. Yanallah, F. Pontiga, J. H. Chen, J. Electrost., 92 54-65 (2018).

#### Acknowledgements

This work has been partially supported by the Spanish Government Agency "Ministerio de Ciencia, Innovación y Universidades" and the European Regional Development Fund, under contract PGC2018-099217-B-I00.

Miscellaneous

### LIQUID DISPLACEMENT BY ATMOSPHERIC PRESSURE PLASMA IN A MICROGAP

<u>Lucia Kuthanová<sup>1</sup></u>, Ján Tungli<sup>1</sup>, Zdeněk Bonaventura<sup>1</sup>, Tomáš Hoder<sup>1</sup>

<sup>1</sup>Department of Physical Electronics, Faculty of Science, Masaryk University, Kotlářská 2,
611 37 Brno, Czech Republic

E-mail: nanai@mail.muni.cz

The liquid droplet put into a confined micro-gap and surrounded by plasma undergoes a thermally induced interfacial instability, stretches its interface and displaces its mass via a viscous fingering process [1, 2]. We map the whole process, which can be very dynamic, via evaluation of multiple visual parameters extracted from the video recordings as well as synchronized temporally resolved electrical measurements. The influence of droplet viscosity, size and applied voltage is evaluated.

The number and size of plasmatic fingers point to the initial perturbation wavelength. The length of evolving fingers and complexity of the produced pattern increase with different rate. We quantify the temporal development of the plasma-liquid interface length and its acceleration and describe the lateral effective force responsible for the interface stretch. The amount of liquid mass displaced out of the original droplet region is determined as another important global parameter. In order to understand the causes of the liquid mass displacement we study the local properties at the plasma-liquid interface via quantified local power density dissipated in plasma and synchronize it with the above mentioned global parameters. We focus on the power density distributions at the base and at the head of the advancing plasmatic finger. The heat exchange in the system is simulated and the results are compared with the experiment.

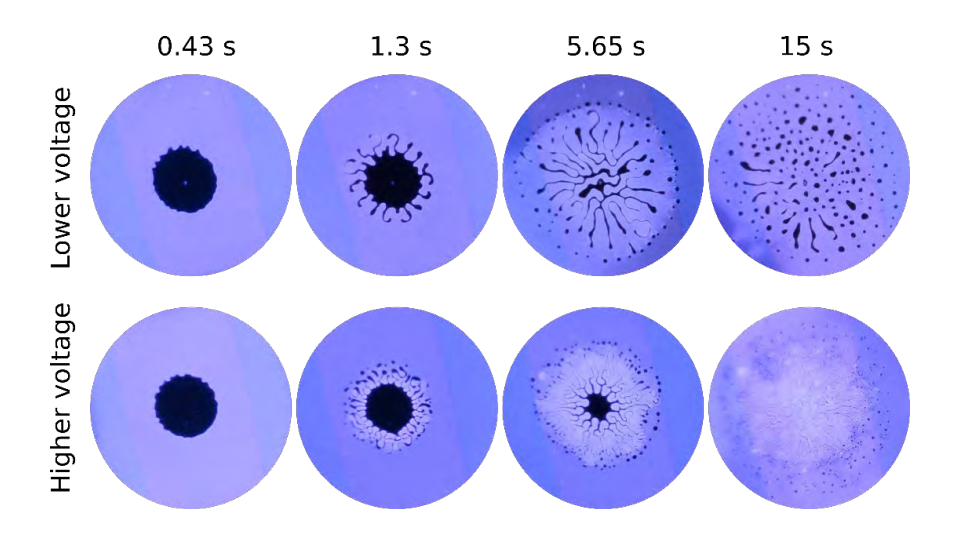


Fig. 1: Two examples of the oil droplet evolution under influence of DBD plasma.

#### **References:**

- [1] Lucia Potočňáková, Petr Synek, and Tomáš Hoder, Phys. Rev. E 101 063201 (2020).
- [2] Shang-Yan Hou and Hong-Yu Chu, *Phys. Rev. E* 92, 013101 (2015).

#### **Acknowledgments:**

This work has been supported by the project LM2018097 funded by Ministry of Education, Youth and Sports of the Czech Republic.

#### Contributed C29 - Yury Gorbanev

Molecular synthesis and decomposition

### PULSED PLASMA JET FOR NITROGEN FIXATION: FUNDAMENTALS AND PROSPECTIVE TECHNOLOGIES

Yury Gorbanev<sup>1</sup>, Elise Vervloessem<sup>1,2</sup>, Lander Hollevoet<sup>3</sup>, Anton Nikiforov<sup>2</sup>, Nathalie De Geyter<sup>2</sup>, Johan Martens<sup>3</sup>, Annemie Bogaerts<sup>1</sup>

<sup>1</sup>Research group PLASMANT, Department of Chemistry, University of Antwerp, 2610 Wilrijk, Belgium

<sup>2</sup>Research Unit Plasma Technology (RUPT), Department of Applied Physics, Faculty of Engineering and Architecture, Ghent University, 9000 Ghent, Belgium

<sup>3</sup>Center for Surface Chemistry and Catalysis: Characterization and Application Team, KU Leuven, 3001 Leuven, Belgium

E-mail: yury.gorbanev@uantwerpen.be

Nitrogen is one of the main elements in agricultural fertilisers, required to meet the increasing world food demand. Converting the chemically inert atmospheric N<sub>2</sub> into chemically accessible nitrogen is one of the utmost important tasks of chemical industry. However, industrial nitrogen fixation remains unsustainable due to non-mild and non-environmentally benign operating conditions, high energy demand, and the need for centralised production. Among the proposed greener substitutes, plasma-based N<sub>2</sub> fixation is of high interest due to the flexibility of its use and synergy with sustainable energy sources, i.e. renewable electricity [1,2]. Here, we demonstrate the use of a pulsed non-equilibrium plasma jet for nitrogen fixation.

Plasma is a promising tool for catalyst-free and H<sub>2</sub>-free NH<sub>3</sub> synthesis via interacting with the plasma-exposed H<sub>2</sub>O. The use of H<sub>2</sub>O as a source of hydrogen enables a facile one-step synthetic route. However, the interaction of plasma with liquid H<sub>2</sub>O largely remains unclear due to the complexity of plasma-liquid systems [1]. In our work, we for the first time, investigated the generation of NH<sub>3</sub> in liquid H<sub>2</sub>O exposed to a pulsed plasma jet fed with an N<sub>2</sub> feed gas saturated with H<sub>2</sub>O vapour (Fig. 1). Using isotopically labelled water and varying the amounts of gaseous water in the feed gas, we discovered that the contribution of the gas-phase H<sub>2</sub>O is dominating in the production of NH<sub>3</sub>, while the liquid serves mostly to accumulate the product [3].

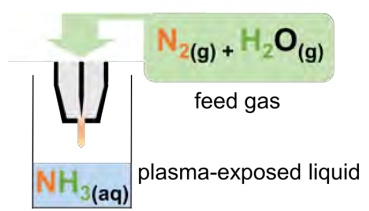


Fig. 1: Nitrogen fixation via reduction of N<sub>2</sub> to NH<sub>3</sub>: catalyst- and hydrogen-free ammonia production with H<sub>2</sub>O vapour.

Besides reduction to  $NH_3$ , nitrogen oxidation to  $NO_x$  is also an attractive route to making nitrogen accessible for agriculture in the form of nitrate salts. Nitrogen oxidation to  $NO_x$  by plasma has been under investigation since the first applications of the Birkeland-Eyde process. To date, various plasma setups have been investigated for nitrogen oxidation, from dielectric barrier discharges to electrodeless microwave plasma [1,4].

However, to meet the techno-economic requirements and to gain a feasible industrial potential, the plasma-based process must have a very low energy consumption (EC) [2]. Our pulsed plasma jet exhibited a very low EC for  $NO_x$  generation, close to the thermodynamic limit – ca. 0.4 MJ/mol. To elucidate the mechanisms leading to this unprecedentedly low value, we performed electrical and optical analysis of the plasma jet. Further, by developing a chemical kinetic model of a pulsed plasma, we demonstrated that the plasma power and the corresponding gas temperature are the reason for the very low EC: they provide a strong vibrational-translational non-equilibrium and promote the non-thermal Zeldovich mechanism reactions in a delicate way (Fig. 2). The exact pulse and interpulse times are critical for finding a balance between the drop in temperature and the fraction of gas treated by the plasma [5].

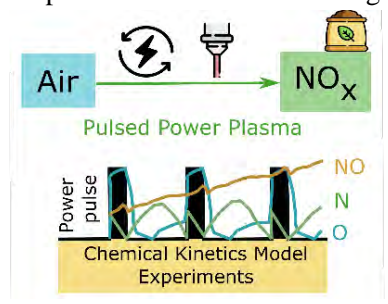


Fig. 2: Nitrogen fixation via oxidation of  $N_2$  to  $NO_x$  using a pulsed plasma jet: chemical kinetic modelling helps elucidate the low energy consumption.

Finally, we show that by using a process which combines the  $NO_x$  production by plasma with subsequent  $NO_x$  capturing and catalytic reduction [6], a highly energy-efficient  $NH_3$  production can be achieved (Fig. 3). This demonstrates direct applicability of the pulsed plasma to both  $NO_x$  and  $NH_3$  production, and paves the way to decentralised nitrogen fixation.

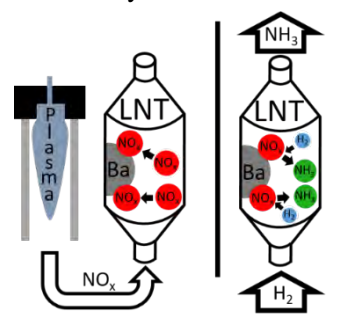


Fig. 3: Plasma N<sub>2</sub> oxidation to NO<sub>x</sub> with subsequent NO<sub>x</sub> trapping and catalytic reduction.

- [1] Winter, L.R.; Chen, J.G., Joule 2021, 5, 300-315.
- [2] Rouwenhorst, K.H.R.; Jardali, F.; Bogaerts, A.; Lefferts, L., *Energy Environ. Sci.* **2021**, 14, 2520-2534.
- [3] Gorbanev, Y.; Vervloessem, E.; Nikiforov, A.; Bogaerts, A., ACS Sustain. Chem. Eng. 2020, 8, 2996-3004.
- [4] Kelly, S.; Bogaerts, A., Joule **2021**, 5, 3006-3030.
- [5] Vervloessem, E.; Gorbanev, Y.; Nikiforov, A.; De Geyter, N.; Bogaerts, A., *Green Chem.* **2022**, 24, 916-929.
- [6] Hollevoet, L.; Jardali, F.; Gorbanev, Y.; Creel, J.; Bogaerts, A.; Martens, J.A., *Angew. Chem. Int. Ed.* **2020**, 59, 23825-23829.

#### Contributed C30 - Ursel Fantz

Molecular synthesis and decomposition

# Enhancement of CO<sub>2</sub> conversion at atmospheric pressure by influencing the gas quenching in the effluent of a microwave plasma torch

A. Hecimovic, <u>U. Fantz</u>, R. Antunes, C. Kiefer, A. Meindl *Max-Planck-Institut für Plasmaphysik, Boltzmannstr.* 2, 85748 *Garching, Germany* 

E-mail: ursel.fantz@ipp.mpg.de

Conversion of CO<sub>2</sub> into the value-added chemical CO by plasmas is an alternative approach to the electrochemical and photochemical technologies. Microwave-generated plasmas are among the plasma reactors with the highest energy efficiencies, when operating at reduced pressure (typically 100 to 200 mbar) [1]. At atmospheric pressure, the figures of merit like energy efficiency and conversion are reduced, with typical values of about 25% for energy efficiency and about 10% conversion. Here, the dominant thermal dissociation at temperatures of about 6000 K is limited by the backward reactions, i.e. recombination of CO with oxygen into CO<sub>2</sub>. This limitation can be overcome by fast cooling, which means fostering fast recombination of oxygen atoms (ideal quenching) and/or production of CO via collisions of CO<sub>2</sub> and oxygen atoms (super-ideal quenching).

The microwave torch (2.45 GHz) is operated in a vortex configuration using tangential gas inlets (up to 100 slm) from the bottom as indicated in Figure 1(a). The transition from the diffuse to the contracted regime is taking place at 150 mbar, such that at higher pressures the gas temperature and the vibrational temperature are in equilibrium at around 6000 K [2]. A method to promote both the gas mixing and gas quenching is the introduction of a nozzle at the top of the microwave resonator which enhances the performance of the microwave torch at pressures above 200 mbar, as shown in Figure 1(b) [3]. At atmospheric pressure and low gas flows of 10 slm, the conversion increases by a factor of 3.5 to 35% at an energy efficiency of 20%, whereas an energy efficiency of 42% could be achieved at 10% conversion and thus being comparable to the operation in the reduced pressure regime.

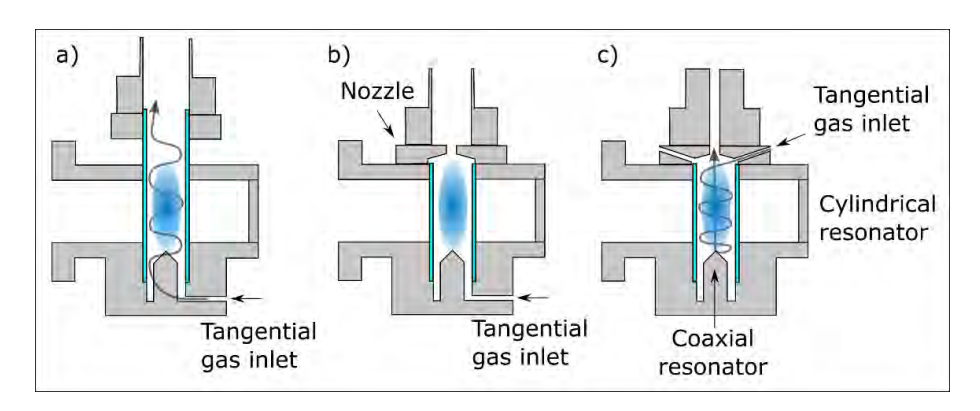


**Fig. 1**: Schematic of the experimental setup showing the plasma torch (comprising a coaxial and a cylindrical resonator) in the standard configuration (a), with the nozzle mounted on the resonator (b), and the configuration for the reversed vortex flow (c).

Changing the gas flow to a reversed vortex configuration with a cooled narrow channel towards the effluent (Figure 1(c)), yields similar performances to the nozzle configuration but enlarges the stable operation regime of the plasma torch at atmospheric pressure, meaning that a higher microwave power can be coupled into the plasma.

The results indicate that both configurations rely on the positive effect of fast gas quenching, thus preventing the recombination of CO and retaining the high CO<sub>2</sub> conversion values. The operation of the plasma torch at atmospheric pressure with performances comparable to those that have up to this point only ever been achieved during low pressure operation, is an important step towards industrial applicability of this technology.

- [1] R. Snoeckx and A. Bogaerts, Chem. Soc. Rev. 46 (2017) 5805.
- [2] F.A. D'Isa, E.A.D. Carbone, A. Hecimovic and U. Fantz, Plasma Sources Sci. Technol. 29 (2020) 105009.
- [3] A. Hecimovic, F.A. D'Isa, E. Carbone, U. Fantz, Journal of CO2 Utilization 57 (2022) 101870.

#### Contributed C31 - Mostafa Elsayed Hassan

Molecular synthesis and decomposition

### THE ROLE OF GAS-WATER INTERFACE SIZE ON SOLVATION OF GASEOUS SPECIES TO WATER

Mostafa Elsayed Hassan, Mário Janda, and Zdenko Machala Division of Environmental Physics, Faculty of Mathematics, Physics and Informatics, Comenius University, Mlynská Dolina, 842 48 Bratislava, Slovakia

E-mail: mostafa.hassan@fmph.uniba.sk

Plasma in contact with water produces "plasma-activated water (PAW)" solution containing various reactive oxygen and nitrogen species (RONS). PAW solution has many potential applications in plant growth promotion, killing microbes, disinfection (e.g., wastewater treatment by ozone), and some PAW solutions have shown anticancer effects. The solubility of RONS in water, under equilibrium conditions, is given by their Henry's law solubility coefficients ( $K_H$ ). Transport of RONS into the water can be enhanced by water aerosolization to microdroplets which have a larger surface-to-volume ratio.

This work compares the solvation of gaseous RONS:  $H_2O_2$ ,  $HNO_2$ ,  $NO_2$ ,  $NO_3$ , and  $O_3$ , having different  $K_H$ , into deionized water through two different reactors. One for solvation to bulk water with fixed surface area, the second for solvation to aerosol microdroplets generated by two techniques. The compressor nebulizer is used to produce non-charged microdroplets of the same sizes ( $\sim 5~\mu m$ ), while electrospray is used to generate charged microdroplets with polydisperse size distribution ( $\sim 10-300~\mu m$ ).

The solvation of RONS into bulk is determined by treatment time regardless of water volume, while solvation of RONS into water aerosol is enhanced due to a larger gas-water interaction interface that is produced [1,2]. Unlike in the case of H<sub>2</sub>O<sub>2</sub> and O<sub>3</sub>; the solvation of HNO<sub>2</sub>, NO<sub>2</sub>, and NO is influenced by chemical changes in water and the formation of NO<sub>2</sub><sup>-</sup> and NO<sub>3</sub><sup>-</sup>. In gaseous mixtures with comparable concentrations of NO, NO<sub>2</sub>, and HNO<sub>2</sub>, the last one is the dominant source of NO<sub>2</sub><sup>-</sup> [3]. The solvation of H<sub>2</sub>O<sub>2</sub>, NO, and O<sub>3</sub> is more efficient in the non-charged than in charged microdroplets due to the smaller size microdroplets generated from the nebulizer, which enables faster saturation. Based on the obtained results, efficient solvation of gaseous RONS in water is not determined purely by Henry's law but also by other key parameters, such as the treatment time, gas-water interface, and chemical reactions of dissolved species in water. These results can lead to optimizing the design of water ozonizers, water sprays, and plasma–water interaction systems used by various air plasma applications in biomedicine, environmental sciences, and agriculture.

This work was supported by Slovak Research and Development Agency APVV-17-0382 and Comenius University grant UK/141/2022.

- [1] M. Janda, et al, J. Appl. Phys., 129, 183305 (2021).
- [2] M.E. Hassan, et al, Water, 13, 182 (2021).
- [3] M. Janda, et al, Appl. Sci., 11, 7053 (2021).

#### Contributed C32 - David Sawtell

Molecular synthesis and decomposition

#### Insights into nitrogen fixation using microfluidic plasma devices

Laila Patinglag<sup>1</sup>, Zaenab Abd Allah<sup>1</sup>, Alex Iles<sup>2</sup>, Louise Melling<sup>1</sup>, Kirsty Shaw<sup>1</sup>, <u>David Sawtell</u><sup>1</sup> Faculty of Science and Engineering, Manchester Metropolitan University, Manchester, UK

<sup>2</sup> Department of Chemistry, University of Hull, Hull, UK

E-mail: d.sawtell@mmu.ac.uk

Methods of fertilizer production predominantly involve the energy intensive Haber-Bosch process. With the drive to reduce carbon emissions and minimize energy consumption, investigations into plasma methods to supplant the Haber-Bosch process are of utmost importance. Current plasma work<sup>1</sup> on nitrogen fixation encompasses a wide range of reactor types, and mostly relies on a two stage process, with nitrate being formed in the plasma, then being dissolved in water in a subsequent process. Modular plasma devices that produce nitrogen based fertilizers at point of use would reduce transportation costs and reduce overall energy consumption. Microfluidic plasma devices allow for plasma initiated liquid phase reactions due to inherent characteristics such as a large surface-area-to-volume ratio and flow control. This essentially removes any mass transfer limitations of plasma species diffusing into the bulk of the liquid. Previous work in the literature using such technology has seen the use of these devices for destroying organic pollutants<sup>2</sup>, inactivation of waterborne bacteria<sup>3</sup>, and nanoparticle synthesis<sup>4</sup>, amongst other applications<sup>5</sup>. This technology allows us to evaluate nitrogen fixation by dielectric barrier discharge in plasma water flows, without the influence of diffusion into the bulk of the liquid. Such devices can be used to both provide insight into plasma nitrogen fixation, and to form a basis for scale up principles.

The microfluidic plasma reactor has been described in previous work<sup>2,3</sup>. Air, argon, nitrogen and oxygen were used as carrier gases, flowed concurrently with de-ionised water, soft domestic water, and hard domestic water respectively. Gas pressures were set to one bar gauge, whilst water flow rates ranged between 35-150  $\mu$ L/min, giving plasma residence times of up to 10 seconds. Outlet gases from the reactor were flowed to a single pass gas cell and analyzed by Fourier transform infrared spectroscopy. Liquid samples were collected from the outlet of the reactor, and anion and cation concentrations were measured by ion chromatography, in addition to pH measurements.

Fig. 1 shows the formation of nitrogen containing cations and anions in deionized water with residence time in an air plasma. Nitrate, nitrate and ammonium ions all increased in concentration with increasing residence time. The formation of nitrate and nitrite is due in part to formation of nitrogen dioxide and nitrogen monoxide in the plasma region rapidly reacting with the water to form these cations. The increased concentration of nitrate cations compared to that of nitrite is thought to be due to the decomposition of nitrite ions to nitrate caused by reactive oxygen and nitrogen species in the plasma. Although concentrations are low, this does represent an extremely short residence time of water in the plasma region, and with higher residence times, the concentrations are believed to scale accordingly. The devices are also

parallelizable, allowing for increased flow rates of water to be treated. This work provides a route towards point of use one stage nitrogen fixation for agricultural purposes.

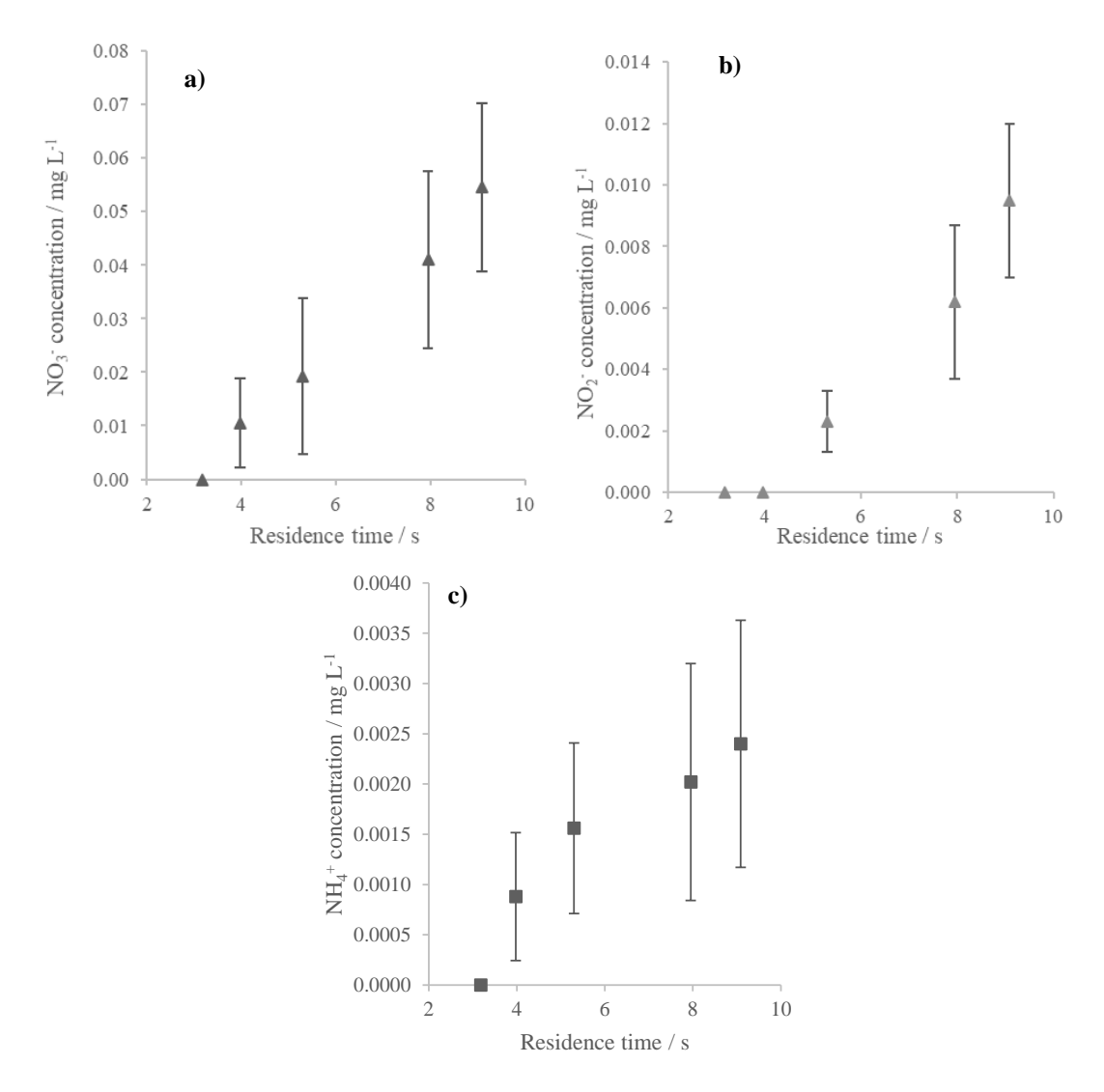


Fig. 1: Concentration against residence time in reactor for a) nitrate, b) nitrite and c) ammonium ions in air plasma treated deionized water. Error bars represent standard error, n = 3.

- 1. E. Vervloessem et. al., Green Chem., 2022, 24, 916
- 2. L. Patinglag et. al., Plasma Chem. Plasma Process., 2019, 39, 561
- 3. L. Patinglag et. al., Water Res., 2021, 201, 117321
- 4. D.-E. Li and C.-H Lin, RSC Adv., 2018, 8, 16139
- 5. L. Lin et. al., Chem. Eng. J., 2021, 417, 129355

#### Contributed C33 - Chiel Ton

Ozone generation and applications

#### Transient plasma for air purification using 400 kV pulses

C.Ton<sup>1</sup>, Tom Huiskamp<sup>1</sup>

Department of Electrical Engineering, Electrical Energy Systems group, Eindhoven University of Technology, PO Box 513, 5600 MB Eindhoven, The Netherlands

E-mail: c.ton@tue.nl

Nanosecond transient plasma generation by high-voltage pulses in corona reactors is proven as an efficient method for air purification. In this research we aim to expand the potential of this method in an industrial setting by using a cylinder-wire reactor with a diameter of 40 cm. This reactor will be driven by pulses with an amplitude up to 400 kV, a pulse width of hundreds of nanoseconds and a rise time of several nanoseconds.

The generator is positioned in a casing filled with transformer oil that transitions into the cylinder of the reactor. This casing contains an integrated D-Dot voltage sensor and a Rogowski coil, alongside custom designed high voltage insulation. The reactor is outfitted with a window for ICCD imaging, synthetic air flow to enable the measurement of ozone yield and both single-wire and multiple-wire configurations.

The Marx generator used to generate the pulses is a refurbished generator from the University of Twente [1]. The original generator has been modified with new charging resistors and a trigger that operates with a nanosecond jitter. This short jitter enables the use of the trigger signal for both the Marx generator and the imaging setup. The imaging setup is used for determining characteristics of the plasma streamers.

We will present the different components of this experimental setup alongside exploratory measurements and an outlook towards a solid-state alternative to the Marx generator. The results from this research will proceed to pave the way for this solid-state alternative which will expand the system's industrial potential by enabling higher repetition rates and a longer longevity.

[1] B.M.H.H. Kleikamp and W.J. Witteman, "High Energy Extraction of Electron Beam Pumped KrF Laster at Multi Atmospheres", optics communication, vol. 49 n. 5 (1984)

Biological applications

### VIRUS AND AEROSOL REMOVAL BY ELECTROSTATIC PRECIPITATOR

Indrek Jõgi<sup>1</sup>, Paap Koemets<sup>1</sup>, Ailar Omler<sup>2</sup>, Sander Mirme<sup>1</sup>, Kaupo Komsaare<sup>1</sup>, Peeter Paris<sup>1</sup>, Jüri Raud<sup>1</sup>, Heikki Junninen<sup>1</sup>

<sup>1</sup>Institute of Physics, University of Tartu, 50411 Tartu, Estonia

<sup>2</sup>Institute of Technology, University of Tartu, 50411 Tartu, Estonia

E-mail: indrek.jogi@ut.ee

There is growing evidence of the significance of aerosols in the spreading of SARS-COV-2 virus [1,2]. The role of infectious aerosols becomes especially important when the aerosols are allowed to accumulate due to the inappropriate indoor ventilation. For example, in recirculating air ventilation systems where it necessary to remove or neutralize the virus loaded aerosols [2]. However, the use of mechanical filters, e.g. HEPA filters, with high resistance to airflow may require the replacement of the whole ventilation system. Electrostatic precipitators with low air resistance are well-established technology for industrial aerosol removal which could be used to retrofit existing ventilation systems. The goal of present study was to build and test a prototype electrostatic precipitator device suitable for air ventilation systems. The removal of virus sized aerosols was investigated together with the power requirement and ozone output. The actual virus removal ability of the device was tested by alphaviruses.

The experimental setup was built on the basis of 100 mm diameter ventilation system components. The two-stage electrostatic precipitator consisted of corona discharge-based charger and parallel plate collector. The charger was built in a 100 mm pipe section with 3 or 6 electrodes (Pt tips or carbon brush) symmetrically placed in the pipe. Two different collector sizes were used with the capacitance of 332 pF and 3.9 nF. DC voltage up to 4 kV was applied to the charger electrodes and to the collector plates. Air flow rate through the system was varied between 200-1000 slm. Test aerosols were introduced into the system using the atomizer, which was filled with salt-water mixture. The concentration and size distribution of aerosols in the outlet of the collector was measured with a Fast Mobility Particle Sizer (FMPS) in the range of 5 to 500 nm and with an Optical Particle Sizer (OPS) in the range of 0.5 to  $10~\mu m$ . The outlet ozone concentration was measured with 2B ozone monitor.

**Total aerosol removal** was a function of specific input energy *SIE* (power divided by flow rate) of the charger i.e. increasing flow rates required correspondingly higher charger power for equal aerosol removal. Carbon brush electrodes were more efficient than Pt electrodes at same *SIE* values. The use of larger number of charger electrodes resulted in increased aerosol removal at the cost of increased power consumption. At all used conditions, the *SIE* values remained below 0.1 J/L and ozone production remained below 20 ppb.

The aerosol removal was also scalable with the collector size. The total aerosol removal was approximately 90% with smaller collector (332 pF) and 99% with larger collector (3.9 nF) with highest applied charger and collector voltages (4kV). The aerosol removal was exponential

function of collector voltage, collector capacitance and inverse of flow rate and could be described by Deutsch model [3]. The aerosol removal was most efficient for aerosol size-range of 10-100 nm while larger aerosols corresponding to the size of the SARS-CoV-2 virus and virus loaded aerosols had relatively constant removal percentage (Fig. 1).

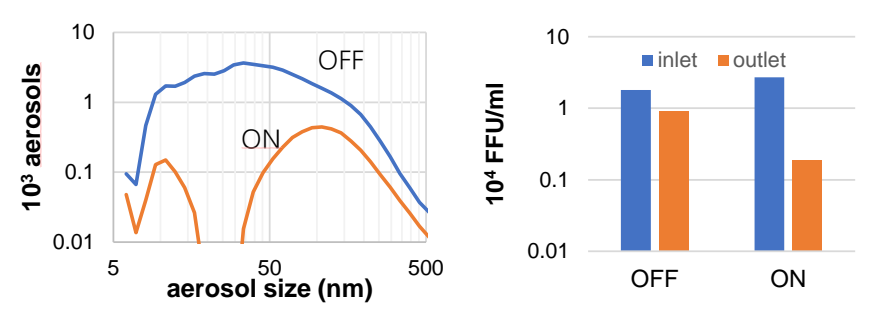


**Fig. 1**: Distribution of removed aerosols and EILV virus removal when electrostatic precipitator was ON or OFF (4 kV charger and collector voltages).

Virus removal ability of the device was investigated by a slightly modified setup with shorter tubes to fit into the fume-hood. Only smaller collector could be used due to the size restrictions. The nebulizer was filled with Alphavirus Eilat virus (EILV) containing physiological solution. EILV has an enveloped virion structure which characterizes several other groups of RNA genomic viruses pathogenic to humans, such as coronaviruses but is only capable of infection in insect cells and is therefore safe for humans. Recombinant EILV encoding for the fluorescent protein mCherry was used in these experiments to assess the viral infection. To produce the aerosol, virus stock solutions with a concentration of 10<sup>7</sup> FFU/ml (focus forming unit) were used. The samples were collected using gelatine filters placed before and after the device. Virus survival was determined by titration using a fluorescent focus formation assay utilizing the mosquito Aedes albopictus cell line C6/36. 10-fold serial dilutions of each sample were prepared and used to infect the cell monolayers. After infection, a viscous cell culture medium was applied to the cell layers. The infected cells were then incubated for an additional 72 h, during which time fluorescent cell foci were formed as a result of viral activity which could be visualized under a fluorescence microscope and counted to determine titers. Calculated titers are in the units of FFU/ml.

Approximately 90% of the viruses were removed when the charger and collector voltages had highest value of 4kV. This result was consistent with the results of aerosol removal.

The results demonstrated that electrostatic precipitator is feasible for the removal of viruses from the ventilation air with low energy costs and negligible production of harmful byproducts, such as ozone.

#### References

- [1] R. Tellier, Interface Focus 12 (2022) 20210072
- [2] V. F. McNeill, Annu. Rev. Chem. Biomol. Eng. 13 (2022) 6.1-6.18
- [3] A. Mizuno, IEEE Trans. Diel. Electr. Insul. 7 (2000) 615

#### Poster P02 - Kubra Ulucan-Altuntas

Depollution and environmental applications

### Degradation of Perfluorooctanoic Acid (PFOA) in Water by Non-Thermal Plasma Enhanced by Boron-Doped Reduced Graphene Oxide

<u>Kubra Ulucan-Altuntas<sup>1,2\*</sup></u>, Marco Oripoli<sup>1</sup>, Mubbshir Saleem<sup>1</sup>, Samuel, Pressi<sup>1</sup>, Giulia, Tomei<sup>1</sup>, Enzo, Menna<sup>1</sup>, Ester Marotta<sup>1</sup>, Cristina Paradisi<sup>1</sup>

<sup>1</sup>Department of Chemical Sciences, University of Padova, Via Marzolo 1, 35131 Padova, Italy <sup>2</sup>Department of Environmental Engineering, Yildiz Technical University, 34220, Istanbul, Turkey

\*E-mail: kubra.altuntas@unipd.it, kubra.ulucan@gmail.com

Per- and polyfluoroalkyl substances (PFAS) are a group of synthetic substances thermally and chemically stable and thus persistent in the environment. They are moreover known to bioaccumulate in living organisms and cause adverse health effects. The widespread use of PFAS since the 1950s in many industrial applications all over the world has caused the contamination of ground, surface and drinking water in many world area. Since 2019, the Stockholm Convention has restricted the use and manufacture of PFOA or PFOA-related compounds and listed these compounds in Annex A. In addition, the European Parliament has also included PFAS in Directive 2020/2184/EU, which sets a limit of 0.1  $\mu$ g/L for the maximum amount of PFAS.

Various treatment methods have been investigated to remove PFAS from water, including physical (i.e. adsorption, membrane filtration), chemical (i.e. electrocoagulation, advanced oxidation processes) and biological treatments. Among them, non-thermal plasma (NTP) has proven to be the most effective method for PFAS decomposition [1] thanks to the production of high energy electrons and other highly reactive species (ions, radicals, and excited species) generated through the collision of the energetic electrons with the gas atoms/molecules and their interaction with the liquid surface. The production of these species *in situ*, the absence of requirement of heat or cooling, pressure or vacuum, and the ease and quickness of switching on and off makes moreover NTP a green technology for water purification.

In this study, the degradation of PFOA was studied using NTP enhanced by boron-doped reduced-graphene oxide (B-rGO) as catalyst. The NTP reactor (Figure 1.a) employs a multipin electrode to generate corona discharge (MCD) and self-pulsed discharges (M-SPD) on each pin as described in Ulucan-Altuntas et al. 2022. DC negative power supply was used to provide the high voltage and operated at different powers (3 - 9 W). In parallel with the plasma reactor, a high-capacitance capacitor of 2 nF was installed. B-rGO was synthesized following the modified Hummers' procedure mentioned in El Hadki et al. 2021. In batch experiments, the reaction progress was monitored as a function of treatment time, and PFOA and its degradation products were analyzed via LC-MS. The effects of MCD and M-SPD were compared with and without B-rGO under air atmosphere and at an initial PFOA concentration of 2.5·10<sup>-6</sup> M. Afterwards, the effect of the gas type on the degradation efficiency and reaction products was investigated in experiments with 1·10<sup>-6</sup> M PFOA solutions using either argon or air.

PFOA degradation yield (Figure 1b) obtained in 5 minutes with MCD plasma only was approximately 15%, while with MCD + B-rGO it was significantly higher (38%). The same

electrode was used to generate self-pulsed discharges (M-SPD) and the degradation yield of PFOA approached 70%. Moreover, the presence of B-rGO allowed to degrade PFOA up to 95%. M-SPD was thus much more effective than MCD and for this reason it was selected for further experiments.

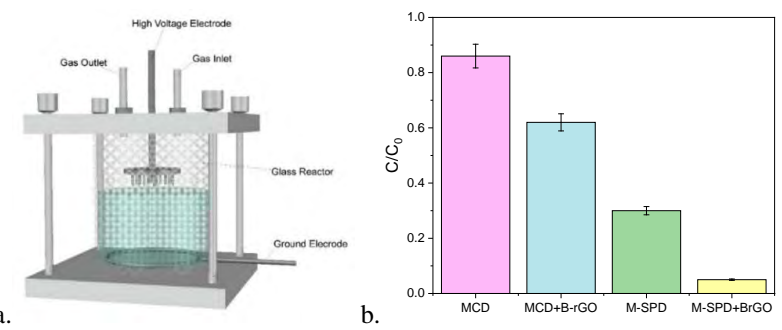


**Fig. 1**: (a) The design of multipin self-pulsed discharge reactor (b) PFOA (2.5x10<sup>-6</sup> M in tap water) degradation with MCD and M-SPD with and without B-rGO (200 mg/L).

The concentrations of PFOA and of its products after 30 min treatment with M-SPD and M-SPD+B-rGO under air and argon atmosphere are shown in Fig. 2(a) and Fig. 2(b), respectively. The detected products are shorter chain homologues of PFOA, namely heptanoic (PFHpA), hexanoic (PFHeA), pentanoic (PFPA), and butanoic (PFBA) acids. The best PFOA degradation yield was obtained with argon plasma in the presence of the catalyst. Moreover, under these conditions the concentration of the byproducts is the lowest. This can be explained considering that Ar<sup>+</sup> and Ar<sup>\*</sup> species produced by discharges in argon play an important role in the degradation of PFAS [4]. B-rGO improves the treatment process both in air and argon but its effect is much higher with plasma in air. The combination of air plasma with B-rGO appears thus promising for the possibility of using air instead of argon, which would make easier the future application of plasma for PFAS removal.

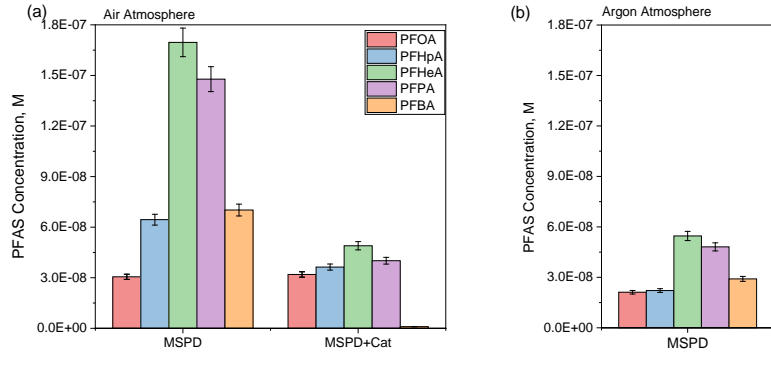


**Fig. 2**: PFAS residual concentration after treatment with M-SPD discharge with and without B-rGO under (a) air and (b) argon atmosphere. Conditions: 200 mg/L B-rGO, 1x10<sup>-6</sup> M PFOA, 9 W power, 30 min treatment.

#### Acknowledgement

This study is funded by European Union's Horizon 2020 research and innovation programme under the Marie Skłodowska-Curie grant agreement No: 898422.

#### References

- [1] Nzeribe et al. (2019) Crit Rev Environ Sci Technol. 49 (10) 866-915
- [2] Ulucan-Altuntas et al. (2022) J. Environ. Manage. 301, 113885.
- [3] El Hadki et al (2021) FlatChem. 27, 100238.
- [4] Singh et al (2021) J. Hazard. Mater. 408, 124452

#### Microwave plasma-based conversion of methane and carbon dioxide

<u>Seán Kelly</u><sup>1</sup>, Elizabeth Mercer<sup>1</sup>, Robin De Meyer<sup>1</sup>, Joachim Slaets<sup>1</sup> and Annemie Bogaerts<sup>1</sup>

<sup>1</sup>Research group PLASMANT, Department of Chemistry, University of Antwerp, Belgium

E-mail: sean.kelly@uantwerpen.be

Plasma-based gas conversion powered by (intermittent) renewable electricity utilising the key greenhouse gases of CO<sub>2</sub> and CH<sub>4</sub> offers great promise for 'net-zero-carbon' chemical and fuel production (e.g., reforming biogas). The resulting syngas (i.e., H<sub>2</sub> and CO mixture) can be used as a feedstock in mature synthesis methods such as Fischer-Tropsch to produce liquid hydrocarbons<sup>1</sup>. In this work syngas production by 'dry-reforming' of CH<sub>4</sub> with CO<sub>2</sub> (equation 1) is interrogated using a microwave (MW) plasma reactor operating in a surface wave mode with a swirling gas flow<sup>2</sup>.

$$CO_{2(g)} + CH_{4(g)} \leftrightarrow 2CO_{(g)} + 2H_{2(g)}$$
 (1)

MW plasmas, under atmospheric pressure conditions (setup shown in **figure 1**), offer the advantage of a high degree of ionisation (i.e., high levels of gas activation), warm plasma conditions (promoting the endothermic chemistry), operate without metal electrodes (i.e., employing a swirling gas flow with a surface wave plasma removes wall interactions) and have a relatively large absolute conversion due to the relatively high gas flows required (e.g., ~ 10 L/min) when compared with other smaller scale plasma reactor designs<sup>3</sup>.

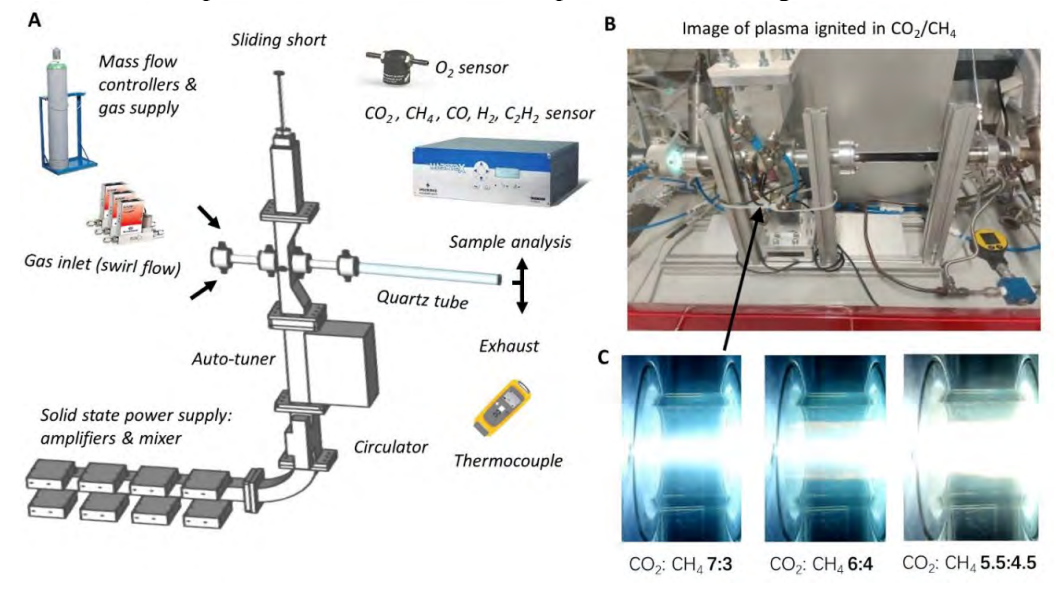


**Figure 1:** A: Illustration of our MW reactor consisting of a solid-state MW power supply, circulator, auto-tuner and tapered waveguide section terminated by a sliding short. The plasma is ignited inside a quartz tube where a swirling flow is injected. Sample analysis of the exhaust gas is carried out using an NDIR and a luminescence O<sub>2</sub> sensor. **B**: Photo of the reactor in operation for 1 kW power and 10 L/min flow rate for a range of CH<sub>4</sub> content. Ignition takes place in a tapered section of a 2.45 GHz WR340 waveguide where a plasma is suspended at the centre of the tube. **C**: In-waveguide photos of the plasma at different CO<sub>2</sub>/CH<sub>4</sub> ratios at 10 L/min; camera viewpoint is looking towards the quartz tube inside the waveguide, as indicated by the arrow.

The total (weighted) conversion is shown in **figure 2 A** for a range of CH<sub>4</sub> content in the CO<sub>2</sub>/CH<sub>4</sub> inlet mixture (photos in **figure 1 C**). The corresponding energy cost is shown in **figure 2 B** (left axis). Notably, our results are found to be amongst the best performing metrics to date<sup>1,3</sup> with promising energy cost of ~3 eV/molecule for total conversion levels of typically ~50 %.

CO and  $H_2$  are the main gaseous products formed. Small levels of  $C_2H_2$  (~2 %) are measured, in agreement with literature<sup>3, 4</sup>, while the exhaust is found to be free of  $O_2$  (~0%). In **figure 2 A** we see CH<sub>4</sub> conversion is higher across the range investigated when compared to  $CO_2$  conversion, a consequence of the lower bond energy required to break CH<sub>4</sub>. At low CH<sub>4</sub> content (i.e., 30 % CH<sub>4</sub>) significant condensation (water) is present in the exhaust. This is attributed to the reaction of  $H_2$  with excess  $O_2$  (i.e., due to the higher  $CO_2$  fraction). At higher CH<sub>4</sub> content (i.e., 45 % CH<sub>4</sub>) condensation is reduced and in **figure 2 B** we see the syngas ratio approaches ~1, consistent with greater selectivity towards  $H_2$  (i.e., over  $H_2O$ ) as per **equation 1**. A small but impactful by-product (i.e., regarding plasma stability) is solid carbon, which is observed to coat the quartz tube for high CH<sub>4</sub> fractions (see **figure 1 B**). Scanning electron microscopy (SEM) analysis of the carbon powder finds that the material is metal-free and has a structure consistent with carbon black with a median particulate size of ~20 nm. Thermocouple measurements of the exhaust taken downstream (~10-15 cm) show (typical) temperatures ~700 °C are maintained in the exhaust, motivating future coupling with downstream catalysis beds and heat/energy recovery configurations.

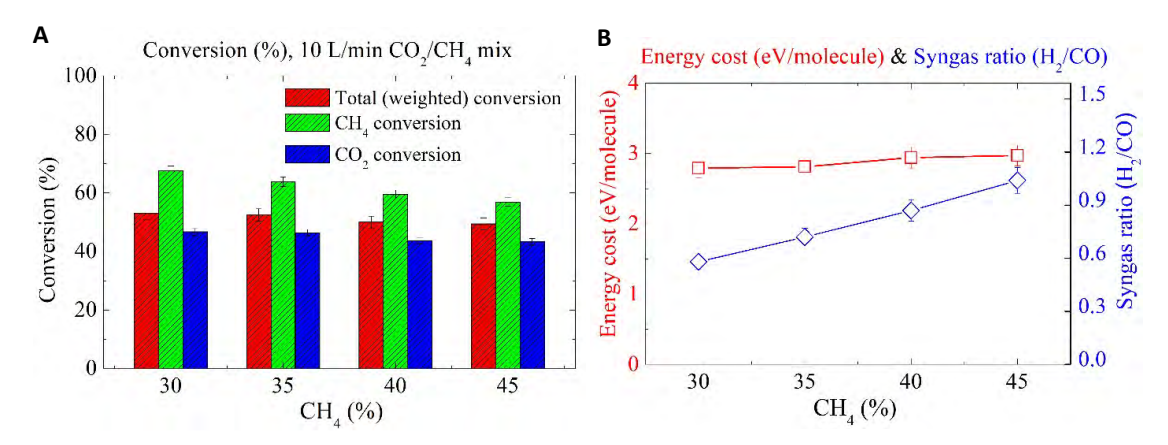


**Figure 2**: **A**: Total conversion (weighted according to inlet fraction of CO<sub>2</sub> and CH<sub>4</sub>) along with individual CH<sub>4</sub> and CO<sub>2</sub> conversion % for a range of CH<sub>4</sub> content in the CO<sub>2</sub>/CH<sub>4</sub> feed mixture for an inlet flow rate of 10 L/min. **B**: Corresponding energy cost (eV/molecule) shown in left axis and the corresponding syngas ratio (i.e., H<sub>2</sub>/CO) present in the exhaust shown on right axis.

#### References

- 1. R. Snoeckx and A. Bogaerts, *Chem Soc Rev*, 2017, **46**, 5805-5863.
- 2. S. Kelly and A. Bogaerts, *Joule*, 2021, **5**, 3006-3030.
- 3. B. Wanten, S. Maerivoet, C. Vantomme, J. Slaets, G. Trenchev and A. Bogaerts, *Journal of CO2 Utilization*, 2022, **56**, 101869.
- 4. E. Cleiren, S. Heijkers, M. Ramakers and A. Bogaerts, *ChemSusChem*, 2017, **10**, 4025-4036.

#### Poster P04 - Francisco Pontiga

Depollution and environmental applications

### CARBON DIOXIDE CONVERSION USING AC AND PULSED DIELECTRIC BARRIER DISCHARGE

A. Fernández-Rueda, H. Moreno, <u>F. Pontiga</u>

Departamento de Física Aplicada II, Universidad de Sevilla, Sevilla, Spain

E-mail: pontiga@us.es

Carbon dioxide emissions are largely responsible for the global warming problem currently affecting the Earth. This fact has promoted research on the possible application of plasmas to decompose carbon dioxide and generate other chemicals of interest, which in turn can facilitate the production of new fuels [1]. However, breaking the OC=O bond of the CO<sub>2</sub> molecule requires a great deal of energy. In this respect, electrons in non-thermal plasmas have sufficiently high energy to decompose the gas molecules [2, 3], while the temperature of the heavy species remains close to room temperature. Among others, the dielectric barrier discharge (DBD) is a non-thermal plasma source that has shown great versatility in many industrial applications, such as in ozone generation. In this work, DBD is used for CO<sub>2</sub> conversion, and two different forms of operations of the DBD reactor are compared: using AC voltage (AC DBD) and using nanosecond high voltage pulses (pulsed DBD).

Figure 1 shows a schematic representation of the experimental set-up. The DBD reactor consisted of two stainless steel plane circular electrodes, 20 mm in diameter, covered with 1 mm thick fused silica glasses. The gap between the two dielectrics was 2 mm. A constant gas flow rate,  $Q = 100 \text{ cm}^3/\text{min}$ , of high purity CO<sub>2</sub> (99.995%) was imposed through the reactor. The composition of gas at the exit of the reactor was analysed using ultraviolet and infrared spectrophotometry to measure the generation of ozone and carbon monoxide, respectively. For the AC DBD, a high voltage amplifier was used to energize the reactor. The voltage amplitude was fixed to 22 kVpp, and the AC frequency was varied between 200 Hz and 2 kHz. The high voltage signal provided by the amplifier was measured using a wide-band probe, and the electrical discharge current was determined by measuring the voltage drop across a monitor capacitor ( $C_m = 1 \text{ } \mu\text{F}$ ). Both the high voltage signal and the voltage drop across the capacitor

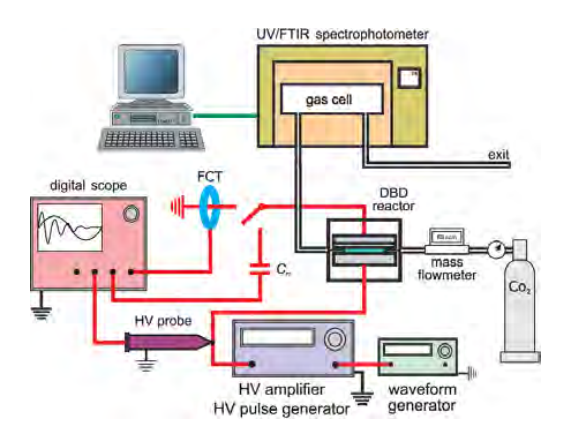


Fig. 1: Experimental set-up.

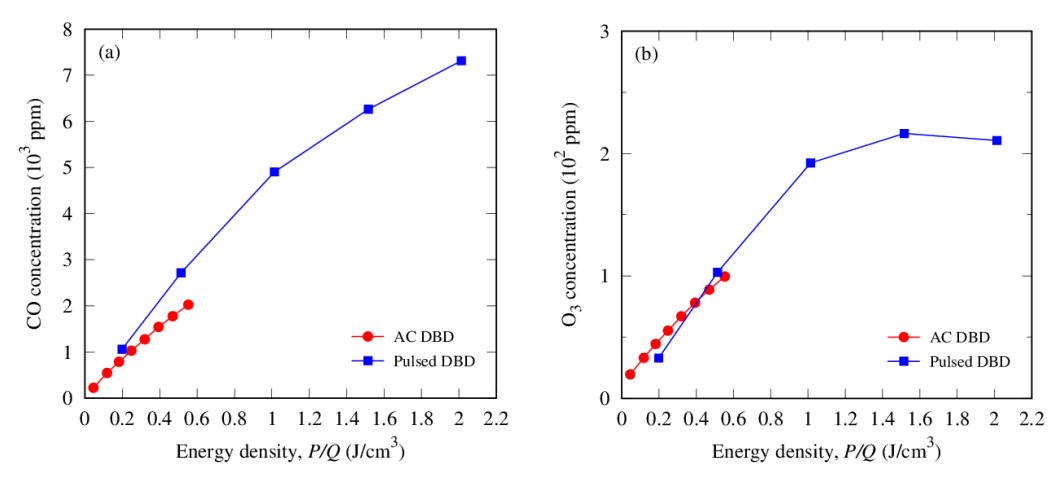


Fig. 2: Concentration of CO and O<sub>3</sub> as a function of the energy density using AC DBD and pulsed DBD.

were recorded using a 2.5 GHz bandwidth digital oscilloscope. For the pulsed DBD, a high voltage pulse generator was used, which produces negative high voltage pulses of 26.40 kV amplitude and duration of about 20 ns. The repetition rate of the pulse was varied in the range 100 Hz to 1 kHz. In this case, a fast current transformer was used for the measurement of the current intensity.

In AC DBD, many short-lived microdischarges occur in each voltage cycle. In contrast, in pulsed DBD, the electrical discharge starts with the pulse and dies out soon after. However, since the pulse amplitude that triggers the discharge is higher, a higher electron density is also generated. Therefore, in order to compare both DBDs, results will be presented as a function of the energy density, that is, the ratio of the electrical power and the gas flow rate, P/Q. Figures 2a and 2b show the concentration of CO and O<sub>3</sub>, respectively, at the exit of the reactor, using the two different DBDs. Note that CO concentration is also a direct measure of CO<sub>2</sub> conversion. As can be clearly seen from the figures, the range of energy densities covered with the pulsed DBD is wider than that when using AC DBD. At low energy densities, the growth of both CO and O<sub>3</sub> is almost linear. This behaviour changes at sufficiently high energies, which are reached in the case of the pulsed DBD: the growth of CO becomes slower and, particularly, O<sub>3</sub> reaches a plateau. However, while ozone concentration was similar in the range of energies shared by AC DBD and pulsed DBD, the growth of CO is faster when using pulsed DBD. This fact implies that CO<sub>2</sub> conversion is more efficient using pulsed DBD.

#### References

- [1] R. Snoeckx and A. Bogaerts, Chem. Soc. Rev., 46 5805–5863 (2017).
- [2] B. Ashford and X. Tu, Curr. Opin. Green Sustain. Chem. 3 45–49 (2017).
- [3] H. Kim, Plasma Process. Polym. 1 91–110 (2004).

#### Acknowledgements

This work has been partially supported by the Spanish Government Agency "Ministerio de Ciencia, Innovación y Universidades" and the European Regional Development Fund, under contract PGC2018-099217-B-I00.

Depollution and environmental applications

### REMOVAL OF AMOXICILLIN AND SULFAMETHOXAZOLE IN WATER USING NON-THERMAL PLASMA

<u>Tian Tian<sup>1</sup></u>, Hervé Rabat<sup>1</sup>, Florin Bilea<sup>2</sup>, Monica Magureanu<sup>2</sup>, Mohamed Ali Antoissi<sup>1</sup>, Olivier Aubry<sup>1</sup> and Dunpin Hong<sup>1</sup>

<sup>1</sup> GREMI, CNRS Université d'Orléans, BP6744, Orléans, 45067 Cedex 2, France
 <sup>2</sup> Department for Plasma Physics and Nuclear Fusion, National Institute for Lasers, Plasma and Radiation Physics, Magurele, Ilfov 077125, Romania

E-mail: tian.tian@univ-orleans.fr

Non-thermal plasma is studied worldwide for water pollution control [1], due to its significant advantages in degrading organic pollutants in water [2], including antibiotic molecules [3], which lead to the contamination of water bodies to an alarming extent.

In this communication, we present the degradation of two antibiotic molecules, amoxicillin (AMX) and sulfamethoxazole (SMZ), in pure water solutions with a non-thermal plasma reactor at atmospheric pressure. A coaxial dielectric barrier discharge (DBD) reactor with water falling film was used in the experiments (Fig. 1). The outer electrode is connected at high voltage, while the inner tube is grounded through a capacitor used for charge measurement. The high voltage has a square waveform with amplitudes in the range of 11 - 15 kV and frequency between 0.3 and 2 kHz. The power dissipated in the plasma was calculated from the charge-voltage diagram and was in the range 10-20 W. The falling film flows along the outside of the central tube with a flow rate of 240 mL/min. Air or oxygen are introduced through the reactor with flow rates of 100 mL/min. In the single component solutions, the AMX concentration was 100 mg/L and the SMZ concentration was 80 mg/L, while the mixture of the two compounds contained half the concentration of each (i.e. 50 mg/L AMX and 40 mg/L SMZ). The initial pH of all solutions was around 6, and the conductivity was several  $\mu$ S/cm. In each experiment, 100 mL of solution was treated up to 60 min.

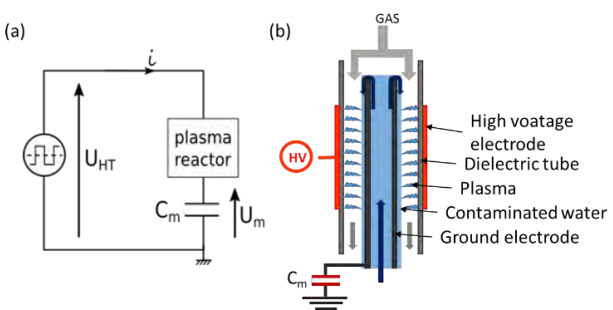


Fig. 1: (a) The schematic diagram of the electric. (b) The plasma reactor of the coaxial DBD configuration.

The concentration of AMX and SMZ in aqueous solutions were measured by high performance liquid chromatography (HPLC); conductivity and pH of the solutions before and after treatment were also measured. The energy yield (EY), defined as the amount (in mass) of target compounds removed per unit of energy spent in the process (equation (1)), was calculated to identify the optimum operating parameters for efficient degradation.

$$EY\left(\frac{g}{kWh}\right) = \frac{(c_0 - c_t) \times V}{\Delta t \times P} \tag{1}$$

where  $c_0$  and  $c_t$  (g/L) are the concentrations of target molecules before and after treatment,  $\Delta t$  (h) is the treatment time; V (L) is the volume of the treated solution and P (kW) is the power dissipated by the plasma.

After the treatment, the pH of all solutions decreased to around 1.4 under air flow and around 2.7 under oxygen flow, while the conductivity became several thousand  $\mu$ S/cm and several hundred  $\mu$ S/cm, respectively. The residual concentration results suggested that the degradation of both AMX and SMZ in both single-component and mixed solutions exhibited quite similar behavior, and obeyed first order kinetics during plasma treatment, as the most frequently observed cases [3]. In single solutions treated by air plasma, the greater the energy, the faster the degradation, but the energy yield depends only on the input energy. The discharge in oxygen considerably improved the degradation of both antibiotics: AMX and SMZ were completely eliminated after about 40 min under air flow and about 20 min under oxygen flow (13 kV, 600 Hz, i.e. 10 W). Another interesting finding is that the degradation of both AMX and SMZ in mixture was slightly faster and more efficient than in the single-component solutions (Fig. 2).

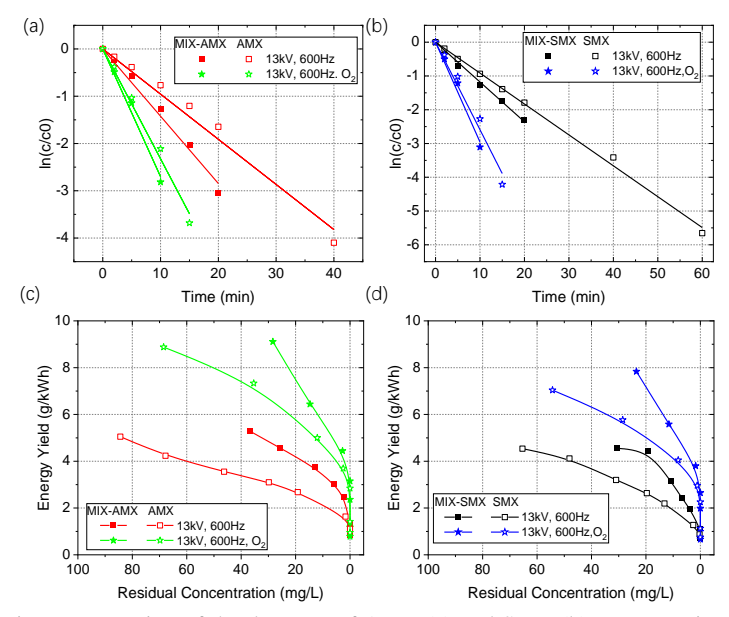


**Fig. 2:** Logarithmic representation of the decrease of AMX (a) and SMX (b) concentration in single-component and mixed solution as a function of the treatment time. Energy yield as a function of the residual concentration of AMX (a) and SMX (b) in single-component and mixed solution.

This study was performed in the frame of a PHC-Brancusi project (2021 No. 43505RC). Tian Tian would like to thank the China Scholarship Council (CSC) for scholarship in the frame of the CSC – Polytech Network PhD program (Student ID: 202009110132).

#### References

- [1] Jiang B., Zheng J., Qiu S., Wu M., Zhang Q., Yan Z., Xue Q., Chemical Engineering Journal (2014), 236, 348–368.
- [2] Murugesan P., Evanjalin Monica V., Moses J. A., Anandharamakrishnan C. Journal of Environmental Chemical Engineering (2020), 8, 104377.
- [3] Magureanu M., Bilea F., Bradu C., Hong D., Journal of Hazardous Materials (2021), 417, 125481.

#### Poster P07 - Rezvan Hosseini Rad

Depollution and environmental applications

# Electrical Characterization of a Coaxial Dielectric Barrier Discharges for CO<sub>2</sub> splitting at Elevated Pressure

Rezvan Hosseini Rad<sup>1</sup>, Volker Brüser<sup>1</sup>, Milko Schiorlin<sup>1</sup>, Ronny Brandenburg<sup>1,2</sup>.

<sup>1</sup> Leibniz Institute for Plasma Science and Technology (INP),

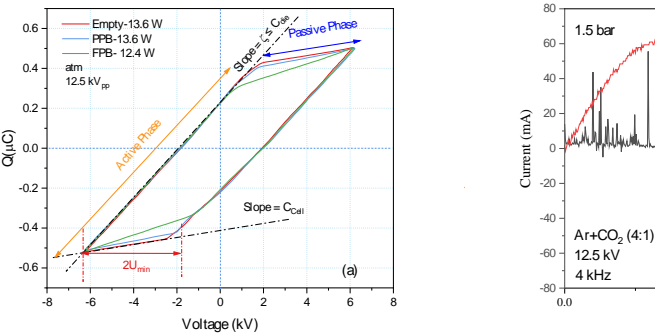
Felix-Hausdorff-Straße 2, 17489 Greifswald, Germany

<sup>2</sup> University of Rostock, Institute of Physics,

A.-Einstein Str. 23-24, 18059 Rostock, Germany

E-mail: rezvan.hosseini-rad@inp-greifswald.de

Global warming by CO<sub>2</sub> emission is one of the main concern in the world. In this regard, CO<sub>2</sub> conversion is more and more in the focus, while CO2 is considered as a source of carbon for value added chemicals production. The CO<sub>2</sub> splitting in coaxial Dielectric Barrier Discharge (DBD) operated at pressures between 1 and 2 bar is investigated in this work. Although, increasing the pressure also increases the breakdown voltage due to Paschen's law, it is increasing the collision rate between the energetic electrons and the CO2 molecules in the plasma zone. It is demonstrated, that CO<sub>2</sub> dissociation can be enhanced by pressure increase. Argon is admixed to CO<sub>2</sub> (electronegative molecules) to reduce the discharge voltage and thus, to enable stable plasma operation at pressures up to 2 bar, but with still moderate high voltage amplitudes (below 25 kV<sub>pp</sub>). Based on an equivalent circuit, the electrode fraction coverage by plasma, the total as well as the effective barrier capacity, the discharge power, and the minimum sustaining voltage as well as the discharge (or burning) voltage are determined by voltagecharge plots. At fixed applied voltage and frequency, the minimum sustaining voltage amplitude changes with the pressure and a maximum discharge power for a specific pressure and applied voltage amplitude is obtained. Furthermore, the addition of a catalyst is studied. The empty coaxial reactor (without catalyst) operation and chemistry is compared with a partially and with a fully packed bed in the discharge zone. The packed bed consists of glass beads, with or without catalyst coating (CeO<sub>2</sub>). An increased conversion of CO<sub>2</sub> to COwith the catalyst is obtained.



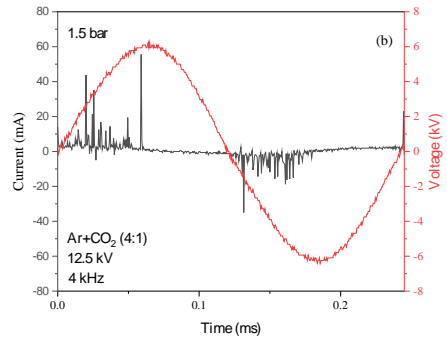


Fig. 1: (a) Voltage-charge plots of three different reactor assemblies, allowing the determination of capacities  $C_{cell}$  and  $\zeta_{die} \leq C_{die}$  as well as discharge power and minimum sustaining voltage. (b) Current and Voltage oscillogram in the DBD operated in Ar/CO<sub>2</sub>=4/1 gas mixture.

#### Poster P08 - Shahriar Mirpour

Fundamental problems of high pressure discharges

# Investigating CO<sub>2</sub> streamer inception in repetitive pulsed discharges

Shahriar Mirpour<sup>1,2</sup>, Sander Nijdam<sup>1</sup>

<sup>1</sup>Department of Applied Physics, Eindhoven University of Technology, PO Box 513, 5600 MB
Eindhoven, the Netherlands

<sup>2</sup>TNO, Geleen, the Netherlands

E-mail: s.mirpour@tue.nl / Shahriar.mirpour@tno.nl

In this study, we investigate the responsible species and processes involved in repetitive pulsed streamer inception in CO<sub>2</sub>. We applied a 10 kV high-voltage (HV) pulse with a repetition frequency of 10 Hz and pulse width of 1 ms to a pin electrode which is placed 160 mm apart from a grounded plane electrode. We measured the inception time (delay between the rising edge of the high-voltage pulse and the rising edge of the photo-multiplier waveform) by a photo-multiplier tube for 600 high voltage cycles. We observed one peak in the histogram of inception times with a median position of 1.2 µs, see figure 1a. To identify the source of this peak, we applied a negative or positive low voltage (LV) pulse before the main HV pulse to manipulate the leftover space charges, see figures 1b-h for examples with positive LV pulses. Three different phenomena are observed: 1) drift, 2) neutralization, and 3) ionization in the LV pulse. At low LV amplitudes and pulse widths, the peak starts to drift toward faster and slower inception times under a positive and negative LV pulse, respectively. However, for an identical LV pulse configuration for positive and negative LV pulse, the observed shift in inception times has a very different magnitude, something which is not observed in air or air-like mixtures. We present a hypothesis to explain this asymmetry based on the differences in the detachment processes between air and CO<sub>2</sub>.

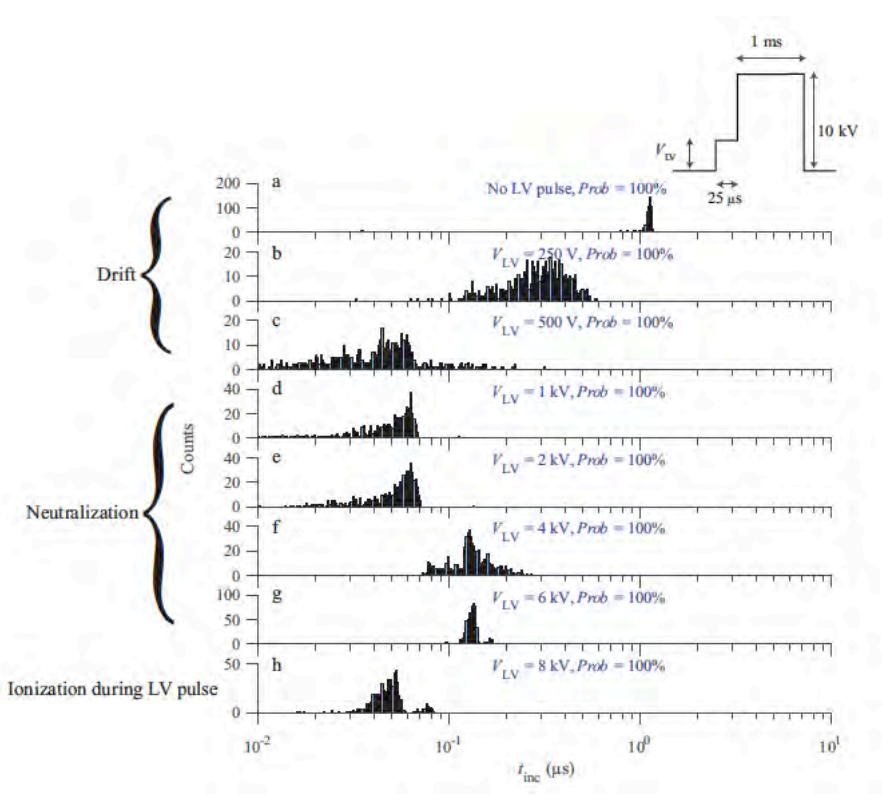


**Fig. 1**: Histograms of discharge inception time ( $t_{inc}$ ) for 600 discharges produced a) for no LV pulse and b-h) by applying a 25  $\mu$ s duration positive LV pulse with the indicated voltage before a 10 kV HV pulse.

#### Poster P09 - Lucia Švandová

Fundamental problems of high pressure discharges

#### Properties of Cr-doped Al<sub>2</sub>O<sub>3</sub> as a dielectric barrier layer

Lucia Švandová<sup>1</sup>, Michal Pazderka<sup>1,2</sup>, Roman Přibyl<sup>1</sup>, Zlata Kelar Tučeková<sup>1</sup>, Jakub Kelar<sup>1</sup> and Mirko Černák<sup>1</sup>

<sup>1</sup>Department of Physical Electronics, Faculty of Science, Masaryk University, Kotlářská 2, 611 37 Brno, Czech Republic

<sup>2</sup>Department of Theoretical Physics and Astrophysics, Faculty of Science, Masaryk University, Kotlářská 2, 611 37 Brno, Czech Republic

E-mail: luciasv@mail.muni.cz

The dielectric barrier discharges are nowadays widely used in various branches of both industry and research. Although the commonly used dielectric layers such as Al2O3 (Alumina) were sufficient, the barrier layer materials have become a subject of extensive research in the last years in order to enhance the discharge properties. The dielectric layer properties could have a significant impact on plasma parameters, e.g. ignition voltage [1], because it is in direct contact with a dielectric layer.

Cr-doped Alumina has been used as a dielectric barrier layer for coplanar dielectric barrier discharges, and its properties have been investigated by various methods. We chose Cr-doped Alumina following previous work [1] because Cr atoms can easily replace Al in the Alumina matrix and form a homogeneous mixture. We investigated both the bulk material properties such as permittivity as well as surface properties such as morphology, roughness, etc. The effect of the Cr-doping on the discharge has been characterized mainly via the ignition voltage measurement by the method invented by our team [2]. The influence of the dopant on the charge trapping properties has been studied using a contactless electrostatic voltmeter by measurement of surface potential decay.

An example of the Cr-doping effect can be seen on the surface potential decay for various levels of Cr-doping, see Fig. 1. To reduce the influence of the environment, the surface potential measurements were conducted in a nitrogen atmosphere with fixed conditions  $T=21.5\,^{\circ}\text{C}$ . The samples were charged under negative corona discharge applied with -4 kV for 10 min. Then, they were rapidly moved under the voltmeter probe. The data were collected for more than  $5000\,\text{s}$ . We can see that there are significant differences in decay rates for various concentrations of Cr dopant.

Furthermore, the connection with surface properties such as roughness and grain size will be made. We will see that for the surface potential decay, two ceramics will play a special role with 1% and 10% Cr-dopant. More interestingly, the 1% Cr ceramics will play an important role in ignition voltage measurements as well.

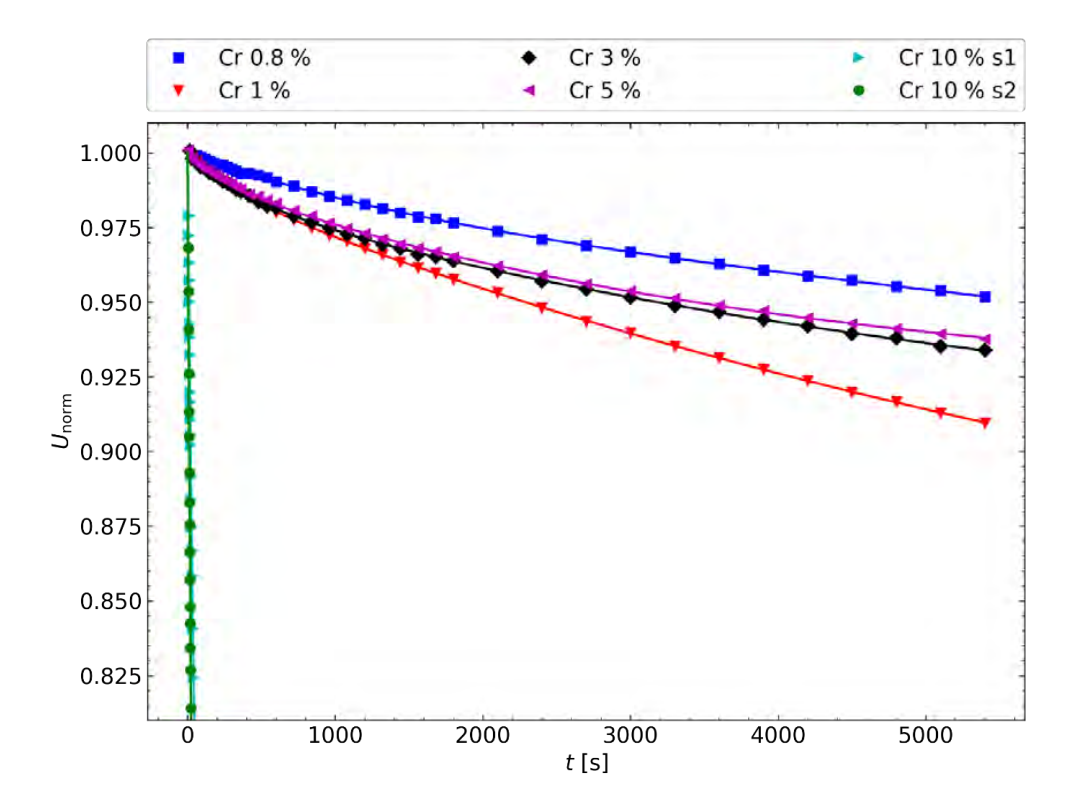


**Fig. 1**: Time evolution of normalized surface potential on various ceramics with Cr concentration from 0.8% up to 10%. Normalization has been done with respect to the surface potential value at t=0 s. The anomalous behavior on 10% ceramics has been verified on samples s1 and s2.

This research was supported by project LM2018097 funded by the Ministry of Education, Youth and Sports of the Czech Republic.

[1] KELAR, Jakub, Roman PŘIBYL, Michal PAZDERKA, Zlata KELAR TUČEKOVÁ, Miroslav ZEMÁNEK a Mirko ČERNÁK. Change of fundamental properties of dielectric barrier discharge due to the alumina-based barrier layer composition. *Vacuum*. Oxford: Pergamon Press, 2020, roč. 174, APR 2020, s. 1-5. ISSN 0042-207X. doi:10.1016/j.vacuum.2020.109180.

[2] PAZDERKA Michal, PŘIBYL Roman, ZEMÁNEK Miroslav, KELAR Jakub, PLŠEK Tomáš, KELAR TUČEKOVÁ Zlata and ČERNÁK Mirko. Robust current peak detection method for dielectric barrier discharges. J. Phys. D: Appl. Phys., 2021. Vol. 54, no. 9, p. 095206.

#### Poster P10 - Mária Cíbiková

Fundamental problems of high pressure discharges

# Characterization of emission current generated by pulse electric field in microdischarge electrode system

Mária Cíbiková<sup>1</sup>, Matej Klas<sup>1</sup>, Peter Čermák<sup>1</sup>, Štefan Matejčík<sup>1</sup>

Department of Experimental Physics, Faculty of Mathematics, Physics and Informatics,
Comenius University, Mlynská dolina, 842 48 Bratislava, Slovakia

E-mail: maria.cibikova@fmph.uniba.sk

Nowadays, nonthermal plasma (NTP) generated by electric discharge at atmospheric pressure applies in many areas such as environmental, biological, medical, or industrial [1-3]. NTP generated at atmospheric pressure has several advantages compared to NTP at low pressure such as avoiding of vacuum system or high chemical reaction rate thanks to a high number of reactive species. On the other hand, in the high pressure NTP, a discharge contraction in spatial inhomogeneities could be a problem. One of the ways how to ensure the homogeneity of the discharge is to generate it at the micrometric distances of electrodes near the minimum of Paschen curve. A key process that influences ignition and preservation of microdischarges is the field emission of electron.

The main objective of this work is to study the microdischarge emission current and breakdown voltage as a function of the pulse electric field rate and the electrode distance [4]. However, direct emission current measurement at high pressures is impossible because it is overlapped by the ionization processes which occur after emission of the electrons. Therefore our measurements were performed in the vacuum where these processes are negligible.

The experimental system is composed of two main parts: the vacuum system and electric equipment. The vacuum system consists of a vacuum chamber made of stainless steel evacuated by a dry forepump and turbomolecular pump. The achieved background pressure is  $\sim 2.10^{-4}$  Pa. Inside the vacuum chamber, the palladium electrodes are set in a sphere (cathode with diameter d = 5mm) to plane (anode) geometry. Air was used as a carrier gas. Electric equipment consists of high voltage power supply (HV), HV probe, current probes, switches, oscilloscope and function generator capable of providing pulses in the range from 10 to  $10^7$  kV/s.

The measurements of the emission current and determination of breakdown voltages were realized at different separations of the electrodes on a micrometric scale. Breakdown voltages were measured before and after conditioning of the electrodes (cleaning the electrode surface from the impurities by the emission current). For the illustration, fig. 1 shows the breakdown voltages measured before and after conditioning at different electrode separations in the regime of fast pulses ( $10^7 \text{ kV/s}$ ) at pressure  $\sim 2.10^{-4} \text{ Pa}$ . It indicates the increase of breakdown voltage with the increasing electrode distances and its dependency on the electrode conditioning process.

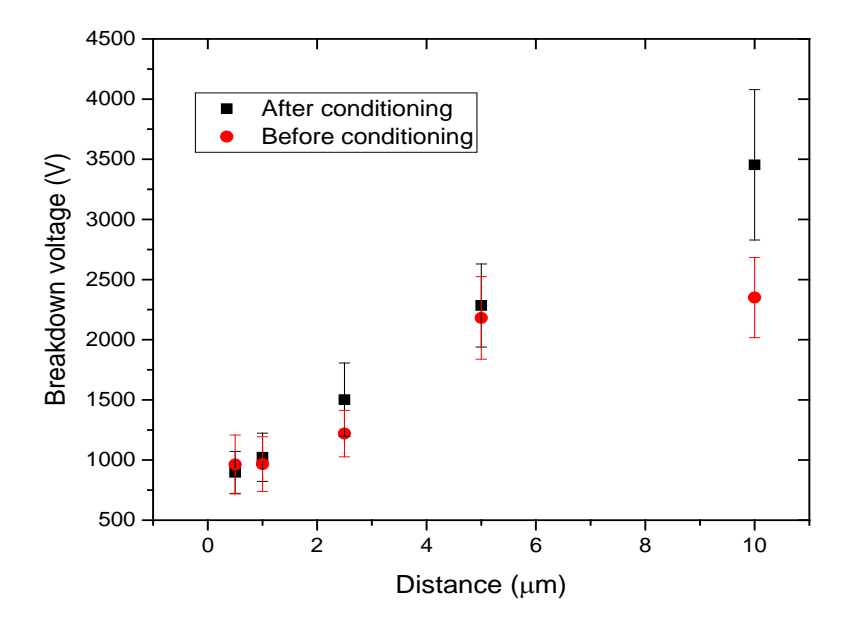


Fig. 1: Breakdown voltage before and after conditioning depending on electrode distance in fast pulse regime ( $10^7$  kV/s) at pressure ~  $2.10^{-4}$  Pa.

The measured data were analysed using the Fowler-Nordheim theory and thermoemission theory which resulted in determination of other important parametres such as enhancement factor  $\beta$ , current density and emitter surface which are important for simulation and optimization of microdischarges at high pressures.

The authors acknowledge partial support by Slovak Grant Agency for Science VEGA Nr. 1/0489/21, Slovak Research and Development Agency under project Nr. APVV-19-0386 and SK-SRB-21-0004.

#### References

- [1] Martišovitš V. (2006), Základy fyziky plazmy. Bratislava: Univerzita Komenského. ISBN 80-223-1983-X
- [2] Mustafa, M. F., Fu, X., Liu, Y., Abbas, Y., Wang, H., & Lu, W. (2018). Volatile organic compounds (VOCs) removal in non-thermal plasma double dielectric barrier discharge reactor. Journal of hazardous materials, 347, 317-324.
- [3] Shenton, M. J., Lovell-Hoare, M. C., & Stevens, G. C. (2001). Adhesion enhancement of polymer surfaces by atmospheric plasma treatment. Journal of Physics D: Applied Physics, 34(18), 2754.
- [4] Klas, M., Čermák, P., Borkhari, A. F., Satrapinskyy, L., Matejčík, Š., Radjenović, B., & Radmilović-Radjenović, M. (2021). Vacuum breakdown in microgaps between stainless-steel electrodes powered by direct-current and pulsed electric field. Vacuum, 191, 110327.

#### Poster P11 - Lucia Kuthanová

Fundamental problems of high pressure discharges

### SPATIOTEMPORAL MEMORY EFFECTS IN BARRIER DISCHARGE AT WATER INTERFACE

<u>Lucia Kuthanová<sup>1</sup></u>, Tomáš Hoder<sup>1</sup>

<sup>1</sup>Dept. of Phys. Electronics, Faculty of Science, Masaryk University, Brno, Czech Republic

E-mail: nanai@mail.muni.cz

The memory effects are generally known to have a significant influence in barrier discharges [1, 2]. The most notable memory propagation agents are usually the electrical 'imprints' of discharge pulses, namely it is the deposition of the charge on dielectric surfaces and presence of residual ionization of the bulk gas. Both of these can modify the local electric field and thus facilitate or delay the subsequent plasma initiation. In such way, a bond between the previous and subsequent discharge pulses is created and a study of this relationship can bring valuable insight into memory propagation in the system and promote proper understanding of the discharge physics and stochasticity of their behaviour.

In this experimental study [3] we investigated the memory effects in a surface barrier discharge in contact with water through the means of electrical measurements and synchronised 2D intensified CCD imaging. Large sets of recordings with high temporal resolution and broad dynamic range were processed into comprehensive database of individual discharge pulses properties, which was then analysed. Evaluating both conditional and unconditional discharge pulse occurrence probabilities confirmed known memory pathways and revealed some new memory patterns. The first discharges in the positive polarity are suspected to be Markov states, without any memory propagated from previous negative half-period. They also tend to cluster into two groups, which significantly impacts further evolution of the discharge, most notably the directly subsequent second discharge pulses. This behaviour is linked with the spatial organization of the filaments and photoemission-induced collective behaviour.

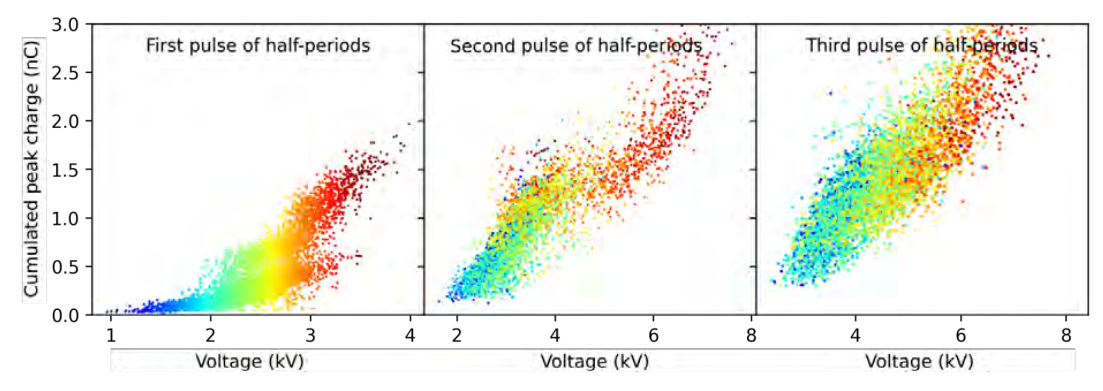


**Fig. 1**: The first three discharge pulses of positive half-periods in *QV* parametric space. The color of individual dots, each representing one discharge, is given by the breakdown voltage of the first discharge of given half-period and then inherited by the second and third discharges of the same half-period. In such way, the memory effect of the first discharge breakdown voltage is visualized.

#### **References:**

- [1] R. J. Van Brunt and E. W. Cernyar, Applied Physics Letters 58 2628–2630 (1991).
- [2] R. Brandenburg R, Plasma Sources Science and Technology 26 053001 (2017).
- [3] L. Kuthanová and T. Hoder, *Plasma Sources Sci. Technol.* (2022)

#### **Acknowledgments:**

This work has been supported by the project LM2018097 funded by Ministry of Education, Youth and Sports of the Czech Republic.

#### Poster P12 - Simon Dap

Fundamental problems of high pressure discharges

### PRE-IONIZATION IN ATMOSPHERIC PRESSURE TOWNSEND DISCHARGES (APTD): SURFACE VS VOLUME MECHANISMS

S. Dap<sup>1</sup>, C. Tyl<sup>1</sup>, X. Lin<sup>1</sup>, A. Belinger<sup>1</sup>, H. Höft<sup>2</sup>, M. Kettlitz<sup>2</sup>, R. Brandenburg<sup>2,3</sup>, N. Naudé<sup>1</sup>

<sup>1</sup> LAPLACE, Université de Toulouse, CNRS, INPT, UPS, Toulouse, France

<sup>2</sup> Leibniz Institute for Plasma Science and Technology (INP), 17489 Greifswald, Germany

<sup>3</sup> University of Rostock, Institute of Physics, 18059 Rostock, Germany

E-mail: simon.dap@laplace.univ-tlse.fr

To obtain a Townsend discharge in  $N_2$ - $O_2$  mixtures, a source of seed electrons between two discharges is necessary to enable uniform breakdown at low electric field strengths. This is referred to as the memory effect, which slows down the ionization process during the gas breakdown and avoids streamer formation leading to filamentary regime. Seed electrons between two discharges can come from the dielectric surfaces but also from the gas bulk. Generally, the dielectric covering the anode is charged with electrons during the discharge. These electrons could be released in the gas gap when the anode becomes the cathode during

These electrons could be released in the gas gap when the anode becomes the cathode during the subsequent half-period. The mechanisms related to the surface charges can be separated into two categories. First, the secondary electron emission leads to the release of trapped electrons from the surfaces. It can be enhanced by collisions of metastable species  $N_2(A^3 \Sigma_u^+)$  with the dielectric surface [1]. These particles are not charged and remain near the anode where they are created during the discharge. According to the literature, the  $N_2(A^3 \Sigma_u^+)$  lifetime is a few tenths of  $\mu$ s for low concentrations of oxidizing species [2]. Depending on the frequency, it may be shorter than the time between two discharges (roughly corresponding to 1/4th of the period). Thus, their density can remain high enough between two discharges to have a significant impact on the production of seed electrons for frequencies down to 2.5 kHz. However, the enhancement of the secondary electron emission by the  $N_2(A^3 \Sigma_u^+)$  collisions on the dielectrics could be negligible for lower frequencies. Moreover, the addition of oxidizing gas to nitrogen increases the quenching of the metastable species and reduces their contribution to the memory effect. Second, the electrons trapped on the dielectric surfaces can also be released spontaneously into

the gas gap [3]. This mechanism allows releasing seed electrons in the gas under low electric field, independently of the gas composition and the applied voltage frequency. At very low frequencies, when the species in the gas bulk are completely renewed between two subsequent discharges this mechanism prevails in the memory effect. It can also play a significant role in air, as the quenching rate of the metastable species of nitrogen such as  $N_2(A^3 \Sigma_u^+)$  is high. It depends of the nature of the dielectric surfaces [4] and in particular to their capacity to retain electrons [5-6]. Their role seems only predominant at very low frequencies, where no other memory effect mechanisms come into play.

The other type of mechanism responsible for the memory effect concerns the production of seed electrons in the gas bulk. Indeed, different chemical reactions occurring in the gas bulk can produce electrons. These mechanisms have been highlighted by the addition of small concentrations of oxidizing gas in nitrogen [7-8]. The creation of seed electrons by the associative ionization of  $O(^3P)$  and  $N(^2P)$  is currently the most likely assumption that can explain the origin of the memory effect in presence of an oxidizing gas [8-9]. However, the

positive ions in the gas created by the associative ionization reactions (for example NO<sup>+</sup> ions produced by the reaction between O(<sup>3</sup>P) and N(<sup>2</sup>P)) can also contribute to the memory effect, as it was suggested by F. Massines [1] and Nemschokmichal *et al.* [10]. When the gas gap voltage increases just before the breakdown voltage, these positive ions increase the secondary electron emission at the cathode and then the production of seed electrons. This hypothesis requires further investigations to be confirmed.

The different mechanisms responsible for the memory effect in APTDs and their quantification depending on the experimental conditions, are summed up in Figure 1. In Figure 1(a), the different memory effect mechanisms are compared as a function of the oxidizing gas concentration, for a fixed power supply frequency of a few kHz. In Figure 1(b), they are compared as a function of the power supply frequency, for gas mixture of nitrogen with a small concentration of oxidizing gas (few 10<sup>th</sup> of ppm). It shows that the dominant physical and chemical mechanisms involved in the memory effect are strongly related to the experimental conditions (gas composition, dielectric material, operating HV, ...). The seed electrons necessary to obtain an APTD are created through a combination of different mechanisms on the dielectric surfaces and in the gas gap, which are named in Figure 1. The understanding of the predominant mechanisms depending on the experimental conditions allows of better control of discharge stability, and the power dissipated in the discharge, for further plasma processes development.

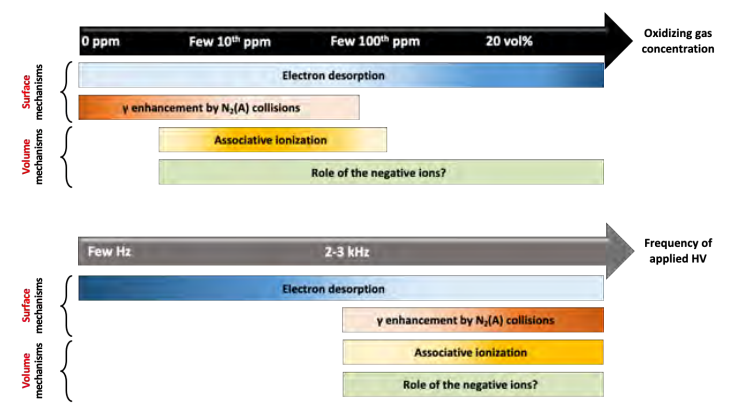


**Fig. 1**: Schematic representation of the dominant memory effect mechanisms as a function of: (a) the oxidizing gas concentration at a fixed frequency of a few kHz, and (b) the power supply frequency in nitrogen with a small concentration of oxidizing gas.

#### References:

- [1] F. Massines et al., The European Physical Journal Applied Physics, 47.2 (2009) 1–10
- [2] G. Dilecce et al., Plasma Sources Science and Technology, 16 (2007) 511–522
- [3] Y. B. Golubovskii et al., Journal of Physics D: Applied Physics, 35.8 (2002) 751–761
- [4] I. A. Kossyi et al., Plasma Sources Science and Technology, 1 (1992) 207–220
- [5] J. Ran et al., Physics of Plasmas, 25.3 (2018) 033511
- [6] H. Luo et al., Transactions on Plasma Science, 42.5 (2014) 1211-1215
- [7] R. Brandenburg et al., Journal of Physics D: Applied Physics, 38.13 (2005) 2187–2197
- [8] C. Tyl et al., Journal of Physics D: Applied Physics, 51 (2018) 354001
- [9] Xi Lin et al., Journal of Physics D: Applied Physics, 53 (2020) 205201
- [10] S. Nemschokmichal et al., The European Physical Journal D, 72.5 (2018) 89

## Poster P13 - Hiroshi Arai

Fundamental problems of high pressure discharges

# SPATIOTEMPORAL MEMORY EFFECTS IN BARRIER DISCHARGE AT WATER INTERFACE

<u>Lucia Kuthanová</u><sup>1</sup>, Tomáš Hoder<sup>1</sup>

<sup>1</sup>Dept. of Phys. Electronics, Faculty of Science, Masaryk University, Brno, Czech Republic

E-mail: nanai@mail.muni.cz

The memory effects are generally known to have a significant influence in barrier discharges [1, 2]. The most notable memory propagation agents are usually the electrical 'imprints' of discharge pulses, namely it is the deposition of the charge on dielectric surfaces and presence of residual ionization of the bulk gas. Both of these can modify the local electric field and thus facilitate or delay the subsequent plasma initiation. In such way, a bond between the previous and subsequent discharge pulses is created and a study of this relationship can bring valuable insight into memory propagation in the system and promote proper understanding of the discharge physics and stochasticity of their behaviour.

In this experimental study [3] we investigated the memory effects in a surface barrier discharge in contact with water through the means of electrical measurements and synchronised 2D intensified CCD imaging. Large sets of recordings with high temporal resolution and broad dynamic range were processed into comprehensive database of individual discharge pulses properties, which was then analysed. Evaluating both conditional and unconditional discharge pulse occurrence probabilities confirmed known memory pathways and revealed some new memory patterns. The first discharges in the positive polarity are suspected to be Markov states, without any memory propagated from previous negative half-period. They also tend to cluster into two groups, which significantly impacts further evolution of the discharge, most notably the directly subsequent second discharge pulses. This behaviour is linked with the spatial organization of the filaments and photoemission-induced collective behaviour.

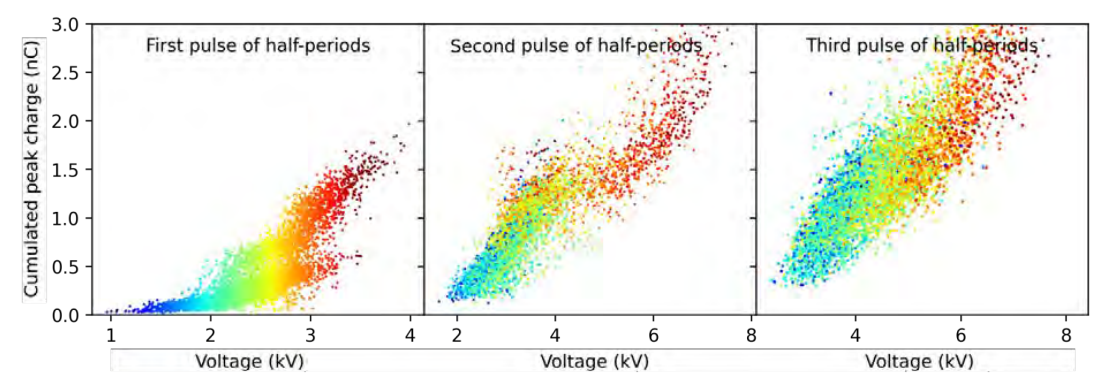


**Fig. 1**: The first three discharge pulses of positive half-periods in *QV* parametric space. The color of individual dots, each representing one discharge, is given by the breakdown voltage of the first discharge of given half-period and then inherited by the second and third discharges of the same half-period. In such way, the memory effect of the first discharge breakdown voltage is visualized.

## **References:**

- [1] R. J. Van Brunt and E. W. Cernyar, Applied Physics Letters 58 2628–2630 (1991).
- [2] R. Brandenburg R, Plasma Sources Science and Technology 26 053001 (2017).
- [3] L. Kuthanová and T. Hoder, *Plasma Sources Sci. Technol.* (2022)

# **Acknowledgments:**

This work has been supported by the project LM2018097 funded by Ministry of Education, Youth and Sports of the Czech Republic.

Fundamental problems of high pressure discharges

# Increase of Penning ionization coefficient proportional to small amount of water vapor admixed with helium

Haruo ITOH<sup>1,2</sup>, Hiroshi ARAI<sup>2</sup>, Susumu SUZUKI<sup>1</sup>, Nobuo SATOH<sup>2</sup>

<sup>1</sup> Department of Electrical and Electronical Engineering

<sup>2</sup> Department of Innovative Mechanical and Electronical Engineering

Chiba Institute of Technology, 2-17-1 Tsudanuma, Narashino-city, Chiba JAPAN

E-mail: haruo.itoh.rcit@gmail.com

Determination is carried out for the first and second Townsend ionization coefficients  $\alpha$  and  $\gamma$  in mixtures of helium and water vapor at 10.4 and 95.4 ppm (hereafter, denoted as He/H<sub>2</sub>O (10 ppm) and (100 ppm), respectively) by the steady state-Townsend method. The obtained first ionization coefficients in the mixture are large compared with those of He and H<sub>2</sub>O in the range of reduced electric field  $E/N \leq 1.13 \times 10^3$  Td; thus, we could conclude that the Penning effect<sup>(1)</sup> between He and H<sub>2</sub>O is formed. Moreover, a surprising result is uncovered, that is, the amount of increased Penning ionization coefficient is directly proportional to the amount of water vapor admixed with helium. If we set up a limitation of the water vapor content up to 100 ppm in helium, quantitatively consistent in these collision processes between the metastable excited helium and water vapor is clearly observable as a linear form Penning effect against the amount of water vapor in helium.

The experimental apparatus used here is the same one as described in a previous paper <sup>(2)</sup>. The observed ionized multiplication currents are analyzed by a linearized least squares method (Nakamura plot<sup>(3)</sup>) to determine the two ionization coefficients.

Figure 1 shows the observed ionization coefficient  $(\alpha/N)_{\text{He/H}_2\text{O}(100 \text{ ppm})}$  of 100 ppm H<sub>2</sub>O in He as filled purple circles against reduced electric field E/N together with that  $(\alpha/N)_{\text{He}}$  of He (blue circles with line). The brown curve is the total excitation coefficient  $(\alpha_{ex}/N)_{\text{He}^*}$  of the metastable states  $\text{He}^*(3\text{s})$  and  $\text{He}^*(1\text{s})^{(4)}$ . Here, we add the values on the brown curve  $(\alpha_{ex}/N)_{\text{He}^*}$  with those of the blue circles with line  $(\alpha/N)_{\text{He}}$  at every E/N value. Then, a theoretical ionization coefficient  $\left[(\alpha/N)_{\text{He/H}_2\text{O}(100 \text{ ppm})}\right]^{theor}$  is obtained, as illustrated by the purple line in the same figure. This purple line coincides well with the purple circles, i.e., observed ionization coefficients  $\left[(\alpha/N)_{\text{He/H}_2\text{O}(100 \text{ ppm})}\right]^{obs}$ . In another words, increments of the increase in the ionization coefficient from that of pure He correspond to the Penning ionization coefficient  $(\alpha_{pen}/N)_{\text{He/H}_2\text{O}(100 \text{ ppm})}$  and are also equivalent to the excitation coefficient  $(\alpha_{ex}/N)_{\text{He}^*}$  of He\*.

valent to the excitation coefficient 
$$(\alpha_{ex}/N)_{\text{He}^*}$$
 of the :
$$\left[ (\alpha/N)_{\text{He/H}_2\text{O (100 ppm)}} \right]^{obs} = (\alpha/N)_{\text{He}} + (\alpha_{pen}/N)_{\text{He/H}_2\text{O (100 ppm)}}$$

$$= (\alpha/N)_{\text{He}} + (\alpha_{ex}/N)_{\text{He}^*}$$

$$= \left[ (\alpha/N)_{\text{He/H}_2\text{O (100 ppm)}} \right]^{theor} . \qquad (1)$$

$$\therefore \quad (\alpha_{pen}/N)_{\text{He/H}_2\text{O (100 ppm)}} = (\alpha_{ex}/N)_{\text{He}^*} \cdot \dots \cdot \dots \cdot \dots \cdot (2)$$

In the same manner, green squares represent observed ionization coefficients  $(\alpha/N)_{\text{He/H}_2\text{O}(10 \text{ ppm})}$  of He/H<sub>2</sub>O (10 ppm). The green curve is consistent with 0.1 times the excitation coefficient,  $0.1 \cdot (\alpha_{ex}/N)_{\text{He}^*}$ , of He<sup>\*</sup> (orange line) and the ionization coefficient  $(\alpha/N)_{\text{He}}$  of He (blue circle with line).

$$\left[ (\alpha/N)_{\text{He/H}_2\text{O (10 ppm)}} \right]^{obs} = (\alpha/N)_{\text{He}} + (\alpha_{pen}/N)_{\text{He/H}_2\text{O (10 ppm)}}$$

$$= (\alpha/N)_{\text{He}} + 0.1 \cdot (\alpha_{ex}/N)_{\text{He}^*} \cdot \dots \cdot \dots \cdot \dots \cdot (3)$$

$$= \left[ (\alpha/N)_{\text{He/H}_2\text{O (10 ppm)}} \right]^{theor} \cdot \dots \cdot (4)$$

$$\therefore (\alpha_{pen}/N)_{He/H_2O (10 \text{ ppm})} = 0.1 \cdot (\alpha_{ex}/N)_{He^*}$$

Therefore, the following expressions are derived, from (2) and (4).

Here, k is the transformation ratio from the excitation coefficient  $(\alpha_{ex}/N)_{\text{He}^*}$  of  $\text{He}^*$  to the Penning ionization coefficient  $(\alpha_{pen}/N)_{\text{He/H}_2\text{O}}(100 \cdot k \text{ ppm})$ . m is the H<sub>2</sub>O content in He. These relations (6) and (7) are acceptable in the range of

and hence, the linear expression (6) of the Penning ionization coefficient from the excitation coefficient is validated in the range of k, as denoted by (8) combined with (7).

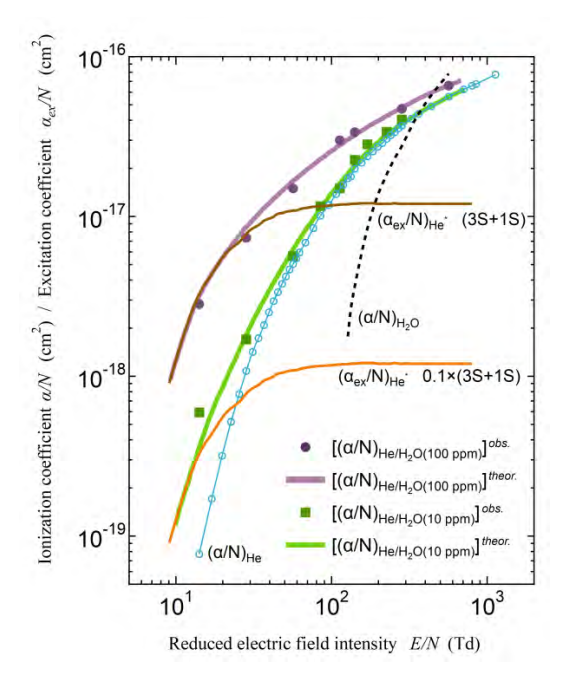


Fig. 1 Observed ionization coefficients in  $He/H_2O$  admixtures (purple circles and green squares). Theoretical ionization coefficients (purple line and green line) calculated from sum of excitation coefficients of  $He^*$  (brown line and orange line) and ionization coefficients of He (blue line with circle). Broken line is  $(\alpha/N)$  in  $H_2O$ .

- (1) A. A. Kruithof and F. M. Penning: Physica IV, No. 6, pp. 430-449, 1937.
- (2) S. Suzuki and H. Itoh: J. Phys. D: Appl. Phys., 52, 235203(11p), 2019.
- (3) Y. H. Paek, Y. Nakamura and T. Mori: T.I.E.E Japan, 97, No.4, pp. 183-188, 1977.
- (4) A.V. Phelps: Phys. Rev., 99, pp. 1307-1313, 1955.

Miscellaneous

# MICROELECTRODE-ASSISTED ATOMOSPHERIC PRESSURE AIR DISCHARGE AND ITS EXTENDED APPLICATIONS

Shuai Zhao<sup>1</sup>, Ana Sobota<sup>1</sup>, Wenzheng Liu<sup>2</sup>

<sup>1</sup>Department of Applied Physics, EPG, Eindhoven University of Technology,

5600 MB Eindhoven, The Netherlands

<sup>2</sup>School of Electrical Engineering, Beijing Jiaotong University, 100044, Beijing, China

E-mail: s.zhao@tue.nl

Based on the ideas of increasing the number of initial electrons and providing an appropriate electric field distribution for discharge space, a method benefitting from microdischarge process is proposed to achieve the atmospheric pressure glow-like discharge in air. With this method, a carbon fibre helical-contact electrode structure is formed and characterized by good discharge phenomenon and low discharge voltage. It is further expanded into a wire-cylindrical device with floating carbon fibres, which contributes to a three-dimensional glow-like discharge in a PFA tube of 6mm inner diameter. All the theoretical features of these electrode structures are explored.

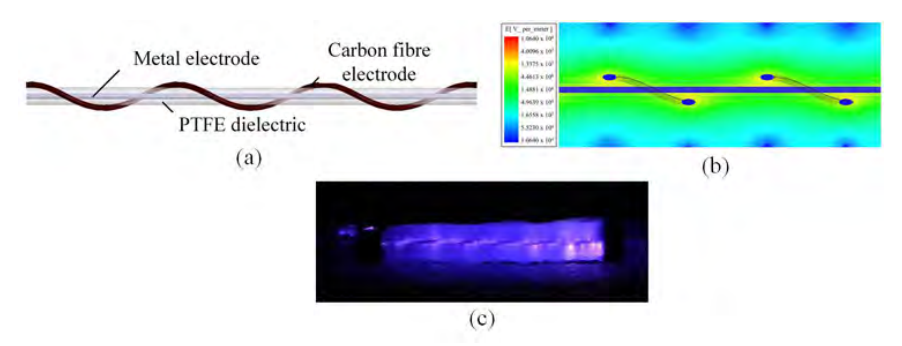


**Fig. 1**: The structure of carbon fibre helical-contact electrode and related discharge phenomenon. a) schematic diagram of the carbon fibre helical-contact electrode structure; b) the electric field distribution of this structure; c) the wire-cylindrical device with floating carbon fibres and its discharge in air. [1-2]

The carbon fibre helical-contact electrode structure is also expanded into a plasma generator for the flue gas treatment, practically the removal of  $SO_2$  and  $NO_x$  in this research. The system is established and the experiments are conducted. The influences of variables including the number of plasma generators, the applied voltage and the gas humidity on the removal rates of  $SO_2$  and  $NO_x$  are respectively discussed. The results are also compared with the corona discharge, a dominant plasma method in flue gas desulfurization and denitrification, and show some advantages in energy efficiency.

Furthermore, for the wire-cylindrical device with floating carbon fibres, a plasma jet will be ready by introducing the gas flow of helium or helium/air admixture into the tube. Optical emission spectroscopy (OES) will be used to get the basic information of gas temperature and of excited particles produced by this jet. Laser induced fluorescence (LIF) spectroscopy will be

used to measure the absolute densities of NO in this discharge. Finally, the parameters of this jet will be optimized with the aims of increasing the average density of NO in the jet effluent and extending its propagation length out of the nozzle. This system is about to build up. Here we just give a guideline about this part and more details will be shown in the poster presentation.

## References:

- [1] W. Liu, S. Zhao, J. Niu and M. Chai, Phys. Plasmas, 24, 093519 (2017).
- [2] S. Zhao, Y. Hao, T. Qiao and W. Cui, EPL, 130, 65001(2020).

Miscellaneous

# DIELECTIC BARRIER DISCHARGES: FROM SPATIALLY RESOLVED ELECTRICAL MEASUREMENTS TO A RECONFIGURABLE ELECTRODE

N. Naudé, S. Dap, A. Belinger LAPLACE, Université de Toulouse, CNRS, INPT, UPS, Toulouse, France

E-mail: nicolas.naude@laplace.univ-tlse.fr

Dielectric Barrier Discharges (DBDs) can be used in many processes such as thin-film coating, sterilisation, treatment of gases, aerodynamic flow control, and lighting devices [1]. Depending on the gas, electrical operation parameters and discharge geometry, the plasma operates in the classical filamentary mode or a homogeneous regime [2]. Therefore, electrical measurements are more convenient than optical measurements to characterise the discharge regime and study the discharge behaviour. However, because of the dielectric presence, it is not possible to directly measure the electrical parameters of the discharge. Usually, the electrical parameters of the discharge (discharge current and gap voltage) are calculated from the measured quantities with the usage of an electrical equivalent circuit [4]. The key parameter for this approach is the discharge area, which is usually considered equal to the electrode surface as long as the discharge is homogeneous. However, even if the plasma seems to cover the electrodes uniformly, its electrical properties (current density, breakdown voltage, duration of discharge, ...) are not precisely the same at any time and any point on the surface. To characterise the discharge behaviour more accurately, we developed an innovative electrical measurement allowing us to obtain a 2D mapping of the local current density [5]. The ground electrode is prepared as a segmented electrode with 64 equally spaced square segments. The high voltage electrode still remained full (figure 1). This system has been successfully used to study the memory effect responsible for the Townsend breakdown in the presence of oxidising species (N<sub>2</sub>+O<sub>2</sub>, N<sub>2</sub>+N<sub>2</sub>O, N<sub>2</sub>+NO) [6]. This electrode arrangement coupled with the measuring system allow a 2D mapping of the discharge electrical parameters (discharge current, power dissipated, gap voltage, etc.) of Townsend but also for Glow discharges, hybrid or patterned regimes.

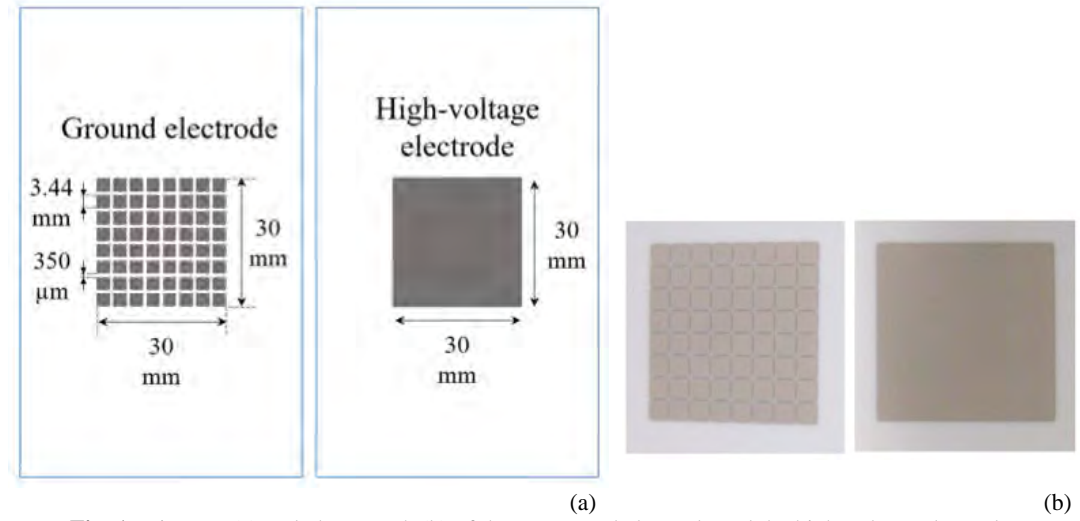


Fig. 1: Diagram (a) and photograph (b) of the segmented electrode and the high-voltage electrode

For now, this system has been used only to study discharge physics. However, it could also be used for plasma processes. Indeed, for a surface coating process, this system can be used to monitor the evolution of the local discharge power, which defines the local deposition rate. Using this segmented electrode as the high voltage electrode with a dedicated power supply, we could reconfigure the electrode and the power transfer to the discharge. Then this system could be used to realise patterns. This opens up new directions, which will be discussed during the presentation.

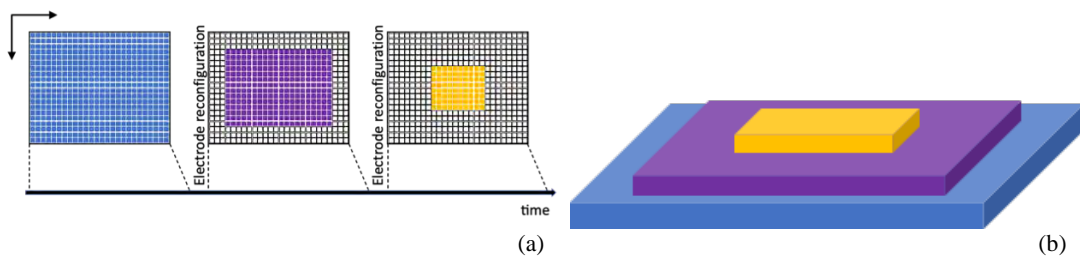


Fig. 2: (a) Illustration of the reconfigurable electrode concept, (b) Illustration of a pattern coating

#### References:

- [1] U. Kogelschatz, Plasma Chem Plasma P 23 (1), 1-46 (2003).
- [2] R. Brandenburg, Plasma Sources Science and Technology 26 (5), 053001 (2017).
- [3] F. Massines, C. Sarra-Bournet, F. Fanelli, N. Naudé and N. Gherardi, Plasma Process Polym 9 (11-12), 1041-1073 (2012).
- [4] A. V. Pipa, J. Koskulics, R. Brandenburg and T. Hoder, Rev Sci Instrum. 83 (11), 115112 (2012).
- [5] C. Tyl, S. Martin, C. Combettes, G. Brillat, V. Bley, A. Belinger, S. Dap, R. Brandenburg and N. Naudé, Rev Sci Instrum. 92 (5), 053552 (2021).
- [6] C. Tyl, X. Lin, M. C. Bouzidi, S. Dap, H. Caquineau, P. Segur, N. Gherardi and N. Naude, J Phys D Appl Phys 51 (35) (2018).

#### Poster P17 - Zdenek Navratil

Modelling and diagnostics

# 2D-resolved electric field measurement in helium coplanar DBD using multi-wavelength single photon counting

Zdeněk Navrátil and David Štegner

Department of Physical Electronics, Faculty of Science, Masaryk University,

Kotlářská 2, 611 37 Brno, Czech Republic

E-mail: zdenek@physics.muni.cz

#### 1 Introduction

2D resolution is often required to capture the true image of the discharge behaviour. Even diffuse barrier discharges exhibit some kind of non-uniformity (perpendicular to the electrode gap), as e.g. radial development of volume DBD with extra current peaks in the half period [1] or local electric field enhancement observed in coplanar barrier discharge [2].

The requirement of 2D resolution strongly favours array detectors as CCD or ICCD. However, coupling of the camera with a monochromator leads to the drop of one spatial dimension in favour of the spectral resolution. The 2D resolution can be preserved when using interference filters in front of the camera [2]. However, a small deviation of the discharge time development or a small error in image matching can lead to erroneous electric field values. The aim of this contribution is to present a novel instrumentation method of line intensity ratio measurement based on multi-wavelength photon counting. The presented method possesses the 2D spatial resolution, a single photon sensitivity and a simultaneous measurement of both spectral lines constituting the line intensity ratio. The method is applied to the diagnostics of coplanar barrier discharge operated in non-uniform gap in helium at atmospheric pressure.

# 2 Experimental set-up

The coplanar barrier discharge was generated in helium (gas purity 5.0) between triangular brass electrodes covered by 0.7 mm thick alumina. The minimal electrode gap was 5 mm. The amplitude of the applied sinusoidal AC voltage was 6 kV<sub>pp</sub>, the frequency was 11 kHz.

The optical diagnostics were carried out using a time-correlated single photon counter (TCSPC) combined with a dual axis scanning galvo mirror system. The light coming from the discharge was projected by a CaF<sub>2</sub> lens through the galvo mirrors onto an iris diaphragm. A bifurcated optical fibre beyond the diaphragm guided the light into two photomultiplier tubes (Becker-Hickl PMC 100), working in the photon counting mode. Interference filters placed at the PMT inputs (Thorlabs FL670-10 and FL730-10) ensured the isolation of light of two spectral lines (He I 668 and 728 nm). The photons arriving into the photomultipliers were counted and sorted according to their arrival times and positions of the mirrors using double TCSPC system (Becker-Hickl, SPC-152). The electric field was obtained from the measured line ratio I<sub>668</sub> /I<sub>728</sub> by method described in [3].

#### 3 Results

The 2D resolved intensity of He I 728 nm line is displayed for three different times within one discharge current peak in Fig. 1, upper row. The patterns clearly display the cathode-directed ionizing wave (CDIW), moving to the right, and anode directed ionizing wave (ADIW), moving to

the left. The discharge development is similar to that of coplanar discharge with uniform gap [3], though the discharge is more constricted to the symmetry axis and the propagation of the waves in later phases is mostly restricted to the dielectric region with metallic electrode located underneath. The axial speed of the CDIW development clearly varies with the distance from the symmetry axis. Whilst the CDIW speed is high at the axis and the light quickly disappears from the observed area, the light emission from regions distant from the axis persists longer. This can be understood from the electric field development, obtained from the line intensity ratio, and displayed in Fig. 1, bottom row.

The maximal values of electric field around 35 kV/cm are observed in early phases of the discharge development, when the CDIW moves above the cathode in narrow region along the symmetry axis. When the CDIW head disappears, a wide region of lower electric field around 20 kV/cm remains. The field seems to be maintained far from the symmetry axis also in the late phase of the discharge development. The electric field in ADIW is lower, around 10 kV/cm. Lower electric field regions must be considered carefully, since that the electric field cannot be interpreted when the plasma is far from ionizing state, required by the collisional-radiative model in [3].

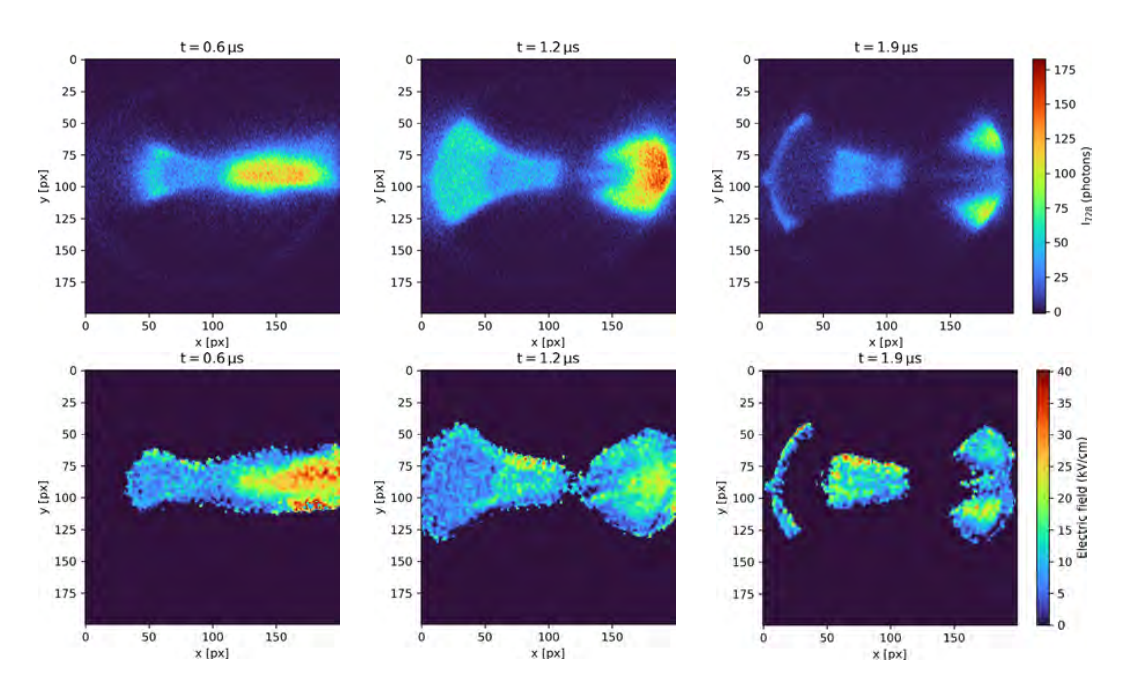


**Fig. 1**: 2D resolved intensity of He I 728 nm line at different times within one discharge current peak (top row). Electric field determined from the line ratio (bottom row).

# Acknowledgement

This study was supported by the project LM2018097 funded by the Ministry of Education, Youth and Sports of the Czech Republic.

#### References

- [1] Mangolini L et al 2002 Appl. Phys. Lett. 80 1722
- [2] Cech J et al 2018 Plasma Sources Sci. Technol. 27 105002
- [3] Ivković S S et al 2014 J. Phys. D: Appl. Phys. 47 055204

#### Poster P18 - Emanuel Maťaš

Modelling and diagnostics

# Ion Mobility Spectrometry diagnostics of NO<sub>x</sub> generated in kHz driven DBD plasma jet in Argon

Emanuel Maťaš<sup>1</sup>, Ladislav Moravský<sup>1</sup>, Štefan Matejčík<sup>1</sup>

<sup>1</sup>Department of Experimental Physics, Comenius University, Mlynská dolina F2, 84245

Bratislava, Slovakia

E-mail: emauel.matas@fmph.uniba.sk

Ion mobility spectrometry (IMS) is a rapid and powerful analytical method that involves the detection, and identification of ionized gas molecules based on their mobility in gaseous environment and presence of electric field [1]. The mobility of ions depends on their shape, size, weight, and charge. The main advantages of this technique are compact design, high sensitivity (ppb-ppt level), fast response (ms range), operation at atmospheric pressure. The IMS instrument consisting of several parts, namely the ion source, the reaction region, the shutter grid, the drift tube, and the detector [2, 3]. The IMS can be used for direct sampling of gaseous substances, for headspace sampling of vapours of liquids and also for thermal or laser desorption of substances from surfaces. It can be applied for monitoring of the ambient air or for online monitoring of different plasma processes producing neutral molecules. The IMS instrument offers fast response (ms - s range) and high sensitivity (ppb-ppt range) [3] and the spectrometer can be operated both in positive and negative polarities. In the negative polarity, the IMS can be used to detect gaseous products of cold atmospheric plasma jet (CAPJ) with high electron affinities.

CAPJ devices have been investigated during the recent decade due to their applications in the field of material sciences and in biomedicine [4]. The advantage of the CAPJ is the high local concentration of chemically active species, such as electrons, radicals, and reactive species (O, OH, O<sub>3</sub>, NO, NO<sub>2</sub>...) while maintaining a low gas temperature.

The studied CAPJ was operated in argon flowing through a quartz capillary with 0.5-mm inner diameter into the ambient air, and the plasma was generated by kHz frequency AC power supply. To identify and determine the concentration of the active oxygen species, optical emission spectroscopy (OES), fluorescent probes, chemical dosimetry, and Fourier transform infrared spectroscopy (FTIR) are frequently used [5]. In present work we are going to demonstrate IMS as a suitable method for fast and efficient monitoring of these products.

In Figure 1 (red line) the IMS spectrum of the CAPJ (AC = 7.68kV) is presented (red line). The ions such as  $NO_2^-$ ,  $NO_3^-$  and  $NO_3^-$ .HNO<sub>3</sub> were detected as indicated in the spectrum. The ionization of neutral  $NO_x$  species was carried out using the negative chemical ionization method, with  $O_2^-CO_2$  ions as Reactant ions (RI):

$$O_2 CO_2 + NO_x \rightarrow NO_x + O_2 + CO_2$$
 (1)

This electron transfer reaction case ionizes molecules with electron affinity, exceeding the bond energy of the electron in the reactant ions O<sub>2</sub>-CO<sub>2</sub>, which is about 1.2 eV [6]. This condition is valid for NO<sub>2</sub>, NO<sub>3</sub> substances. The intensity of the ions is then proportional to the

concentration of the neutral precursors. For the quantitative measurements of these substances, calibration of the IMS response to the precursor molecules must be carried out.

The blue line in the Figure 1 represents an IMS spectrum of neutral NO<sub>2</sub> standard at a concentration of 5 ppm. We can see that the intensity of the NO<sub>2</sub> from NO<sub>2</sub> mixture at concentration of 5 ppm is much higher than the NO<sub>2</sub> from the CAPJ. This indicates that in the CAPJ lower concentrations of NO<sub>2</sub> were generated. There exists need to perform detailed calibration measurements for NO<sub>2</sub>. In order to achieve reliable quantitative results regrading NO<sub>2</sub> production in the CAPJ. The preliminary results indicate, the IMS has potential for fast and sensitive detection of NO<sub>2</sub> at sub ppm concentrations.

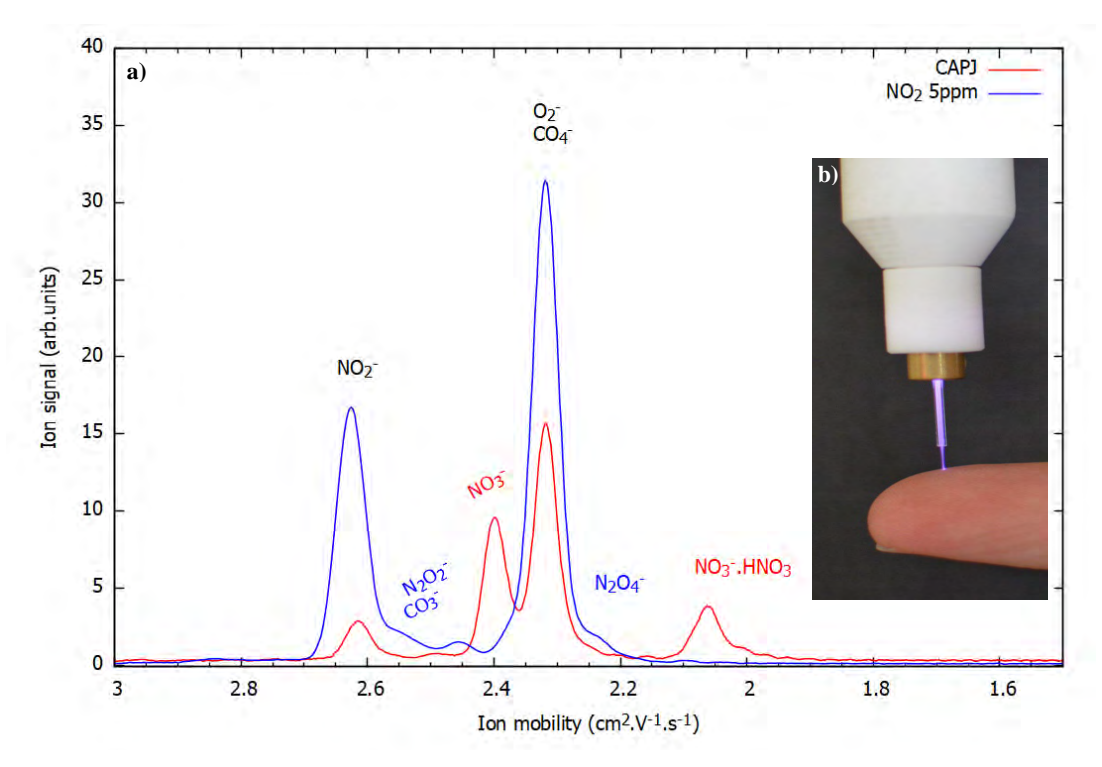


Fig. 1: a) IMS spectrum of CAPJ (red line) and 5 ppm NO<sub>2</sub> (blue line), b) picture of CAPJ.

The present studies were carried out with the support of Slovak Research and Development Agency under project Nr. APVV-19-0386.

#### **References:**

- [1] EICEMAN, Gary Alan; KARPAS, Zeev. Ion mobility spectrometry. CRC press, 2005.
- [2] HILL JR, Herbert H., et al. Analytical Chemistry, 1990, 62.23: 1201A-1209A.
- [3] SABO, Martin; MATEJČÍK, Štefan. Analytical chemistry, 2011, 83.6: 1985-1989.
- [4] JÖGI, Indrek, et al. Contributions to Plasma Physics, 2020, 60.3: e201900127.
- [5] MORAVSKÝ, Ladislav, et al. Contributions to Plasma Physics, 2020, 60.7: e202000014.
- [6] LEE, Sang Hak, et al. The Journal of Physical Chemistry A, 2021, 125.26: 5794-5799.

#### Poster P19 - Sara Ceulemans

Modelling and diagnostics

# Effect of quenching on the afterglow temperature to improve CO<sub>2</sub> conversion in a rotating gliding arc plasma reactor

<u>Sara Ceulemans</u><sup>1</sup>, Colin O'Modhrain<sup>1</sup>, Joshua Boothroyd<sup>1</sup>, Ivan Tsonev<sup>1</sup>, Senne Van Alphen<sup>1</sup>, and Annemie Bogaerts<sup>1</sup>

<sup>1</sup>Research group PLASMANT, Department of Chemistry, University of Antwerp, Universiteitsplein 1, BE-2610 Wilrijk-Antwerp, Belgium

E-mail: sara.ceulemans@uantwerpen.be

Due to global warming, there is a large interest in lowering the concentration of CO<sub>2</sub> in the atmosphere. This can be achieved by capturing the CO2 and storing it (Carbon Capture and Storage, CCS), but a more interesting approach is to use the captured CO<sub>2</sub> to create fuels and chemicals (Carbon Capture and Utilization, CCU). A promising way to do this is by the use of plasma, which has important advantages over other CO<sub>2</sub> conversion techniques, e.g. it does not require any rare earth metals, the plasma can be created using renewable electricity and it can instantly be switched on and off [1]. The aim in plasma conversion of CO<sub>2</sub> is to simultaneously obtain a high conversion and a high energy efficiency, which is why different methods to increase both are being investigated. One way to do this is by quenching in the afterglow, i.e. immediately cooling down the gas after the plasma reactor. This will limit the recombination of CO and O2 molecules back into CO2, which lowers both the conversion and the energy efficiency. It has already been shown through simulations that quenching the gas in the afterglow can improve the results [2], and experiments in a microwave reactor and a thermal plasma reactor have also reported better conversions or energy efficiencies [3,4]. In this research, we investigate the effect of quenching in a rotating gliding arc (RGA) reactor. This type of reactor creates a warm plasma, causing dissociation of CO<sub>2</sub> mainly by thermal reactions, it can operate at atmospheric pressure and, in contrast to a classical gliding arc reactor, it has a 3D geometry, enabling more gas to pass through the discharge zone.

To investigate the effect of quenching in the afterglow, we created a thermal model of an RGA reactor. In this model, we assumed that the plasma is in local thermodynamic equilibrium and at this stage we included no reactions in order to keep the model as simple as possible, while still obtaining valuable insights. There are different methods of cooling the afterglow, two of which we tested in our RGA model: the use of a quenching nozzle and the addition of an extra gas inlet after the reactor that supplies room temperature gas. When using a quenching nozzle, we varied the geometry of the nozzle and speed of the gas, reaching both subsonic and supersonic velocities after the nozzle. For the extra gas inlet, we tested the effects of both Ar and  $CO_2$  as the cooling gas in addition to the position of the inlet. In further research, we hope to experimentally validate these results.

#### References

- [1] R. Snoeckx, and A. Bogaerts, *Chem. Soc. Rev.*, **46**, 5805 (2017)
- [2] V. Vermeiren, and A. Bogaerts, J. Phys. Chem. C, 124, 18401 (2020)
- [3] W. Bongers, H. Bouwmeester, B. Wolf, F. Peeters, S. Welzel, D. van den Bekerom, N. den Harder, A. Goede, M. Graswinckel, P. W. Groen, J. Kopecki, M. Leins, G. van Rooij, A. Schulz, M. Walker, and R. van de Sanden, *Plasma Process Polym.*, **14**, 1 (2017)
- [4] J. Li, X. Zhang, J. Shen, T. Ran, P. Chen, and Y. Yin, J. CO<sub>2</sub> Util., 21, 72 (2017)

#### Poster P20 - Dennis Bouwman

Modelling and diagnostics

# Theoretical approximations for macroscopic parameters of positive streamer discharges

Dennis Bouwman<sup>(\*),1</sup>, Hani Francisco<sup>1</sup>, Ute Ebert<sup>1,2</sup>

Multiscale Dynamics, Centrum Wiskunde & Informatica (CWI), Amsterdam, The Netherlands
 Department of Applied Physics, Eindhoven University of Technology, Eindhoven, The Netherlands

 (\*) Dennis.Bouwman@cwi.nl

We present a self-contained theoretical model that describes a positive streamer with three parameters: velocity  $\nu$ , radius R and the thickness of the space-charge layer  $\ell$ . The model input is a one-dimensional function  $\lambda$  which represents the on-axis width-integrated space-charge in the channel. We show how to obtain the three streamer parameters and that they agree with results from simulation.

Characterizing the streamer discharge with only a few macroscopic parameters is a classic unsolved problem, with the first 'order-of-magnitude' approximations dating back to 1989 [1]. This is an important missing step in the development of simplified streamer models which are crucial for advancing our understanding of multiscale streamer discharge phenomena such as repetitively pulsed discharges and sprite discharges.

In this work we derive and evaluate semi-analytic approximations for macroscopic parameters of a positive streamer. We identify three streamer parameters that are sufficient for an on-axis description of positive streamer propagation. These three parameters are: velocity v, radius R and thickness of the space-charge layer  $\ell$ . Moreover, we show how to solve v, R and  $\ell$  given a one-dimensional function  $\lambda$  which is the on-axis width-integrated space-charge. We have assumed  $\lambda$  to be known, since it was shown in [2] how this function can be calculated using an on-axis macroscopic model. In order to calculate v, R and  $\ell$  we first have to calculate the on-axis electric fields (roughly following [2]) and the on-axis electron density ahead of the streamer head. Then we reformulate first-principle physical laws (e.g. conservation of total current) into three equations which the parameters v, R and  $\ell$  have to satisfy. It turns out that this problem is implicit, coupled and nonlinear. Therefore the streamer parameters are obtained numerically. We do so by recasting the problem into the *streamer root-equation*:

$$S(v, R, \ell) = 0$$
,

which can be solved, for instance, by iterative root-finding algorithms. In other words, solving for the roots of the (three-dimensional vector) function S yields the desired macroscopic streamer parameters. The result of our approximation for a streamer with length of 15 mm in an electric field of 14 kV/cm is shown in Table 1. Using the approximated parameters R,  $\ell$  and  $\lambda$  we are then able to reconstruct the (full) electric field along the axis of propagation, shown in Figure 1.

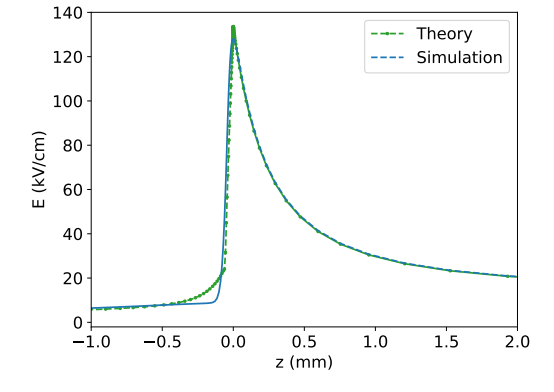
This theoretical model addresses a big hiatus in the development of macroscopic streamer models. Moreover it is particularly well-suited to be used in combination with streamer tree-models, e.g. [2, 3], which often require v, R and  $\ell$  in order to calculate the evolution of  $\lambda$  (note that the two models thus complement each other exactly).

Furthermore, the theoretical framework also allows us to develop understanding into the nonlinear behaviour of positive streamer discharges. For example in Figure 2 we show our (nonlinear) relation between v and R as a function of the electric field at the streamer head ( $E_{\rm max}$ )

- [1] M. I. D'yakonov, V. Y. Kachorovskii, Zh. Eksp. Teor. Fiz 95 (1989) 1850-1859
- [2] A. Luque, M. González, F. J. Gordillo-Vázquez *Plasma Sources Science and Technology* **26** (2017) 125006.
- [3] A. Luque, U. Ebert New Journal of Physics 16 (2014) 013039

Parameter	Simulation	Theory	Relative error
v	0.77 mm/ns	0.79 mm/ns	1.9%
R	0.66 mm	0.64 mm	3.1%
$\ell$	92 μm	60 μm	36%
$E_{\rm max}$	128 kV/cm	134 kV/cm	4.3%
$E_{\mathrm{ch}}$	8.6 kV/cm	10.3 kV/cm	20%
$n_{e,\mathrm{ch}}$	$6.2 \cdot 10^{19} / \text{m}^3$	5.8·10 <sup>19</sup> /m <sup>3</sup>	6.7%

Table 1: Approximation of important macroscopic parameters of a positive streamer in a  $14\,\mathrm{kV/cm}$  background field with a length of 15 mm: velocity  $\nu$ , radius R, width of the space-charge layer  $\ell$ , electric field at the streamer head  $E_{\mathrm{max}}$ , electric field in the channel  $E_{\mathrm{ch}}$  and electron density in the channel  $n_{e,\mathrm{ch}}$ . All parameters are approximated within several tens of percent.



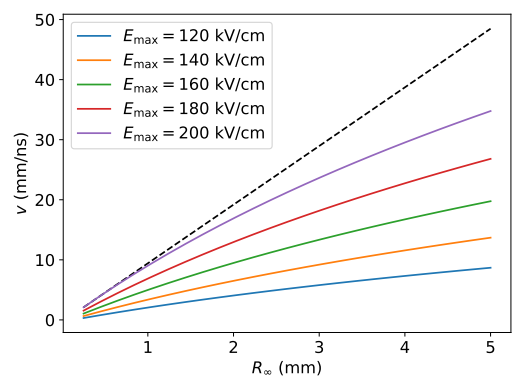


Fig. 1: The electric field on the axis of propagation (to the right) at the streamer head located at z=0, reconstructed using approximated parameters R and  $\ell$  from Table 1 and  $\lambda$ .

Fig. 2: A *nonlinear* relation between velocity v and radius R as a function of electric field at the streamer head  $E_{max}$ .

#### Poster P21 - Tomas Hoder

Modelling and diagnostics

# KINETICS OF THE $N_2(A^3\Sigma^+_u, v)$ STATE IN ATMOSPHERIC PRESSURE TOWNSEND DISCHARGE IN $N_2$

Petr Bílek<sup>1</sup>, Lucia Kuthanová<sup>2</sup>, <u>Tomáš Hoder<sup>2</sup></u>, Milan Šimek<sup>1</sup>

<sup>1</sup>Institute of Plasma Physics of the Czech Academy of Sciences, Prague, Czech Republic

<sup>2</sup>Department of Physical Electronics, Faculty of Science, Masaryk University, Brno, Czech Republic

E-mail: hoder@physics.muni.cz

Barrier discharges in gases at atmospheric pressure are important sources of non-equilibrium plasma and are studied both for fundamental and applied research reasons [1]. In most cases these discharges operate in a filamentary regime [2] where the discharge consists of many microdischarges of filamentary shape, bridging the space between the two dielectrics-covered electrodes. The second important regime in which the barrier discharges may operate at atmospheric pressure is the so-called homogeneous or diffuse barrier discharge [3]. Such discharge does not present structural variation in the plane perpendicular to the axis connecting the electrodes and appears to be homogeneous or diffuse. The memory effects play here an important role, maintaining the residual electron/metastable densities between the half-periods over a certain threshold, so the subsequent discharges start in a sufficiently preionised environment. There are two types of homogeneous barrier discharges at atmospheric pressure, the Townsend discharge type (usually denoted as "atmospheric pressure Townsend discharge", i.e. APTD, or as "Townsend dielectric barrier discharge", TDBD) and the glow discharge type ("atmospheric pressure glow discharge", APGD, or glow dielectric barrier discharge, GDBD). Both types were observed and studied under different conditions or operated in different gases. Concerning molecular gases, the APTD was studied in pure nitrogen [4] as well as in nitrogen with small admixtures of oxygen or nitric oxide [5-7].

This work reports our effort and findings in the investigation of the APTD operated in barrier discharge setup in pure nitrogen. We focus on the two lowest vibrational levels of the  $N_2(A^3\Sigma^+_u)$  metastable state since they are thought to play an important role in the secondary emission of electrons from dielectric surfaces in the APTD. In order to grasp the complex nature of the  $N_2(A^3\Sigma^+_u, v)$  state we developed a detailed state-to-state vibrational kinetic model of  $N_2$  applicable mainly at low reduced electric fields (< 200 Td). The model includes the four lowest vibrationally-resolved electronic states of the molecular nitrogen:  $N_2(X^1\Sigma^+_g)$ ,  $N_2(A^3\Sigma^+_u)$ ,  $N_2(B^3\Pi_g)$ ,  $N_2(W^3\Delta_u)$  and  $N_2(C^3\Pi_u)$  state, which are produced by the electron-impact excitation of  $N_2(X^1\Sigma^+_g, v=0)$ . Moreover, the model benefits from the determination of the electric field and the electron density profile using the equivalent electric circuit analysis, see Fig. 1(a). The knowledge of the electric field and the electron density significantly reduces the number of free parameters of the model and thus improves the accuracy of kinetic predictions.

Results of the kinetic model are compared with the measured emission spectra of the Second Positive System (SPS) and the Herman InfraRed (HIR) system of  $N_2$ . The peak intensity of the SPS correlates with the discharge current peak as shown in Fig. 1(b), which proves that during the active discharge phase the  $N_2(C^3\Pi_u)$  state is created mainly due to the electron impact

excitation. Conversely, during the postdischarge phase (30  $\mu$ s < t < 50  $\mu$ s) the  $N_2(C^3\Pi_u)$  state is populated due to the energy pooling between  $N_2(A^3\Sigma^+_u, v=0\text{-}1)$  metastables. The upper states of the HIR are produced exclusively by the energy pooling between  $N_2(A^3\Sigma^+_u, v=0\text{-}1)$  metastables and Fig. 1(b) shows the maximum of the HIR intensity delayed about 15  $\mu$ s after the discharge current peak. This delay is caused due to radiative/quenching cascade  $N_2(C^3\Pi_u) \rightarrow N_2(B^3\Pi_g)/N_2(W^3\Delta_u) \rightarrow N_2(A^3\Sigma^+_u, v=0\text{-}1)$ , populating the  $N_2(A^3\Sigma^+_u, v=0\text{-}1)$  states with a lag beside the active discharge phase.

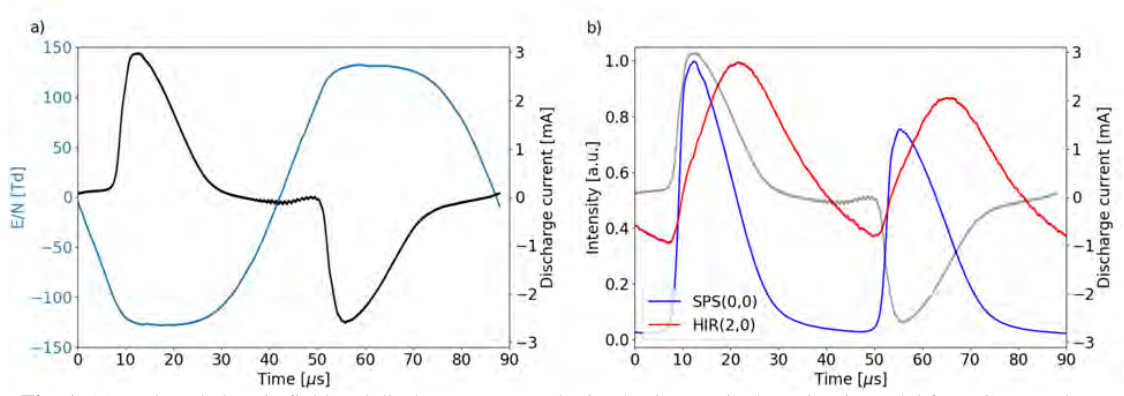


**Fig. 1**: (a) Reduced electric field and discharge current obtained using equivalent circuit model for AC HV voltage 14 kV (peak-to-peak). (b) Monochromatic waveforms collected using a set of suitable bandpass filters selecting SPS(0, 0) and HIR(2, 0) emissions at 337 and 710 nm, respectively.

The comparison of the kinetic model and experimental HIR intensity leads to the determination of the density of the two lowest vibronic levels of  $N_2(A^3\Sigma^+_u)$ . Finally, a method suitable for the purely experimental determination of  $N_2(A^3\Sigma^+_u)$ , v=0-1) metastable density based on the decay constant of the HIR intensity is proposed.

The work demonstrates that the complex kinetic modeling in the combination with the emission spectroscopy in the APTD setup can improve understanding of elementary processes in pure nitrogen plasmas. Such a strategy can be efficiently used even in more complex gas mixtures in the APTD regime.

**Acknowledgements:** This work was supported by the Czech Science Foundation (Project No. 15-04023S) and by the Strategy AV21 project. TH a LK acknowledge the support of the project LM2018097 funded by the Ministry of Education, Youth and Sports of the Czech Republic. We would like to thank prof. Andrey S. Kirillov (Polar Geophysical Institute Murmansk, Russia) for his beneficial advice and the discussion concerning intermolecular and intramolecular energy transfers.

- [1] F. Massines et al., *Plasma Processes and Polymers*, 9(11-12), 1041–1073, (2012).
- [2] U. Kogelschatz, IEEE Transactions on plasma science, 30(4), 1400–1408, (2002).
- [3] F. Massines et al., The European Physical Journal-Applied Physics, 47(2), (2009).
- [4] Y. B. Golubovskii et al., Journal of Physics D: Applied Physics, 35(8), 751, (2002).
- [5] R. Brandenburg et al., Journal of Physics D: Applied Physics, 38(13), 2187, (2005).
- [6] C. Tyl et al., Journal of Physics D: Applied Physics, 51(35), 354001, (2018).
- [7] X. Lin et al., Journal of Physics D: Applied Physics, 53(20), 205201, (2020).

## Poster P22 - Tomas Hoder

Modelling and diagnostics

# DEVELOPMENT OF A METHOD FOR DETERMINATION OF THE ELECTRIC FIELD IN TRANSIENT ARGON DISCHARGES

Tomáš Hoder<sup>1</sup>, Lukáš Kusýn<sup>1</sup>, Markus M Becker<sup>2</sup>, Zdeněk Bonaventura<sup>1</sup>, Detlef Loffhagen<sup>2</sup>

<sup>1</sup>Department of Physical Electronics, Faculty of Science, Masaryk University, 611 37 Brno, CZ <sup>2</sup>Leibniz Institute for Plasma Science and Technology (INP), 17489 Greifswald, DE

E-mail: hoder@physics.muni.cz

We present an analysis of a recently developed non-steady-state (time-dependent) collision-radiative model for the electric field determination in a highly transient dielectric barrier discharge in argon at atmospheric pressure. Collision-radiative models are well-established methods used for plasma diagnostics in various gases by means of optical emission spectroscopy. Typically, they are applied under steady-state assumptions, i.e., in time-independent form, to determine the density of metastable excited states or electrons in argon or air discharges [1,2]. The steady-state assumption simplifies the governing equations and can be conveniently applied to spectral recordings acquired by instrumentations lacking the high temporal resolution. In highly transient discharges, e.g., pulsed discharges, streamers, ionization waves, fast decay phases etc., the time-dependent processes taking place in the plasma remain thus mostly hidden or highly uncertain, although some tendencies can be uncovered (e.g. [3]) even if the simple steady-state model is used.

This contribution analyzes the methodology based on above mentioned non-steady-state collision-radiative model and synthesized optical emission spectroscopy data. Transient discharges in argon are considered as a suitable theoretical playground also for its high applicability potential. Experimentally, a high temporal resolution technique of time-correlated single photon counting is considered for spectroscopy data acquisition. For the collisional-radiative model in argon, we combine a fully time-dependent kinetic chemistry model with a fluid model for dielectric barrier discharges to obtain model-predicted optical emissions. This complex model provides us with synthetic optical emission profiles as an input for testing the collision-radiative model as well as with the detailed spatiotemporal distribution of the original electric field and densities of considered species.

Several approaches and line-intensity ratios are probed to find the most suitable method for the electric field determination with high spatiotemporal resolution. An example of such probing to find the best approach is exemplified in Fig.1 where the electric field development is shown as a result of the fluid model and as a result of the re-computation from the line intensity ratio via the developed collision-radiative model under given conditions. The sensitivity of the ratio to the electric field change and the possibility to experimentally obtain the effective lifetimes for the use in the kinetic scheme are the focus of interest. While the whole process is analyzed theoretically, the final intention is to develop an independent experimental method for the electric field determination with reasonable sensitivity and accuracy. Therefore, we also use methods of sensitivity analysis and uncertainty quantification to identify the main reaction

pathways in the collisional-radiative model and their influence on the electric field determination in the evaluated theoretical framework.

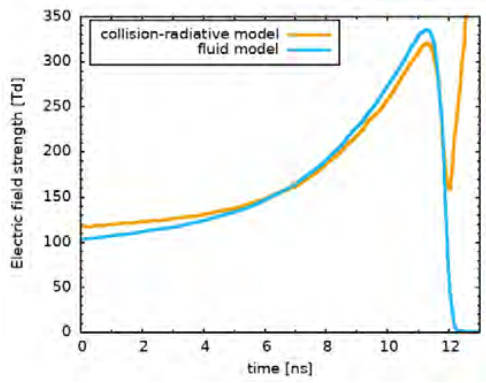


**Fig. 1**: The electric field development in the streamer head is shown as a result of the fluid model and as a result of the re-computation from the line intensity ratio via the developed collision-radiative model under given conditions.

- [1] D. Mariotti et al. Appl. Phys. Lett. 89 (2006) 201502.
- [2] X.-M. Zhu, Y.-K. Pu J. Phys. D: Appl. Phys. 43 (2010) 403001.
- [3] M. Šimek, P. Ambrico, T. Hoder et al. Plasma Sources Sci. Technol. 28 (2018) 055019.

This contribution was supported by the Czech Science Foundation grant project number 21-16391S. This research was also supported by Project CEPLANT (LM2018097) funded by the Ministry of Education, Youth and Sports of the Czech Republic.

Modelling and diagnostics

# GAS HEATING DYNAMICS IN A CO<sub>2</sub> PULSED GLOW DISCHARGE RESOLVED BY KINETIC MODELING

Omar Biondo<sup>1,2</sup>, Chloé Fromentin³, Tiago Silva³, Vasco Guerra³, Gerard van Rooij²,⁴,
Annemie Bogaerts¹

<sup>1</sup>Research Group PLASMANT, Department of Chemistry, University of Antwerp,
Universiteitsplein 1, Wilrijk B-2610, Belgium

<sup>2</sup>DIFFER, 5612AJ Eindhoven, The Netherlands

<sup>3</sup>Instituto de Plasmas e Fusão Nuclear, Instituto Superior Técnico, Universidade de Lisboa,
1049-001 Lisboa, Portugal

<sup>4</sup>Faculty of Science and Engineering, Maastricht University, 6229 GS Maastricht, The
Netherlands

E-mail: Omar.Biondo@uantwerpen.be

Renewable energy is a fast-growing market and is expected to become the largest power source by 2040 [1]. However, its intermittent nature makes a full exploitation of the natural energy sources hardly achievable [2]. Moreover, climate change is putting increasing pressure onto society and actions to drastically reduce our CO<sub>2</sub> emissions are more than ever needed. Therefore, the development of technologies able to simultaneously reduce CO<sub>2</sub> emissions and store the excess of renewable energy into chemical bonds of fuels is of vital importance.

To this end, plasma technology stands out as a viable tool to achieve splitting of CO<sub>2</sub>, which opens up to the different chemical routes to convert the undesirable waste product into valuable chemicals or fuels [3]. Extensive research has been conducted during the last decades to find out the optimal conditions to obtain energy-efficient conversion of CO<sub>2</sub> and make the technology attractive to the industrial sector while concurring to reduce our carbon footprint.

Vibrational excitation of the asymmetric stretch mode of CO<sub>2</sub> to its dissociation limit is believed to be an efficient channel for splitting, having the lowest threshold energy amongst the possible dissociation pathways [4]. However, the stepwise excitation up to the dissociation threshold, also called "ladder-climbing", is typically sustained only at limited reduced electric fields (E/N) and low gas temperature. Such favorable conditions can be offered by pulsed low-pressure discharges, where the modulation of the pulse and inter-pulse time allows to selectivity trigger the vibrational chemistry while limiting the gas heating [5].

In this perspective, we developed a zero-dimensional (0D) kinetic model to reproduce the evolution of the gas and vibrational temperature measured by Klarenaar *et al.* [6] in a pulsed glow discharge and determine the underlying heating dynamics. The kinetic scheme was established upon our previous modelling efforts and includes an extensive description of the CO<sub>2</sub> vibrational chemistry (101 vibrational levels) and the main gas heating pathways. The successful validation of our kinetic scheme (see Figure 1) enabled the resolution of the heating dynamics (see Figure 2), disclosing the importance of the symmetric vibrational levels and electronic excitation of CO<sub>2</sub>. Finally, this study provides useful insights into the limitations to the stepwise excitation and lays the foundation to clarify its possible contribution to the dissociation of CO<sub>2</sub> in future modelling efforts.

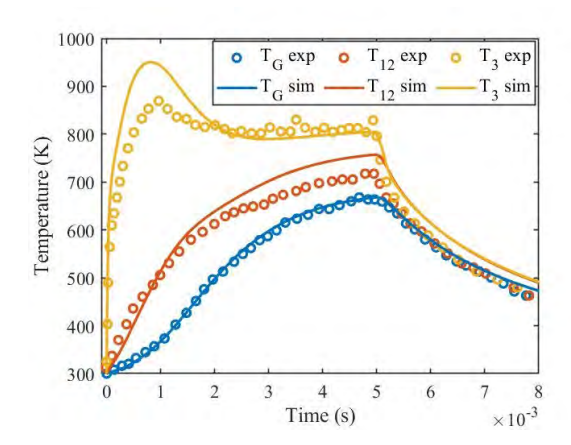


**Fig. 1**: Experimental (circles) [6] and simulated (solid curves) gas  $(T_G)$  and vibrational (symmetric  $(T_{12})$ ) and asymmetric  $(T_3)$ ) temperatures as a function of time. Note that the pulse time is 5 ms; for t > 5 ms, the plasma is turned off.

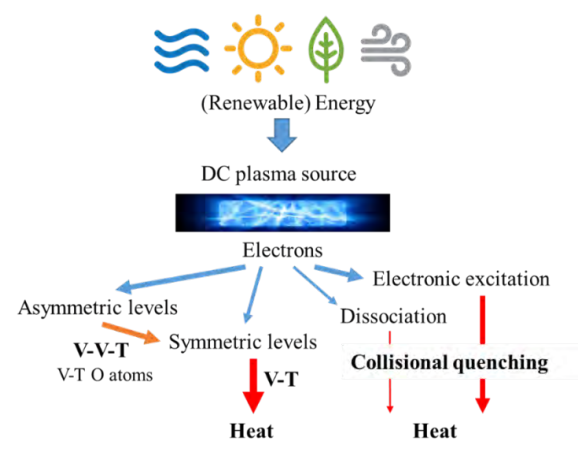


**Fig. 2**: Schematic overview of the flow of energy in a pure CO<sub>2</sub> low-pressure discharge. The red arrows stand for the main heating mechanisms involved: vibration-vibration-translation (V-V-T) relaxation, vibration-translation (V-T) and deactivation by collisions with oxygen atoms (V-T O atoms) and collisional quenching of electronic states coming from direct excitation or electron-impact dissociation of CO<sub>2</sub>.

**Acknowledgments**: This work was partially supported by the European Union's Horizon 2020 research and innovation programme under grant agreement MSCA ITN 813393, and by Portuguese FCT-Fundação para a Ciência e a Tecnologia, under projects UIDB/50010/2020, UIDP/50010/2020 and PTDC/FIS-PLA/1616/2021.

#### References

- [1] BP Statistical Review of World Energy, (2019).
- [2] G.J. van Rooij, H.N. Akse, W.A. Bongers, M.C.M. van de Sanden, Plasma Phys. Control. Fusion 60 (2018) 014019.
- [3] A. Bogaerts, G. Centi, Front. Energy Res. 8 (2020) 111.
- [4] A. Fridman, Plasma Chemistry, Cambridge: Cambridge University Press, 2008.
- [5] V. Vermeiren, A. Bogaerts, J. Phys. Chem. C 123 (2019) 17650–17665.
- [6] B.L.M. Klarenaar, R. Engeln, D.C.M. van den Bekerom, M.C.M. van de Sanden, A.S. Morillo-Candas, O. Guaitella, Plasma Sources Sci. Technol. 26 (2017) 115008.

Modelling and diagnostics

# 3D reconstruction and analysis of branching streamer discharges in air

<u>Yihao Guo</u>, Martijn van der Leegte, Siebe Dijcks, Sander Nijdam *Eindhoven University of Technology, Eindhoven, The Netherlands* 

E-mail: y.guo@tue.nl

Streamers are ionized fingers that propagate through gases, liquids, and solids when a high voltage is applied quickly to a gap. Streamers usually break up into separate channels during their propagation, which is called branching. Traditional imaging of streamer discharges usually results in two-dimensional (2D) projections of these three-dimensional (3D) phenomena. This may lead to loss of information of the 3D spatial structure of streamer discharges, such as branching angle, propagating velocity and radius.

For this reason, we have developed a method to semi-automatically reconstruct the streamer discharges into 3D representations from stereoscopic and stroboscopic images. The stereoscopic setup we used was also described in [1]. Combined with an ICCD system (LaVision PicoStar HR) operating in stroboscopic mode where its gate can be controlled at up to 1 GHz, it enables us to obtain two 2D stroboscopic images from two different viewing angles of the same discharge on one camera, as shown in Fig. 1(a). A calibration with a known-size checkerboard was done before the measurements.

A semi-automatic program was developed in MATLAB to analyse these images and reconstruct the streamers into 3D streamer trees. In this program, Gaussian blur and K-means clustering algorithms are applied successively to detect the individual dots representing propagating streamers in the stroboscopic images. Then the two detection sets from the different viewing angles (left and right sides) are matched by a triangulation method or by manual selection from top to bottom. Finally, all the detected dots are connected based on a shortest path tree weighted with their Euclidean distance. The 2D images are then reconstructed into 3D models, as is shown in Fig. 1(b). From the reconstructed 3D models, branching angles and radius and velocity of each segment (a streamer channel that does not branch) can be analysed.

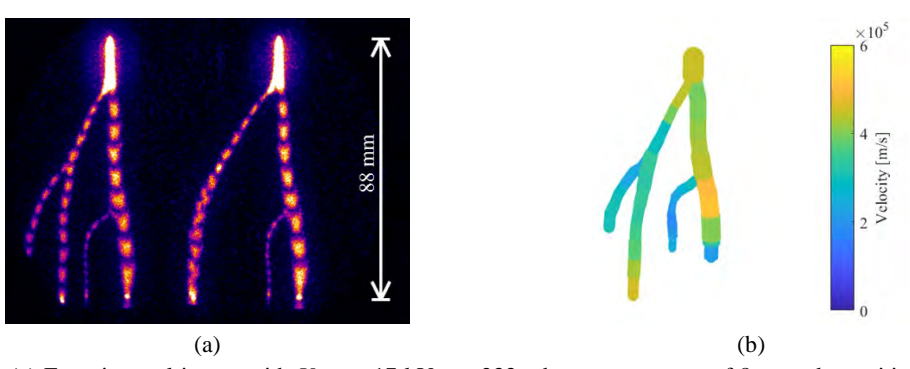


Fig. 1: (a) Experimental image with  $U_{app} = 17 \text{ kV}$ , p = 233 mbar, camera gate of 8 ns and repetition rate of 50 MHz; (b) corresponding reconstructed 3D model. The colour scale indicates the velocity of the streamer, while the segment width is a measure of the real streamer diameter

In this work, we performed experiments on positive streamer discharges in air and air-like mixtures at pressures around 200 mbar in a protrusion-to-plate gap (100 mm separation of two plates and 12 mm protrusive length of the pin) with voltages between 10 and 30 kV. Our method shows promising results for analysing large numbers of streamer discharges that contain multiple (up to about 10) branches. More details and the experimental results will be presented at the conference.

# Reference

[1] S. Nijdam, J. S. Moerman, T. M. P. Briels, E. M. van Veldhuizen, and U. Ebert, *Applied Physics Letters*, **92**, 101502 (2008).

## Poster P25 - David Rauner

Modelling and diagnostics

# Spectroscopic determination of rotational and vibrational temperatures in molecular MW plasmas for gas conversion

<u>David Rauner</u><sup>1</sup>, Ante Hecimovic<sup>2</sup>, Christian Kiefer<sup>2</sup>, Arne Meindl<sup>2</sup>, Vinzenz Wolf<sup>1</sup>, Wenjin Zhang<sup>2,3,4</sup>, Ursel Fantz<sup>1,2</sup>

<sup>1</sup>AG Experimentelle Plasmaphysik, Universität Augsburg, 86135 Augsburg, Germany <sup>2</sup>Max-Planck-Institut für Plasmaphysik, Boltzmannstrasse 2, 85748 Garching, Germany <sup>3</sup> Institute of Plasma Physics, Hefei Institute of Physical Science, Chinese Academy of Sciences, Hefei 232001, People's Republic of China.

4 University of Science and Technology of China, Hefei 232006, People's Republic of China

E-mail: david.rauner@physik.uni-augsburg.de

In view of the goal to electrify chemical industry, processes for the production of value-added chemicals that can be driven or enhanced by (non-)equilibrium plasmas have gained considerable interest in the past years. A frequently considered process in view of the carbon cycle is plasma driven CO<sub>2</sub> conversion, targeted at CO production (to be utilized e.g. for syngas) [1]. This topic is also closely related to hydrogen production via CH<sub>4</sub> (dry or steam) reforming as well as pyrolysis, a field where plasma processes have also gained a lot of attention in the past [1]. Beyond that, the larger topic of plasma-assisted nitrogen fixation is heavily discussed,

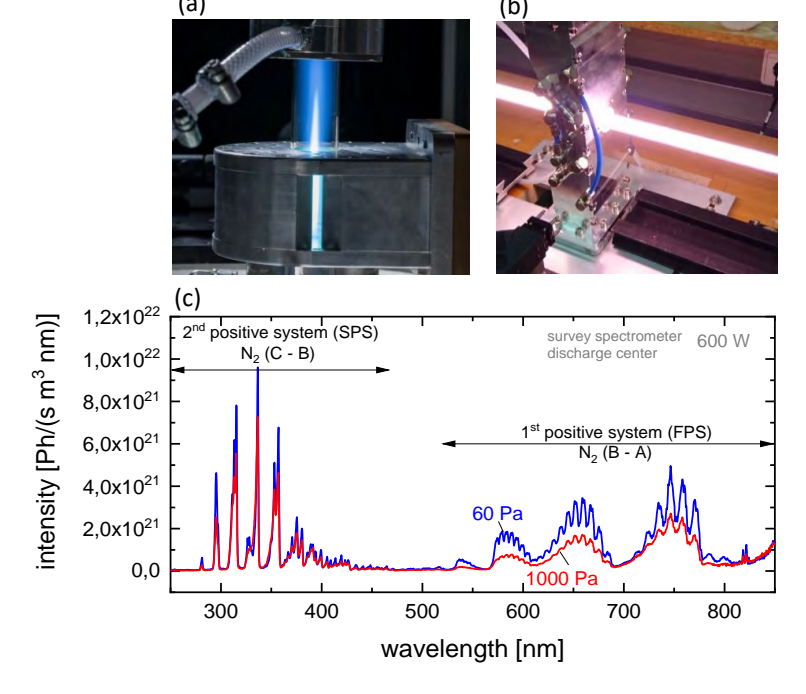


**Fig. 1**: (a) Atmospheric, MW (2.45 GHz) driven plasma torch operating a  $CO_2$  discharge (photograph taken by Axel Griesch). (b) Surface wave discharge (surfaguide) driven at 2.45 GHz operating a  $N_2$  plasma at 60 Pa. (c) Survey spectra and most prominent molecular transitions of a nitrogen discharge (surfaguide setup) at 60 Pa and 1000 Pa.

comprising mainly two pathways: NO<sub>x</sub> and NH<sub>3</sub> synthesis [2,3]. For many of these processes, a combination with heterogenous catalysis is also required or beneficial [4].

Hence, a variety of different plasma sources and technological concepts are investigated. However, an essential common challenge remains: understanding the specific role of the plasma in the process chemistry - which can differ strongly for different discharge types and/or operating parameters. Generally, the plasma can serve both as a supplier of heat (several 1000 K can easily be achieved within seconds, depending on the discharge type) or – if suitable non-equilibrium conditions can be achieved – as means to facilitate reaction pathways entirely inaccessible by purely thermal approaches. The latter relies on processes induced via electron collisions such as electron impact dissociation of molecules or vibrational excitation of ground state molecules. In this context, simultaneous diagnostic access to rotational and vibrational populations of molecules (that can be characterized by temperatures  $T_{\rm rot}$  and  $T_{\rm vib}$  in case of Boltzmann distributions) is a powerful tool to understand the plasma chemistry and characterize (non-)equilibrium conditions: while the vibrational distributions can be heavily influenced by the electronic ensemble, rotational distributions are typically closely coupled to the translational kinetics of heavy particles, which consecutively provides a frequently exploited tool to access the gas temperature in discharges [5].

In this contribution, rotational and vibrational temperatures of several excited molecules in microwave (MW) discharges are determined by applying emission spectroscopy. Measurements are carried out at different MW-driven setups, which allows to cover a large parameter space from atmospheric conditions (MW-driven plasma torch, see Figure 1(a)) down to pressures of several Pa (surface wave discharges, surfaguide see Figure 1(b)). This grants diagnostic access to regimes characterized by a vibrational-rotational equilibrium, distinctly non-equilibrium conditions and highly dynamic transition regions. In various gases ( $N_2$ ,  $H_2$ ,  $O_2$ ,  $CO_2$  and mixtures therefore), rotational and vibrational temperatures are determined and compared, applying techniques based on the measurement of molecular emission spectra and their consecutive simulation and/or fitting. Considered are for example emitting systems of  $N_2$  (first and second positive system) and  $N_2$ + (first negative system), as displayed in Figure 1 (c). In addition, evaluations conducted for molecular  $C_2$  [6], CO or CO emission are presented and compared, alongside methods applied for CO, utilizing the Fulcher-system of the CO molecule [7].

#### **References:**

- [1] R. Snoeckx and, Chem. Soc. Rev. 46 (2017) 5805.
- [2] S. Li et al, *Processes* **2018** (2018), 248
- [3] M.L. Carreon, J. Phys. D: Appl. Phys. 52 (2019) 483001
- [4] A. Bogaerts et al., J. Phys. D: Appl. Phys. 53 (2020) 443001
- [5] P. J. Bruggeman et al., Plasma Sources Sci. Technol. 23 (2014) 023001
- [6] E. Carbone et al., Plasma Sources Sci. Technol. 29 (2020) 055003.
- [7] S. Briefi et al., J. Quant. Spectrosc. Radiat. Transfer 187 (2017) 135 44

# Poster P26 - Julia Mrotzek

Modelling and diagnostics

# Characterization of the plasma torch of an APPJ for thin film deposition

Julia Mrotzek<sup>1,2</sup>, Wolfgang Viöl<sup>1,2</sup>

<sup>1</sup>Laboratory of Laser and Plasma Technologies, University of Applied Sciences and Arts, Von-Ossietzky-Str. 99, 37085 Göttingen, Germany

E-mail: julia.mrotzek@hawk.de

Plasma powder deposition by means of an Atmospheric Pressure Plasma Jet (APPJ) allows the deposition of thin films of metal, metal oxide or polymers also on temperature sensitive surfaces such as paper or wood. In the process, particles are melted in the plasma and applied to the surface. For broad application, understanding of the underlying mechanisms and influence of relevant parameters is necessary, while process stability must be guaranteed.

In this study, the afterglow plasma of a pulsed DC arc jet (2 kW input power, 50 kHz repetition frequency, pulse period 5–10  $\mu$ s) was studied using optical emission spectroscopy (Figure 1). The development of reactive species along the gas flow direction was investigated for different process gases (N<sub>2</sub>, air) and gas flow rates. Spectra are dominated by N<sub>2</sub><sup>+</sup> (B-X), N<sub>2</sub> (C-B) and NI. With increasing distance to the nozzle, the intensity of species (OH, NO) originating from the surrounding atmosphere is increasing due to the turbulent flow. Determination of plasma temperatures proofed, that the jet is far from LTE conditions with rotational temperatures at the nozzle exit around 4500 K and excitation temperatures around 6000 K.

In a next step, investigations will be carried out during injection of metallic powders.

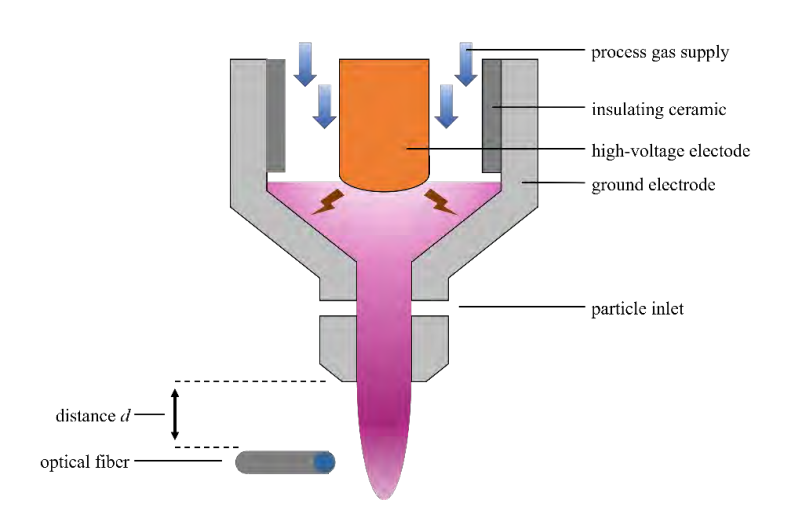


Fig. 1: Schematic Setup of the Atmospheric Pressure Plasma Jet (APPJ).

<sup>&</sup>lt;sup>2</sup>Application Center for Plasma and Photonics, Fraunhofer Institute for Surface Engineering and Thin Films, Ossietzky-Str. 100, 37085 Göttingen, Germany

## Poster P27 - Gerard van Rooij

Molecular synthesis and decomposition

Unravelling Transport in CO<sub>2</sub> Microwave Plasma by Comparing Flow Geometries

A.W. van de Steeg, A. Hughes, M.C.M. van de Sanden, G.J. van Rooij A. Van Rooij A.

E-mail: g.vanrooij@maastrichtuniversity.nl

Plasma is gathering momentum as CO<sub>2</sub> utilization technology due to the compatibility with intermittent power sources as well as high obtainable energy efficiencies in the dissociation reaction of CO<sub>2</sub> to the chemical building block CO.<sup>1</sup> Microwave plasma is considered as most promising and generally approached in a vortex-stabilized configuration.<sup>2</sup> In contrast to the early research claiming low gas temperature and high vibrational activation as essential,<sup>3</sup> recent work demonstrated core temperatures up to 7000 K,<sup>4</sup> equal gas and vibrational temperatures,<sup>5</sup> hence thermal chemistry to dominate for dissociation.<sup>5,6</sup>

In this work, we provide a first in-situ characterization of the Reverse Vortex (RV) CO<sub>2</sub> microwave plasma to gain more insight in transport phenomena in microwave plasma. We use Raman scattering to create maps of composition (CO<sub>2</sub>, CO, O<sub>2</sub> and O) and temperature over a large volume. These results are compared with Forward Vortex (FV) results of our earlier work<sup>5</sup> to illustrate the effects of a change in core transport mechanism and timescale.

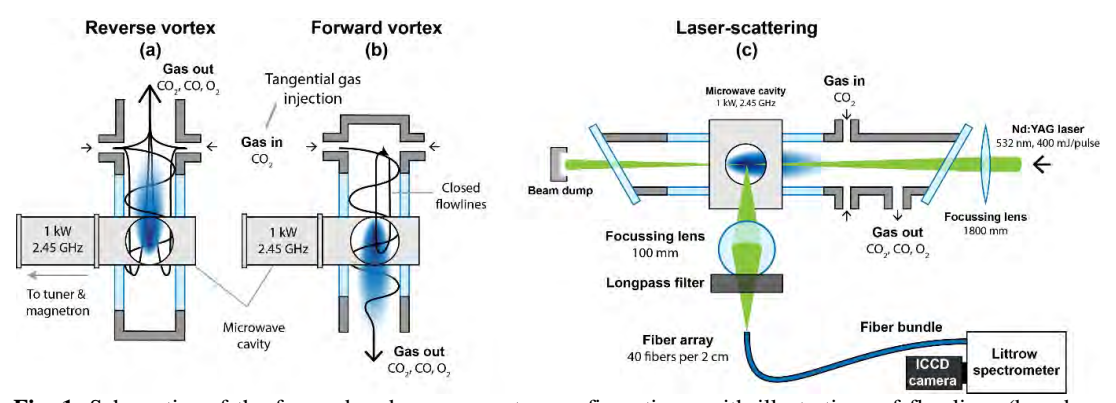


**Fig. 1**: Schematics of the forward and reverse vortex configurations, with illustrations of flowlines (based on Gutsol and Bakken<sup>7</sup>), and a schematic of the laser setup used to assess local densities in the reverse vortex (and forward vortex in our previous work<sup>5</sup>).

Fig. 1 shows schematics of the two flow configurations as well as the details of Raman scattering layout in RV. In all systems, a quartz tube of 27 mm inner diameter is placed in a 1 kW 2.45 GHz microwave cavity. Both RV and FV have two tangential gas injection nozzles

<sup>&</sup>lt;sup>1</sup> A. Bogaerts et al., ACS Energy Lett. 3, 1013 (2018); R.G. Grim et al., Energy Environ. Sci. 13, 472 (2020).

<sup>&</sup>lt;sup>2</sup> R. Snoeckx et al., Chem. Soc. Rev. 46, 5805 (2017).

<sup>&</sup>lt;sup>3</sup> Y.P. Butylkin et al., Sov. Phys. Tech. Phys. 26, 555 (1981); V.D. Rusanov et al., Sov. Phys. Usp. 24, 185 (1981).

<sup>&</sup>lt;sup>4</sup> A.J. Wolf, et al., Plasma Sources Sci. Technol. 28 (2019); A.W. Van de Steeg et al., Opt. Lett. 46, 2172 (2021).

<sup>&</sup>lt;sup>5</sup> A.W. Van De Steeg et al., ACS Energy Lett. 6, 2876 (2021).

<sup>&</sup>lt;sup>6</sup> D.C.M. v.d. Bekerom et al., Plasma Sources Sci. Technol. 28 (2019); A.J.J. Wolf et al., J. Phys. Chem. C 124, 16806 (2020).

<sup>&</sup>lt;sup>7</sup> A. Gutsol et al., J. Phys. D. Appl. Phys. 31, 704 (1998).

located 100 mm from the waveguide center. The FV creates a swirling flow around the tube edge, with a recirculation cell in which the plasma center resides. In the RV, gas injection and exhaust are placed at the same side of the waveguide.

In-situ characterization of the reverse vortex is carried out at a pressure of 120 mbar with a fixed input power of 1 kW and 10 slm gas flows. These conditions are inspired by our previous work in the FV and the general observations that efficiency peaks in this pressure regime. Fig. 2 shows a plasma emission image and the results of the Raman scattering measurements in both RV and FV configurations for the high-flow condition.

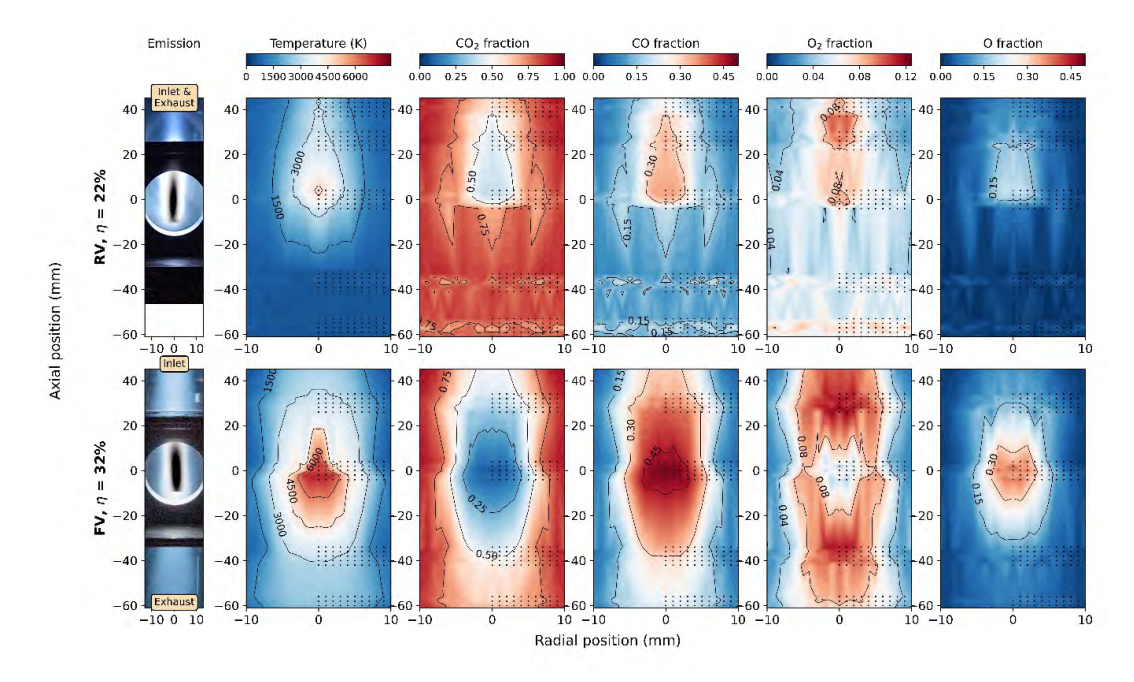


**Fig. 1**: Schematics 2D results of rotational Raman scattering in a 120 mbar, 1000 W, 20 slm reverse vortex (top) and forward vortex (bottom, from earlier work<sup>5</sup>). From left to right: Plasma emission (an overlay of total emission and 777 nm O-atom emission), rotational temperature, CO<sub>2</sub> fraction, CO fraction, O2 fraction and O fraction.

While the operating conditions are identical, large differences in temperature and composition are observed; temperatures in the RV do not exceed 4500 K versus 6000 K in FV, dissociation in the plasma core is less for RV than for FV. The difference in reactor conditions is due to the higher particle transit rates in RV compared to FV. Rough velocity estimates yield for the RV up to 200 m/s, with core velocities approximately 150 m/s. Much lower, the FV has diffusion velocities up to 40 m/s. Moreover, the diffusion velocities occur over a very small range, as gradients become less sharp outside of the plasma core.

Through the convective core transport, the reverse vortex allows for control over core residence times, which enables convective cooling of the discharge. Moreover, a decoupling of core temperature and composition with power density is observed, enabling contracted plasma conditions at lower gas temperature. Such aspects underline the importance of gas flow geometry for reactor parameters and are expected to play an important role in future reactor engineering and design.

# Poster P28 - Hemaditya Malla

Ozone generation and applications

# Identifying the Major Reactive Oxygen-Nitrogen Species in a Pulsed Streamer Discharge

## Hemaditya Malla<sup>1</sup>, Jannis Teunissen<sup>1</sup>, Ute Ebert <sup>1,2</sup>

<sup>1</sup>Centrum Wiskunde & Informatica, Multiscale Dynamics, Amsterdam, The Netherlands <sup>2</sup>Department of Applied Phyiscs, Eindhoven University of Technology, Eindhoven, The Netherlands E-mail: hemaditya.malla@cwi.nl

Plasma-activated water (PAW) generated by electrical discharges in air contains reactive oxygen-nitrogen species (RONS) [1]. Depending on the type of chemical species, plasma-activated water can for example be used for disinfection or to increase the shelf-life of agricultural products. In [4, 5], extensive chemical reaction sets were used to theoretically predict the dominant species in a plasma jet. In [2, 3], it was shown using experiments that using sub-nanosecond high voltage pulses can be used to generate RONS in an energy efficient way. It is not fully understood how various RONS are produced/consumed on a nano-second timescale. Various operating conditions such as voltage amplitude, voltage rise time, pulse shape, repetition frequency, and gas composition influence the yield of different RONS. In this work, we investigate the effect of varying the water percentage in the gas composition on the streamer discharge properties, and RONS yield for a single pulse+afterglow regime.

#### References

- [1] Bruggeman, P. J., et al. "Plasma-liquid interactions: a review and roadmap." *Plasma sources science and technology* 25.5 (2016): 053002.
- [2] Wang, Douyan, and Takao Namihira. "Nanosecond pulsed streamer discharges: II. Physics, discharge characterization and plasma processing." *Plasma Sources Science and Technology* 29.2 (2020): 023001.
- [3] Huiskamp, T., et al. "(Sub) nanosecond transient plasma for atmospheric plasma processing experiments: application to ozone generation and NO removal." *Journal of Physics D: Applied Physics* 50.40 (2017): 405201.
- [4] Norberg, Seth A., Eric Johnsen, and Mark J. Kushner. "Formation of reactive oxygen and nitrogen species by repetitive negatively pulsed helium atmospheric pressure plasma jets propagating into humid air." *Plasma Sources Science and Technology* 24.3 (2015): 035026.
- [5] Van Gaens, W., and A. Bogaerts. "Reaction pathways of biomedically active species in an Ar plasma jet." *Plasma Sources Science and Technology* 23.3 (2014): 035015.

## Poster P29 - Dušan Kováčik

Surface processing and technology (cleaning, coating, etching and modification, equipment)

# AIR PLASMA TREATMENT FOR IMPROVING THE SAFETY PROPERTIES OF LAMINATED GLASSES CONTAINING IONOPLAST INTERLAYER USED IN CIVIL ENGINEERING

<u>Dušan Kováčik</u><sup>1</sup>, Richard Krumpolec<sup>1</sup>, Leila Zahedi<sup>1</sup>, Pedram Ghourchi Beigi<sup>1</sup>, Monika Stupavská<sup>1</sup>, Slavomír Sihelník<sup>1</sup>, Evžen Rainer<sup>2</sup>, Mirko Černák<sup>1</sup>

<sup>1</sup>Department of Physical Electronics, CEPLANT, Faculty of Science, Masaryk University, Kotlářská 2, 611 37 Brno, Czech Republic

<sup>2</sup>OGB s.r.o. Karla Čapka 1739/6, 415 01 Teplice, Czech Republic

E-mail: dusan.kovacik@mail.muni.cz

Laminated glasses used in civil engineering are produced by layering two and often more glass plates, between which a safety foil (interlayer) is placed. The layering and lamination of plates allow not only to increase the standard load-bearing capacity and improve the acoustic insulation properties of the glass, but above all, it enables its residual load-bearing capacity after breakage and prevents the release of glass shards due to their high adhesion to the safety film. For several decades, PVB (Polyvinyl butyral) foils have been the most commonly used interlayer in the laminated safety glasses (LSGs) for building glazing of the standard design to the simplicity of lamination, good safety after breakage and low cost. However, LSGs are increasingly used as a load-bearing and structural support element in modern functional buildings. For these applications, an ionoplast (ionomer-based) interlayer is more suitable, due to its several times higher strength, up to 100 times greater toughness, and considerably higher stability under prolonged load and at higher temperatures. The ionoplast interlayer in LSGs does not depend on the type of glass support and has greater resistance to ageing and clarity. The listed properties of ionoplast interlayer enable to production of thinner and lighter, more safety and high-quality LSGs with the larger dimensions of the minimal framing and point supporting as well as load-bearing glass elements (beams, stairs, floors, railings, etc.).

The ionoplast interlayers have a very different chemistry than that of PVB, which requires slightly modified processing compared to PVB. Special lamination settings are necessary to achieve optimum adhesion and optics. The lamination must be done using the tin side of the glass, or when not possible, using a chemical primer on the thoroughly cleaned air side of the glass to achieve good adhesion. In general, the low adhesion of ionoplast to glass and the associated increased demands on the quality of lamination are persistent technical problem that limits its use, e.g. in the production of thin SLGs and photovoltaic panels. Based on our previous experiences and results of the project solved in the past on a related topic, a possible alternative method leading to an increase in the adhesion of the ionoplast interlayer to the air side of the glass without the use of the primer appears to be the application of the atmospheric-pressure plasma to activate the air side of the glass as well as the ionoplast prior laminating process.

Within a joint ongoing project with the OGB s.r.o. company, a manufacturer of laminated glasses for civil engineering, we are investigating the possibility of using atmospheric-pressure

plasma generated by diffuse coplanar surface barrier discharge (DCSBD) to enhance the adhesion and thus the mechanical properties of SLGs containing the ionoplast interlayer. DCSBD is a robust plasma source generating the macroscopically homogeneous plasma with a high ratio of diffuse plasma in ambient air (Fig. 1) without the necessity of any stabilization by flowing gas or admixture of the noble gases. Moreover, it is practically infinitely scalable, which predetermines it for the surface treatment of large-area planar and flexible samples, including glass and polymer foils.

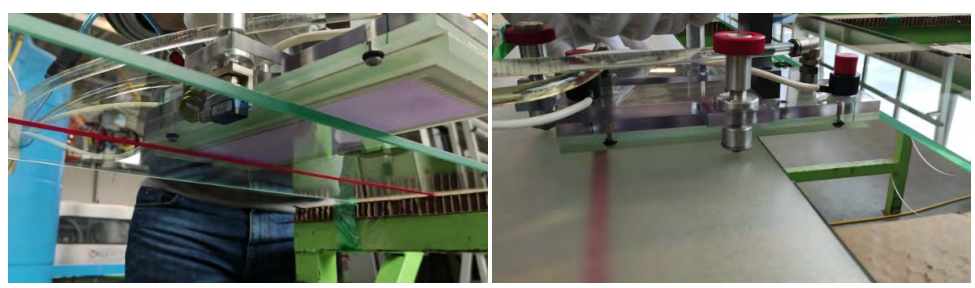


**Fig. 1**: The real photos capturing the DCSBD plasma treatment of the air side of the glass instead of the application of the primer (left) and the ionoplast interlayer (right) used for the production of SLGs in the OGB company.

Based on experimental laboratory research, we tried to determine the optimal conditions for the plasma treatment of float glass and ionoplast interlayer by DSCBD, which were continuously verified during the production of SLGs glasses at the OGB company. The research included a study of the DCSBD plasma cleaning effect on the surface of the tin/air side of the float glass and a comparison with cleaning using solvents and detergents or ultrasonic cleaner with an emphasis on uniformity. The effect of DCSBD plasma on the surface of glass and ionoplast was studied using modern surface analyses, including the measurement of water contact angle, surface free energy, adhesion by tape peel test method, XPS, roughness using a laser confocal microscope and VIS transparency. The stability of the plasma treatment due to its ageing was also studied. The optimal power input of the DCSBD plasma source was determined to be 400 W at the frequency of ~15 kHz, and the optimal exposure time was 4 sec for treating the air side of the glass and 5 sec for treating the ionoplast at the kept effective distance of 0.3 mm between the treated surfaces and the thin plasma layer of DCSBD. Under such conditions, largearea glass and ionoplast interlayer of the thickness 8 mm and 0.8 mm with dimensions of 25 cm and 450 cm were plasma treated using DCSBD at the OGB company. These were used to produce the structural glass beam LSGs for civil engineering and were subjected to a test of their strength under bending stress. The results confirmed that plasma treatment of the air side of the glass before lamination with inoplast leads to an increase in the strength of the beams.

#### Acknowledgement

This research has been supported by the project "Increasement of production efficiency and improving the safety properties of glasses laminated with ionoplast foil intended for use in construction", FW03010109 funded by the Technology Agency of the Czech Republic (program TREND), and project "R&D centre for plasma and nanotechnology surface modifications (CEPLANT)", LM2018097 funded by the Ministry of Education, Youth and Sports.

## Poster P30 - Katerina Polaskova

Surface processing and technology (cleaning, coating, etching and modification, equipment)

# EFECT OF PLASMA AND LIGHT IRRADIATION ON MORPHOLOGY OF DEPOSITED TIO<sub>2</sub> NANOPARTICLE STRUCTURES

Kateřina Polášková<sup>1,2,3</sup>, Miloš Klíma<sup>2</sup>, Lenka Zajíčková<sup>1,2,3</sup>

<sup>1</sup>Departement of Condensed Matter Physics, Masaryk University, Kotlářská 2, 611 37 Brno, Czech Republic

 Department of Theoretical and Experimental Electrical Engineering, Brno University of Technology, Technická 12, 616 00 Brno, Czech Republic
 Central European Institute of Technology – CEITEC, Brno University of Technology, Purkyňova 123, 612 00 Brno, Czech Republic

E-mail: polaskova.katerina@mail.muni.cz

Titanium dioxide (TiO<sub>2</sub>) is a highly stable, environment and human-safe, cheap semiconductive material. It exists in several polymorphs, the most abundant ones being tetragonal structured anatase and rutile phases [1, 2]. The rutile phase is a more stable polymorph of two. It is often used in theoretical studies as a model system in the surface sciences of metal oxides [2]. For many applications (self-cleaning, antibacterial, or antifouling coatings; solar cells, wastewater treatment), the photoreactive anatase phase is preferred, especially in the form of the more photocatalytic effective nanoparticles (NPs) [1]. The TiO<sub>2</sub> can be prepared by sputtering and annealing [2]. The eco-friendly plasma deposition is an attractive alternative to these processes, especially the cost-efficient fast atmospheric pressure variant. The plasma-enhanced chemical vapor deposition using Ti-based precursors is usually utilized [3], though, recently, studies using a solution of pre-synthesized TiO<sub>2</sub> nanoparticles emerged [4,5]. Compared to more standard methods, plasma deposition of pre-synthesized TiO<sub>2</sub> nanoparticles offers a high degree of nanoparticle coverage and thickness control.

The plasma was generated inside a quartz capillary (Fig. 1) with an inner diameter of 2.5 mm at the power of 50 W and an Ar flow rate of 3 slm. The TiO<sub>2</sub> NPs were deposited with both the plasma ON and OFF onto a Si substrate (10 × 15 mm), moving at 22 mm/s with one pass. The distance between the capillary exit and the sample was fixed at 10 mm. The commercial solution TiZonic (Nanozone) composed of TiO<sub>2</sub> NPs (0.5%, 2–5 nm in diameter) dispersed in a mixture of water (95%) and isopropanol (4.5%) was nebulized into micrometer-sized droplets and carried into the discharge region by an Ar flow. During the deposition, the particles were irradiated by different wavelength light sources focused by Fresnel lenses into the area inbetween the substrate and the capillaries exit. In the UVA range, the Hg lamp (with the emission cut off at 300 nm by Fresnel lenses) was used. A set of three LED reflectors (MultiLED QT from GSVITEC) provided light in the VIS range. The NIR light was produced by a pulsed laser CAVILUX HF, with the emission line at 810 nm and the power of 500 W. All the light sources were used separately. The background radiation of fluorescent lights was present for all the experiments.

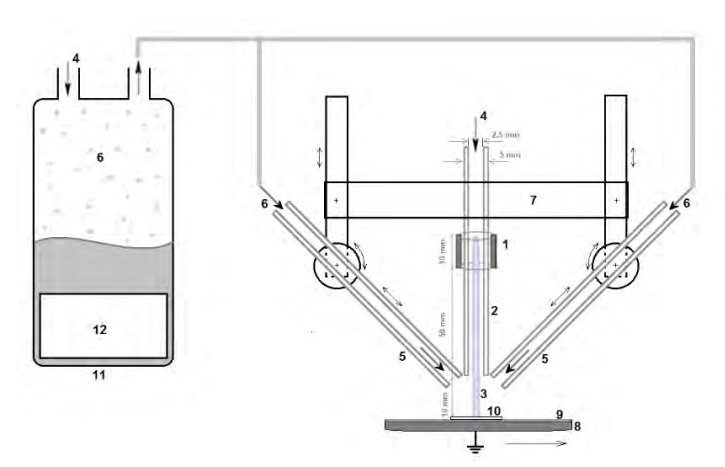


**Fig. 1**: Experimental set-up. 1 – RF electrode, 2 – quartz capillary, 3 – plasma, 4 – main Ar flow, 5 – aerosol inlets, 6 – aerosol carried by Ar, 7 – movable jet holder, 8 – grounded electrode, 9 – mica composite, 10 – Si substrate, 11 – vessel with the TiZonic solution, 12 – ultrasonic vaporizer

At the fixed treatment time (0.7 s), we deposited TiO<sub>2</sub> NPs in dried droplet patterns, the morphology varying for each studied condition. The most noticeable differences were observed between the samples prepared with and without the plasma. Without the discharge, the quasispherical TiO<sub>2</sub> NPs were densely packed, forming small disks (3–5 μm) with elevated edges and almost a uniform NP layer inside. The presence of plasma caused the NP shape to become sharper, akin to ellipsoids or plates rather than spheres. The dried droplet patterns had increased in size (9–15 µm) while simultaneously becoming less symmetrical and 'thick'. The changes are probably caused by a combination of the plasma-induced decrease of droplet surface tension and an increase in particle hydrophilicity. The influence of the different wavelength irradiation was not as significant as that of the plasma. The UVA exposure reduced the dried disk size, likely by the change in the droplet pH level induced by the water-splitting reaction on the photoactivated surface of TiO<sub>2</sub> NPs. The morphology of disks deposited while irradiated by the VIS diodes was the most similar to the structures formed without any additional light source, as the TiO<sub>2</sub> NPs were not photoactivated in the higher wavelength light. Surprisingly, the NPs exposed to the NIR laser had a similar structure to the UVA irradiated sample. With the addition of the plasma, the patterns were concentric rings rather than disks. The changes are probably connected to high-powered laser pulses quickly heating and evaporating the droplets.

In this work, we compare structures of TiO<sub>2</sub> NPs deposited with and without plasma. In addition, different light sources were used to irradiate the particles during the deposition. The morphology formed by deposited NPs differed in each condition based on the presence of plasma, the strength of photocatalytic NPs reactions, and the droplet evaporation rate.

# References

- 1. S. M. Gupta et al., Sci. Bull. 56(16), 1639–1657(2011)
- 2. U. Diebold, Appl. Phys. A 76(5), 681–687(2003)
- 3. S. Banerjee et al., Mater. 13(13), 2931(2020)
- 4. J. Profili et al., J. Appl. Phys. 120(5), 053302(2016)
- 5. T. Peng et al., Plasma Process. Polym. 16(6), 1800213(2019)

## Poster P31 - Richard Krumpolec

Surface processing and technology (cleaning, coating, etching and modification, equipment)

# ULTRA-FAST LOW TEMPERATURE ATMOSPHERIC PLASMA TRIGGERED REDUCTION-EXFOLIATION OF HIGHLY POROUS AEROGEL-LIKE GRAPHENE OXIDE

<u>Richard Krumpolec</u>, František Zelenák, Mirko Černák

Department of Physical Electronics, CEPLANT—R&D Center for Plasma and

Nanotechnology Surface Modifications, Faculty of Science, Masaryk University,

Kotlářská 267/2, 61137 Brno, Czech Republic

E-mail: krumpolec@mail.muni.cz

Additive-free 3D reduced graphene oxide (rGO) aerogels are promising candidates for energy storage, fuel cells, photocatalysis, sensing and medical applications etc. [1] The simplest way to prepare the graphene-like rGO is to reduce low-cost graphene oxide (GO). However, the complicated 'reduction–exfoliation' of GO become a major bottleneck that restricts the large-scale production of rGO. We present simple, fast, low-cost and chemical-free fabrication of rGO aerogel-like 2D sheets and 3D cakes [2] using an electrical plasma-triggered reduction-exfoliation of highly porous GO aerogel-like materials starting at temperatures not higher than 100 °C.

For plasma triggered reduction-exfoliation of GO we prepared a sample of highly porous aerogel-like graphene oxide. A 1 mm thick sheet of dimensions roughly  $1\times 2$  cm of brown colour shown in Figure 1a was fabricated under mild conditions from an aqueous solution of graphene oxide (GO flakes size < 45  $\mu$ m) by drying in a vacuum oven (modified lyophilization method).

The GO sheet was exposed to low-temperature plasma generated by atmospheric Diffuse Coplanar Surface Dielectric Barrier Discharge (DCSBD) plasma source in technical nitrogen. The plasma triggered the self-propagating reduction-exfoliation modification of brown GO into black rGO (Figure 1b-h). The highly porous (2-4 mg.cm<sup>-3</sup>; ~ 500 m<sup>2</sup>.g<sup>-1</sup>) rGO sheet (Figure 2) retained its original shape without abrupt disintegration unlike as often described in previously published work [3]. Subsequently, the sheet was hydraulic pressed into a thin 60  $\mu$ m sheet and examined using XPS, SEM, and Raman spectroscopy. We observed an approximately 10<sup>5</sup> fold decrease of the rGO sheet resistivity compared to unmodified GO sheet. The rGO sheet exhibited sheet resistance 257  $\Omega$ . $\Box$ <sup>-1</sup> (sheet conductivity 225 S.m<sup>-1</sup>) as measured and analysed by four-point probe method. XPS analysis of C1s spectra revealed the decrease of Oxygen concentration (from 45 to ~ 8 at.%) and significant decrease of C-O-C, C-O(C-OH), and C=O bonds together with the increase of sp2 C-C bonds.

Fast plasma-triggered reduction-exfoliation process of GO was studied using DCSBD units with various electrode geometry generating atmospheric plasma with different ratio of diffuse and filamentary plasma. The results are discussed as well as the comparison of GO reduction using a 'conventional' heat treatment method.

The novel plasma-triggered reduction-exfoliation method opens new opportunities for low-cost industrial-scale production of conductive rGO sheets and rGO-based composites for various modern industrial applications.

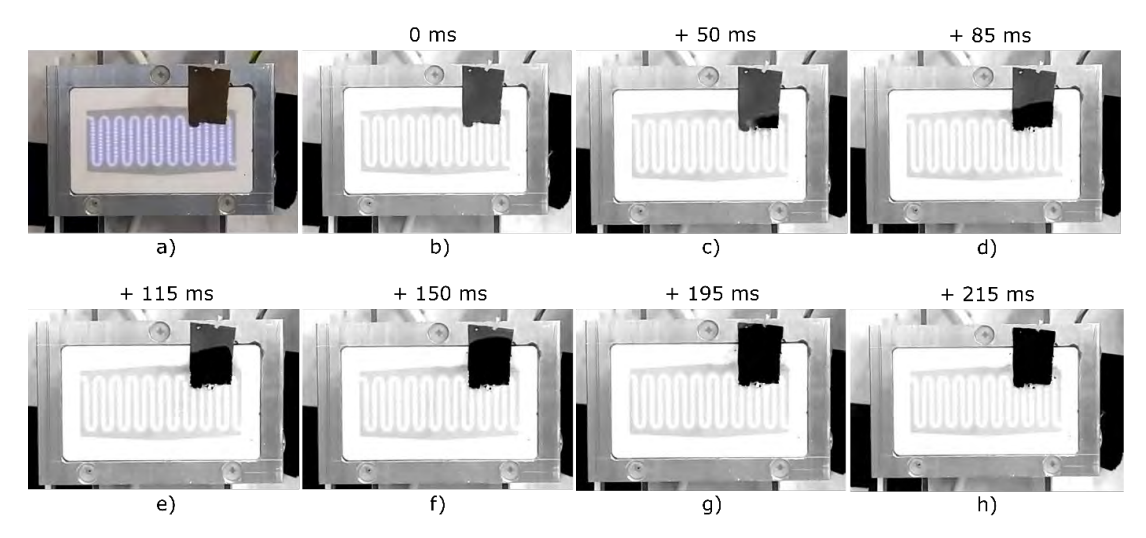


**Fig. 1**: Time evolution of plasma-triggered reduction-exfoliation of graphene oxide into rGO. a) Self-standing 1 mm thick GO sheet situated partly on the surface of DCSBD electrode system; b) the moment of the onset of plasma generation; c-h) illustrate the fast reduction-exfoliation process propagating in the volume of GO material (original brown colour) forming black rGO. (Plasma volume is not discernible in Fig. 1 b)-h) because of an intense external light necessary for taking the snapshot).

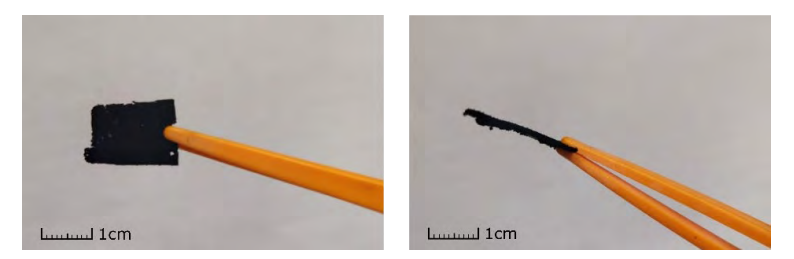


Fig. 2: Self-standing rGO sheet after the plasma-triggered reduction-exfoliation process.

## **Acknowledgement:**

This research was supported by project LM2018097 funded by the Ministry of Education, Youth and Sports of the Czech Republic and project MUNI/31/03202005/2020 funded by the Technology Agency of the Czech Republic.

#### **References:**

- [1] X. Zhang, J. Zhou, Y. Zheng, H. Wei, Z. Su, Graphene-based hybrid aerogels for energy and environmental applications, Chem. Eng. J. 420 (2021) 129700. https://doi.org/10.1016/j.cej.2021.129700.
- [2] R. Krumpolec, F. Zelenák, T. Kolářová, M. Černák, High conductive rGO sheets fabricated by mild, low-cost and scalable plasma-triggered reduction-exfoliation of 3D aerogel-like graphene oxide, submitted in FlatChem, under review.
- [3] K. Wang, M. Xu, Y. Gu, Z. Gu, J. Liu, Q.H. Fan, Low-temperature plasma exfoliated n-doped graphene for symmetrical electrode supercapacitors, Nano Energy. 31 (2017) 486–494. https://doi.org/10.1016/j.nanoen.2016.11.007.

## Poster P32 - Maria Luíza de Azevedo

Surface processing and technology (cleaning, coating, etching and modification, equipment)

# Fast pyrolysis in methane plasma

<u>Maria Luiza Azevedo</u><sup>1</sup>, Thomas Buttwerworth<sup>1</sup>

<sup>1</sup>Maastricht University, Plasmalab - Chemelot Brightside Campus, The Netherlands

E-mail: m.moreiradeazevedo@maastrichtuniversity.nl

Plasma technology offers the potential to electrify high-temperature processes, being in line with the chemical industry's transition towards renewable energy. This project will focus on optimizing the methane (CH<sub>4</sub>) pyrolysis process to directly produce ethylene (C2H<sub>4</sub>) using high temperatures, short residence times, and fast quenching.

Since the 1940s, the industrial-scale Hüls process has applied arc plasma to convert natural gas into acetylene ( $C_2H_2$ ). However, when we consider the reaction enthalpies of methane pyrolysis to  $C_2H_2$  and  $C_2H_4$  (reactions 1 and 2), it is more energy-efficient to directly produce  $C_2H_4$ :

$$2CH_4 \to C_2H_2 + 3H_2 \quad \Delta H = 378 \, kJ/mol$$
 (1)

$$2CH_4 \rightarrow C_2H_4 + 2H_2 \quad \Delta H = 202 \, kJ/mol$$
 (2)

In this project, we will investigate methane pyrolysis using a microwave (MW) plasma discharge, which allows fine temporal control over the plasma input power. Using laser scattering diagnostics we will measure temporally resolved temperature and composition. With this approach, we will reveal the chemistry and kinetics of CH<sub>4</sub> pyrolysis.

## Poster P33 - Wouter Graef

Modelling and diagnostics

# Status report on the LXCat project

J. Stephens<sup>1</sup>, L. Pitchford<sup>2</sup>, M. Hopkins<sup>3</sup>, B. Yee<sup>4</sup>, <u>W. Graef</u><sup>5</sup>

<sup>1</sup>Texas Tech Univ, Lubbock, Texas, United States of America

<sup>2</sup>CNRS & Univ of Toulouse, Toulouse, France

<sup>3</sup>Sandia Nat'l Lab, Albuquerque, New Mexico, United States of America

<sup>4</sup>Lam Research, Tualatin, Oregon, United States of America

<sup>5</sup>Plasma Matters BV, Eindhoven, the Netherlands

E-mail: info@lxcat.net

LXCat [1] (www.lxcat.net) is an on-line platform for the curation of data needed for modeling the electron and ion components of Low Temperature Plasmas (LTPs). LXCat is open-access and no sign-up is required. The platform is organized in databases which are named and maintained by individual contributors. Nearly 60 people from around the world participate in this project, either by contributing data or by volunteering time to work on other aspects of the project. The data types available now are electron-neutral or ion-neutral scattering cross sections, oscillator strengths, and transport parameters (e.g., mobility, diffusion coefficients) and rate coefficients. The LXCat team does not recommend data and hence data for the same process can appear in one or more of the databases. On-line tools are available that allow visitors to search for specific data, plot and compare data from different databases, download data, or use the available complete sets of electron-neutral scattering cross sections in an on-line Boltzmann solver to calculate transport and rate coefficients in pure gases or gas mixtures. The LXCat team is interested in contacting members of the LTP community about data needs and about how people can volunteer to participate in this project.

[1] E Carbone et al, Atoms 2021, 9(1), 16; https://doi.org/10.3390/atoms9010016

Acknowledgment
Presented on behalf of the LXCat Team.

#### Poster P34 - Daan Boer

Modelling and diagnostics

# A Novel Data Platform for Low-Temperature Plasma Physics

Daan Boer<sup>1</sup>, Wouter Graef<sup>2</sup>, Emile Carbone<sup>3</sup>, Jan van Dijk<sup>1</sup>

<sup>1</sup>Department of Applied Physics, Eindhoven University of Technology, Campus Eindhoven University of Technology, P.O. Box 513, 5600 MB Eindhoven, The Netherlands

<sup>2</sup>Plasma Matters BV, Campus Eindhoven University of Technology, P.O. Box 513, 5600 MB Eindhoven, The Netherlands

<sup>3</sup>Institut National de la Recherche Scientifique, Centre Énergie Matériaux Télécommunications, 1650 Blvd Lionel Boulet, J3X 1P7 Varennes, QC, Canada

E-mail: d.j.boer@tue.nl

Reliable input data is of key importance in any low-temperature plasma (LTP) simulation. The ability to access and share such data within the community is reliant on the presence of capable data platforms. However, current platforms are often very specific, enforcing a strict structure on states and reactions, severely limiting the range of data they support. Moreover, the lack of a proper data format and schema renders the data inconvenient to use in a general context.

This work presents a novel data platform for low-temperature plasma physics. It is designed and implemented from the ground up, using modern data science and web technology, and the experience of the well-established LXCat platform [1]. The primary accomplishment regards the ability to serve any complex atomic, or molecular state as a structured object, including compound and less well-defined state designations. As a result, the platform has excellent support for state-to-state, as well as less precise data. Whereas contributors can provide data describing individual interactions, self-consistent reaction mechanisms remain a core concept. Other accomplishments include support for arbitrary n-ary reactions, and the representation of potentials and cross sections as parameter sets for well-established models.

These results are realized through the development of an extensible LTP type library, written in TypeScript [2, 3], which provides the means to accurately and conveniently control the structure of all data objects that enter and leave the platform. In conjunction, JSON (JavaScript Object Notation) is introduced as the general-purpose data format, to leverage its clear structure and excellent tooling [4, 5]. Furthermore, a prototypical backend implementation is realized. The prototype uses an ArangoDB [6, 7] database instance, which provides native support for JSON and allows to accurately capture the molecular, ro-vibrational substructure and reaction networks by means of graph modeling.

The potential of the platform is shown through the joint development of multiple carrier applications, including the open-source LoKI Boltzmann solver (LoKI-B) [8, 9], and the Magnum potential integrator (MagnumPI); in development at the Eindhoven University of Technology. Both applications are updated to support the novel data format, are integrated in a web environment, and can retrieve input data by directly interacting with the platform. This pioneering work on LTP data treatment has led to some exciting prospects with regards to future directions and collaborations. The current focus is on charged particle interactions, although the presented solutions can be extended to serve as an LTP chemistry data platform.

# **Bibliography**

- [1] Carbone, E., Graef, W., Hagelaar, G., Boer, D., Hopkins, M. M., Stephens, J. C., Yee, B. T., Pancheshnyi, S., van Dijk, J., & Pitchford, L. (2021). Data Needs for Modeling Low-Temperature Non-Equilibrium Plasmas: The LXCat Project, History, Perspectives and a Tutorial. Atoms, 9(1), 16. <a href="https://doi.org/10.3390/atoms9010016">https://doi.org/10.3390/atoms9010016</a>
- [2] Bierman, G., Abadi, M., & Torgersen, M. (2014). Understanding TypeScript. In ECOOP 2014 Object-Oriented Programming (pp. 257–281). Springer Berlin Heidelberg. <a href="https://doi.org/10.1007/978-3-662-44202-9\_11">https://doi.org/10.1007/978-3-662-44202-9\_11</a>
- [3] The TypeScript GitHub repository, https://github.com/microsoft/TypeScript, accessed July 13, 2022.
- [4] Bray, T. (2014). The JavaScript Object Notation (JSON) Data Interchange Format. RFC, 8259, 1-16.
- [5] Pezoa, F., Reutter, J. L., Suarez, F., Ugarte, M., & Vrgoč, D. (2016, April 11). Foundations of JSON Schema. Proceedings of the 25th International Conference on World Wide Web. WWW '16: 25th International World Wide Web Conference. https://doi.org/10.1145/2872427.2883029
- [6] The ArangoDB website, <a href="https://www.arangodb.com/">https://www.arangodb.com/</a>, accessed July 13, 2022.
- [7] The ArangoDB GitHub repository, https://github.com/arangodb/arangodb, accessed July 13, 2022.
- [8] Tejero-del-Caz, A., Guerra, V., Gonçalves, D., da Silva, M. L., Marques, L., Pinhão, N., Pintassilgo, C. D., & Alves, L. L. (2019). The LisbOn KInetics Boltzmann solver. Plasma Sources Science and Technology, 28(4), 043001. <a href="https://doi.org/10.1088/1361-6595/ab0537">https://doi.org/10.1088/1361-6595/ab0537</a>
- [9] Tejero-del-Caz, A., Guerra, V., Pinhão, N., Pintassilgo, C. D., & Alves, L. L. (2021). On the quasi-stationary approach to solve the electron Boltzmann equation in pulsed plasmas. Plasma Sources Science and Technology, 30(6), 065008. https://doi.org/10.1088/1361-6595/abf858

## Poster P35 - Jakub Kelar

Surface processing and technology (cleaning, coating, etching and modification, equipment)

# High quality UV digital printing on various materials with plasma enhanced surface

Jakub Kelar<sup>1</sup>, Zlata Kelar Tučeková<sup>1</sup>, Oleksandr Galmiz<sup>1</sup>, Michal Fleischer<sup>1</sup>, Eva Kosová<sup>1</sup> Lukaš Obšel<sup>2</sup>, and Dušan Kováčik<sup>1</sup>

<sup>1</sup>Department of Physical Electronics, Faculty of Science, Masaryk University, Kotlářská 2, 611 37 Brno, Czech Republic

<sup>2</sup>Effetec s.r.o., Ruská 255, Čelechovice na Hané, Česká republika

E-mail: jakub.kelar@mail.muni.cz

The UV digital printing technology is widely used for high variety of surfaces. However, the ink composition, UV light intensity and surface chemistry must be perfectly tailored for the printed layer to adhere to the desired material. An industrially proven process for tailoring of surface chemistry of the printed material often uses aggressive chemicals (so-called primers). This process is cumbersome with limited use for larger surfaces since the application of the primer is done by hand.

During our cooperation with UV digital printer manufacturer, we have been able to prove that plasma modification of the surfaces can yield adhesion improvements satisfactory for industrial standards even without introducing any other chemical into the mix.

Plasma discharge used for the treatment of polycarbonate, polymethyl methacrylate, and acrylate layer on top of aluminium plate was our Diffuse Coplanar Surface Barrier Discharge and its novel modification suitable for printer implementation.

Every material has been evaluated by various measurement methods from which the free surface energy measurement, peel test (adhesion), and crosscut test (industrial adhesion test) were performed in most detail. For all materials, the surface energy and peel test adhesion values rose with a higher exposure time. However, for industrial partners, the most critical test is the crosscut adhesion test according to the prescribed ISO norm. For this evaluation method, we have discovered significant differences for each material that lead to development of the treatment process with separate parameter adjustments from the printing head – so the printing will not be slowed down by plasma treatment. For example, results on the acrylate layer on top of aluminium showed the best adhesion improvement for short exposure times (1-3s) and worsening of the adhesion for any exposure time over 5s, which is in sharp contrast to polymethyl methacrylate surface that needed exposer times in an interval of 60s to properly improve adhesion.

This and all other results are presented at the poster presentation.

## Acknowledgment:

This research has been supported by the project FV40114 funded by the Ministry of Industry and Trade of the Czech Republic by the project FV40114, funded by the Ministry of Industry and Trade of the Czech Republic.

#### Poster P36 - Tao Zhu

Surface processing and technology (cleaning, coating, etching and modification, equipment)

# Tracing model of in-flight particles during a plasma spray process

Tao Zhu, Margarita Baeva, Holger Testrich, Rüdiger Foest

Leibniz Institute for Plasma Science and Technology, Felix-Hausdorff-Str. 2, Greifswald, 17489, Germany E-Mail: tao.zhu@inp-greifswald.de

Due to its powerful versatility of high temperature, high velocity and high energy density, atmospheric plasma spray has been widely utilized for the production of functional coatings. Besides the working conditions of the plasma torch, characteristics of injected particles, such as size distribution, the velocity, the angel, and the position of injection are essential for the formation of the coatings.

This work presents studies on the combined effect of injection parameters. Normal statistical distributions dispersion of the injection parameters are considered in order to follow the transport of Al<sub>2</sub>O<sub>3</sub> particles fed into the jet of a plasma spray torch. The thermal and flow field of a turbulent plasma jet is obtained in previous modelling of the plasma spray torch Oerlikon Metco F4MB-XL[1], in which the cathode boundary layer and the bulk plasma are coupled in a self-consistent way. The particles are heated and become melting in the plasma jet. Their trajectories (Figure 1), velocity (a), and temperature (b) are obtained by solving the equation of motion for a given number of particles accounting for drag, thermophoretic, and gravity forces. The computed values of velocity and temperature agree well with the measured values of about 400 m/s and 3000 K, respectively. The particle tracing model allows us to evaluate the K-Sommerfeld number that characterizes the impact behavior of the droplets. The tracing model is benchmarked against published data.

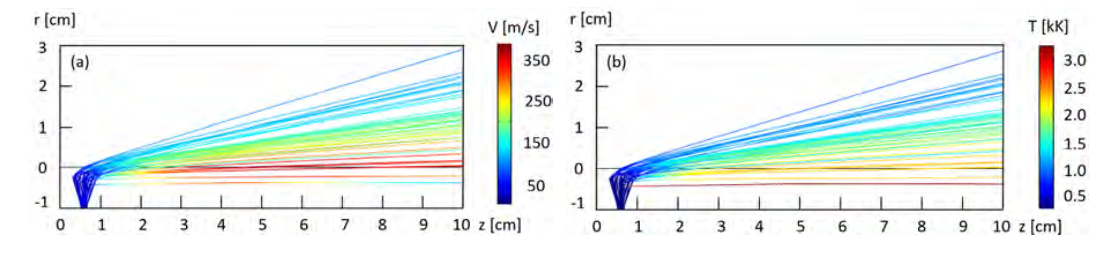


**Fig. 1:** Image of the computed particle trajectories after injection into the plasma jet. The colours of the trajectories indicate the particle velocity (a) and the particle temperature (b).

## References

[1] Baeva, M., Zhu, T., Kewitz, T., Testrich, H., Foest, R., Journal of Thermal Spray Technology (2021), DOI 10.1007/s11666-021-01261-4.